UNIVERSITÀ DEGLI STUDI DI TRIESTE

XXXIII CICLO DEL DOTTORATO DI RICERCA IN NANOTECNOLOGIE

DEVELOPMENT OF A RECYCLABLE NATURAL BASED THERMAL INSULATOR NANOCOMPOSITE

Settore scientifico-disciplinare: ING-IND/22

DOTTORANDO
MATTEO CIBINEL

COORDINATORE
PROF. ALBERTO MORGANTE

SUPERVISORE DI TESI
PROF. VANNI LUGHI

ANNO ACCADEMICO 2019/2020

Università degli Studi di Trieste

XXXIII CICLO DEL DOTTORATO DI RICERCA IN NANOTECNOLOGIE

DEVELOPMENT OF A RECYCLABLE NATURAL BASED THERMAL INSULATOR NANOCOMPOSITE

Settore Scientifico-Disciplinare: ING-IND/22

Dottorando:
Matteo Cibinel

Coordinatore:
Prof. Alberto Morgante

Supervisore:
Prof. Vanni Lughi

Anno Accademico 2019/20

"We are the first generation to feel the sting of climate change, and we are the last generation that can do something about it."

-Jay Inslee

Contents

List of Figures

List of Tables

List of Acronyms

Acronym	Description
AF	Alginate Foam (suffixes and prefixes defined in (Par. 4.1))
AG	Alginate Gel (suffixes and prefixes defined in (Par. 4.1))
AS	Alginate Solution (suffixes and prefixes defined in (Par. 4.1))
ATH	Aluminium hydroxides
CAF	Composite Alginate Foam (suffixes and prefixes defined in (Ch. 4))
CC	Cone Calorimetry
DSC	Differential Scanning Calorimetry
EPS	Expanded polystyrene
fGO	Funcionalized Graphene Oxide (suffixes defined in (Par. 4.3))
FR(s)	Flame retardant(s)
GO	Graphene Oxide
GWP	Global Warming Potential
HBDC	Hexabromocyclododecane
HCFC	Hydrochlorofluorocarbons
HFC	Hydrofluorocarbons
HFM	Heat Flow Meter
HFR	Halogenated Flame Retardant
HRC	Heat Release Capacity (Micro Combustion Calorimetry)
HRR	Heat Release Rate (Cone calorimetry)
LCA	Life Cycle Assessment
LDH	Layered double hydroxides

LOI	Limited Oxygen Index
MCC	Micro Combustion Calorimetry
MH	Magnesium hydroxides
MLC	Mass Loss (Cone calorimetry) Curve
MLR	Mass Loss Rate (Cone calorimetry)
MMT	Montmorillonite
nFR	Nano Flame Retardant
oCAF	Original Composite Alginate Foam (suffixes defined in (Par. 4.1))
PBDE	Pentabromodiphenyl ether
PFR	Phosphorous based Flame Retardant
pHRR	Peak of Heat Release Rate (Cone calorimetry)
PO	Original Material(oCAF) - Product System LCA (suffixes defined in (Ch. 5))
PP	Polypropylene
PR	Recycled Material(rCAF) - Product System, rCAF-G variant (LCA) (suffixes defined in (Ch. 5))
PRI	Recycled Material(rCAF) - Industrial Product System, rCAF-G variant (LCA) (suffixes defined in (Ch. 5))
PS	Polystyrene
PTFE	Polytetrafluoroethylene
PU	Polyurethane
rCAF	Recycled Composite Alginate Foam (suffixes defined in)
rGO	Reduced Graphene Oxide
SEM	Scanning Electron Microscopy
TEM	Transmission Electron microscopy
TGA	Thermogravimetric analysis
THR	Total Heat Release (Cone calorimetry)
TIM(s)	Thermal Insulation Material(s)
TOF	Time of Flame Out (Cone calorimetry)
TTI	Time To Ignition (Cone calorimetry)
XPS	X-ray photoelectro spectroscopy

XPS	Extruded polystyrene

Part I

Introduction

Abstract

This work was focused on the development of a fully recyclable thermal and acoustical insulation nanocomposite with improved fire resistance behavior in which Graphene Oxide (GO) was used as flame retardant. The nanocomposite was based on a previously developed alginate-based insulator foam, in which fibre-glass waste is down-cycled by incorporation into the polyanionic gel matrix before lyophilization. The complete functional recycling was carried out by designing a new process capable of disassembling and then rebuilding the ionic matrix – which is initially formed by the interaction between a cation (e.g. calcium) and the negatively charged alginate backbone – with the use of a chelator (Ethylenediaminetetraacetic acid disodium salt, EDTA) easily controlled via pH shift. The effectiveness of the recycling process was primarily assessed through characterization of the functional properties on an optimized version of the alginate composite, at first, and on the GO nanocomposite afterward. Data showed that thermal, acoustical and mechanical properties were maintained or even improved in the recycled samples. A multi parametric life cycle assessment (LCA) study showed that, at the lab scale, the recycling option is preferable to simple material disposal and substitution due to the reduction of the environmental footprint of the recycling process. A second comparative analysis, operated also by defining an industrial scaled version of the recycling process, allowed to identify, in the electric energy consumption and in the EDTA syntheses, the most environmentally critical contributors associated with the recycling process, paving the way to futures developments. Cone calorimetry was used to evaluate the fire resistance effect of the introduction of GO in the nanocomposite: data show major improvements at a concentration of only $2\%_{wt}$ with the GO acting with a physical barrier mechanism. In addition both the recy-

cled foam and nanocomposite showed an improved fire resistance behavior respect to their original counterparts primarily ascribed to modifications introduced by the recycling process. Eventually, to improve flame resistance activity of GO and compatibilization with the alginate matrix, different GO functionalization, with polyamines and nano-aluminium hydroxides, were synthesized and fully characterized.

Introduction and Purposes

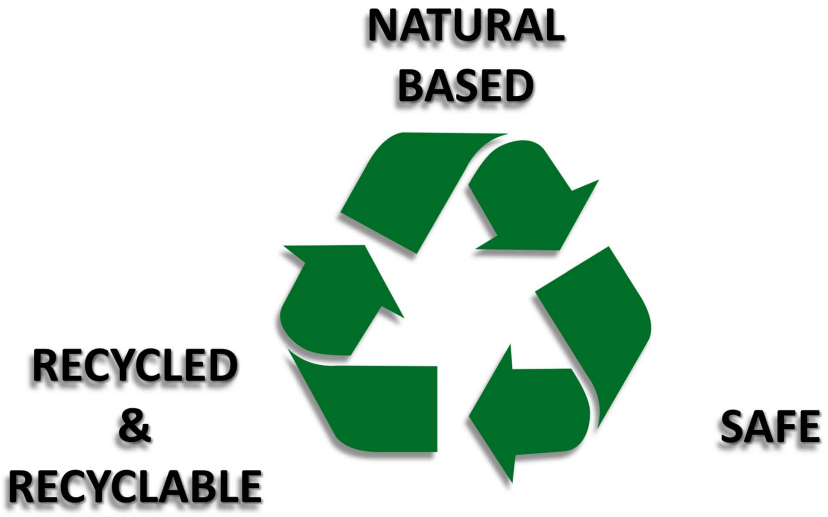

Figure 1

With the rolling out of the *European Green Deal* project, the European Union is currently pledging to drastically reduce its carbon footprint with the goal to become the first carbon-neutral economy by 2050. To fulfil this objective all the member states committed to promote energy efficiency policies which have seen in the Construction & Building one of the leading sector toward which efforts have to be directed. Hence, the adoption and development of new thermal insulation technologies is a key element that has to be put in place due to its major role in the reduction of energy waste. As a matter of fact, it has been estimated, in a realistic scenario, that a retrofit of the current EU building stock could save

up to 5-6% of overall EU energy demand and leading also to the abatement of about 5% of CO_{2eq} EU emission. However, the advancement toward a carbon-neutral economy cannot be only based on simple energy spending review policies. Reduction of generated waste and non-renewable resources depletion are two other key-points which are handled in the *Circular Economy* and *Bio-economy* European action plans; and again, the building sector represents one of the leading actors. At the present, the most widely adopted thermal insulation solutions are based on non-renewable resources (synthetic polymers) and their recycling strategies, in a circular economy vision, are facing numerous problems. For this reason, the attention of the research community is currently focused on the development of new natural based solutions and on the re-use of industrial waste as new thermal insulating materials. Unfortunately, little attention is actually paid to end-of-life options of the developed alternative thermal insulator materials that do not involve landfill disposal or incineration.

This work is focused on the development of a completely recyclable alginate insulator nanocomposite with improved fire resistance properties. This material is based on a previously produced thermal and acoustic insulator obtained from glass industrial waste embedded in a calcium-alginate foam (CAF)[1]. More in the details, after a initial optimization stage the attention was primarily focused on finding an efficient recycling strategy capable to preserve the material's functionalities (thermal, mechanical and acoustical): herein a new functional chemical recycling process for alginate-based material was developed and its environmental impact was evaluated, through Life Cycle Assessment (LCA). The improvement of fire resistance was approached with the use of Graphene Oxide (GO), used as flame retardant (FR) nano-filler. GO efficacy was initially evaluated in the original (non-recycled) material and its functional compatibility with the recycling process was also assessed. Graphene Oxide has been chosen as flame retardant candidate, as an alternative to conventional systems, for two main reasons: the composite alginate foam (CAF) had been originally developed to host different industrial waste with the calcium-alginate acting as a binding agent, therefore an additive with a physical flame retardant mechanism was preferred due to limited dependencies with the polymeric system. In addition, nano-structured flame retardants

generally require a reduced loading concentration to be effective respects to conventional systems. At the end, to improve flame resistance activity of GO and compatibilization with the alginate matrix, different GO funcionalization, with polyamines and nano-aluminium hydroxides, were studied.

Chapter 1

Thermal Insulators materials (TIMs)

Thermal insulators constitute a wide and heterogeneous family mainly composed of foamed and fibrous materials of both organic and inorganic origin [Fig. 1.1]. Globally, the thermal insulator market value was estimated, in 2018, at nearly 52 billion USD[2] with a share of the building segment of 28 billion USD [3]. Glass wools and expanded polyester (EPS) represent together the largest product segment (by volume) with the latter accounting for the bigger share, 27% (mainly due its extensive used in thermal packaging), while glass-wools still dominates in building insulation applications[2]. By order, mineral and inorganic wools (which compete for the second position with EPS in regional building markets), extruded polyester (XPS) and foamed polyurethanes (PU and PIR) represent the others major players while use of cellulose, aerogels and vacuum insulation panels are still limited. However, the market value is expected to rise, with a forecasted value of 73 billion USD in 2025[1], mainly due to the growth in construction activities in developing countries and as a result to the extensive retrofitting of pre-existing buildings. This is caused by the expected growth in energy and combustible cost and the consequent interest in reducing energy waste coupled with the increase in the need of maintaining a comfortable indoor temperature in residential buildings[2]. Jointly,

[1] base year for estimation: 2018

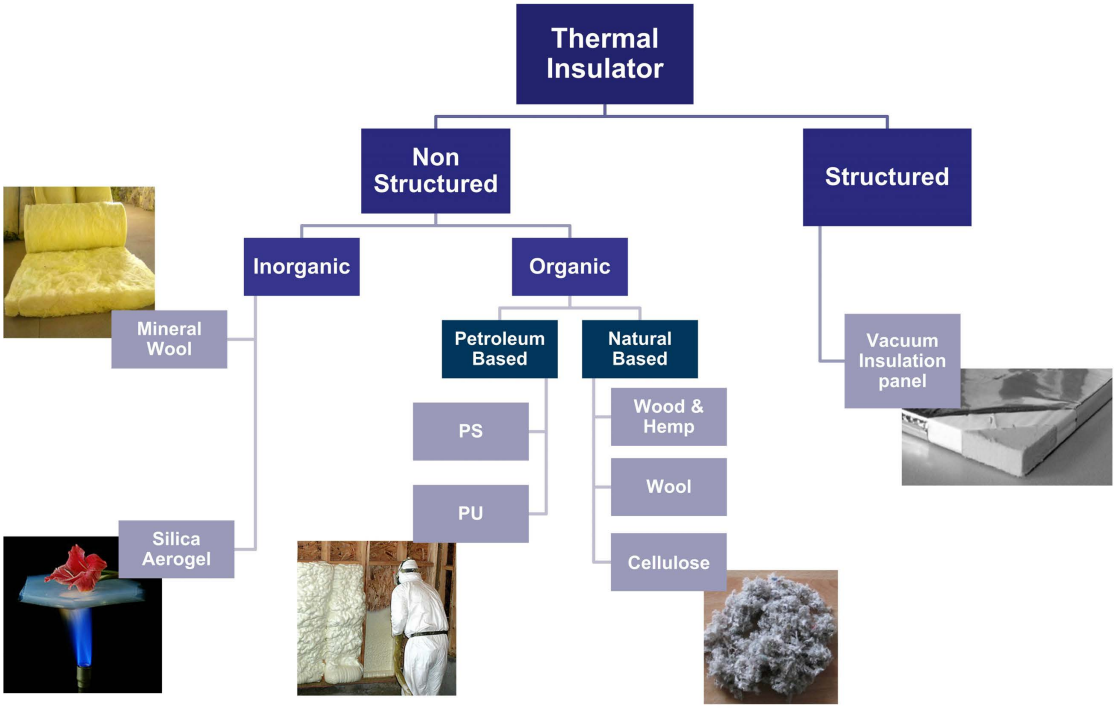

Figure 1.1: Thermal Insulators families examples

growing environmental awareness has been driving economic policies around the word, actively promoting energy efficiency actions and carbon emission reductions efforts.

1.1 An European glimpse

Together with a 20% cut in greenhouse gas emission[2], in its "*2020 Climate & Energy Package*" the European Union (EU) set an additional goal of an overall 20% improvement in energy efficiency to be reached by the end of 2020 [3]. These targets have been recently updated, as a part of the new development plan toward 2030[4]

[2] from 1990 levels

[3] The 2020 Climate & Energy Package (EU2020) is a complex set of law and communications ruled by the EU starting from 2007: detailed policies and related documentations can be found at https://ec.europa.eu/clima/policies/strategies/2020_en

[4] 2030 climate & energy framework: main communication (COM(2014) 15), other information can be found at https://ec.europa.eu/clima/policies/strategies/2030_en

setting a 40% reduction in greenhouse gas emission[5] and an improvement of 32.5% in energy efficiency[6]. Numerous technical reports have already identified the Constructions and Buildings sector as one of the critical areas in which urgent actions have to be put in place in order to comply with environmental goals [4][5][6]. As a matter of fact, buildings are responsible for 36% of all CO_{2eq} emission[7] and for 40% of total EU energy demand[5], with heating and cooling loads accounting for 60 - 80% of the total energy consumed (averaged values which varies, primarily, across residential and non-residential buildings and climate zones)[8][9]. For these reasons, in its *Energy Performance of Buildings Directive* (EPBD)[8], the EU required that all new public buildings must comply with *nearly zero-energy building standards* (nZEB) from 2019, and the same applies to all new building from 2021. This particular action was coupled with other efficiency policies which committed each single European state government to establish specific long term strategies to boost the energy efficiency of pre-existing building. As a matter of fact, only 1% of the buildings, with respect to the entire EU building stock, is currently "built new" (or efficiently renovated) and, even more important, the majority of pre-existing buildings ($\approx$ 75% [9,10]) are outdated and built before the introduction of single state energy efficiency laws[10][11]. Both [Fig. 1.2] and [Fig. 1.3] highlight this situation, by subdividing average thermal transmittance of buildings with respect to the building ages and by displaying the building stock distribution by EPC[11] label. The *Energy efficiency directive* (EED)[12] stressed the fundamental importance of old building retrofitting to meet environmental targets and required member state to increase to 3% the annual renovation rate of public building. Nevertheless, a massive intervention on private sector is still pivotal and was partially addressed

[5] As a part of the European Green Deal, the EU recently proposed to further raise the greenhouse gass emission target for 2030 to 55%, (COM(2020) 562)

[6] Directive on Energy Efficiency (2018/2002)

[7] allocated from consumed energy[7]

[8] (2002/91/EC),(2010/31/EU) and (2018/844/EU) directives, see also Energy Efficiency Directive (2012/27/EU) and (recast 2018/2001/EU)

[9] https://ec.europa.eu/energy/topics/energy-efficiency/energy-efficient-buildings/energy-performance-buildings-directive_en

[10] https://www.bpie.eu/publication/97-of-buildings-in-the-eu-need-to-be-upgraded/

[11] Energy Performance Certificates, see: https://ec.europa.eu/energy/eu-buildings-factsheets-topics-tree/energy-performance-certificates_en

[12] (2012/27/EU) and (recast 2018/2002/EU)

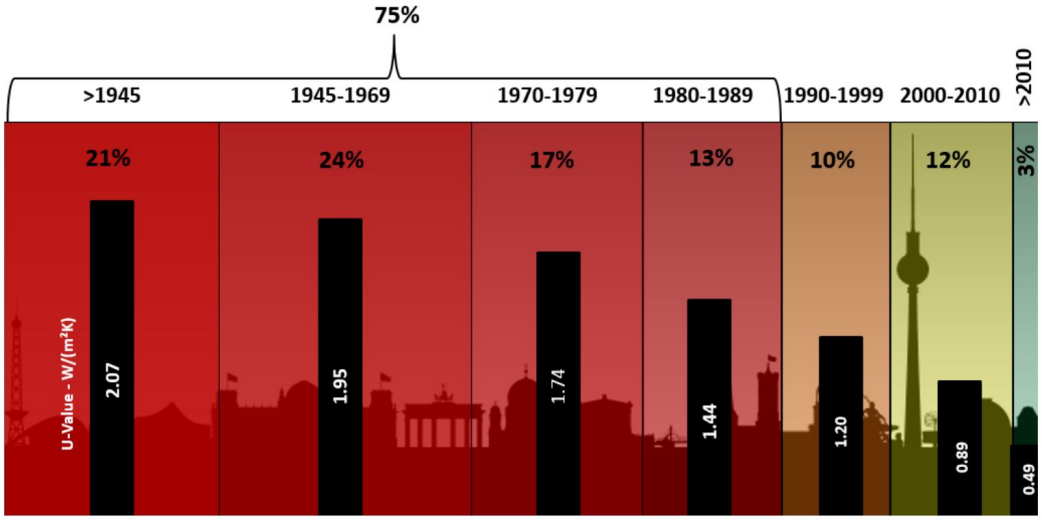

Figure 1.2: Age of the EU building stock and corresponding average U-value (illustrated by the black bars) for building envelopes. The 2010 data for U-Value is based on an average of just 7 countries, while the others are based on average of all 28 Member States ((Source: EU Building Stock Observatory), from [14])

by the EPBD 2018 amending directive[13] which calls member states for instituting financial mechanisms to promote energy efficiency refurbishment of private buildings[12]. It has been estimated that a deep renovation scenario of the entire building stock[14] would lead, by 2050, to a save of 80% of energy consumed for heating[15] and a reduction up to 91% in CO_{2eq} emission in the building sector[13]. Despite not being *the* solution to the energy inefficiency of buildings, the improvement of the thermal insulation level of the external envelope (*i.e.* reducing the U-value) can substantially contribute: in a deep high thermal efficiency, retrofitting the impact of the envelope on heating and cooling loads, weights around 50% and it is mainly shared between *opaque insulation* layers[16] and windows, followed by air sealing technologies, solar reflective technologies and passive solar design[15]. Others upgrades, that can substantially contribute to the efficiency target, consist

[13](2018/844/EU)

[14]Base year 2015, 2.3% annual renovation rate to nZEB standard, high contribution of renewable for electric and heating, 1% new building nZEB standard (15 kWh/m^2)

[15]hot water included

[16]with "*opaque insulation*" it is refereed to insulation of walls, roofs foundations and floors

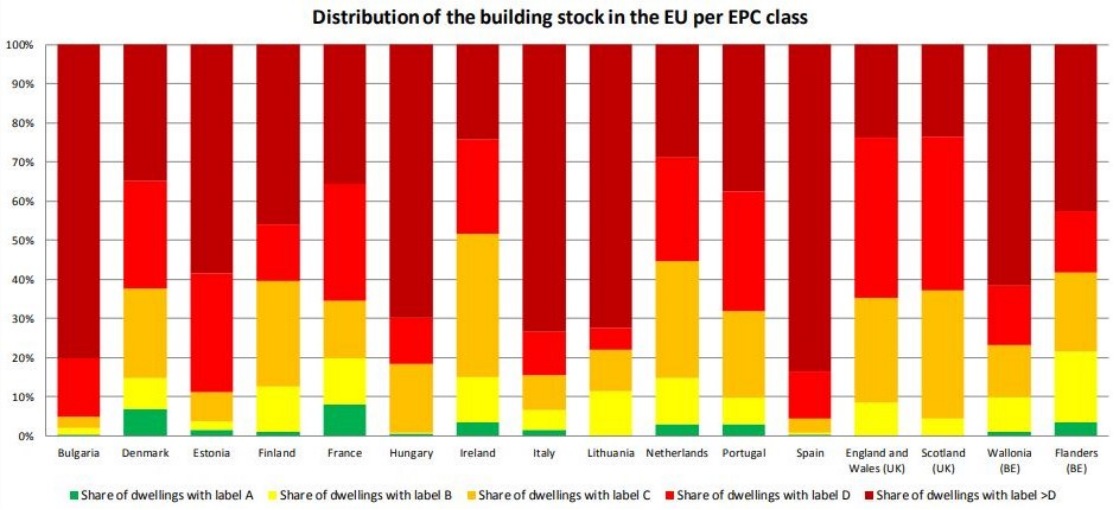

Figure 1.3: EPC data retrieved from the EU Building Stock Observatory (BG, FR, ES, NL, IT, FI), national databases (DK, HU, PT, EN & WAL, IE, LT, , FL) and reports by the Concerted Action EPBD (EE, SL, WL). The sample covers half of EU Member States, with a minor bias toward Western European countries. Data update to 2017, from [14])

in the use of solar-thermal, photovoltaic, heat pumps, district co-generative systems, instantaneous heaters for hot-water, solid state lightings and high reflective paints and coatings[15]. Nevertheless, in a complex work, published by Gulotta *et al.*[9], in which the impact of the retrofit of the sole external insulation layer on the majority of the European building stock, was simulated a potential reduction of 20-30% of heating-related thermal loads and 13% of CO_{2eq} emission from the entire sector was displayed, taking account for differences among climate zones, single state energy mix, types and ages of the buildings using a consequential Life Cycle Assessment approach. Understanding the enormous potential of the building sector, in an effort to promote also private buildings retrofitting, the EU recently published its "*Renovation Wave Strategy*"[17] which aims to double the current 1% annual renovation rate[18] in the next decade, leading to a potential cut in

[17] A Renovation Wave for Europe – Greening our buildings, creating jobs, improving lives (COM(2020)662)[16]

[18] EU real deep energy renovation rate, >60% in savings, is much lower: 0.2 - 0.3% annual. The 1% value, often presented, is a weight averaged energy renovation rate for all energy related renovations achieving a minimum of 3% energy savings[17]

buildings final energy consumption of 14% (which correspond to 5-6 % of total EU energy demand) and a greenhouse gas emission reduction of 60% (corresponding to a $\approx$ 5% decrease of EU CO_{2eq} emission)[7][18][16].

However, the renovation wave is just a piece of a new long-term strategic plan, named *European Green Deal*[19], that the EU is currently deploying with the aim of making the EU a climate neutral continent hinged on a sustainable economy by 2050. In order to fulfill this ambitious target, emission cutting policies are currently implemented side by side with integrated circular[20] and bio-economy[21] strategies that work together toward a zero-waste society, less dependent on non-renewable resources. Circular economy aims to interrupt the *"take-make-use-dispose"* linear pattern, that generate an enormous stream of waste and it is incompatible with the natural constrains on the availability of non renewable resources, by implementing a closed loop in which products are reused, repaired and recycled as long as possible, while retaining their value. The building sector (construction and demolition stages, C&D) is responsible alone for 35% of total waste generation in EU[22] and has been identified as one of the critical sectors for waste management policies since 2008, with the publishing of the first Waste Framework directive(WFD)[22] and with the following 2015 circular economy action plans[23]. In the amended WFD the EU pledged to improve the recycling share of C&D waste to 70% by 2020, target that was successfully accomplished but mostly by down-cycling mineral waste part[23]. Data on non-mineral waste fraction in EU C&D waste are scarce or missing thus preventing an efficient implementation of valorization & recycling policies for these materials. As a matter of fact, numerous reports and reviews highlighted, during the last years, the problem related to the poor waste stream characterizations in the C&D sector [23][24][25]. For this reasons in the new circular economy action plan[24] the EU stressed the importance of the introduction of material-specific re-

[19] https://ec.europa.eu/info/strategy/priorities-2019-2024/european-green-deal_en

[20] in particular plastic waste strategy [19] in circular economy action policies[20]. Latest update: (COM(2020)98)

[21] Bioeconomy agenda [21]

[22] 2008/98/EC, amended 2018/851

[23] (COM(2015) 614 final) and following (COM(2020) 98 final)

[24] A new Circular Economy Action Plan For a cleaner and more competitive Europe (COM(2020) 98 final)[22]

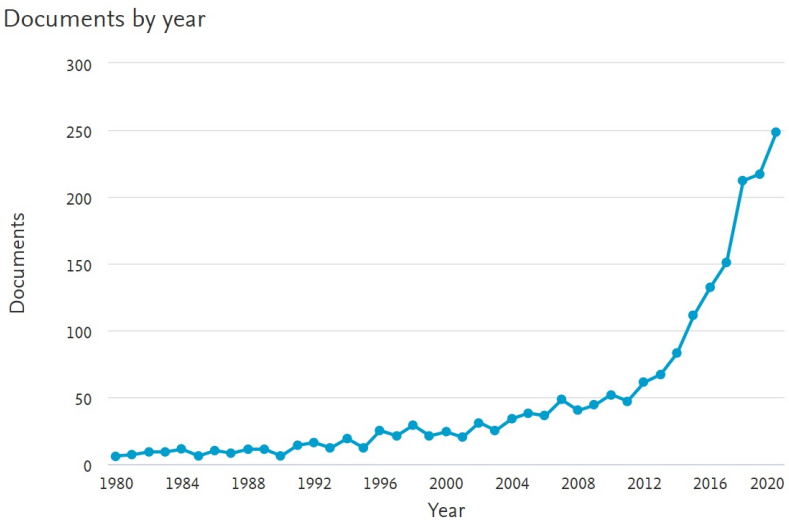

Figure 1.4: By year number of research article in natural or bio based thermal insulator topic, Scopus database: TITLE-ABS-KEY ("Thermal" AND ("Insulator" OR "insulation") AND ("natural" OR ("bio" AND "based"))) AND (LIMIT-TO (DOCTYPE , "ar"))

cycling targets in C&D, specifically appointing to thermal insulation materials due to their growing waste stream.

On the bioeconomy policy side, one of its main objective is the reduction of dependency on non-renewable resources, not only from fossil fuels but also from raw materials used in industries and consumer products, pushing for the development, among others, of bio-based substitute materials, in line with the commitment under the Paris Agreement objective[26]. Research interest in bio-based thermal insulation material has grown in recent years [Fig. 1.4], in particular towards those derived from agricultural by-products and cellulose. Alongside, for example, it is worth mentioning that the natural thermal insulation market share expanded from 1% in 1998 to 11% in 2014 in central Europe; with cellulose, wood fiberboard and wood-wool as principal products[27]. This is mainly due to the above mentioned motivations and due to the reduced potential environmental impact that natural sources posses. As a matter of fact, a recent report drawn up by the European Environment Agency, has highlighted that the use of recycled and natural based materials as substituent for petroleum derivates or hazardous alternatives consti-

tutes a core foundation for a sustainable circular economy transition[23].

The same report also highlighted another critical factor: the lack of the application of the "*design for disassembly*" concept. Design for disassembly enables the reclamation of individual components limiting or excluding the damaging of others. This deficiency, other than extremely limiting an efficient waste differentiation during demolition also prevents a possible reuse or recycle of materials. Analogously, in the reviewed literature little or no attention was directed toward different end-of-life options, excluding landfill disposal, for natural based systems: although the value of recycling industrial waste or agricultural by-products is not questionable, a recycling outlook is always preferred. As a matter of fact, the use of grinded waste/by-products in a cascade recycling cycle, in which the value of the original material is inherently loss at every step better fit the definition of downcycling. Examples of this are PU bonded foams[28], wood particleboard[29], textile off-cuts boards and natural fibres panels with non reversible binders[30]. The concept of including the valuable reuse or functional recycling (in which the performance or their original primary function is maintained) as end-of-life option is contained in the "*design for recycling*" concept. *Design for recycling* and *design for disassembly* are two faces of the same coin that has to be invested, together with the development of new recycling technologies, in building a real sustainable society.

1.2 Conventional TIMs

[Fig. 1.1] proposes a classification of TIMs depending on their complexity and on the material family they are based on. As stated above, most of the TIMs present in the market are mineral wools and polystyrene and polyurethane foams while natural derived and more structured materials such as aerogel or vacuum insulation panels (VIPs) are still emerging. One of the most important properties of TIMs is the thermal conductivity $\lambda\ [W/m\,K]$: the capacity to transmit a heat flux through a thermal gradient per unit of space (thickness). The lower the thermal conductivity is, the thinner the insulation layer can be build, for a target thermal

transmittance ($U\ [\,W/m^2\,K\,]$)[25]. Another important parameter is the Specific Heat Capacity $c_p\ [\,J/kg\,K\,]$, which express the capability of a material to store thermal energy per unit of mass, therefore its capacity of inducing a thermal inertia effect. This thermal inertia can be exploited to store energy inside the insulation layer, during high temperature peaks (*e.g.* day-time), to be released in concomitance with the low temperature peak (*e.g.*night), thus preventing overheating and excessive thermal loads. This approach, however, is far more effective in temperate and hot climate, with relevant temperature excursion across the comfort temperature levels, than in cold climates[31]. Thermal conductivity, density and specific heat can be combined together in a single term, named thermal diffusivity $\alpha = \lambda/c_m\,\rho\ [\,m^2/\,s\,]$, which is more useful in non-steady condition since it describes the propagation of thermal waves inside the media. Often, TIMs can be used to contemporaneously fulfill another function: sound absorption barriers. When a sound wave passes through a porous media it can dissipate its energy through friction or thermal losses. For this reason TIMs are also frequently acoustically characterized, normally in terms of their sound absorption coefficients. Fire resistance is another factor that has to be seriously taken in to account, specifically when organic polymers are involved, since its underestimation cal lead to serious safety issue[32][33].

1.2.1 Mineral Wools

The term mineral wool principally cover stone wool and glass wool products that can be presented as tiles, mats and rarely also as fibrous filling materials. Stone wools (also named Rock-Wools) are manufactured by melting at 1600 °C volcanic rocks, such as basalt and diabase, and/or industrial slag which are then spun to produce fibers that are eventually bonded together with an organic (phenolic resoles resins) or inorganic binder. Glass wool is produced in a similar way starting from a mixture of sand, limestone, soda, borax and recycled borosilicates (glass) waste, that can be processed at a lower temperature (1300-1400 °C). However, glass-wool possess a lower maximum service temperature, 250-400°C, respect to

[25] thermal transmittance reflect the insulation capacyty of a building envelope, or section, by taking accounts thickness and thermal conductivity value of each layer and refers to the total heat that can be transferred through a temperature gradient per unit of area

700-800 °C of Rock-Wool. Generally speaking, due to their limited organic content (5-10$\%_{wt}$), mineral wools are inherently resistant to fire damage. Stone wool, in addition, since possessing a higher density, 40-200 kg/m^3, with respect to 15-75 kg/m^3 of glass wool, is also suitable as flame stopper, capable of withstanding flames penetration. Common mineral wools TIMs are commercialized with a λ of 30 - 44 $mW/m\,K$ and a c_p of 0.8 - 1.0 $kJ/kg\,K$. In addition, mineral wool possess excellent sound insulation performances and in particular rock-wool due to its higher density[34]. These considerations, combined with their low-price and flame resistance determined their leading position in the market[35][36]. Unfortunately, despite not being anymore categorized as carcinogenic to humans[26], the long term toxicity of mineral wools is still debated and full body protection is still required (or highly recommended by the producers) during installation to reduce skin irritation[34][39]. From the recycling point of view, mineral wools are reported to be easily recycled by re-melting by the same producers or they can be reused in ceiling tiles or even down-cycled in cement industry or in other fiber reinforced products[36][40][41]. However serious problems limit the effective recycling of these waste despite the options presented above (*e.g.* limited material-selective waste differentiation during deconstruction and limited data on real waste streams). In addition, recycling could not be always economically valuable, with respect to landfill disposal, caused by the low cost of the new mineral insulator and the high cost of transport (thanks to the looseness and bulkiness of the material). Moreover, wools produced before ≈1996 were made without those important process changes that eventually reduced the carcinogenicity (bio-solubility) of fibres (chemical composition and possible asbestos-like content of fibres). Therefore, without any certification, unidentified mineral wools TIMs have to be treated as hazardous waste and excluded from recycling[41][37].

1.2.2 Polystyrene based (EPS & XPS)

Polystyrene (PS) is a thermoplastic polymer and is commercialized, as TIM, either in its rigid expanded form or the extruded one. Expanded polystyrene (EPS) is the

[26] since 2002 by IARC, in EU the REACH regulation (907/2006) and CPL regulation (1272/2008) require specific bio-solubility test to be conducted in order to not be categorized as "possible carcinogenic"[37][38]

most common and it is usually produced by introducing a blowing agents (such as pentane, or HCFC in the past) during the suspension polymerization of PS beads, which are then expanded (using a hot pressurize steam or air) and sintered inside the mold. The final product is extremely performing, possessing a low thermal conductivity, 31-35 $mW/m\,K$, and a good specific heat $\approx 1.25\ kJ/kg\,K$. In addition, it is lightweight (15 - 75 kg/m^3) and can be easily cut and manipulated during installation[36]. Extruded polystyrene (XPS) is produced by a continuous extrusion of melted PS pellets with the addition of a blowing agents and it generally performs slightly better than EPS (with the same density). XPS possess a lower thermal conductivity 25 - 35 $W/m\,K$, higher specific heat ≈ 1.3 - $1.7\ kJ/kg\,K$ and, avoiding sinterization, it shows a higher compression strength being less prone to crumble[36]. Both XPS and EPS posses a closed cell structure but, due to incomplete bonding of PS beads, EPS still shows open cavities which leads to a reduced water permeation resistance with respect to XPS, thus partially limiting its use in wetted environment[42][36]. However, EPS still represent the best solution due to the higher cost of XPS (10 - 20% more). As far as sound insulation is concerned, both EPS and XPS, show no significant properties, primarily due to their closed cell structure and low density[36]. Differently from mineral wools, PS insulators compulsory need the addition of flame retardants to reduce their flammability. Unfortunately, in the past, HBCDs (Hexabromocyclododecanes) were extensively used as flame retardants before their EU ban in 2015 due to increasing warnings and scientific evidences about their toxicity and accumulation potential[27][45][46]. Despite having been banned, HBCDs still pose a major problem since all previously installed panels containing banned chemicals cannot be recycled and have to be incinerated[47]. An experimental recycling technology, named Creasolv®, is currently under testing, with an industrial pilot-plan, claiming to separate the HBCDs from the EPS/XPS via physical methods[48]. A similar problem comes from the presence of some prohibited HCFCs ,used as blowing agents for XPS before their ban was introduced in 2014[28]: waste specialized treatment is mandatory in this latter case. Taking account of these problems, PS can be easily recycled

[27] REACH regulation[43] annex XIV, and PoP (Persistent Organic Pollutant) regulation under Stockholm Convention[44].

[28] Regulation (EU) No 517/2014 of the European Parliament and of the Council on fluorinated greenhouse gases and repealing Regulation (EC) No 842/2006

by re-melting and used along with new virgin material as feedstock or it can be down-cycled as filler (*e.g.*) cements[49]). Currently, only a very limited fraction of PS, coming from C&D, is recycled in Europe: less than 70% EPS is incinerated and almost 29% is disposed to landfills (with peaks of >50% in France, Italy and East Europe countries)[49]. However, it is worth to note that, the EUMEPS (*"European Manufacturers of EPS"* association) submitted a voluntary pledge to the EU[29] in which they indicate their intention to rise up to 27% the recycling fraction of EPS coming from buildings deconstruction by 2025[48].

1.2.3 Polyurethanes FOAMS (PU & PIR)

Polyurethane foams (PU or PUR) are produced through an exoteric polymerization reaction between polyisocyanates and polyether polyols and simultaneously expanded with a blowing agent(pentane or low impact HFC). Cell structure, thermal, physical and mechanical properties of the final product are closely related to the chemical structure and molecular weight of the chosen precursors: open and closed cell, rigid, flexible, thermosetting and thermoplastic polyurethane can be synthesized. For thermal insulation purposes thermosetting, rigid, closed cell foams, produced starting from low molecular weight precursors (1000 Da), are usually preferred and some formulations can also be directly sprayed (polymerized and expanded) directly *on-site*, making them extremely suitable for insulating cavities or low accessible positions. Thermal conductivity varies from 22 to 44 $mW/m\,K$, depending primarily on cell sizes and structure, density from 15 to 45 kg/m^3. They are also characterized by a high specific heat 1.3 - 1.45 $kJ/kg\,K$[36]. Like EPS and XPS, they do not posses excellent sound insulation properties but average mechanical properties are better, leading to lower installation problems (*e.g.* walkability, bonding, layering and supporting capability) at a slightly higher cost of the insulation material. Unfortunately, PU foams are extremely susceptible to fire damage and the use of flame retardants is mandatory: similarly to what happened with HBDC, PBDE (pentabromodiphenyl ether) was a widely used FR which was found out to be extrimely dangerous to human health before its ban

[29] as requested in Annex III of the EU Plastics Strategy, COM(2018)28 final

in 2004 in EU[30][47][45]. Nowadays, phosphorous based flame retardant are commonly used in polyurethane, such as additive TDCPP[31] or reactive Fyrol 6 and Levagard 4090 (Par. 2.4.2). In addition to the problems already discussed for PS (*e.g.* collection and identification of presence of banned substances), recycling of PU can be even more critical: polyols oligomers and isocyanates can be recovered from de-polymerization processes and can therefore be used as feedstock for new PU production. However, this process can be impaired by the presence of unknown legacy chemicals and the final product composition largely depend on original chemical composition of waste. For these reason chemical recycling is often limited to PU waste of known chemical composition (*e.g.* industrial or construction off-cuts),excluding, in this way demolition waste which chemical composition is largely unknown. Currently, only a limited number of companies operate PU chemical recycling, mainly through acidolysis and glicolysis technologies, which unfortunately do not allows FR separation [52][53][54]. On the other hand, mechanical recycling can be easily performed in a similar way in which PS foams waste are processed[52][54]. Polyisocyanate foams (PIR) are produced with an analogous process by using an higher proportion of isocyanate (in general methylene diphenyl diiso-cyanate) wwith respect to polyols fraction (polyester- derived) to produce a highly reticulated polymer formed by interconnected isocyanurate ring. PIR panels generally posses better fire resistance properties than PUR but flame retardant additives are still necessary[36]. The same considerations made for PU, as far as recycling is concerned, apply to PIR panels.

1.2.4 Cellulose

Cellulose fibres TIMs commonly refers to panels or flakes made from recycled waste paper newsprint. The paper is shredded and, after that contaminant as paper clips are removed, is fiberized before being sold as flakes or moulded using organic binder such as polyester resins[55]. However, before commercialization flame retardants and biocides (to prevent mould attack) have to be added to the material: a mix of borax and boric acid, which act at the same time as flame retardant and an-

[30] EU has banned the use of pentaBDE since 2004 (2003/11/EC)

[31] TDCPP is currently listed by ECHA as suspected carcinogenc[50] and scientific literature already highlighted its toxicity[51]

tifungal, is generally used at 20% - 25% of loading[55][56]. Common values of thermal conductivity for cellulose fibres are in between 37 and 42 $mW/m\,K$ with a density of 30 and 80 kg/m^3 and a specific heat of 1.3 - 1.6 $kJ/kg\,K$ and are also capable to provide good sound insulation[36]. Flakes can be used to easily fill cavities but cannot be compressed without loosing their thermo-acoustic performances. Beside this, one of the main attractiveness of cellulose TIMs is represented by its reduce environmental impact, which is one of the lowest, in terms of Global warming potential and embodied energy, among thermal insulation materials: respectively 0.73 $kg\,CO_{2eq}$ and 20 MJ_{eq}/kg compared, for example, with 5 $kg\,CO_{2eq}$ and 127 MJ_{eq}/kg of expanded polystyrene (for the same functional unit)[36]. Unfortunately, high hygroscopicity and a marked sensibility to fungal ingrowth tend to limit the widespread use of cellulose in construction and renovation projects[55]. After its use, despite producer states that it can be easily recycled as TIM, cellulose is mainly incinerated[57] or landfilled (if no contaminants are present)[47][55].

1.2.5 Wood and Cork

Common Wood based products, used for insulation, are wood-wools, fibre-boards and Corks. These materials can be commercialized as panels or in loose form used to fill cavities such as cellulose. Regarding wools and fibrous wood products, numerous types of panels are already present in the market having their properties that vary according to their final density, the used binder (frequently organic or mineral, gypsum) and averaged strips (part of wood-wools) or fibres sizes. The density of the final product can vary between 50 - 600 kg/m^3 and they generally possess a thermal conductivity of 38 - 107 $mW/m\,K$ followed by a specific heat ranging between 1.9 to 2.1 $kJ/kg\,K$ [36][34]. Generally, wood insulation panels shows excellent mechanical properties but a resistance to vapour uptake that dramatically decreases with density. The wood used for panel production can derive from primary sources or, more often, from sawmill waste or recycled structural wood elements from which fibres are extracted. Recently, Ceitner and co workers examined the thermal properties of non-binded grounded wood waste: the results shown a thermal conductivity of 48-55 $mW/m\,K$ and, although having a

reduced resistance to water permeation, these binderless aggregates possess the economic advantage of representing an extremely low-cost alternative[58]. Flame retardants have to be obviously added and intumescent systems (Par. 2.4.2.1) are commonly used together with, amino resins (compounds used for their manufacture are dicyandiamide, phosphoric acid, formaldehyde, melamine, and urea) and borax-borates additives[59]. On the other hand, Cork is an extremely valuable insulation material: is possess excelent sound insulation performances and it is waterproof and does not need addition of binders due to its high content of lignin resin. Moreover, thermal conductivity are comprised between 37 an 50 $mW/m\,K$ with densities of 110 - 170 kg/m^3 and with a specific heat of 1.5-1.7$kJ/kg\,K$. Unfortunately it represent an extremely expensive alternative with respect to other natural based materials.

1.2.6 Structured TIMs

In this category are categorized non conventional TIMs whose thermal insulation properties do not directly derive by the simple reduction of thermal conductivity contribute of the bulk material λ_s (*e.g.* fibres, foams or granular matrices which rely on the low thermal insulation coefficient of still air ($\approx$ 21$mW/m\,K$). Extremely low thermal conductivity can be reached by exploiting the combination of different materials or specific structures: vacuum insulation panels (VIPs) and silica aerogels are the two main representative of this category and are the most promising high-performance thermal insulation materials, with values of thermal conductivity as low as $4\,mW/m\,K$. Aerogel's extremely low thermal conductivities are reached by reducing both λ_s and λ_g (respectively the thermal conductivity of the solid matrix and the gaseous phase, in this case air)[32]. Gaseous thermal conductivity can be lowered by the so called *Knudsen effect*: when the average pore diameter of the material is smaller than the average free length of path of gas molecules, the air molecules start to collide, elastically, with the pore surfaces

[32] λ_r: radiative thermal conductivity plays a major role when higher temperature are considered and its treatment is not trivial since light is absorbed and emitted all along the inner structure of the material. Detailed treatment of aerogel's λ_r contribution can be found in [60].

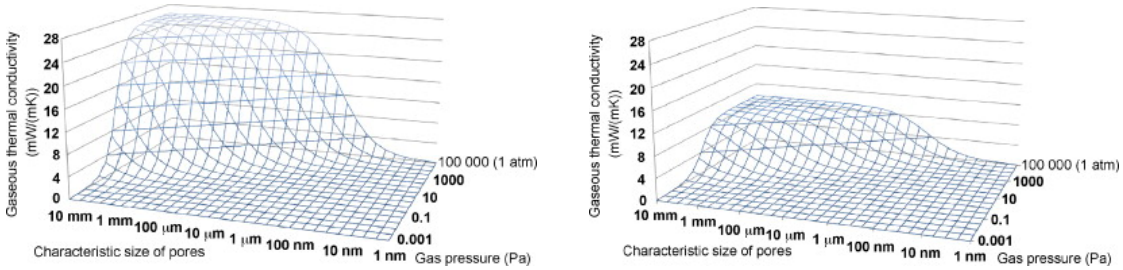

Figure 1.5: Gaseous thermal conductivity of **(a)** air and **(b)** Krypton as a function of gas pressure and pore diameter, from[61].

without transferring energy[61], the new λ_g can be calculated as follow[33]:

$$\lambda_g = \frac{\lambda_{g,0}}{1 + 2\beta K_n} \tag{1.1}$$

with

$$K_n = \frac{k_B T}{\sqrt{2}\pi d_g^2 P_g \delta} \tag{1.2}$$

As it can be seen in [Fig. 1.5], (Eq. 1.1) and (Eq. 4.8), λ_g can be drastically reduced by reducing the pore diameter and/or the gas pressure. Silica aerogel are made via a sol-gel process in wich silicon precursors are polimerized and aged to create a tortuous interconnected-beads gel structure which is, after-that, dried in specific conditions to prevent structure collapse (*e.g.* supercritical drying). The final material possess a particular microstructure with a pore size of 20 - 50 nm, a particle size of 1 - 20 nm and densities as low as $3\,kg/m^3$ with porosities values up to 99.8%[62][36][62]. This particular structure do not only allows to contribute to reduce λ_g but also λ_s contribution, thanks to the high tortuosity of the interconnected network and the enhanced phonons' scattering caused by the fact that particle sizes are close to the phonon mean free path[60]. Despite their attractive properties their widespread use is impaired by technological problems related

[33] $\lambda_{g,0}$ is the thermal conductivity of the gas phase, β depends on the gas type, K_n is the Knudsen number, d_g^2 is the molecules gas diameter, P_g is the gas pressure inside the pores and δ is the characteristic pores' size

to their extreme fragility and elevated cost. However, different strategies can be adopted to overcome these problems: enhanced mechanical strength and even flexible aerogel can be produced by changing silane precursor (*e.g.* high methylated silane) or by adding fibres or fibrous matrix in to the sol-gel process[63]. In a similar way, solvents changes and adoption of different drying technologies can also be used to improve aerogel mechanical properties[62]. In addition,silica aerogel can also be used as granular filler in different material, such as in plasters (50 $mW/m\,K$) [64], polymeric foams, stone wools (19 $mW/m\,K$ in[36]) and even as packed granulated panels (13 $mW/m\,K$[36]). Some aerogel products of this kind are already present in the market such as Spaceloft® from Aspen Aerogels[65] or Thermal Wrap^{TM} from CABOT[66]. Typical densities of these materials are in between 100 and 200 Kg/m^3 but the prices are still high if compared with other conventional TIMs solutions. Moreover, due to high transmittance in the visible domain silica aerogels can also found application in windows. Despite ofthe fact that silica aerogels remains the most performing option, carbon, alumina, copper and even natural polymers such as polysaccharides[67] can be used to produce aerogel structure for insulation purposes[64].

Vacuum insulation panels, differently from silica aerogels, mainly take advantage of the Knudsen effect by reducing the pressure of the air inside the porous material which is enveloped by a vapour and pressure tight barrier to maintain the vacuum. Polyurethane, EPS, XPS, rock-wools, fumed silica or, even better, aerogels can be used qs core material to produce a panel with a central thermal conductivity that can be as low as 4 $mW/m\,K$. The envelope is the most critical part of each VIP: it has to maintain the vacuum inside along the service life of the TIMs and any failure of the protective film will result in a drastic increase of the thermal conductivity (up to 20 $mW/m\,K$), leading to the fact that VIP cannot be cutted or punctured during, or after, the installation[61]. Multiple metal foils (aluminium) or metallized films are used to produce the envelope and proper design is fundamental to reduce vacuum leaking, vapour uptake and thermal bridges effect (due to high conductivity of the envelope's material which can be avoided by enclosing the VIP in a conventional insualtion foam). Getters and desiccants are normally used in the core materials to absorb gas and water vapours, extending the service

life. However, similarly to aerogels, VIP's fragility and cost, joined with the impossibility to be shaped *on-site* still limit its use to situation where the insulation thickness is constrained[36][64].

1.3 Unconventional sustainable TIMs

In this section new TIMs solution are presented, which have been developed and tested in laboratory, in particular those derived from industrial or agricultural waste or bi-products. More traditional materials such as wools and hemp fibres, whose market share is still limited with respect to that one of the materials presented in the previous section, are also considered. Examples of detailed reviews on this topic have been produced by Schiavoni *et al.*[36], Asdrubali *et al.*[34] and Abu-Jdayil *et al.*[64].

1.3.1 From Industrial waste

Textiles represent one major stream of primary industry wastes (mainly polyester and cotton)[68][34] and different strategies for recovering and recycling discarded or used fibres are under investigation to reduce land-filling. For examples, Valverde *et al.*[69] produced a thermal insulation panel with polyester and polyurethane offcuts with a thermal conductivity of 41 - 53 $mW/m\,K$ whereas Tilioua *et al.* studied the thermal conductivity of a panel composed of an inhomogeneous mixture of discarded textiles (composed of wool, cotton and polyester) with a thermal conductivity of 39 $mW/m\,K$ [70]. Some producers also started to recycle their textile waste: this is the case of thermo-acoustic insulation panels made out of multiple fibres waste, such as wools and kenaf, leading to the production of a material with a thermal conductivity as low as 35 $mW/m\,K$ with excellent insulation properties and mechanical resistance[71], or made of denim and cotton bonded with a synthetic binder[72]. Additional examples of recycled textile as TIMs can be found in[68]. PET (Polyethylene terephthalate) is one of the most widely used polymers in packaging application, in particular for bottles, and inadequate disposal can lead to enormous problems of environmental pollution. Exhausted PET bottles can be recycled as TIMs when mixed with virgin PET fibres (25 - 15 $\%_{wt}$,

used as low melting binders), thus producing a material characterized by a low thermal conductivity, $35 mW/m\,K$ and density, $30 kg\ m^3$[73]. What is worth mentioning is that a life cycle assessment study highlighted the non-trivial fact that the environmental impacts of the recycled panel is lower than the one of an original panel produced starting form virgin-PET: in particular, the reduction of CO_{2eq} emissions was estimated to be about 42%[73]. Similar materials, but with higher sound insulation capabilities, are already present in the market[71]. Benkreira *et al.* reported the use of elastomeric particle waste from tyres and PVC-backed carpet fibres bonded using a specific tailored virgin polyurethane adhesive as bonding agents ($\approx 10\%_{wt}$. The best thermal conductivity obtained by the autohors was 34 $mW/m\,K$ with a density of $96\,kg/m^3$. Other examples of TIMs produced form industrial waste can be found in [74].

1.3.2 From Natural resources and bi-products

Natural fibres are excellent starting material for TIMs production: bagasse, cotton stalks, hemp, sheep wool are just few examples, a complete review has been written by Asdrubali *et al.*[75]. Bagasse is a residue of sugar production which is currently treated as waste material but has the potential to be used as TIM due to its low cost and high cellulose content. Binderless bagasse particleboard, for example, can be produced with a thermal conductivity value of 46 $mW/m\,K$ and a density of 250 kg/m^3[76]. Anyway, the addition of a synthetic binder allows the production of stiffer, and more suitable board for building insulation[77][78]. Rice and wheat husks can be used as starting materials for TIMs as well: panels has been produced and tested by Muthuraj et al, using a biodegradable but not bio-derived binder (Ecoflex®), with a thermal conductivity of 80 and 100 $mW/m\,K$ and densities of $\approx 400\,kg/m^3$[79]. The same work studied the use of wood and texitile fibres, but higher thermal conductivities where reported. Buratti *et al.* on the other hand, produced a panels from rice husk using polyurethane as binder ($\approx 70\,mW/m\,K$) but characterizing its sound absorption capabilities[80]. Rice is one of the most cultivated farming products, therefore finding a way to use one of its main waste can be extremely beneficial[34].

1.3.3 Alginate and other Polysaccharides

Beside the use of natural resources waste as TIMs it is definitely worth to cite the use of natural biopolymers, in particular polysaccharides, to produce aerogels with comparable thermal properties to that of silica aerogels. Different polysaccharides such as cellulose, chitosan, pectin and alginate can be used to prepare aerogels with enhanced thermal resistance by taking advantage of the Knudsen effect: two main strategies are used to produce a small pore size distribution which are ionotropic gelation (in particular for pectin and alginate) and alcohol gelation. Polysaccharides are natural polymers formed by carbohydrates monomers bonded together by glycosidic linkages and are mainly extracted by plants (*e.g.* cellulose and pectin) or algae (*e.g.* *alginate*). Due to the extensive presence of hydroxyl groups (in the carbohydrate monomers), polysaccharides are readily dispersible in water and side-side chain interaction can be enhanced by solubilization in less polar media (*e.g.* alcohols) resulting in the formation of a gel structure. On the other hand, polysaccharides salts (*e.g.* sodium alginates) or acid polysaccharides (*e.g.* carboxymethyl-cellulose or pectin) are capable to form more stable gels by forming inter-chain ionic junctions through chelation of externally added cations (preferably divalent or trivalent, *e.g.* Ca^{+2})with their de-protonated carboxylic and polar hydroxyl group: this method is generally referred to as *ionotropic gelation*[81][82]. Similarly to what happens for silica aerogel, to prevent structure collapse lyophilization or supercritical CO_2 extraction are used to extract the solvent. In general, gel structures produced trough hydrophilic interaction posses a smaller pore size with respect to the one produced through ionotropic gelation, but the latter method leads to superior mechanical properties[82]. In addition, in order to produce a mesoporous pores distribution (pore sizes $< 100\,nm$) the use of lyophilization is discouraged, since ice crystal growth tends to modify the gel pores structure providing at the same time a densification of the solid gel structure with an increase of the solid thermal conductivity contribution (λ_s)[81][83]. Numerous polysaccharides super-insulating (*i.e.* $\lambda < 26\,mW/m\,K$) aerogel are reported in literature and referenced materials can be deadly found in [81], [64] and [82], but some examples are herein reported. The most widely studied polysaccharide is cellulose and its derivate, nano cellulose fibres, due to the fact that it is the most

abundant natural polymer on earth. Ayady and co workers produced a cellulose aerogel, starting form microcrystalline cellulose via solvent exchange and alcohol gelation technique with a λ of 24 $mW/m\,K$[84]. Seantier *et al.* synthesized a multi-scale aerogel with cellulose and nanocellulose fibres via freeze-drying with a final thermal conductivity of 24 $mW/m\,K$ and a density of 40 kg/m^3[85]. A good example of super insulator is found in the work of Kobayashi *et al.* where an ordered crystalline nanocellulose skeleton reaches λ values as low as 18 $mW/m\,K$[86]. Another example is reported by Wicklein et al.[87] where directional freezing and subsequent lyophilization lead to the production of a nanocellulose aerogel with a thermal conductivity of 15 $mW/m\,K$ (in the transversal direction). In addition, in this case, graphene oxide was also used to enhance the flame resistance of the nano-cellulose aerogel(Par. 2.5.3). As far as other polysaccharides are concerned, Horvat *et al.* [88] managed to produce a pectin alcohol induced aerogel with a thermal conductivity of 21 $mW/m\,K$ with a mesoporous pore size in the range of $17 - 19\,nm$. Other examples for alginate can be found in [81] and, in particular, in the work os Gurikov et a. where thermal conductivity of 18 $mW/m\,K$ have been reached with CO_2 induced ionotropic gelation followed by drying[89]. In a similar way, super insulation foam can be produced starting from starch [90] and chitosan[91]. Beside being more mechanically stable than silica aerogel and possessing the advantage of being naturally available, biocompatible and compostable, a strong limitation to the use of polysaccharides aerogel comes from their high hydrophilicity that negatively affects their thermal properties[81]. In addition, as a matter of fact, the production of super-insulating aerogel, with extremely low thermal conductivity and pore size, is not easy and not always feasible or scalable (due to the adoption of particular gelification and solvent extraction techninque, *e.g.* use of supercriticality drying technique), for this reason there is also a strong interest in producing and studying polysaccharides fibrous or foams TIMs which, beside not taking any advantage of the Knudsen effect, still posses a thermal conductivity values comparable to conventional insulating materials[81]. Examples of nano-cellulose fibrous insulation can be found in the work of Fan *et al.* where they obtained, by freeze casting-drying, a insulation foam with $\lambda = 39\,mW/m\,K$ showing a remarkable fire resistance behavior due to the *in-situ* precipitation of $Al(OH)_3$ [92]. With a different approach, slightly higher values of thermal conduc-

tivity, $43\,mW/m\,K$, where obtained by combination of cellulose (from pineapple leafs) with cotton waste fibres but, in this case, the authors manage to produce a full flexible material in a scalable process[93].

Alginate is a poly-anionic, high hydrophilic material which is capable to form strong, thermally stable hydrogel upon interaction with multivalent cations. In addition, it possess an inherent excellent fire resistance capabilities and has the potential to be a sustainable alternative to oil derived polymers[94]. Due to its biocompatibility, it is currently largely used in food and pharmaceutical applications[94]. Recently alginate has found application as thermal insulation material and different works have been already published in which it is used both as main constituent of a bio-based thermal insulator[95][96][67][88][97][98][99] and as natural binder[100][101][102][103][104]. Horvart *et al.* sensitized a hybrid foam with alginate and a silane (TMSO) as gelling agent followed by supercritical drying which possessed a thermal conductivity of 32 $mW/m\,K$ with enhanced thermal degradation resistance, tested with TGA[67]. In contrast, exploiting ionotropic gelation, Shang and co-workers manage to fabricate alginate foams with enhanced compression modulus and fire resistance (tested with cone calorimeter) and a thermal conductivity of 49 $mW/m\,K$. The gelling method, in particular, is comprised of a first freeze casting - freeze drying followed by a second crosslink via Ca^{2+} in ethanol solution[99]. With a completely different approach, Vincent *et al.*, in two recent works[96][95], produced an innovative alginate foam ionotropically cross-linked with Cu^{2+} and Ca^{2+} with thermal conductivity varying between 28 and 39 $mW/m\,K$. The addition of sodium lauryl sulfate as foaming agent led to the production of a stable foam capable to retain its macro-porous structure after air-drying, avoiding catastrophic pore collapse (under specific range of concentration of the ionic cross-linking and the release agent, *i.e.* glucono-δ-lactone). In the subsequent work, the fire resistance of the material was assessed (with cone calorimetry) and by comparison with flame retarded polyurethane, the produced alginate foam showed a better resistance to flame propagation and heat release without any addition of flame retardants additives.

1.3.4 Use of Alginate as Eco-Binders

The majority of TIMs described above, which are produced from industrial or natural waste or bi-products, use petroleum-based binders (*e.g.* polyester and polyurethane) which clash with the concept of *green* and *eco-sustainable* economy. For this reason much more attention was payed to the research of alternative ecological binders derived from minerals or plants: gypsum [105], geopolymers[106], PLA[79] or polysaccharides[107] such as starch[100], chitosan[104] and alginate[101][102][103][107][103][1] are just few examples. Mati-Baouche *et al.* studied the composition of a bio based binder, composed of chitosan and alginate for the production of a TIM made of sunflower stalks, thus obtaining a material with comparable compressive and tensile strength to that of other insulation materials already commercialized[107]. Similar studies were performed using only alginate, as main binder, for lignocellulosic materials [103], or alginate based mixtures for wood-fibres and textile waste composites[100]. In this last example, alginate was cross-linked with glyoxal and glutaraldehyde to improve final mechanical strength. Palumbo *et al.* took advantage of ionotropic gelation of alginate with Ca^{+2} to increase the mechanical strength of corn pith based TIMs, producing a material with good fire and mould resistance and a thermal conductivity of 38 $mW/m\,K$[101][102].

Recently, in our laboratories, Kyaw Oo D'Amore *et al.*[108][1] developed a new foamed material in which alginate was used as *highly-porous-binder* to produce a thermal-acoustical insulation material in which glass and fiber-glass waste can be recycled. The problem of fiber-glass waste is gaining higher and higher concerns all over the worldwide technical community, since clear and well established recycling route are not yet available in the market (principally due to the low cost of glass raw material) and landfill is still the current preferred end-of-life treatment[109][110][111]. The naval, aviation (ship and aircraft hull), electronic(printed board) and energetic (wind turbines blades) sector are among the bigger contributors to the fiber-glass[34] waste stream, with an estimated $10^9\,kg/year$ of wastes

[34]the term fiber-glass it is commonly referred to glass fibre reinforce polymers or resins. In the shipbuilding industry the most widely used fiber-glass composites are polyester reinforced resin and epoxy reinforced resins

generated in Europe coming only from turbine blades dismantling in 2030 [112]. In the presented work, Kyaw Oo D'Amore *et al.*, were able to produce open porous materialby freeze-drying a ionotropically gelled alginate matrix, without the aid of foaming agents, showing an averaged better acoustical performances whit respect to rock wool, and possessing a thermal insulating value of 45 $mW/m\,K$ [108][1].

1.3.5 What after ...

All the above-mentioned solutions for producing recycled TIMs can undoubtedly represent an extremely valuable and greener alternative to conventional end-of-life options for primary waste or by-products coming from the industrial or the agricultural sector. However, the aims of using a natural base material in place of a petroleum-based polymers, to limit the use of non renewable resources in the primarily feedstock, does not always couple with an overall reduction of waste. In a *linear economy* paradigm, little or no consideration is given to the treatment of the generated waste from goods production. As presented in the previous sections, a considerable large number of thermal insulator materials, made from agricultural and industrial waste, are already present in the market but, again, little or no attention has been paid into studying their end-of-life options (with some limited exception which are focused on their biodegradability[113][114][115]). Therefore, final landfill disposal or incineration seems to be again the only available end-of-life option. What's more, this reuse of "waste" comes often with a reduction of the quality or functionality of the original material. This approach is commonly referred to as *down-cycling*. On the other hand the key-point of the *circular economy* paradigm ***is*** the reduction of waste and this can be achieved only by taking in consideration, during the material design phase, a closed product-system where goods are produced to be eventually recycled by returning as feedstock in the main production-system.

Chapter 2

Flame Retardants (FR)

Due to their high carbon and hydrogen content, polymers are highly inflammable and actions, in order to improve their fire safety (of both polymeric artefacts and composites), have to be taken due to their widespread presence in everyday life. Published, for the first time, in 1974, by the National Fire Protection Association (NFPA), the Fire Safety Concepts Tree, outlined the two fundamental strategies to be adopted fo achieving a fire-safety environment by use of materials whose performance could be improved by the use of flame retardants: the first one focus on preventions mechanisms to minimize the likelihood of ignitions events, the second one involves the manage of the fire events. In particular in this part the main goal is to delay or avoid the flashover by controlling the heat, the smoke and the toxic and corrosive volatile released during gasification and combustion[116]. It worth mentioning that, in 2015, the global market for flame retardant was valued for 6.29 billion USD with a demand of flame retardants additives exceeding 2 mega tons (2 x 10^9 kg) per year and with the building and the electrical and electronic industry taking the lead of the market[117].

2.1 Polymers Combustion

Combustion is a catalytic exothermic reaction that takes place when combustible (reducing agents) and combustive (oxidizing agents) species are mixed and ignite

by the presence of heat. Combustion mechanisms vary enormously across polymeric materials due to differences on chemical composition, crystallinity, cross-link degree, molecular weight distribution and additives presence[45][59][118]. Furthermore, environment conditions should also be taken in consideration such as temperature and oxygen concentration[59]. Nevertheless, despite these differences a general description of a combustion pathway (or cycle, as it will described below) can be given [Fig. 2.1][119]:

1. The process usually starts with an increase of the polymer temperature. This can be caused by an external source (e.g. fire), by a proximal source (e.g. adjacent propagating flame) or even by an internal exothermic process (such as fermentation, in case of natural materials, or oxidation)[120]. However, in this initial stage the internal (*i.e.* in the condensed phase) thermal decomposition processes are mainly non-oxidative (radical and disproportionation chain splitting under pyrolysis[Fig. 2.2]) leading to the evolution of principally free radicals and combustible gases together with non-volatile carbonaceous residues (char)[59][118]. At this point, volatile products migrate above the surface (*i.e.* the gas phase) of the polymer and mix with the oxygen present in the air (combustive) to reach the lower flammability limits[121].

2. Flaming start upon ignition. This can occur by additional heat that can be provided by an external source (such as a spark, or a pre-existing flame) and in this case the temperature at which the ignition take place is called flash-ignition temperature[1]. At higher temperature auto ignition can also take place (*i.e.* without any additional source), the temperature at winch this occur is defined self-ignition temperature(SIT)[122]. [Tab. 2.1] reports some ignition and decomposition temperature reference value for common polymers.

3. At this point, to sustain the combustion, a complex mass and energy balance has to be present. The heat released by the combustion has to be sufficient to continuously sustain further polymer decomposition (i.e. thermal feed-

[1]this normally refers to tests conducted using clean air at atmospheric pressure as combustive mixture. See ASTM D1929-16[122] and ASTM E176-15a[123] for further information.

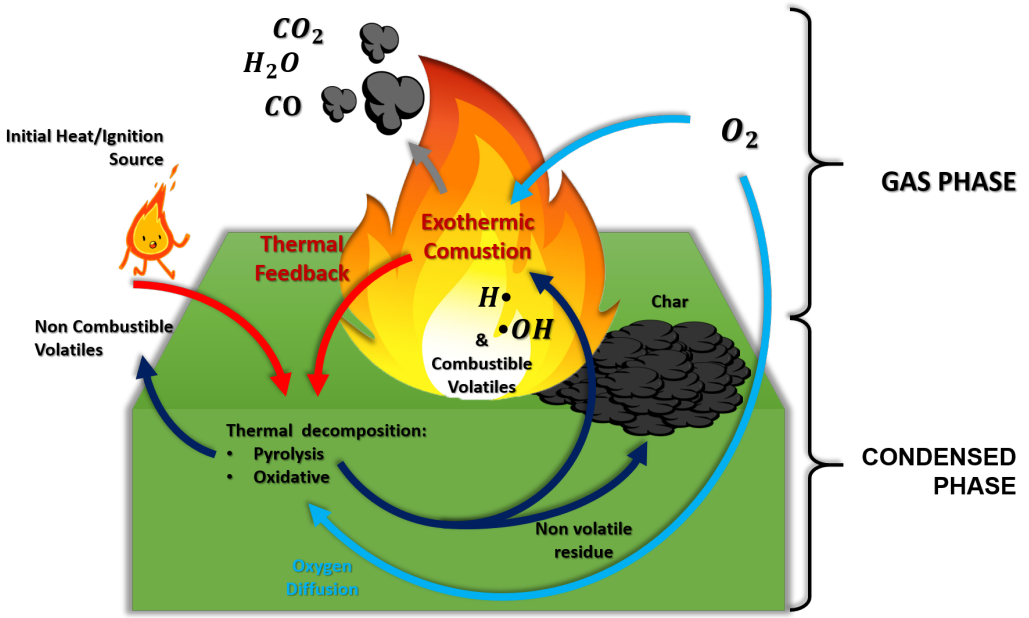

Figure 2.1: Combustion cycle schematic representation of processes involved in polymer combustion.

back) and the combustible species and free radical evolved have to diffuse toward the gas phase to maintain their concentration above the low flammability limit. In particular, the presence of highly reactive free radicals ($H^\bullet$ and $OH^\bullet$) maintain the combustion process by a cascade-chain mechanism by reacting oxygen with other reactive species(in particular carbon centered radicals $RO\cdot$ which result in a further increase of $R\cdot$)[116][120][124]. Polymer decomposition is further promoted by oxygen diffusion into the condensed phase, fuelling oxidative decomposition reactions that lead to evolution of low molecular weight products (e.g. alcohols, ketones, aldehydes)[124]. Flameless combustion reaction, referred to as smoldering, can also take place in the condensed phase if oxygen concentration is not sufficient. Unlike flame combustion, smouldering combustion is less efficient and releases a lower amount of heat[125]. If these condition are met, the combustion cycle is complete and flames start to propagate.

Another important factor that influence ignition is the oxygen concentration (in

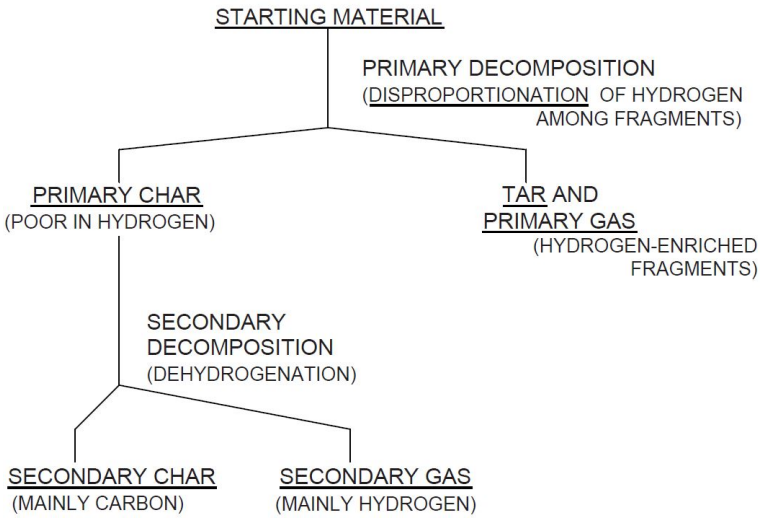

Figure 2.2: Basic mechanism of pyrolysis[126]

air): definitions such as the lower flammability limit (LFL) and the upper flammability limit (UFL), defined for vapours and gases, can be applied to the fuel/oxygen mixture in the gas phase but are not meaningful if the whole system is considered (since no vapor pressure for the flammable species evolved from the solid polymer specimen can be calculated); the Oxygen Index (OI) can be used instead[2]. OI is defined as the minimum concentration of oxygen that will support candle-like polymer combustion [128]: OI can be therefore be used as first estimator for polymer flammability[59]. As a mater of fact, during OI determination, different oxygen/nitrogen ratio mixtures are tested on a previously ignited sample and no additional heat is provided during the test. This kind of test, also defined as "small heat source tests"[3], is specifically designed to reproduce the initial condition of a fire event caused by a "bening" ignition source in order to rank different materials to reduce their risk of causing a major catastrophic fire[116]. Unfortunately, these tests do not provide any specific information about polymers performance in heavy fire condition or under continuous external heating exposure. Nevertheless,

[2]sometimes the Oxigen Index is also referred to as Limited Oxygen Index (LOI) in scientific literature with the same meaning. However, international standard organizations (such as ASTM [127] and ISO[128]) prefer the term OI for plastic materials testing.

[3]other examples can be found inside the UL-94 standards collection[129]

Table 2.1: Decomposition and ignition temperature of common polymers. If not specified data source from[59], expect for (a) that are from [120]

	Decomposition range [°C]	Flash ignition Temperature [°C]	Autoignition Temperature [°C]
LDPE	340-440	340	350
Polypropylene	330-410	350-370	390-410
Polystirene	300-400	345-360	490
PVC (rigid)	200-300	390	455
PMMA	170-300	300	450
Cellulose	280-380	210	400

industries extensively use these test to assess quality assurance of fire retardant treated products (e.g. in R&D) mainly due to their good -benefit ratio resulting from the high repeatability, sensibility to chemical composition and reduced costs. National and international safety codes and regulations (such as the EUROCLASS System[130] or the 2010 FTP code[131]) requires a better fire resistance products characterization and "small heat source tests" are therefore jointly used together with other bench-scale tests (e.g. heat release[4] and smoke production[5] tests) and full-scale fire test (e.g. room corner test[6]).

Another important test, which involves a more detailed scientific approach, is the cone calorimeter heat release test. Standardized by ASTM E1354 and ISO 5660, cone colorimetry (CC) allow the live measurement of multiple combustion parameters such as the heat release rate (HRR), the peak of heat release rate (pHRR), the time to ignition (TTI) and the total heat released (THR) from a sample subjected to a constant heat radiative flux. Moreover, if coupled with mass spectroscopy and optical sensors, information about density and toxicity of evolved gas are available in CC trough the specific extinction area calculation[45]. Thanks to its versatility, the CC test, since its development by the National Institute of Standard and Technologies (NIST) in 1982, gained popularity despite of an increased technical

[4]EN ISO 1716 - Gross calorific potential test

[5]ISO 5659-2 - Plastics - Smoke generation -Part 2: Determination of optical density by a single-chamber test

[6]ISO 9705-1: 2016 - Room corner test for wall and ceiling lining products

complexity. A scaled-down variation of CC is represented by the microscale combustion calorimetry (MCC)[7] which is particularly recommended for textile and thin products or were only small samples are available[119][132].

At this point it has been made clear that polymer combustion is a particularly complex system that can be schematically represented in [Fig. 2.1]. Across the multiple above mentioned tests, which only represent a relatively small part of those available, a relevant number of parameters such as dimension and geometry of the sample, ignition source, ventilations and heat flux are not fixed and represent a relevant source of results discordances. This prevents an easy correlations between different tests results also mainly because different materials, fire-retardant mechanisms(that will be discussed subsequently), simulated fire condition are examined and tested[45]. It is worth mentioning that, following these reasons, the ASTM introduced a mandatory disclaimer that has to be included in each fire test standards, highlighting that *"This test method measures and describes the response of materials, products, or assemblies to heat and flame under controlled conditions, but does not by itself incorporate all factors required for fire hazard or fire risk assessment of the materials, products, or assemblies under actual fire conditions"*.

2.2 Flame Retardant Strategies

In the previous paragraph the combustion cycle was introduced underling the fact that flame propagation is regulated by the presence of a stationary energy and mass balance. In the case of an exceeded production of heat and free radicals, combustion proceeds at an increasing rate until an explosion occurs, whereas, if the heat is not sufficient (e.g. caused by a reduction of the thermal feedback) or combustible species are unable to fuel the reactions the combustion rate becomes negative and, eventually, the fire is extinguished. Fire retardants strategies, obviously, are intended to interfere within the combustion cycle to overbalance the energy and mass transport phenomena towards the latter scenario. The term

[7] ASTM D7309 - Determining Flammability Characteristics of Plastics and Other Solid Materials Using Microscale Combustion Calorimetry

Fire (Flame) Retardant system is normally refereed to a chemical (or a group of chemicals) compound that is added to the polymer (as bulk additive or surface treatments) to reduce fire treats. A single FR system can act relying on a single or multiple flame retardant strategies, these can be divided in two categories according to their action mechanism [45][120][133]:

- **CHEMICAL**
  - **Gas Phase Reaction**
    Release of reactive chemicals in the gas phase able to react with free radicals to form less reactive or inert molecules[45], mainly scavenging H•and OH•. This mechanism reduces the reaction rate of the branching (*e.g.* $H^{\bullet} + O_2 \longrightarrow OH^{\bullet} + O^{\bullet}$) and the highly exothermic propagation steps (*e.g.* $OH^{\bullet} + CO \longrightarrow CO_2 + H^{\bullet}$) of the combustion reactions[124][134].
  - **Condensed Phase Reaction**
    Formation of a dense (char) or expanded (intumenscent) carbonaceus or vitreus layer by promoting solid products reactions during polymeric degradation (*e.g.* cyclization, aromatization, dross-linking dehydration). This layer act as barrier toward heat and volatiles diffusion.

  Depending on how they are incorporated into the polymeric matrix, chemical-active FR can be classified as additives and reactive. Reactive FR are usually introduced during polymeric synthesis (as monomers or precursors) or with a post-reaction process to become incorporated into the polymeric structure. Additives FR are generally incorporated during processing and do not react with the polymer during standard operating temperatures[120].

- **PHYSICAL**
  - **Gas Dilution**
    Release of inert gases/vapours species (e.g. H_2O, CO_2, NH_3, N_2) in the gas phase which dilute the oxygen, leading to a reduction of the combustion rate.
  - **Cooling**

Specific compounds endothermic decomposition reactions that act as heat sinks, cooling the reaction environment and therefore reducing the thermal feedback directed to the polymer.

– **Protective Layer Forming**
Formation of a protective surface layered structure by accumulation of non-volatile organic and inorganic residues. It limits the direct heat transfer to the polymer (heat shield), reducing the thermal feedback, and hinder the diffusion of reactive species from the condensed phase to the gas phase and of oxygen into the condensed phase[116].

Despite the fact that a general rule can not be defined and that the choice of the FR system is dependent on the considered polymer formulation, some considerations apply. FR systems that primarily act through physical mechanisms tend to be less system-dependent with respect to chemicals FR (in particular reactive FR and some particular intumescent system (Par. 2.4.2.1)[45]) since their mechanism of action involves fewer reactions with the polymers but as drawback their efficacy tend to be limited. Localizing the concentration of flame retardants where they are majorly needed, *i.e.* on the surface, can be a successful strategy to reduce FR use and the detrimental side effects that high FR loading have on materials properties. However, the use of FR coating encounters other challenges such as long-term stability, durability and compatible coating application technologies (to secure strong substrate adhesion)[119]. In addition, sometimes a FR system relies not only on a single mechanism and other problems, such as compatibility, dispersibility and aging effects of FR chemical within the polymeric matrix have to be addressed[59][45].

2.3 Consideration on polymer structure

Some general guidelines on polymers thermal stability and flammability from their chemical structures can be derived as well. In fact, even though thermal stability doesn't necessarily implies a better fire resistance, since flammability (particularly in flame combustion) is more associated with oxidation pathways of volatiles degradation products, some degradation pathways can hinder the complex combustion

process promoting, for example, the formation of char residues, reducing in this way the availability of volatile products in first instance[59](e.g. polysaccharides and oxidized polysaccharides[45]). These mechanisms, that can be further promoted by FR activity, lead towards an inherently flame resistant behavior in some polymers[116]. Effects of polymeric structure on thermal stability of polymers are summarized in [Tab. 2.2].

Polymers having a higher carbon to hydrogen ratio tend to be less susceptible to combustion, due to their reduced ability to generate volatile and flammable species[116]. On the contrary, the presence of a high hydrogen to carbon ratio and unsaturated bonds concentration tend to reduce the resistance of the polymeric chain to oxidative degradation[118]. These are, for example, some of the reasons for general high flammability of polyolefins[59]. Highly fluorinated polymers, on the other hand, are highly thermally stable and thanks the intrinsically low concentration of combustible species that evolves during their degradation, they generally show a high flame resistant behavior(*e.g.* PTFE posses a LOI 96). As a matter of fact, the presence of halogenated substitutes, typically, induces flame retardancy effects due to their activity in the gas phase (Par. 2.4.1). PVC is one of the best example and, although it possesses a limited thermal stability, it is considered as inherently flame-retardant (nevertheless for some specific applications incorporation of FR are still needed) [45]. High nitrogen presence has also been reported to reduce flammability, mainly due to gas dilution mechanism (*e.g.* in polyamides and amino resins)[45][116][135]. Both thermal stability and fire resistance are enhanced by the presence of aromatic or hetero-cyclic structure[126]) and by high cross-linking degree [116][59]. A high cross-linking degree reduces the volatilization of decomposition products, which is the reason why thermoset polymers exhibit, in general, a better flame retardancy than thermoplastics[59].

To conclude, the following considerations about polymeric degradation pathways and flame resistance can be done. Polymeric materials degrade via one of the following process (simplified)[118]:

Table 2.2: Factors which affect the thermal stability of polymers, $T_{50\%}$ is defined as the temperature at which a polymer has lost half of its initial weight in 30 min [116]

Polymer	Effect on thermal Stability	Examples	$T_{50\%}$ [°C]
Chain branching	Weakens	Polymethylene	415
		Polyethylene	406
		Polypropylene	387
		Polyisobutylene	348
Double bonds in polymer backbone	Weakens	Polypropylene	387
		Polyisoprene	323
Aromatic ring in polymer backbone	Strengthens	Polybenzyl	430
		Polystyrene	364
High molecular weight	Strengthens	PMMA	327
Cross-linking	Strengthens	Polydivinyl benzene	399
		Polystyrene	364
Oxygen in polymer backbone	Weakens	Polymethylene	415
		Polyethylene oxide	345
		Polyoxymethylene	<200

(**A**) **Chain scission**: chain scission starts by the cleavage of the weaker bond, this can occur randomly (i.e. in any position of the polymeric backbone) or at the end of the chain (i.e. unzipping).

(**B**) **Chain stripping**: cleavage of side groups (or atoms) attached to the main polymeric backbone.

(**C**) **Cross-linking**: new bonds creation (mainly via intra-chain chemical reaction) that lead to generation of a cross-linked network.

These processes can occurs simultaneously in the same system and their predominance is a function of: heating time, sample size and additives presence. Polymers that degrade mainly following the first mechanism (**A**) are more susceptible to combustion, due to the high volatiles combustible species that are produced and by the reduced formation of condensed products [45]. This is the case of polyethylene (PE), polystyrene (PS) and polyethylene-terephthalate (PET) and poly(methylmethacrylate) (PMMA)[135]. The second mechanism (**B**) is particular effective, in enhancing its flame retardancy, in PVC where HCl is liberated. In addition, with the leaving of pendants groups, cyclicization, condensation and recombinations reactions are favored, ultimately leading to an increased production of char due to the presence of reactive conjugated bounds[118][59]. Following, the latter mechanism (**C**), for what was explained before about cross-linked structure, could induce a flame resistance behavior. As a matter of fact, some aliphatic polyamides (*e.g.* PA 6.6), polyacrilonitriles and phenoilic resins take advantage of this mechanism[116]. Other examples are reported in [Tab. 2.3] and in [136].

Table 2.3: Typical Decomposition Products for Each Generalized Mechanism of Polymer Decomposition [116]

Mechanism	Examples of Polymer	Typical Products
Random chain scission	Polyethylene	Alkanes, alkenes, very little monomer
	Polypropylene	Alkanes, alkenes, very little monomer
	Polystyrene	Styrene monomer, dimer, and trimer
	Generally	*Monomers and oligomers*
End-chain scission	Polymethylmethacrylate	90%–100% monomer
	Polytetrafluoroethylene	90%–100% monomer
	Generally	*Monomer*
Chain stripping	Poly (vinyl chloride)	Hydrogen chloride, aromatic hydrocarbons, and ***char***
	Polyvinyl alcohol	Water and ***char***
	Generally	*Small molecules and* ***char***
Cross-linking	Polyacrylonitrile	***Char*** (and HCN), ***High char content***, *few volatile products*
	Generally	

As largely highlighted, the above mentioned considerations are not to be considered as strict rules from which flame behavior of polymers can be accurately inferred, not to mention the fact that pure polymers rarely have any technological application and additives are almost always used, having thus a huge impact on flame resistance. Polyurethanes (PU) behavior represent, for example, a model case: flammability of PU is expected to be low due to the high nitrogen content and high cross-link degree, however it finds the majority of its applications as flexible or rigid foams[59]. Due to the increased active surface, in contact with oxygenated environment, in practice the fire performance of PU materials is poor and extensive use of FR is needed.

2.4 Conventional Flame Retardants

Flame retardants active species can be firstly classified in halogenated and non-halogenated (due to the high effectiveness of the first). Among the non-halogenated FR, phosphorous and nitrogen based, together with the inorganic FR, compose the main FR families.

2.4.1 Halogenated FR (HFR)

Experimental works and long industrial experience in FR technology highlighted that among the thousand reactions that can take place during combustion, burning velocity is most sensitive to those that involve $OH^{\bullet}$, $R^{\bullet}$, $H^{\bullet}$ and $O^{\bullet}$ [45]. Halogenated FR act, therefore, by interfering within the combustion cycle by free-radical scavenging effect in the gas phase with the following mechanism:

$$MX \longrightarrow R^{\bullet} + X^{\bullet} \tag{2.1}$$

$$X^{\bullet} + RH \longrightarrow R^{\bullet} + HX \tag{2.2}$$

$$HX + H^{\bullet} \longrightarrow H_2 + X^{\bullet} \tag{2.3}$$

$$HX + OH^{\bullet} \longrightarrow H_2O + X^{\bullet} \tag{2.4}$$

where MX is the flame retardant molecule, RH is the polymer/fuel and $X^{\bullet}$ is the halogen. Chlorine and bromine containing molecules are the most suitable whereas fluorine and iodine do not act in an effective way as FR. High stability of fluorine derivates and high reactivity of $F^{\bullet}$ limit both (Eq. 2.1) and radical quenching effect of (Eq. 2.3) and (Eq. 2.4). As far as iodine compounds are concerned, their exclusion derives from the low stability of iodine bond which makes them less thermally stable than commercial polymers: release of iodium could therefore occur during polymer processing [45][118]. Following (Eq. 2.2) it is clear that hydrogen halide, the real FR molecules, is reformed after quenching of $OH^{\bullet}$ and $H^{\bullet}$The permanence of the hydrogen halide molecules in the gas phase originates a secondary FR physical effect: the dilution of combustible gas concentration [59]. Hydrogen halide can also catalyse the oxidation of the solid phase, promoting in this way cyclization and char forming pathways, however this is dependent

on the FR-polymer system[118]. Reactive halogenated FR posses further advantages, such as the increased compatibility between the FR and the polymer (since they are directly incorporated into the polymeric structure) reducing migration and segregation phenomena. However, an additional synthesis step is needed and it is not always remunerative on the industrial scale[118][120][137]. Halogenated FR also show a synergistic effect with other compounds firstly antimony-based, with antimony trioxide (Sb_2O_3) being the most widely used. The main synergistic effect comes from the reaction of Sb_2O_3 with hydrogen halides to form both antimony halides and oxyhalides in a cascade-chain reactions that were proven to be much more effective as scavengers in the gas phase with respect to halogens and antimony alone[116][118]. Mixes of brominated and chlorinated FR, as well as brominated and phosporous FR systems are reported to produce synergistic FR effects[45]. Halogenated FR were among the first FR systems extensively introduced with the growth of the polymeric industry (and the consequent rise of fire hazards) in the first part of the 20^{th} century. They owe their own success to their high efficacy and to their reduced dependency to the polymeric system (regarding the gas phase mechanism)[45]. A typical load between 5-20% (further reduced for bromine-FR) is typically needed. Unfortunately, serious concerns about their toxicity rapidly forced the authorities to place restrictions on their use[8]. As a matter of fact, hydrogen and metal halides, which evolves during combustion, are toxic and corrosive. In addition toxic compounds can also be dispersed as a results of leaching phenomena, posing a serious threat during handling. Many halogen-FRs, such as Hexabromocyclododecane (HBCD)[9][45], have been proved to be environmentally persistent and toxic (with adverse effect toward the immune system with bioaccumulation tendency)[116]. Another major concern related to the use of halogen-FRs is linked to the evolution of dioxins over combustion (and in some cases, it occurs even during polymers thermal processing)[45]. Following these considerations the current use of halogen-FR is in decline despite of, at the end, only some specific molecules have been specifically banned but the research on alternative halogen-free FR system is strongly encouraged by regulators. Despite

[8] In the European Union legislation the following directives can be found: RoHS (Restriction of Hazardous substances), REACH (Regulation on Registration, Evaluation, Authorization and Restriction of Chemicals) and the WEEE (Waste Electric and Electronical Equipment)

[9] widely used in EPS and XPS thermal insulation panels

their reduced popularity, it is worth mentioning that, HFRs still shared for more than 40% of the global FR market (by sales) in 2015[117]. This is mainly caused by the fact that their use is still widespread in PS and PU foams, ABS and in many polyolefine-based systems since, for these polymers, the use of reliable full non-halogenated systems is not yet consolidated in the industry[138].

2.4.2 Phosphorous based FR (PFR)

Phosphorous based flame retardants compounds compose one of the fastest growing segments in flame retardants chemicals. This is due their limited environmental impact and their wide range of applications. PFRs can act whether in the condensed phase or in the vapour phase (or simultaneously) but the prevalence, or the suppression, of one mechanism with respect to the other, highly depend on the specific FR system: chemical structure of the polymer and of the PFR compound and fire exposure conditions[45][139]. Gas phase activity is based on the volatilization of reactive phosphorous radicals, such as PO$^{\bullet}$ and HPO$^{\bullet}$, that act as scavenger in analogy with the mechanism discussed for HFR. However, PFR are mainly used due to their condensed phase mechanisms: by participating in decomposition reactions PFR are capable to promote the formation of a char or intumescent layer[139][116].

Red phosphorous, which is a tetrahedral phosphorous polymerized form, is commonly used as FR additive, mainly in polyesters and polyamides[116]. When compounded in nitrogen or oxygen containing polymers, it decomposes at high temperature by producing both phosphoric acids and anhydrides, which eventually reacts into polyphosphoric acid[120]. Phosphoric and poly-phosphoric acid tend to promote char-forming reactions which eventually leading to an increase in char yield during polymer combustion, mainly through dehydratation, cyclicization and transesterification reactions[120][116][45][139]. Red phosphorous is also known to have some limited FR effect on polyolefins (which do not decompose producing char) mainly through the gas phase mechanism [120]. Some limitations to the widespread use of red-phosphorous comes from its relative high flammability risk, when it is present in high concentrated powered form (*e.g.* during polymer compounding) which implies the adoption of safety measure for its han-

dling, (*e.g.* inert gas blaket)[45], and from the evolution, in limited amounts, of toxic phosphine gas (PH_3) upon decomposition[120]. The addition of metallic salts can help to reduce this phenomenon, in addition, their combination in the condensed phase with phosphoric acid can lead to the formation of a protective glassy layer[116].

Another important family of inorganic PFR is composed by Phosphate (or polyphosphates) salts such as ammonium polyphosphate (IPP, $[NH_4 \cdot PO_3]_n$) or melamine polyphosphate: these salts represents a readily available form of phosphoric acids whose thermal degradation temperature (and therefore activity) can be easily tuned, by changing the chain length and branching, to match those of the polymer matrix [120]. Upon decomposition they can also release active molecules (such as melamine) or directly ammonia (in the case of API) which primarily both act by gas diluting mechanism [59][45]. They are mainly used in intumescent FR systems (Par. 2.4.2.1).

Several others PFRs are commercialized: organophosphorous (*e.g.* phosphate and phosphonate) constitute the largest family and, depending on the application, they can be both be used as reactive or additive compounds. For example, a reactive PFR approach is commonly used for PET, PU and Epoxy whereas in PS, ABS and PC additives are usually preferred. As stated above, the main action mechanism of PFRs depends on the FR-polymer interaction: Pawlowski *et al.*[140], reporting the use of different organic PFR on carbon fibre reinforced epoxy resins (EP-CF), highlighted that gas phase mechanism (*i.e.* release of radical scavengers) is stronger in less oxidative phosphate compounds (*e.g.* phosphine oxide) and decrease with the oxidation state (phosphates). Other examples include the use of PFRs in PET, which mainly acts in the gas phase (despite a condensed phase action is still present[116]), whereas in polyamides the condensed phase mechanism is predominant. It is worth to cite that some PFRs systems are also capable to act in the condensed phase in PMMA, by changing the decomposition pathways thus leading to char formation (which normally does not occur in PMMA, mainly degrading through chain unzipping[59])[116][120]. In particular, char forming in PMMA seems to be enhanced with the use of reactive PFR (such as diethyl(methacryloyloxy) methyl phosphonate, DEMMP[141]). Other examples of PFR system are

ICL Fyrol 6 (Diethyl bis(hydroxyethyl) aminomethyl phosphonate) and Levagard® 4090 N (N,N-bis-(2-hydroxylethyl) aminomethane phosphonic acid diethyl ester) which are reactive compounds used in rigid PU and PIR foams[45]. What that can be generally inferred by the literature, is that PFRs mainly act in the gas phase with polymers possessing low charring capabilities whereas the presence of hetero-structure (and in particular the presence of $-$OH and O and N bonds) tends to "induce" the char forming mechanism of PFR[139]. The increased probability of new bond formations with the presence of P$-$N bonds, due to their higher reactivity, is commonly referred to as a the between phospshorous and nitrogen synergic effect[120].
Poly(phospahzenes) and ciclic-poly(phospahzenes) are another class of organic PFRs, in which phosphorous atoms are convalently bonded nitrogen by a double bond ($-\left[\mathrm{RR'-P=N}\right]_n-$) in which $-$R and $-$R$'$ can be hydroxyl, amino, epoxy or unsaturated carbon groups. These groups ease the way to their use as reactive FR in numerous polymer, such as PU, polyester[142][137]. In conclusion, despite of PFR have been proved to be versatile (by tailoring organic-inorganic content, phosphorous content and oxidation state), their use is highly system dependent: in order to maximize the FR capabilities PFR structure has to be individually formulated for each polymer composition[45][137][119]. In addition, their cost is higher with respect to their halogenated counterpart and other FR systems[116].

2.4.2.1 Intumescent system

Intumescent systems have been initially developed to protect fabrics and wood but they are now widely used in rubber,plastic and as protective paints in steel structures in building and ships as well[45]. The term intumescence refers to the formation, upon heating, of a stable expanded char layer that acts as physical barrier toward heat transfer and volatile diffusion. The formation of a stable barrier also reduce smoke production during fire, which is a great advantage with respect to halogenated FRs which lead to a dense smoke production instead[45]. Intumescent systems are generally composed by three elements[59][120]:

- Acid source: promote char forming reaction, mainly by dehydration of the carbonizing agent

- Carbonizing agent: a polymer/compound that upon heating decompose, assisted by the acid source, by char forming reaction. In char forming polymers, the polymer itself, that has to be flame retarded, acts as carbon source. Otherwise, external carbonizing agent are used. In the latter case mainly branched polyols (*e.g.* pentaerythritol) and carbohydrates(*e.g.* mannitol), in a lesser extent, are used[120][116].
- Blowing agent: a compound that upon heating release non combustible volatile (*e.g.* NH_3) during charring reactions of the carbonizing agent that lead to the expansion of the char layer

It is clear that intumescent behavior is not an exclusive prerogative of phosphorous based systems. [Tab. 2.4] reports different chemicals that can be used in intumescence system. API is one of the main chemical bases for intumescent systems, together with melamine phosphates which add the advantages of melamine based systems (Par. 2.4.3). Inorganic based intumescent systems are also available in the market such as those based on borates and alkali silicates. Alkali silicate are capable of formimg an inorganic char, whereas the foaming step is provided by the water entrapped in the hydrated structures which is released as vapour[116]. Zinc borates ($n\mathrm{ZnO} \cdot m\mathrm{B_2O_3} \cdot x\mathrm{H_2O}$), on the other hand, are capable of promoting charring reactions thought boric acid release (that acts as catalyst in nitrogen or oxygen containing polymers)[120][45], at the same time oric acid is also capable to form a stable glass layers by oxidation into boric oxide (a low melting glass). As a matter of fact, for example, ammonium pentaborate ($(\mathrm{NH_4})_2 \cdot 5\mathrm{B_2O_3} \cdot 8\mathrm{H_2O}$) is an effective intumescent system that can act both as a blowing agent, due to water and ammonia release, and as glass forming agent due to the conversion into boric oxide in intumescent paint formulations[116]

Table 2.4: Composition examples of Intumescent systems, from [116]

Acid source	Carbonizing agent	Blowing agents
Inorganic acid source	Starch	Urea
Phosphoric	Dextrins	Urea-formaldehyde resins
Sulphuric	Sorbitol, mannitol	Dicyandiamide
Boric	Pentaerythritol (monomer, dimer, trimer)	Melamine
	Phenol-formaldehyde resins	
	Methylol melamine	
Ammonium salts	char former polymers: (PA-6, PA-6/clay nanocomposite PU, PC, . . .)	
Phosphates, polyphosphates		
Borates, polyborates		
Sulfates		
Halides		
Phosphates of amine or amide		
Products of reaction of urea or guanidyl urea with phosphoric acids		
Melamine phosphate		
Product of reaction of ammonia with P2O5		
Organophosphorus compounds		
Tricresyl phosphate		
Alkyl phosphate		
Haloalkyl phosphate		

2.4.3 Nitrogen based FR

Nitrogen based FR are mainly used in synergism with phopshorous-FR and in intumescent systems. However, some compounds are effective as "*stand-alone*" FR, such as melamine (and derivates) or Alkoxyamines. Nitrogen based flame retardant are capable of releasing inert gases (such as NH_3) during decomposition and are therefore used as blowing agents in intumescent systems. Melamine is a typical example but also amine or amides are used[138][116].
Melamine primarily acts through endothermic decomposition and release of ammonia (upon decomposition) leading to the formation of higher molecular weight products: melam ($\sim$ 330 $°C$), melem ($\sim$ 390 $°C$) and melon($\sim$ 550 $°C$) [Fig. 2.3][143][144][145]. These products remain into the condensed phase contributing to char formation[120]. Melamine alone is slightly soluble in water but it can be dispersed in polyols and polyurethanes in which melamine (and melamine based) FR systems found extensive application (20-30$\%_{wt}$ is normally required)[145]. Melamine sublimation ($\sim 200-300$ $°C$) competes with the above mentioned mechanism: in fact, despite being an endothermic reaction, its energy demand is lower ($\sim$ 25 kcal/mole vs $\sim$ 450 kcal/mole). Nevertheless, melamine presence in the vapour phase also contribute to gas dilution. Melamine sublimation also limits its application to polymers that can be processed below its sublimation temperature (*e.g.* therefore excluding PP, PA or PEs)[120]. In order to reduce sublimation melam can be used instead or melamine can be directly attached to the polymer (*i.e* used as reactive FR) or it can be used in form of one of its salts. Melamine salts generally posse an higher thermal stability and can also add new FR mechanism such as for melamine-polyphosphates (MPP) and melamine cyanurate (MC). MPP is stable up to 350 °C, temperature at which endothermically decompose releasing phosphoric acid and melamine. MPP is therefore used as common base for intumescent system. Melamine cyanurate, on the other hand, is particularly effective on polyamides in which, upon decomposition at 300 °C, it drastically reduces the polymeric melt viscosity: polymeric droplets then drip away without flaming (thanks to the gas diluting effect). A 7$\%_{wt}$ of loads is commonly sufficient in PA. However, this mechanism is highly specific and is effective only in PA[145]. Endothermic decomposition and gas diluting effect remain the predominant FR

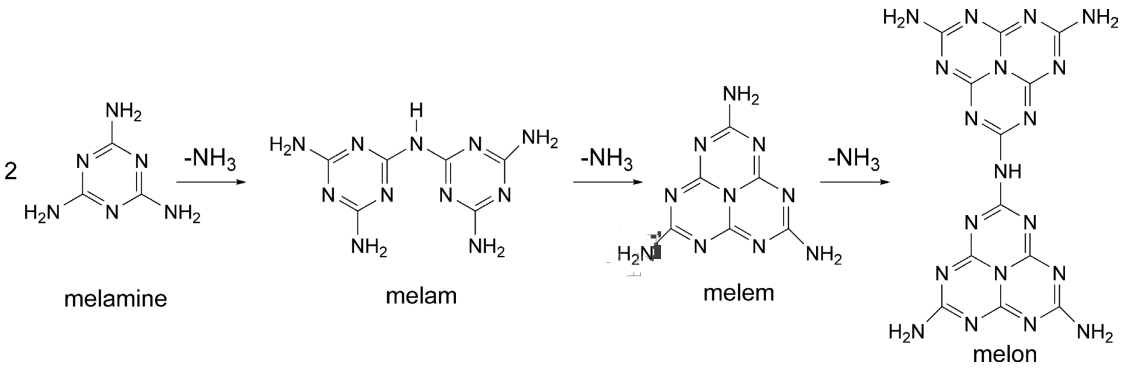

Figure 2.3: thermal decomposition of melamine[120]

mechanism of melamine systems. As anticipated, amine are also used due to their capability of releasing non combustible gas upon combustion: ethylenediamine, for example is used in combination with phosphate (Ethylenediamine Phosphate, EDPA), with its trade name Amgard® EDAP, in epoxy resins and polyurethanes foams[138][146] whereas polyethylenimine has been used as charbonizing and blowing agent in Ramie fabrics [147] and polypropylene[148].

2.4.4 Minerals filler and other Inorganic FRs

Minerals FR represent the main group of FR fillers. Metal hydroxides (alluminum and magnesium principally), carbonates and hydroxycarbonates compose the majority of mineral filler FR family with aluminium hydroxide ($Al(OH)_3$, ATH[10]) alone that dominate accounting for more than 80% (by tonnage) of mineral FR market[45] which, overall, accounts for more than 45% of global FR sales (by tonnage)[116]. Their extensive use is derived by their low cost, non-toxicity (during handling, compounding, combustion and disposal) and their efficacy as smoke suppressors. However, as principal drawback, a higher load of mineral FR is needed in order to effectively meet flame retardancy standards: typical loads lay between 20-50 $\%_{wt}$ but with peaks exceeding $70\%_{wt}$ for some specific applications[45]. Such a high filler loads generally have a detrimental effect on mechanical properties of the

[10]aluminium hydroxide, when used as fire retardant, is commonly referred to as alumina trihydrate(ATH) and formulated, sometimes, as Al2O3·3H_2O, even though it is neither an alumina, nor a hydrate [133]

treated polymer, making then unsuitable for some specific applications. Use of FR surface coating (with organosilanes or hydrocarbons) or size and shape tuning can limit these adverse effects by improving FR dispersion and adhesion to the polymeric matrix, therefore reducing the loading content needed[45]. Metal hydroxides, such as ATH and magnesium hydroxide (MH) decompose endothermically subtracting heat from the reaction environment and releasing water which further cools and dilute the vapour phase. The inorganic residue of hydroxides decomposition contributes to build an inorganic char layer in char forming polymer[45]. The decomposition temperature of ATH ($\approx$ 300 $^{\circ}C$) and MH ($\approx$ 400 $^{\circ}C$) limits their use to polymer whose process temperature do not exceed respectively 200 $^{\circ}C$ and 300 $^{\circ}C$: PE, particular formulation of PP, rubbers (*e.g.* styrene–butadiene based), EVA composites, epoxy and phenolic resins[116]. Another limitation comes form the release of water in the condensed phase, that can induce hydrolysis of the polymeric chain. This limits the use of mineral hydrate FR (in particular MH) in sensible polymers such as polyamides (in particular PA 6 and PA 6.6) and polyester[45][116].

Carbonates and hydroxycarbonates act in a similar way to hydroxides but possess an higher decomposition temperature, in addition, by releasing CO_2 they can further dilute the vapour phase.Example of these compouds are hydromagnesite $4\,MgCO_3 \cdot Mg(OH)_2 \cdot 4\,H_2O$ or $5\,MgO \cdot 4\,CO_2 \cdot 5\,H_2O$. Several synergic effect are reported in literature from the combination of hydrates fillers with other FR. Examples of these synergistic effects are the use of ATH and MH with red phosphorous, which limits the release of toxic phospine, or with silicones (*e.g* organosilicones) in which in a variety of polymers, included polyolefins, a reduced amount of additives is needed to produce a FR effect[120]. The same synergic effect, in polyolefines, has been observed with the addition of metal nitrates or oxide together with hydrates[116].
Boron FRs represent another class of inorganic fillers but, contrary to those mentioned above, a reduced loading is generally needed. Zinc and calcium borates, borax and boric oxides are the mostly used with the first having the highest commercial importance (with the trade name of Firebrake®)[116]. Borax ($Na_2O \cdot n_2B_2O_3 \cdot mH_2O$) is mainly used for treating woods and polysaccharides and is active thanks to its

endothermic decomposition and char promoting capabilities when boric acid is present (beside that boric acid is a weaker acid than phosphoric). Boric acid ($B(OH)_3$) is also an effective anti smoldering combustion agents. Boron oxide B_2O_3, on the other hand, being a low melting glass (450 °C), is capable to form an insulating inorganic glassy layer wich also help to stabilize the char, this has been proved to be effective in PEE and HIPS based system[116]. This effect is improved in zinc borates (*e.g* $2\,Zn \cdot 3\,B_2O_3 \cdot 3.5\,H_2O$) which can form an eutectic with metal oxides/hydroxides [116][149]. Zinc borates are also capable of acting in synergism with halogenated systems(*e.g.* PVC or particular HFR) as char promoters and, in contrast with antimony synergism, zinc borates also act as smoke suppressants[45].
Silica gel, dispersed into polymeric matrix, has also been evaluated as FR. In particular, tests performed on various type of silica (gel,fumed and fused), with different densities and porosity, have shown that the lower the density and higher is the surface area the better the FR activity, with a significant reduction of the HRR both in char (*e.g.* PE-oxyde) and non-char (*e.g.* PP) forming polymers[150]. Another study, conducted on PMMA, highligthed that this FR mechanism is highly influenced by polymer melt rheology since it relies on the formation of a protective, non combustible, thermal insulating layer derived by the accumulation, on the surface, of silica particles[151]

2.4.5 Organo-Silicon Based FR

Silicon based materials (silicones, silicas, organosilanes, silsesquioxanes and silicates) have been explored as FR thanks to their high thermal resistance, reactive chemistry and due to the fact that upon thermal degradation they tend to be transformed into an inert and non-volatile residue[45][138]. One of the mechanism of action of organosilanes is the char promoting effect observed, for example, in PC with branched-structure methyl phenyl-silicone[138]. However, this cross-linking mechanism, that promotes the formation of a silicon-carbonaceous char, is highly system dependent and has been proved to be effective principally in aromatic thermoplastics (in particular PC, PS and ABS) with phenyl and methyl substituents in organosilanes backbones[45][120]. The main FR mechanism of organosilane (silox-

anes and silanes) remains their capability of accumulating, on the burning surface, and decomposing in non volatile residue, building up an inorganic protective layer and/or stabilizing the carbonaceous char. In addition, organosilane and other silicon derivates, produce silica upon decomposition thus increasing the oxidation stability of the char and improving the thermal shielding effect due to the reduced thermal conductivity[120][45]. The production of a compact and continuous inorganic layer highly depends on the capability of organosilanes to migrate to the surface, their initial dispersion into the polymeric matrix and on their specific chemistry that dictate the decomposition pathway[45]. Organosilanes FR offer a promising alternative to halogenated flame retardants, however their production and functionalization cost is still high[138].

2.5 Nano Flame Retardants (nFR)

Introduction of nanotechnology in the world of flame retardancy was firstly brought by Gilman *et al.*, researcher at the NIST[152], as an extension of a research finally published by Toyota in 1993 on mechanical properties of nylon 6/nano-clay[153]. Nanometric particles are currently used in a variety of applications, in polymer technology, to enhance materials properties such as rheological, mechanical, thermal, electrical, gaseous barrier and fire resistance[154][116]. The extremely high specific surface area, net of specific nanoparticle properties, incredibly increases the interface between the nanoparticles and the polymer, commonly allowing a reduction of $\%_{wt}$ loading with respect to conventional fillers for the same application. Nanostructured FR represent a relatively novel group of FR materials that attracted numerous interests. This is, indeed, mainly due to their potential capacity to contribute to the simultaneous enhancement of multiple properties such as mechanical, thermal and flame resistance[120]. This section, which is far from being exhaustive, will analyse the contribution to flame retardancy of some restricted, but important, classes of Nano-FR which are: nanoclays ,nanohydroxides and graphene based. Others nano FR systems are based on silsesquioxanes (POSS), metal oxides nanoparticle, carbon nanotubes (MWCNTs) [120].

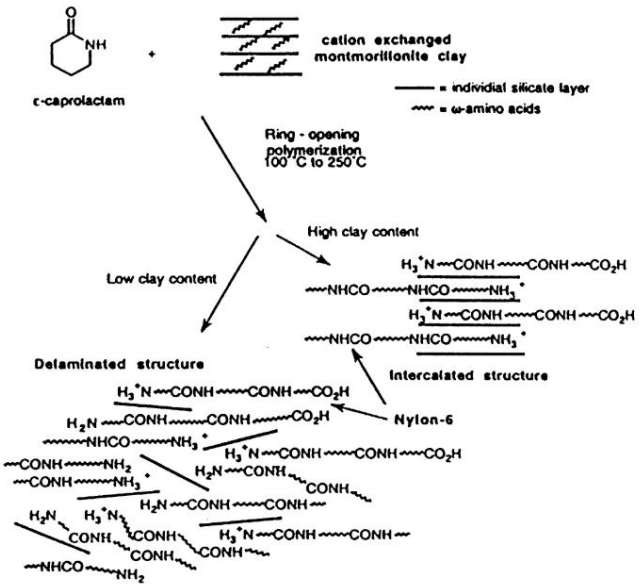

Figure 2.4: Original description on nylon6/nanoclay structure in the first published observation of nanoclay used as flame retardant[152]

2.5.1 Nano-Clays

Nanoclays are natural silicates that possess an ordered layered structure of tetrahedral $SiO_4{}^{4-}$ coupled with an octahedral sheet of $Al_3{}^{+}$ or $Mg_2{}^{+}$. One of the most commonly used nano-clay is Montmorillonite (MMT): a 2:1 phyllosilicate in which the Si tetrahedral sheet is sandwiched between two octahedral layers in which $Al_3{}^{+}$ and $Mg_2{}^{+}$ are present, the non stoichiometric ratio between $Mg_2{}^{+}$ and $Al_3{}^{+}$ leads to a net negative charge of the single nano-clay layer that is counterbalanced by cations in the interlayer. MMt can be easily hydrate due to its hydrophilicity and each layer has a thickness of $0.96\,nm$ and a lateral size of $\approx 400\,nm$. Its repeating unit is $(Na, Ca)_{0.3}(Al, Mg)_2Si_4O_{10}(OH)_2 \cdot (H2O)$. Intercalation with organic charged molecules(*e.g.* alkylammonium or alkyl phosphonium), between the nano-clay layer, or covalent functionalization (*e.g.* alkylamines) is possible, to enhance polymer compatibility. These modified nanoclays are commonly referred to as organoclay or organonano-clay. However, some organo-modified silicates tend to decompose at low temperature, which can limits their use or requires strict controls during processing (*e.g.* polymer compounding and extrusion)[45]. A better

compatibility between the polymer and the nano-clay also improves polymer intercalation between the layers leading to intercalated nanocomposite or, if the layers are completely separated, to exfoliated nanocomposites [Fig. 2.4][116][45]. In the pioneering work of Gilman *et al.*, it is described how the addition of only a small amount of nano-clay (2 - 5 $\%_{wt}$) leads to a drastic reduction of the pHRR without the normal drawbacks of high flame retardant loading on mechanical properties and acting as a physical barrier against volatile out-gassing[152]. After their discovered FR use, nano-clay (or organonano-clay) have been extensively studied and are currently commonly used a FR systems for ethylene-vinyl acetate (EVA) but also, and not only, for acrylonitrile-butadiene-styrene (ABS), polyethylene (PE) and polypropylene (PP)[45]. The typical FR mechanism of nano-clay is physical: thanks to their high aspect ratio, they are able to produce, by migration (in thermoplastics) or accumulation (in thermosettings), a protective layer on the surface that limit the oxygen/volatile inter-diffusion reducing in this case the HRR and the pHRR but without a strong reduction of the THR (total heat released). Furthermore, the interlocking of polymeric chain between the nano-clay layers tends to enhance their thermal stability and the formation of carbon char structure, even in non-charring polymers if organonano-clay are used[155][156]. Organo- modification, and in particular for organo-MMT (oMTT), leads upon thermal decomposition of the alkyl graft to the presence of Brønsted acidic sites on MMT surface, which catalyze thermal decomposition pathways that lead to formation of char [155][120]. Typical loading of nano-clay (MMT) is 5$\%_{wt}$. In all the applications, however, a good grade of nano-clay dispersion and the formation of a intercalated or exfoliated structure is fundamental[116][45][120]. Nanoclays have also been used in polysaccharides materials to enhance fire resistance: in the work of Shang *et al.* (previously cited in (Par. 1.3.3) different nano size FR, such as ATH, LDH (Par. 2.5.2) and MMT, were tested as filler in alginate foam, with a loading of 50$\%_{wt}$. None of the prepared samples, with the addition of FR, ignited under CC test and only flameless combustion appears with reduced HRR and pHRR. In addition, great improvement of mechanical properties (*i.e.* compression modulus) was also reported[99]. Example of MMT used in cellulose are also reported in literature; both as a coating [157] and as bulk filler[158].

2.5.2 Nano Hydroxides

Some studies reported the effect of nano-sized Aluminium hydroxides (ATH) and magnesium hydroxides (MH). As previously stated for the use of nano-clay two major benefits arise form reducing the size of the FR filler to nano scale: a reduction of the minimum FR loading and a general increase of the mechanical properties, with respect to the neat polymer. In a work where the effects of MH powders of different grain size (form $2.5\mu m$ to $100nm$) were compared in EPDM elastomer, the lower HRR and greater time of ignition were achieved with the use of nano MH, accompanied with an increase in mechanical properties and a reduced tendency of melt dripping during LOI test (although LOI index was unchanged[159]). Similar results were obtained in two others works were nano-MH[160] and nano-Boehmite[11][165] were successfully tested respectively in polypropylene and poly(butylene succinate) (PBS) with a reduction of flame propagation with a load of just $12\%_{wt}$ and $2\%_{wt}$. It is worth also mentioning another publication, of Silva and co workers [166] were nano-ATH was used to reduce flame spreading of linear low density polyethylene (LLDPE), tested through UL94 horizontal and vertical burning test with promising results. In particular, in this last publication, nano-ATH crystals were obtained from recycling of aluminium anodization industrial wastes. Nano-boehmite wa also used to enhance flame resistance of nano-cellulose: Fan *et al.* used an *in-situ* nucleation of boehmite nanoparticle in cellulose aerogel via hydrothermal reaction to finally produce a cellulose foam through freeze-drying[92]. Others examples of the use of nano MH and ATH in EVA, PVC and epoxy nanocomposite can be found in [Ch. 9 of [45]].

Another class of nano-hydroxide FR is represented by layered double hydroxides (LDH) which are anionic clays formed by hydroxides layer: LDHs have the huge potential to combine together the layered FR mechanism of nano-clays (*i.e.* continuous inorganic layer builder) with the endothermic decomposition of hydroxides, which is extremely effective into delaying the ignition time due to their multiple decomposition temperatures and water release from the interlayer, thus acting both

[11] Boehmite is an aluminium polymorph oxide-hydroxide (AOH), $\gamma - AlOOH$, that can originate from the thermal decomposition of ATH[161], and that find application as FR due to its endothermic decomposition in Al_2O_3[162][163][164]

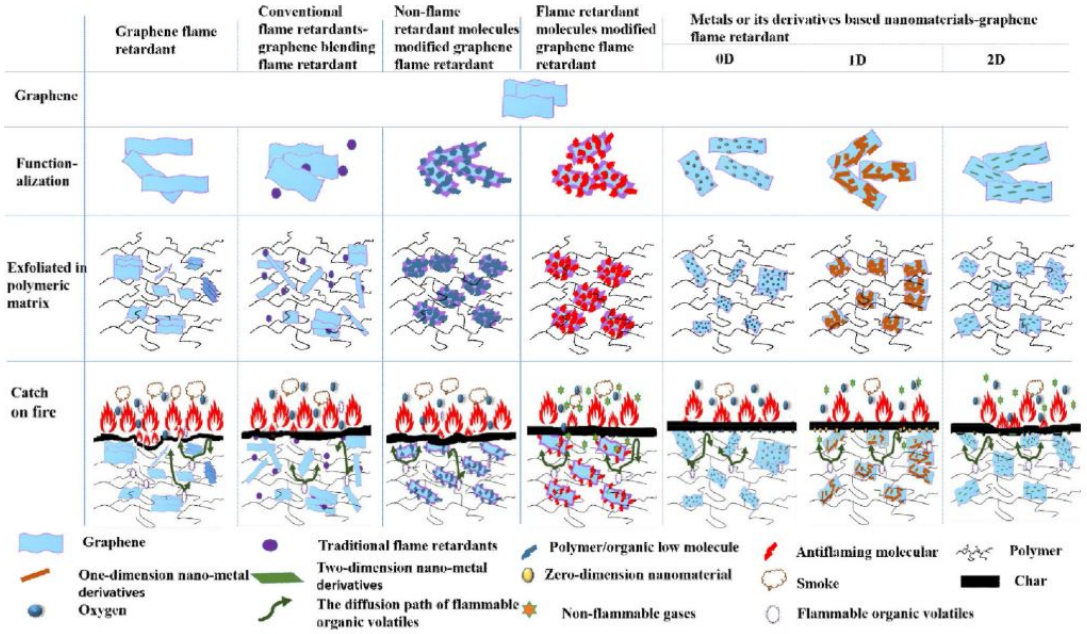

Figure 2.5: Schematics illustration of Graphene and Graphene Oxide (GO) flame retardant mechanism, from[168]

in the gas phase (*i.e* dilution) and in the condensed phase (*i.e.* protective layer forming and cooling) and be effective, at the same time as rheological modifier and mechanical strengthener (similarly to nano-clay)[Ch. 20 of [45]]. A detailed review on LDH has been produced by Gao *et al.*[167] , where LDH use are reported for multiple polymers such as: polyethylene (PE), ethylene vinyl acetate (EVA), poly(methylmethacrylate)(PMMA).

2.5.3 Graphene Based Nano-FR

Carbon nanotechnological, Fullerenes[169], Carbon Nanotubes[170], graphene and graphene oxide[168] fillers have been extensively reviewed to be good candidate as FR. Graphene (G) and Graphene Oxide (GO) are composed by a single layer carbon sheet with important applications in polymer nanocomposite (Par. 3.1.2)[Fig. 3.4]: recently graphene based materials have gained access to FR research due to their strong barrier effect and high thermal stability (as fa as concerns graphene and rGO). There are three main ways in which G, GO and rGO can acts

as flame retardants: the first comes from their high aspect ratio that act both as diffusion limiter (via the so called *labyrinth effect* in which a tortuous pathway is created for volatile inter-diffusion) and as char former template in the bulk polymer or on its surface, the second mechanism involves its adsorption capabilities of flammable organic volatiles during combustion[171][168]. Finally, especially GO and rGO contain numerous functional groups (*i.e.* carboxyl, hydroxyl, carbonyl and epoxy) that ease their functionalization to improve compatibilization with the polymer or to covalently attach conventional FR[Fig. 2.5][168]. Gao *et al.* reported how a minimum concentration of $0.20\%_{wt}$ of Graphene in PLA is necessary to improve its flame retardancy, due to arise of barrier effect that hinder volatile diffusion reaching a decrease of the pHRR of 40% with a loading of 2% and a decrease of mass loss rate. However due to the high thermal conductivity and the infrared absorption of graphene the time of ignition is reduced[172]. This behavior of reduction of the ITT is commonly reported for graphene based nanocomposite[168][173] Graphene efficacy has been also reported in epoxy[174] composites and polystirene[175] and polypropylene[176]. Interesting, Han *et al.*[175] studied the effect of Graphene and GO (with different oxidation grades) in polystyrene nanocomposite and, via cone calorimetry studies, highlighted the fact that the lower the oxygen content of GO the better the flame resistance of the final nanocomposite. Graphene ($5\%_{wt}$), indeed, leads to optimal resistance with a drop of 50% of the pHRR with a stable char formation, which is a remarkable result since PS, recalling its decomposition pathway (Par. 2.3), does not form char upon combustion. However, pHRR reduction, reported for GO with oxygen content ranging from 37% to 25%[12], was about $\approx 30 - 40\%$ and with a reduced char formation with respect to graphene/PS nanocomposite. Other reports studied the effect of GO on PS and PP with similar results at 0.5 - 2 $\%_{wt}$ ladings, calling, however, the attention to the fact that THR and LOI index were not altered after the addition of GO, which is compatible with previously reported nano-layered FR mechanism (*e.g.* for non-organomodified nano-clay)[171]. Obviously another fact has to be taken into account in these studies, beside the higher thermal stability of graphene with respect to the GO counterpart; GO posses a highers polar structure and hydrophilicity due to the presence of oxygen moieties which negatively

[12] from elemental XPS analysis

impacts its compatibility with apolar polymers such as PS or PP. GO efficacy was also studied in polyurethane, both as a coating[177][178] and bulk FR[179]: Zhang *et al.* [178] used a GO protective coating to protect PU foams, created by layer-by-layer assembly, taking advantage of negative charge of GO present in alternate layers of chitosan and alginate. Smoke production, pHRR and THR were significantly reduced with respect to the neat PU. In this case polysaccharides were used to enhance char forming properties of the layer (Par. 2.6). Currently, a commercial graphene based paint is commercialized with the name of FireStop™, developed to be used as flame retardant coating for timber[180]. As stated above, GO and rGO can be easily functionalized to enhance polymer compatibilization, also preventing re-stacking of graphene-like structure, or modified with other FR to achieve synergist effects. This is the case, for example, of pentaerythritol grafted on GO surface which was used to enhance the functionalized GO dispersion in PP, enhancing in this way mechanical and fire resistance properties of the composite promoting the formation of a continuous char[181]. Cao *et al.*, similarly, grafted polypropylene on GO surface [182].

Conventional flame retardant have been attached to GO surface. This is the case of phosphorous [183][184], amine-based (*e.g* melamine[185]) and hydroxides[168]. In particular, covalent grafting of phosphoric acid precursors can be particularly beneficial due to their capability of promoting char formation(Par. 2.4.2). This is the case, for example, of organic phosphate functionalized GO for epoxy composite where char yield was enhanced together with the pHRR, with respect to the addition of non functionalized GO ($5\%_{wt}$)[184]. A similar work was also conducted in PS with an hyperbranched phosphorous and nitrogen based novel FR by Hu *et al.*[183]. Another example of FR functionalization of GO is represented by Melamine grafting, via esterification aided with SOCl2, by Monji *et al.*[185] to be used in PP: a reduction of both pHRR and the THR was achieved with the addition of only $2\%_{wt}$ of the novel FR. As far as mineral flame retardants are concerned, an interesting work was published by Edenharter *et al.*[186] in which LDH (Par. 2.5.2) and GO where used as a filler at different loadings (up to $5\%_{wt}$) in PS (both the GO and the LDH where functionalized to improve organophylicity). Upon combustion LDH and GO start to etherocoagulate (due to their opposite

charge) and concentrate on the burning surface of the PS, the flame resistance of the nanocomposite is therefore improved by reduced the thermal feedback and volatile exchange. Alginate and cellulose flame resistance have also been improved with graphene: in a work published in nature nanotechnology, Wicklein *et al.*[87] produced acellulose aerogel with extremely low thermal conductivity (Par. 1.3.3) using GO as FR filler. Cone calorimetry show a reduction of pHRR with the prevalence of smouldering combustion with respect to the complete flame evolution observed without the addition of GO. Thermally reduced GO was also used in Alginate to increase its resistance to thermal degradation, assessed through TGA[187]. Numerous other examples of the use of G, GO and rGO can be found in the review written by Wang *et al.* [188] and Sang *et al.* [168] and Malucelli [189].

2.6 Alginate Role in Flame Retardancy

Alginate, and oxidized polysaccharides in general, are well known to be char forming polymers able to form intumescent layers (by creating a swelled char layer upon combustion). Oxidized starch and lignin can, for example, be used to reduce flammability of pine-wood if used as a coating (Ch. 7 [45]). This is mainly due to the decarboxylation and dehydroxylation reaction that take place along the polymeric backbones which promote char formation (*i.e.* chain stripping (Par. 2.3)). Alginate, among its multiple uses, has recently attracted the attention of thermal insulation and FR research community: multiple thermal insulation material based on alginate (used both as bulk constituent or as binder) have been presented in (Par. 1.3.3 and 1.3.4) and, for the above mentioned reasons, alginate possesses an intrinsic flame resistance with an EHC[13] of about $\approx 3\,MJ/kg$ while standard polymers posses an EHC comprised between $\approx 16 - 45\,MJ/kg$ (Ch. 2 [45])[190]. As described in the previous chapter 1.3.3, Vincent *et al.* produced a calcium-alginate foam, with an air drying method, with excellent flame resistance capacity. Indeed, comparison between the alginate foam, and a commercial flame retarded PU foam revealed high self-flame extinction capacity (seconds *vs.* min-

[13] **EHC**: the effective heat of combustion is a parameter which can be calculated from cone-calorimetry test and represents the heat released, during combustion, for a unit of mass

utes for FR-PU), reduced pHRR (17 *vs.* 80 kW/m^2,) and char properties (61% *vs.* 26% of residue)[14][95]. Alginate has shown to enhance flame retardancy of composite materials even when used as binder: Palumbo *et al.* reported a reduction of the THR and pHRR up to 30% when alginate was used as binding agent for bio based TIMs from agricultural bi-products[191]. In another study, alginate was used as in polyamide (PA) fibres ($50\%_{wt}$), showing a reduction of 50%, 59% and 66% of pHRR, total heat release and smoke release respectively. The FR properties were atributed to the charring capabilities of alginate, that limited the melt dripping of PA fibres coupled with a vapour-phase mechanism of gas dilution due to adsorbed water release[192]. It has been reported (in the previous paragraph (Par. 2.5.3)) the use of alginate and chitosan as FR coating system coupled with GO(Par. 2.5.3); in a similar work, this type of coating (composed only by alternate layers of chitosan and alginate) was applied to flexible polyurethane foams obtaining a decrease of the pHRR of 66% [193]. Literature also highlight that alginate fire behavior is highly influenced by the metal used during ionotropic gelation (*e.g.* Ca^{2+},Cu^{2+},Ni^{2+}). Ionotropic gel structure possesses higher thermal stability (TGA) with respect to non crosslinked alginate (as a matter of fact, neat Na^{+}-alginate do not show self-extinguishing behavior). In addition, specific metal ions (*e.g.* Fe^{3+}[194] Al^{3+}[195] ,Ni^{2+} [196] [94] Ca^{2+}[197][198], Cu^{2+}Liu2015) intercalate metal ions, in the alginate matrix, seems to participate in polymer degradation reactions, promoting char formation (*e.g.* decarboxylation, dehydroxylation and scission of the glycosidic bond). The magnitude of this effect is also dependent on the metal ion[194][94][199]. In addition, formed metal oxides, can effectively contribute to a stable char formation in particular in fibrous or foamed alginate materials with high specific area[197]. Numerous other examples of the use of alginate as co-flame retardant can be found in[94].

[14] All these values are reported for Cone calorimetry test with spark ignition at 50 kW/m^2 of radiative heat flux.

Part II

Experimental

Scopes and Experimental Approach

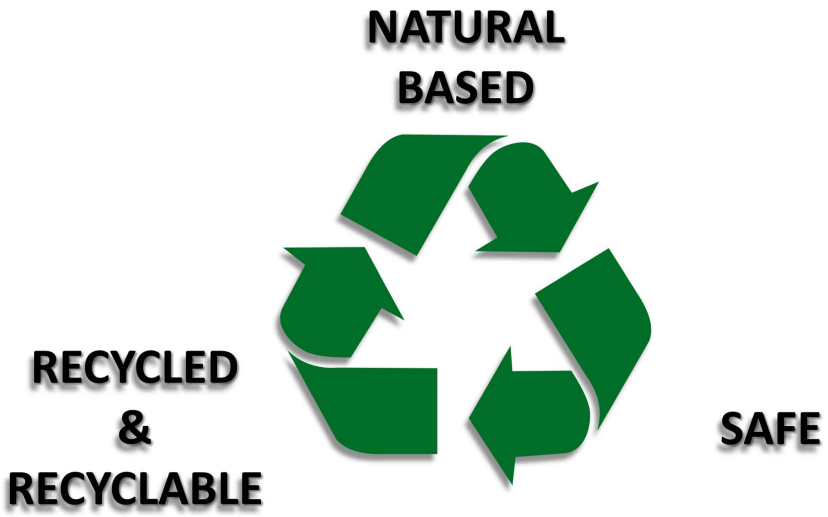

Figure 2.6

As described in the introduction, the final objective of this work is the development of a fully recyclable thermal insulating nanocomposite, with improved flame resistance, as evolution of an insulation material which was previously developed in our laboratories[1] with a patented process[200]. The original material was designed as an innovative solution to recycle industrial waste (fiber-glass and glass waste) in a valuable thermal and acoustic insulator by embedding them in a porous calcium alginate matrix, produced without the use of external foaming agents (ini-

tially described in Par. 1.3.4). The main results of this work are subdivided in five different chapters, as they are presented in Section III: the initial optimization step of the foam composition (Ch. 6), the development of the recycling process (Ch. 7), a life cycle assessment study (Ch. 8), the fire resistance characterization of Graphene Oxide filled foam (Ch. 9) and, at the end, a section dedicated to the characterization of functionalized GO(Ch. 10).

Initial Optimization

An initial optimization stage, that eventually delivered the composition detailed in (Par. 4.1), was performed and the results are presented in (Ch. 6): initially, the composite alginate foam (CAF) was optimized to be used in the ship-building sector as a part of the *GGTDoors* project conducted in collaboration with industrial partners, delivering the CAF-*GGTD* composition. Being destinated to be used in the shipbuilding sector some restrictions applied to its composition, in compliance with the FTP code[15] as far as waste filler concentration is concern: for this reason both fibre-glass and glass waste were used in CAF-*GGTD*. Due to the industrial nature of this project, these data are covered by a *non-disclosure agreement*, therefore only relevant informations with respect to the final composite alginate foam composition (oCAF), used in the all the following sections, will be briefly discussed. The CAF, studied in this work, was obtained via freeze-drying of an alginate ionic-gel in which waste fillers and additives were dispersed before gelification. The gel was obtained via *internal-gelation* technique, by which an homogeneous structure can be obtained by dispersion of insoluble $CaCO_3$ which Ca^{2+} release is triggered by glucono-δ-lactone (GDL) hydrolyzation (*i.e.* ionotropic gelation, (Par. 1.3.3)). Before that the gelification step occurs, as far as CAF-*GGTD* composition is concerned, both fiber-glass and glass waste were added, together with a natural plasticizer. In the following experimental sections, in which the oCAF composition is used, only fiber-glass are added as waste filler, without the use of any plasticizer: this change in the foam composition, was operated to reduce any interference coming from the use of additives (*i.e. the plasticizer*) in the development of the recycling process and to maximize the critical waste frac-

[15] 2010 FTP code: Fire testing Procedures adopted by the *Maritime Safety Committee*[131]

tion content (*i.e.* the fiber-glass waste, see (Par. 1.3.4)) within the material . In addition, this simplification allowed the avoidance of any conflict with the signed *non-disclosure agreement* N.D.A. and was possible due to the discard of the FTP code restrictions since the intended use of the material is no longer restricted to the shipbuilding industry.

Recycling Process Development

In (Par. 7) the problem of the development of a complete functional recycling process is considered. Such a result can be obtained, without degradation of the polymeric binder (*e.g.* alginate), by interfering with the ionic junctions that build up the matrix, via competitive chelation of the cation with EDTA (ethylenediaminetetraacetic acid disodium salt) which possesses a higher affinity toward the calcium at neutral or basic condition. As a consequence of the disruption of the ionic junctions, the gel is dismantled and the material regresses to it viscous state. A complete recovery of the foam is possible upon deactivation of the chelating activity of the EDTA, under mild acid condition: as a consequence, the ionotropic gelation reoccurs and, by freeze-drying, a dried composite alginate foam can be re-obtained. The effects of the initial EDTA concentration, together with the additional use of new complexing cations ($CaCO_3$) and HCl were studied. Initially, rheometry was used to asses the efficacy of the dissolution and the recovery step (without the addition of waste filler). Lately, the functional properties of the recycled foam were studied as far as thermal (thermal conductivity and specific heat), acoustical (sound absorption coefficients) and mechanical (compression test) behavior are concerned, together with the evaluation, through micro-tomography (μ-CT), of the foam morphology. We are well aware that natural derived materials are marked by a general poor resistance to vapour permeation and mould attack but no specific tests were conducted regarding these condition since they were out of the scope of the present work. Nevertheless, these characterization will be considered in future works.

LCA Study

The evaluation of the environmental impact of the recycling process was calculated and analysed with respect to the original production process of oCAF material with the main aim of identifying the most impacting activities involved in each production stream-line and, most important, to actually gain information about the potential environmental benefit associated to oCAF recycling with respect to its landfillig and simple substitution. This was done, initially by modelling two lab-scale products systems: the first for the original and the second for the recycled process (PO and PR). Eventually via a third production system was defined, in which an industrial scaled version of the recycling process was simulated to better understand the potential impact of the extremely energy demanding oCAF recycling process, in different energetic scenarios(Ch. 8)

GO as FR study

GO capability to enhance fire resistance of both the original and the recycled foam was studied primarily through cone-calorimetry (CC) and the results are presented in paragraph (Ch. 9). GO was dispersed in the alginate solution before addition of the waste filler with a mechanical homogenizer (Ultra-Turrax®) and compatibilization was assessed through High frequency Rheometry before fire testing. The functional properties (*i.e.* thermal, acoustical and mechanical) of the original and recycled GO-Composite alginate foam were also evaluated and the result are presented. Micro-combustion calorimetry (MCC) was also used to study the FR effect of different concentration of GO in pure alginate foam, without the addition of waste filler (*i.e.* fiber-glass).

GO functionalization and characterization

Finally, different GO functionalizations (fGO), with amines and nano aluminium hydroxide (nATH), were synthesized and completely characterized mainly through X-Ray Photoelectron Spectroscopy (XPS), TEM and termogravimetric analyses (TGA). The results are presented in (Ch. 10). Two strategies were used to produce

amino-fGO: the first via simple amination of GO ketones and aldehyde groups via Leuckart reaction with ammonium formate and the second through alkylamine grafting through GO epoxy opening reaction. Ethylenediamine, tetraethylenepentamine and branched polyethylenimine were grafted on GO surface. The main aim of the amino-fGO is to improve fGO-alginate interaction thus increasing its dispersibility and flame retardant effect: alginate is a polyanionic polymer hence capable of interacting with the positively charged amino groups. Zeta potential was therefore used to characterize the surface charge of amino-fGO. A more direct approach to enhance GO flame retardant efficacy was studied by conventional flame retardant functionalization with Melamine (see Par. 2.4.3) and nATH (see Par. 2.4.4). Melamine grafting was attempted via epoxy opening and XPS and Z-potential were used to asses reaction efficacy. nATH was deposited on GO surface via in situ precipitation and X-Ray diffraction (XRD) and differential scanning calorimetry (DSC) were used as characterization techniques.

Chapter 3

Materials

3.1 Starting Materials

3.1.1 Alginate

Figure 3.1: Kelp forest of *laminaria Hyperborea*, sea of Scotland, UK.

The term alginates is commonly referred to the wide families of salts coming from the neutralization of alginic acid with the most common commercialized form being Na-Alginate. Alginate is a polysaccharide extracted principally from brown

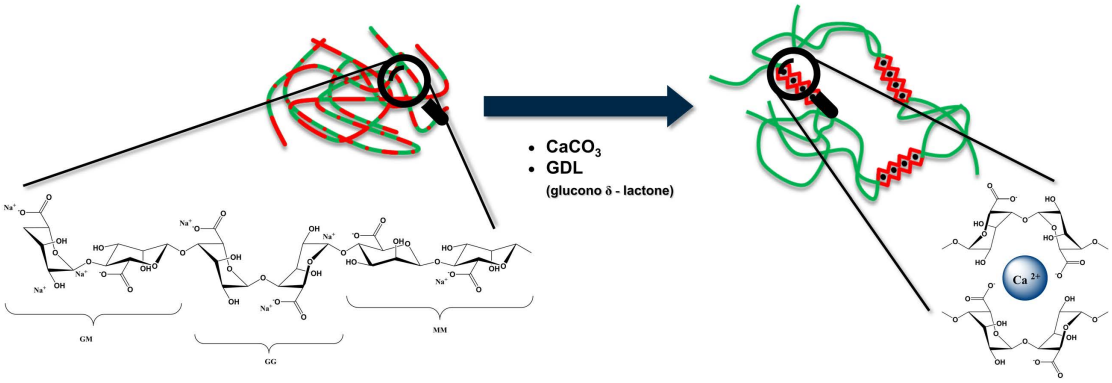

Figure 3.2: Alginate structure and ionotropic gelation mechanism for calcium alginate (egg-box model). M = β-D-mannuronate, G = α-L-guluronate

seaweed (mainly kelp of the order of *Laminariales* and focoids of *Fucales* order) and, in a far less extent, from bacteria with an overall worldwide market that is valued approximately 318 millions USD[94][201]. From the chemical point of view, alginate is a linear, anionic, random block-copolymer, part of the polysaccharides family composed by two monomer: β-D-mannuronate (M) and α-L-guluronate (G) linked together by a $1 \rightarrow 4$ glycosidic bond and arranged to form MM, GG and MG blocks [Fig. 3.2]. MM and GM blocks are more flexible than GG blocks, which provide stiffness to the alginate forming a helix-like structure due to their di-axial linkage. Molecular weight and block length and distribution vary across different algae species depending also on other conditions such as the harvesting timing and location inside the algae[201].

As anticipated in (Par. 1.3.3), alginate is capable of forming water insoluble gels via *ionotropic gelation* in the presence of divalent (Ca^{2+}, Cu^{2+}, Mg^{2+}, Zn^{2+}, Ca^{2+}) or trivalent cations (Fe^{3+}, Al^{3+}, Cr^{3+}) which are chelated by alginate backbone. Differences among the gel structures produced with different cations are presented (from micro-scale chain conformation to mechanical properties of final gel) and are discussed elsewhere[202][203]. A general accepted gelation model, studied from the gelation mechanism of Ca-Alginate systems, is the so called "*egg-box*" model: due to the tridimensional conformation of GG alginate blocks the cation can be easily chelated by the carboxyl groups (aided by hydrogen interactions) and hosted inside the cavities formed between two adjacent chains therefore producing

a ionic cross-link zone extended along the GG blocks [Fig. 3.2]. Therefore, only GG blocks concur into ionic-gel formation whereas MG and MM segments remain free [204][201]. Alginate is also capable to form gel, in acid conditions, even without the presence of specific cations: by lowering the pH below the pK_a of M and G carboxylic groups (3.4 and 3. respectively) the arising of Van der Waals force and hydrogen bonds between the protonated alginate chains (which now are no longer charged) induce an initial increase in viscosity and eventually gelation occur. Acid alginate gels are less stable and possesses a lower mechanical resistance[205]. In addition, temperature rise reduce their gel stability whereas once the ionic gel is formed, it can withstand temperatures up to 100 $°C$ [206].

3.1.1.1 Sodium Alginate Extraction

Alginate production derives mainly from wild algae, harvested worldwide with approximately 38 different species (in 13 countries) that are commercially exploited [Fig. 3.3][201]. Alginate is one of the main structural components of cellular walls and extracellular matrix in brown algae representing from 12% to 55% of their dry weight. Inside the algae alginate is present in various form: mainly complexed with calcium ions (or other sea-available cations) or as alginic acid, depending on the species, cultivation stage and condition and position inside the algae[201].
One of the main extraction methods for the production of alginate is the ethanol-alkaline-extraction as reported by Gonzalez-Lòpez *et al.*[207] and Villanueva *et al.*[208][209]. The process involves three main steps: pre-extraction, neutralization and final precipitation for the production of Sodium Alginate.

- **Pre-treatment**
  Before the first step, normally, algae are washed, grounded and treated with a formaldehyde solution (0.1-1%) to remove pigments and extensively washed with water.

- **Pre-extraction**
  The algae biomass is then treated in acid condition (H_2SO_4) to enhance the alginate extraction by increasing its solubilization and to remove impurities and contaminants (such as polyphenols and proteins) by subsequent water washing.

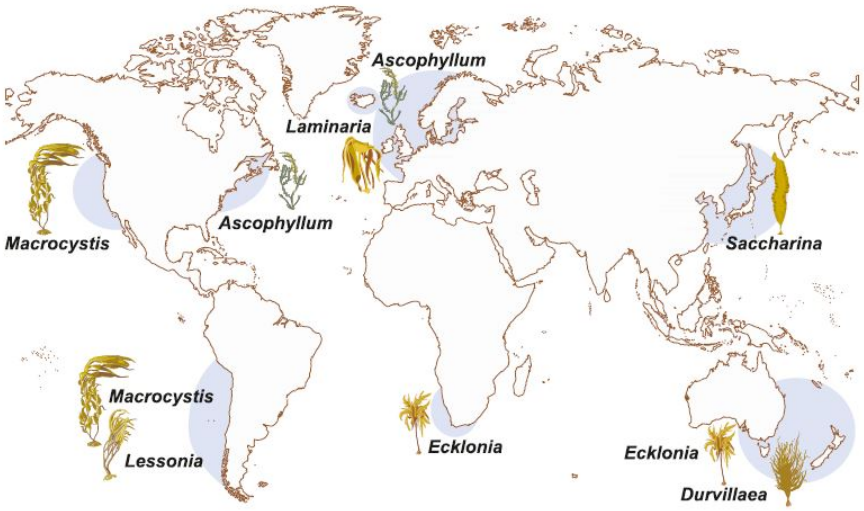

Figure 3.3: Worldwide distribution of commercially exploited seaweed resources for Alginate production. From [201].

- **Neutralization (alkaline extraction)**
  A Sodium carbonate solution is added ($Na2CO_3$) and the pH is brought to 9-10. During this stage alginic acid is converted to water soluble Na-alginate and impurities are removed by filtration.
- **Precipitation**
  In this final step Na-Alginate powder is directly obtained by precipitation in ethanol and subsequent washing in ethanol and acetone before air drying.

The process, as it is described here, has been used as model for PO.2 in the LCA analysis in (Par. 5). Others alginate extraction routes, such as the calcium-alkaline and acid-alkaline extraction, are described in [201].

3.1.2 Graphene Oxide (GO)

Graphene Oxide (GO) is an extremely promising material, whose properties mainly depend on its oxidation or reduction stage, that is finding application in graphene related fields such as optics[], chemistry, biology, energy storage and electronics[211]. Chemically, GO is an oxidized form of graphene with a high oxygen func-

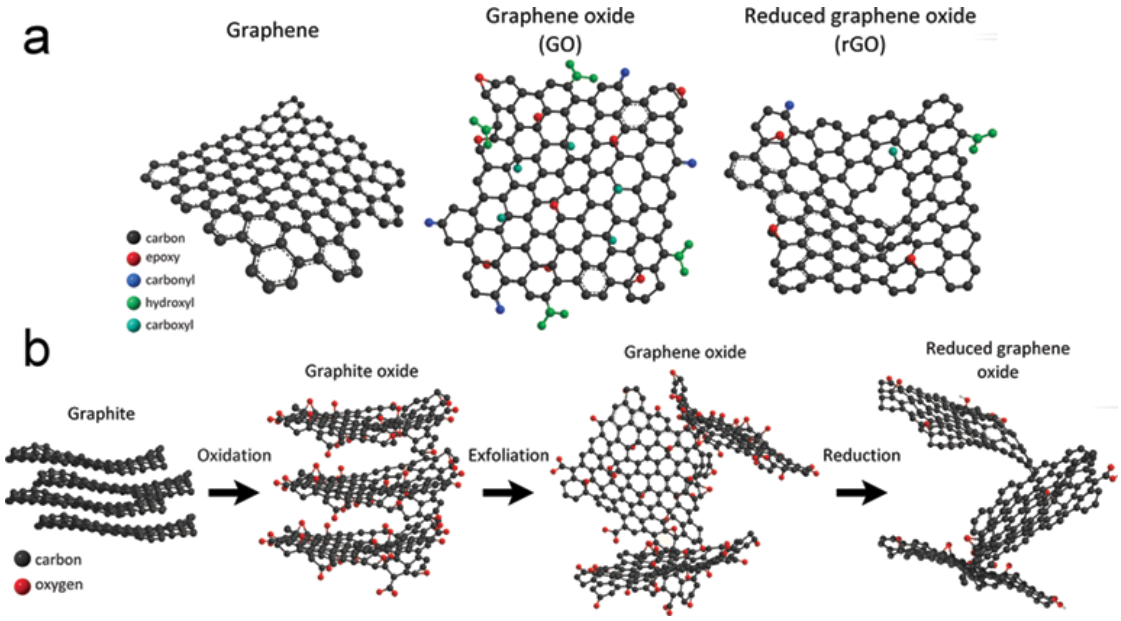

Figure 3.4: Graphene, Graphene Oxide (GO) and reduced Graphene Oxide (rGO) structure and synthesis route, from[210].

tional groups content: even though a precise structure cannot be defined, epoxy and hydroxyl groups are mainly present, together with carbonyl and ester groups, while carboxyl groups are situated predominantly on the edges[Fig. 3.4]. The presence of oxygen makes GO more prone to chemical functionalization. Nevertheless the disrution of the extended sp^2 network of the graphene hexagonal lattice leads to an overall drastic reduction of the electrical conductivity and the thermal stability of GO. Oxygen moieties also make GO easily dispersible in water in which stable dispersions are possible without the use of surfactants at concentration up to $\approx 4\,mg/mL$ $(0.4\%_{wt})$.

The most common route to produce GO is through oxidation and exfoliation of graphite via the modified Hummer method[212][213]: at first, graphite is oxidized in concentrate H_2SO_4 in the presence of $KMnO_4$ and other strong oxidant, (such as K_2FeO_4 to replace $NaNO_3$ used in the original process that leads to toxic gas evolution and low yield) that intercalate between the graphite layers (oxidizing at the beginning the edges) and, by further addition of oxidizing agents, lead to inner oxidation and exfoliation at 95 ° C. The reaction is then quenched by addition of

water and H_2O_2[212]. Mechanical stirring, ultra-sonication and even high shear reactors[214] have been used to improve GO exfoliation and single layer yield of the process[213]. Different modified versions of the Hummer methods have been developed in the literature to overcome the several problems related to the process, such as the evolution of toxic gasses or the dangerous condition of oxidation that could lead to a risk of explosion (if not well managed, which makes difficult the up scaling of the process) or the enormous amount of water needed for the process workup (1000:1 with respect to graphite initial load) that is eventually contaminated[212]. Nevertheless, recently also bottom-up approach have been developed to produce GO such as the hydrothermal treatment of glucose or chemical vapour deposition methods but Hummers related approach remain the best candidate to full industrial scale GO production[211]. GO finds numerous applicatioFns, it is easily functionalizability and reduced cost (with respect to graphene) makes it a valuable alternative to be used in polymeric nanocomposite and in medicine and biology as sensor or carrier (where specific target molecules can be attached to GO structure) thanks to its low cytotoxicity[211]. The sp^2 network can be partially restored by GO reduction leading to production of reduced graphene oxide (rGO). The difference between rGO and graphene lies on the amount of structural defects that are still present on rGO and from the non complete removal of oxygen. rGO can be obtained by chemical (*e.g.* hydrazine) thermal, or mechanical or electrochemical reduction route of GO[213]. The reduced graphene oxide possesses some usefull properties, such as a mantained controllable functionality from the GO and an increased electrical and thermal conductance (typical of graphene despite not being comparable with those of high pure graphene) making it a good candidate for electronics(*e.g.* sensors, photovoltaic, supercapacitors). It is also worth mentioning that GO and rGO can be easily produced at the kilogram scale and still represent one of the best candidate scalable routes to produce high quality graphene.

3.1.3 List of Solvents and Chemicals Used

- **Alginate sodium salt** (MW = 200–250 KDa; M/G ratio = 1.44; shear viscosity = 0.99 [Pa s] at 1.4% w/v, 25 ° C, pH 7.5 and 1 s^{-1} of shear rate)

was purchased from *Carlo Erba*

- **Hydrochloric acid** (37 % solution) was purchased from *Carlo Erba*
- **D-glucono-δ-lactone (GDL)** was purchased from *Sigma Aldrich*
- **Calcium carbonate** $CaCO_3$ was purchased from *Sigma Aldrich*
- **Ethylenediaminetetraacetic acid disodium salt (2Na-EDTA)** was purchased from *Sigma Aldrich*
- **Milli-q water** used to prepare all aqueous solutions. Purified with a Direct-Q 5 UV Millipore® system.
- **Fiber-glass powder waste** were derived from final grinding of industrial fiber-glass products:
  - **Batch 1**: resin 55%, glass 13%, aluminium hydroxide $Al(OH)_3$ 32 %, residual fraction at 1000 °C 35%, (values calculated from TGA and DSC data). If not differently specified, this batch was used in all the formulations.
  - **Batch 2**: resin 55%, glass 2% , aluminium hydroxide $Al(OH)_3$ 43 %, residual fraction at 1000 °C 30%, (values calculated from TGA and DSC data).
- **Graphene oxide**: GO-powder and stock GO-water solution ($0.4\%_{wt}$) was purchased from *Graphenea*
- **Solvents**: acetone, ethanol and methanol were purchased from *Sigma Aldrich*
- **Glass powder waste**: grounded glass Pirex waste $< 500\ \mu m$ ($< 20\ \mu m$ 20%, $< 50\ \mu m$ 70%,$< 200\ \mu m$ 90%).
- **Aluminium Sulfate Hexadecahydrate** ($Al_2(SO_4)_3 \cdot 16H_2O$) was purchased from ThermoFisher.
- **Ethylenediamine** was purchased from *Sigma Aldrich*
- **Tetraethylenepentamine** was purchased from *Sigma Aldrich*

- **Polyethylenimine, branched**, M_w = 25 kDa was purchased from *Sigma Aldrich*
- **Kaiser Test kit** was purchased from *Sigma Aldrich*

Chapter 4

Methods

In this section the procedure and the methods used to produced all the sample of the alginate foam (both pristine and recycled), the GO dispersion method used to produce the GO-Alginate foams and the synthesis route adopted to produce the functionalized graphene oxide are described. The following general notation applies:

- **oCAF**, Original Composite Alginate Foam: **all the sample produced following the method described in (Par. 4.1) with the final optimized composition detailed in (Par. 6)** in which alginate is used as binding agent, for fibre-glass waste, to produce a porous matrix.
- **AS**, Alginate Solution: all alginate solution samples produced following point **1** of (Par. 4.1). These samples were used in rheological evaluation.
- **AG**, Alginate Gel: all gelled samples produced following (Par. 4.1) without the addition of fibreglass waste and whose properties were evaluated before freeze-drying. These samples were used in rheological evaluation.
- **AF**, Alginate Foam: all the samples produced following (Par. 4.2) without the addition of fibreglass waste. These sample were used in micro combustion calorimetry (MCC) to assets GO efficacy as flame retardant at various concentration and as starting material to produce recycled alginate gel (rAG)

- **rCAF**, Recycled Composite Alginate Foam: all the sample produced following (Par. 4.2) in which oCAF were recycled with the method developed in this work. Exact composition is identified with a suffix described in detail in (Par. 4.2).
- **rAS**, recycled Alginate Solution: all alginate solution samples obtained at the end of point **2** following the procedure described in (Par. 4.2) starting from AF samples. These samples were used in rheological evaluation.
- **rAF**, recycled Alginate Foam: all the samples produced following (Par. 4.2), starting from AF samples. Different samples are designated as described in (Par. 4.2)
- **rAG**, recycled Alginate Gel: all the samples produced following (Par. 4.2), starting from AF samples whose properties were evaluated before freeze-drying. Different samples are designated as described in (Par. 4.2)
- **GO**: Pristine, non functionalized Graphene Oxide
- **fGO**: functionalized GO as described in (Par. 4.3). Suffix identify the specific functionalization process.
- **SA**: Sodium alginate

4.1 Production of Composite Alginate Foam (CAF)

The composite alginate foams (CAF) used in this work were produced with the method previously reported by Kyaw Oo D'Amore *et al.*[1] and that is herein summarized. Reagents concentration refers only to oCAF samples:

1. SA was dispersed in milli-q water to obtain a homogeneous viscous solution at a concentration of 1.4% w/v.
2. Fiber-glass (powdered) and CaCO3 were added, to obtain a final concentration of 5.3% w/v and 15 mM, respectively, to the SA solution. Stirring was maintained until a homogeneous suspension was obtained.

3. To initiate the internal gelation, a freshly prepared GDL solution (180 mM) was finally added before pouring the viscous mixture in a rectangular die(200 mm × 200 mm × 18 mm).
4. The gel was aged for 12h at 4 ° C and then placed at -20 ° C for 12h
5. The forzen gel was lyophilized (Lio 5P DIGITAL freeze drier), the samples are extracted from the freeze drier, not before 48 h, once a plateau in the readings of the internal pressure gauge was reached.

All the concentrations are expressed for a final gel volume of 700 mL which corresponds to a single foam tile (200 mm × 200 mm × 18 mm). The considerations that lead to the development of this exact composition are described in (Par. 6). With the same method, Alginate Foam (AF) and Alginate Gel (AG) samples (without the addition of fibre-glass waste), used in rheological evaluation, were also produced.

NOTE The procedure and concentrations presented above apply to **all** the composite alginate foam sample produced in this work with the exception of:

I The recycled sample whose production is described in (Par. 4.2).

II The non optimized composite alginate foam (CAF) from which the optimized composite alginate foam (oCAF) was developed (as described in (Par. 6)). CAF were produced, varying reagents concentrations, with the above described procedure. Initially, different mix of fibre-glass and glass waste and a natural plasticizer were used, together with the CaCO3, in the step Num. 2.

Table 4.1: oCAF composition, values for 700 mL of final gel volume.

Alginate		**Fiber-Glass**		**$CaCO_3$**		**GDL**	
[g]	[$\%_{wt,dry}$]	[g]	[$\%_{wt,dry}$]	[g]	[$\%_{wt,dry}$]	[g]	[$\%_{wt,dry}$]
9.80	17.59	37.38	67.10	1.05	1.88	7.48	13.43

4.1.1 GO dispersion in Alginate

Graphene Oxide stock water solution ($0.4\%_{wt}$) was used for the preparation of Alginate graphene nanocomposite. The GO solution was sonicated, in a bath sonicator, for 30 minutes at room temperature and subsequently treated with a mechanical homogenizer (Ultra-Turrax®) for 8 minutes at 20k rpm before its addition to a previously prepared SA solution. The obatained SA-GO solution was further treated with a mechanical homogenizer (Ultra-Turrax®) for 8 minutes before its use.
The suffix **"-GOx"** identify the presence of GO in the sample, where x stands for GO percentage weight with respect to the final organic weight fraction $\%_{wt,org.frac.}$. oCAF-GO2, rCAF-GO2, AF-GOx and oCAF-ED oCAF-NH3 were produced with this method.

4.2 Recycled Composite Alginate Foams production (rCAF)

In this section the method used to produce the recycled composite alginate foams (rCAF) is described. Each single rCAF sample was produced with a final volume equivalent to the volume of the starting oCAF used in the recycling process. The concentrations herein presented refers to a final volume of 700 mL (lyophilized tile dimension 200 mm × 200 mm × 18 mm).

1. 44 mM of 2Na-EDTA were dissolved in Milli-q water at pH 8 (stabilized with 1 M NaOH solution) to obtain a clear solution.

2. A single foam tile of the oCAF material, produced as previously described (Par. 4.1), was ground and then added to the solution. The pH was stabilized at 7.5 using a 0.1 M NaOH and maintained under vigorous stirring for 1 h at a constant pH level. After one hour, a homogeneous viscous solution was obtained. At this point the alginate and fiber-glass concentration in the water solution was equivalent to the one present in the oCAF production process prior to the gelification step (Step. 2 in (Par. 4.1)).

3. At this point four different routes have been tested to re-establish the gel structure:

   rCAF–CG addition of CaCO3 (final concentration of 15 mM) followed by the addition of GDL (180 mM)

   rCAF–G addition of GDL (180 mM) without the use of additional CaCO3.

   rCAF–CG–A addition of CaCO3 (final concentration of 15 mM) followed by the addition of GDL (180 mM) and HCl 6 M (0.5 % v/v) at 75 ◦C

   rCAF–G–A addition of GDL (180 mM) and HCl 6 M (0.5 % v/v) at 75 ° C.

   Immediately after the addition of GDL the viscous solution was poured in a rectangular mold before the gelification occurs.

4. The gel was aged for 12h at 4 ° C and then placed at -20 ° C for 12h

5. The dried foam was obtained following the previously described freeze-drying procedure (Par. 4.1).

In the above defined process, three different steps can be identified: dissolution, inhibition and gelification. The initial dissolution of the gel correspond to step **2-3**, the inhibition of the chelator starts at point **3** unitl the Ca^{2+} cation starts to be chelated by the alginate. The gelification step can be identified between point **3** and **4**. Alginate nanocomposite oCAF-GO2 have been recycled following the "-G" route, producing rCAF-GO2-G samples.

4.2.1 Recycling of the rCAF (2rCAF)

A second-recycling test was made by dissolution of the rAF – G composition following the procedure described for the production of rAF samples(Par. 4.2), without the addition of new EDTA. Briefly, a single foam tile of the rAF – G material was ground and then added to a water solution, and the pH was stabilized at 7.5 using a 1 M NaOH solution. The solution was maintained under vigorous stirring for 1 h at a constant pH level. After one hour, a homogeneous viscous solution was obtained. Following the addition of GDL (180 mM), the viscous solution was poured in a rectangular mold prior to gelification. The dried foam was obtained following the previously described freeze-drying procedure. All the concentrations are expressed for a final gel volume of 700 mL.

Table 4.2: rCAF compositions, values for 700 mL of final gel volume.

		rCAF-G	**rCAF-GC**	**rCAF-G-A**	**rCAF-GC-A**	**2rCAF-G**
Alginate	[g]	9.80	9.80	9.80	9.80	9.80
	[$\%_{wt,dry}$]	10.90	10.78	10.90	10.78	8.73
Fibre -Glass	[g]	37.38	37.38	37.38	37.38	37.38
	[$\%_{wt,dry}$]	41.59	41.11	41.59	41.11	33.28
$CaCO_3$	[g]	1.05	2.10	1.05	2.10	1.05
	[$\%_{wt,dry}$]	1.17	2.31	1.17	2.31	0.93
GDL	[g]	29.92	29.92	29.92	29.92	52.36
	[$\%_{wt,dry}$]	33.29	32.90	33.29	32.90	46.62
EDTA	[g]	11.73	11.73	11.73	11.73	11.73
	[$\%_{wt,dry}$]	13.05	12.90	13.05	12.90	10.44
HCl	[%v/v]				0.50	0.50

4.3 Graphene Oxide Functionalization

GO powder was used as starting material fro the production of fGO. Funcionlized graphene Oxide has been produced with amine (to improve the compatibility of GO with SA) and with $Al(OH)_3$ and melamine to enhance FR capability of GO.

4.3.1 Amine Functionalization

fGO functionalization was attempted with the following nitrogen containing compounds: ammonium formate (NH_2OCHO), ethylenediamine (ED), tetraethylenepentamine (TEPA) and branched polyethylenimine (pN), with the main objective of inducing a neat positive charge on the surface of GO. Initial precursors concentration were calculated in order to maintain constantthe final ratio of NH_2/g_{GO} equal to 0.166 mol/g_{GO} (*i.e.* theoretical final primary amine concentration), with a 100% theoretical reaction yield.

Ammonium Formate-fGO (fGO-NH3)

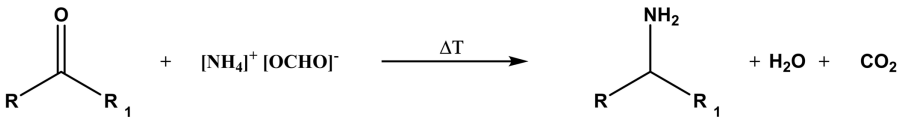

Figure 4.1: Reductive amination reaction of ketones, Keuckart reaction.

Amination of GO with ammonium formate (NH_2OCHO) was conducted with a method reported in literature through reductive amination of ketones groups of GO via Leuckart Reaction[Fig. 4.1][215]. First, 100mg of GO powder and 0.5g of ammonium formate were mixed together in a mortar and transferred in a round bottom flask fitted on a condenser. The temperature was raised up to 135 °C and maintained for 4 h. Afterwards, the reacted GO was collected and repeatedly vacuum filtered (0.45 μm PTFE omnipore membrane) with milli-q water until neutral pH of the filtered solution was reached. Final product was labeled fGO-NH3-5. Following the same procedure fGO-NH3-10 was also synthesized, the final number represent the Ammonium Formate/GO initial weight ratio). The theoretical final primary amine concentration was theoretically obtained in fGO-NH3-5 sample. Control reaction, labeled fGOctr-135°C was performed wollowing he same described procedure but without the addition of ammonium formate.

Amine-fGO (fGO-ED),(fGO-TEPA),(fGO-pN)

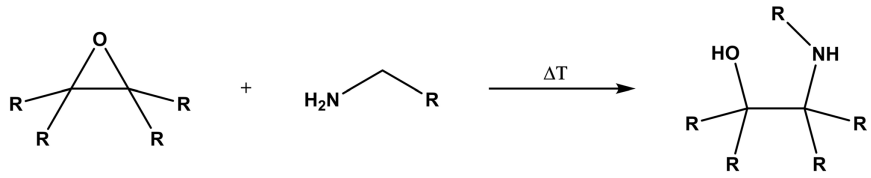

Figure 4.2: Graphene, Graphene Oxide (GO) and reduced Graphene Oxide (rGO) structure and synthesis route, from[210].

Due to the high reactivity of amine toward oxygenated moieties, amine functionalization of GO with ethylenediamine (ED), tetraethylenepentamine (TEPA) and branched polyethylenimine (pN) was conducted via simple epoxy ring opening of GO, with a method adapted from literature[Fig. 4.2][216]. To produce fGO-ED, $1g$ of ethylendiammine was dispersed, togheter with $100mg$ of GO in 100 mL of ethanol in a round bottom flask and sonicated for 40 min. The flask was therefore fitted on a condenser and the reaction was maintained, under stirring at 80 °C, for 24 h. Subsequently the mixture was washed by vacuum filtering (0.1 μm PTFE omnipore membrane) in clean ethanol, methanol and acetone and then dried in vacuum overnight to finally get the fGO-ED. The complete elimination of unreacted amine was assessed through stabilization of total nitrogen concentration ($\%_{wt}$) determined with XPS. The same method was used to graft tetraethylenepentamine (TEPA) and branched polyethylenimine (pN) to GO, respectively labeled fGO-TEPA and fGO-pN. Calculation for maintaining the theoretical final primary amine concentration were based on the fact that only one primary amine is required for grafting. An average value of amine 0.5 amine for each monomer unit was used to calculate initial pN amounts. Control reaction, labeled fGOctr-80°C was performed wollowing he same described procedure but without the addition of any amine.

Melamine-fGO (fGO-MEL)

fGO-MEL was produced by dispersion of 4.1 g of melamine in 200 ml of milli-q water at 80 °C until a clear solution is obtained before that 100 mg GO was added.

The mixture was sonicated, maintaining the temperature at 80 °C, and then fitted on a condenser to react at 90 °C for 24 h. To wash out the un-reacted melamine the solution was washed several times with hot water (80 °) via vacuum filtering (0.1 μm PTFE omnipore membrane) to obtain fGO-MEL. The product was then placed under vacuum drying, overnight. The complete elimination of un-reacted melamine was assessed through N-fraction determination with XPS.

Table 4.3: list of nitrogen fGO produced in this work

Code	**Parameters (T [°C] - solvent - time)**	**N-rich precursor**
fGO-NH3	135°C - dry - 4h	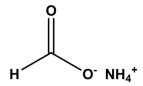
fGO-ED	80°C - EtOH - 24 h	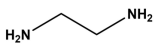
fGO-TEPA	80°C - EtOH - 24 h	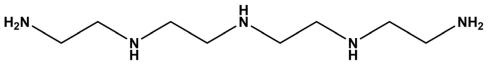
fGO-pN	80°C - EtOH - 24 h	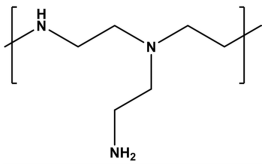
fGO-MEL	90°C - H_2O - 24 h	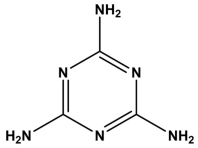

4.3.2 Aluminium Hydroxide Functionalization

Aluminium Hydroxide $Al(OH)_3$ was deposited on GO surface, to produce fGO-Al, via hydrolyzation of $Al_2(SO_4)_3 \cdot 16H_2O$ and subsequent nucleation and precipitation over GO surface. $Al_2(SO_4)_3 \cdot 16H_2O$ was dispersed in 100 mL milliq-water and $NH_{3,liq}$ was added until a clear solution was obtained at pH 11. GO was dispersed in 100 mL of mill-q water and added to the $Al_2(SO_4) \cdot 16H_2O$ solution. The mixture was then sonicated at 50°C for 50 min before being placed in oil bath un-

der vigorous stirring at 90 °C for 60 min. After 12 h the supernatant was decanted off and the grey suspension at the bottom was centrifugated and the pellet was collected until neutral pH was obtained. The pellet was subsequently re-suspended in water and vacuum filtered (0.45 μm PTFE omnipore membrane) several times until no trace of SO_4^{2-} were detected with $BaCl_2$ test. fGO-AL powder was then collected, after ethanol and acetone filtering and vacuum dried overnight.

4.4 Characterization Techniques

4.4.1 Rheometry

Rheology is a branch of physic that studies the flow and the deformation of matter and it find wide applications in polymers technology and in the study of viscous solution suspensions. As a matter of fact, the viscosity of a fluid is not an intrinsic property of a system (depending, for example, on the sole temperature and concentration) but it also depends on the nature of the applied mechanical load (*i.e.* static or dynamic stress) and on the microstructural arrangement of the system. The so-called *Newtonian fluids model* adopts a constant value of viscosity which is independent on the mechanical load applied and is well suitable for interpreting the behavior of low molecular weight fluids but fails in describing complex behaviors typical of structured system arising from the re-arrangement of long polymeric chain under over wide shear stress range, or different frequency loads, or the aggregation of nano or micro constituents. Shear Viscosity is defined as the ratio between the shear stress and the shear rate applied to a viscous system(Eq. 4.1) and can be used to describe (non-time dependent) non-linear behavior of viscous solutions:

$$\eta(\dot{\gamma}) = \frac{\tau(t)}{\dot{\gamma}} \tag{4.1}$$

In [Fig. 4.3] the general behaviors that Non-Newtonian fluids can produce (not taking account for time-dependent behaviors) as a function of shear stress rate applied are represented. *Dilatant* behavior is, for example, typical of highly dense nanoparticle dispersion in polymers solution that tends to hinder the mobility of

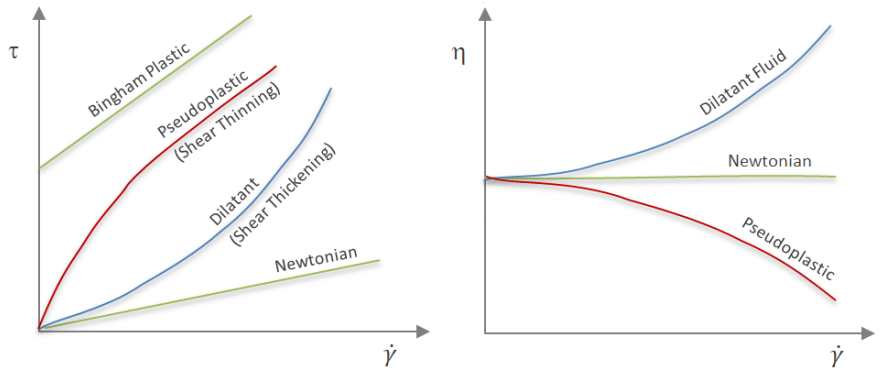

Figure 4.3: Representation of non-time dependent fluid behavior, from[217].

the polymeric chain at high stress. *Pseudo Plastic* behavior, on the contrary, is the most common response that polymers shows under high shear rate: this is due to the disentanglement of polymeric chains and their re-arrangement parallel to the direction of the flow, which reduce the viscosity of the system as depicted in 4.4. Differences on the polymer molecular weight (MW) and on the polymeric weight distribution (MWD) also affect the viscoelastic behavior of fluids and the pseudoplastic regime. As it can be seen in [Fig. 4.4], polymeric solutions of the same polymer having higher MW possess an higher zero-low shear viscosity (η_0) whereas a narrow distribution of the MWD drastically affecs the shear thinning regime which shift to higher shear rate with a reduced broadening. The Cross model can be used to correlate the flow curve (shear viscosity vs shear rate) and was used to fit the flow curves for oAG and rAG sample in order to have information about possible degradation of the alginate as a consequence of the recycling process which was subjected[219] (Eq. 4.2):

$$\eta(\dot{\gamma}) = \eta_\infty + \frac{\eta_0 - \eta_\infty}{1 + (\tau \cdot \dot{\gamma})^m} \tag{4.2}$$

where η is the viscosity at the shear rate s, η_0 and η_∞ are the extrapolated viscosity at zero and infinite shear rate, respectively. τ is the shear rate $[1/s]$ at which the viscosity assumes the mean value. m is the exponential fitting parameter, which

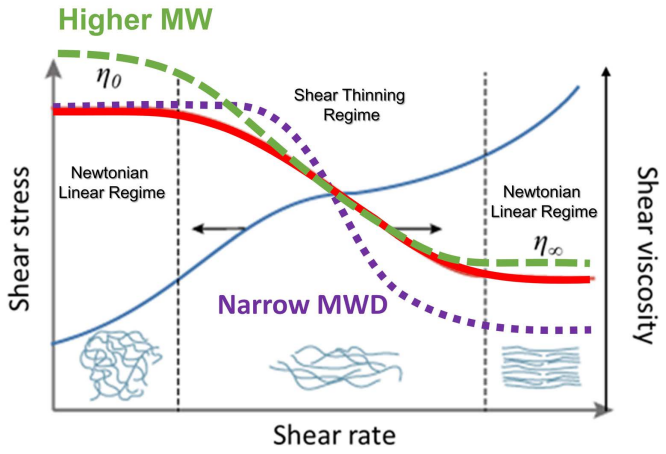

Figure 4.4: Non-newtonian shear thinning behavior, flow curve representation. Different regimes and influence of the molecular weight (MW) and molecular weight distribution (MWD) are displayed. Adapted from[218].

is inversely proportional to the polydispersity index (PI) of the polymer (Eq. 4.3):

$$m \propto (PI)^{-1} = \left(\frac{M_w}{M_n}\right)^{-1} \tag{4.3}$$

where M_w is defined as the weight averaged molecular weight and M_n is the number averaged molecular weight.

Structural informations, such as sol-gel transition and nano-filler exfoliation, can be inferred from oscillatory rheometry test, in which loads (or strains) are applied sinusoidally (with an angular frequency ω). In such a system the viscous component leads to a out-of-phase strain (or stress) response, hence it is easier to separate the elastic response, with the storage modulus (G'), from the viscous response, with the the *loss-modulus* (G''), by decoupling their contribution:

$$\gamma(t) = \gamma_0 sin(\omega t) \tag{4.4}$$

$$\sigma(t) = \gamma_0 \left[G'(\omega) sin(wt) + G''(\omega) cos(\omega t)\right] \tag{4.5}$$

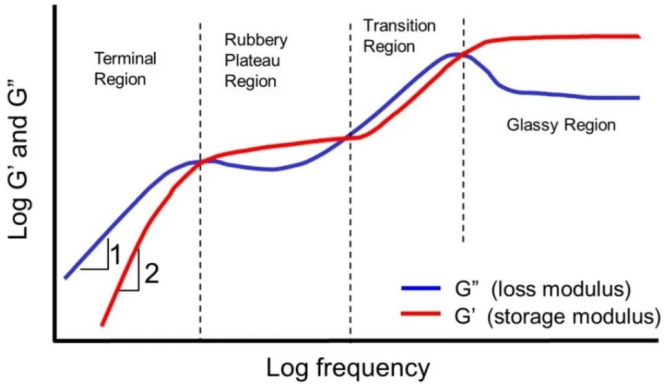

Figure 4.5: Typical Mechanical spectrum of a viscous polymeric solution, from[220].

and from which complex viscosity con be defined ($|\eta^*|$):

$$|\eta^*(\omega)| = \frac{\sqrt{G'(\omega) + G''(\omega)}}{\omega} \tag{4.6}$$

Frequency-Sweep test, in which the system response is recorded during the application of a variable frequency stress-load (in the linear regime), have been used to asses the behaviors of alginate gels and solution. By investigating the low frequency region of the mechanical spectrum, (*i.e.* the terminal zone), it is possible to obtain information about the long-range polymeric chain-chain or chain-filler interactions. Gelled systems posses high elastic response ($G'' < G'$) with the value of G'' and G' that are independent of the angular frequency whereas viscous polymer solutions usually respectively show a linear ($G'' \propto \omega$) and a quadratic ($G'' \propto \omega^2$) relation of the storage and loss modulus with the frequency[Fig. 4.5]. Nano-filler interaction with the polymeric chain contribute to the increase in system viscosity toward the building of a gel-like structure, which correspond to the creation of a long-range interconnectivity (rheological percolation) continuous mechanical with the slope of $G''(\omega)$ and $G'(\omega)$ approaching zero.

A rotational rheometer was used to characterize the visco-elastic response of the original and recycled material, in order to highlight the influence of 2Na-EDTA concentration and of the use of additional $CaCO_3$ and HCl in the recycling process(Par. 4.2). To prevent interferences derived from the dispersed particulate, the

rheological characterizations were performed on samples that had been prepared as previously described, but without the addition of fiberglass powder (oAS, rAS and rAG and oAG). Different concentration of 2Na-EDTA were tested: 15 mM and 45 mM. Since a single de-protonated EDTA molecule ($EDTA^{4-}$) is capable of chelating a single Ca^{2+} ion; the tested concentration corresponded respectively to one and three equivalents of Ca^{2+} present in the original sample (15 mM). Steady-state shear viscosity (flow curves) was used to characterize the homogeneous solution obtained after the dissolution of the dried foam (rAS samples); 2 mL of solution were sampled to this purpose. A clean sodium alginate solution at the same concentration and pH (7.5) of the previous has been used as reference. The Cross model was used to fit the flow curves (Eq. 4.2)[219]. The mechanical behavior (*i.e.* the mechanical spectrum) of the re-formed gels (rAG samples) was determined by performing a dynamic frequency sweep test (FS) within the linear stress regime (2 Pa) previously identified with a short stress sweep test (f =1 Hz; stress range 2-5 Pa; maximum deformation <0.02 %). The viscous (G'') and the elastic (G') components of the mechanical response were then calculated for each sample. A clean sodium alginate gel (AG) has been used as reference. With the same approach, GO-solution, prepared as described in (Par. 4.1.1), where characterized by dynamic frequency sweep test. All the rheological tests were performed at 25 °C using the controlled stress rheometer Haake Mars III equipped with Peltier temperature control system and using the cone–plate geometry (flow curves) and a cross-hatched plate–plate geometry (frequency sweep and stress sweep).

4.4.2 Thermal-Characterization

Specific heat capacity (c_p) and thermal conductivity (λ) of oAF and rAF samples have been measured using a Heat Flow mether apparatus (NETZSCH HFM 446 Lambda Series), according to ASTM C518 and ASTM C1784 standards. Each sample was tested immediately after the completion of the lyophilization cycle. The typical sample size was 200 mm × 200 mm × 18 mm. To ensure a proper contact between the specimen and the sampling area of the instrument, a 2 kPa load was applied. Thermal conductivity was calculated using a steady-state Fourier model at an average temperature of 20 °C and 40 °C. Specific heat values were cal-

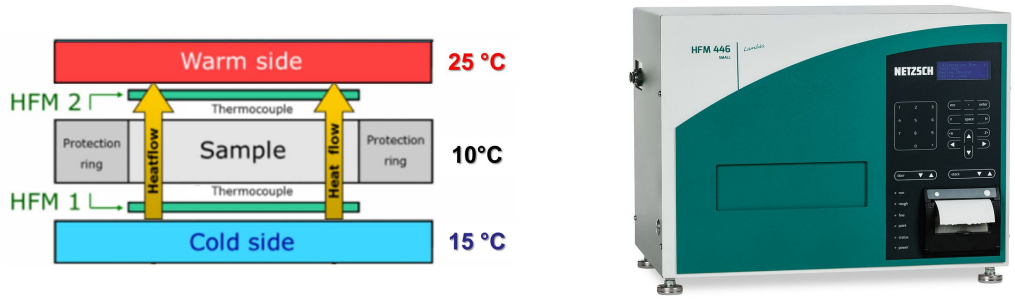

(a) Heat Flow Meter apparatus **(b)** NETZSCH HFM 446 Lambda Series

Figure 4.6: Images taken from [221]

culated by integration of the heat flux over time at an average sample temperature of 20 °C and 30 °C. Sample apparent density (ρ) was automatically calculated by the system, on previously weighed sample and thermal diffusivity (α) was calculated as follow:

$$\alpha = \frac{\lambda}{\rho c_p} \tag{4.7}$$

4.4.2.1 Material Index

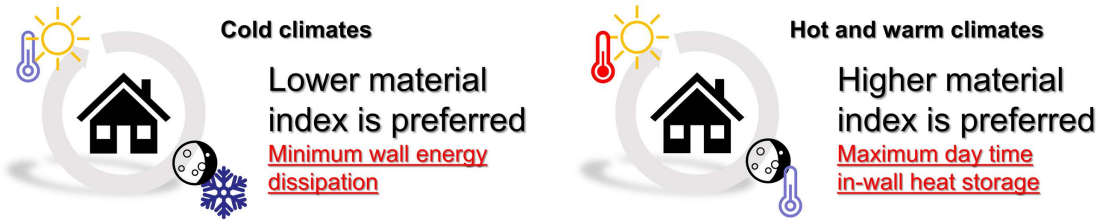

Figure 4.7: Material indexes scheme.

A material index that group specific material properties values, as defined by M. Ashby in (Ch. 6 [222]), was used to rank the oCAF and rCAF with respect to other TIMs depending on their use in different climate zones: in a hot/warm climate, characterized by a large diurnal temperature excursion, an optimal thermal insulation solution is represented by a system capable to take advantage of the passive

solar heating, by simply storing thermal energy inside the wall for then releasing it during the night without heating the internal premises. In a cold climate, on the contrary, where environmental temperature are constantly below the comfort level such a strategy cannot be applied and a high heat capacity of the wall can be unfavourable. In the latter case, the total energy flux (per unit area) expression contains two terms (Eq. 4.9): the first takes in account the heat losses due to conduction through the wall and the second due to absorption by the insulation material in the time interval t.

$$K_n = \frac{k_B T}{\sqrt{2}\pi d_g^2 P_g \delta} \tag{4.8}$$

$$Q_{cold} = \frac{\lambda \Delta T \ t}{w} + \frac{c_p \rho w (\Delta T)}{2} \tag{4.9}$$

ΔT is the difference between the internal and external temperature ($\Delta T = T_i - T_e$) whereas w is the insulation thickness. By differentiating (Eq. 4.9) with respect to the wall thickness the optimum value (which depends on the selected insulation material) is obtained and can be substituted to obtain a new expression for Q_c (Eq. 4.11).

$$w_{cold} = \left(|w|_{\frac{\partial Q_{cold}}{\partial w}=0} \right) = (2\alpha t)^{\frac{1}{2}} \tag{4.10}$$

$$Q_{cold} = (T_i - T_e)\,(2t)^{\frac{1}{2}}\,(\lambda\ c_p\ \rho)^{\frac{1}{2}} \tag{4.11}$$

The heat losses can therefore be minimized by selecting the material with the **lowest value of M_c**:

$$M_h = (\lambda c_p \rho)^{\frac{1}{2}} \tag{4.12}$$

On the other hand, to reduce energy losses and to take advantage of the warm daily temperature and cold night, a time dependent approach to the heat diffusion is needed: a high thermal mass is needed to slow down the diffusion of the heat

through the wall such that the heat front need a time t to reach the opposite side of the wall. Through this time-lapse, energy is stored inside the wall and is equal to:

$$Q_{hot} = w\ \rho\ c_p\ \Delta T \tag{4.13}$$

where ΔT is equal to the temperature gradient between the wall. The insulation thickness (w), in this case, is chosen so that it equals to the distance (across the wall) that the heat front crosses in the time lapse t (Eq. 4.14). In first approximation this is expressed in eq. 8. In such a way it takes t for the heat front to reach the inside surface of the wall during the day before the external temperature change and so the heat flux direction (in a warm-day/cold-night semi period $t = 12h$).

$$w_{hot} = \sqrt{\rho\ c_p\ t} \tag{4.14}$$

As it has been done in the previous example, by substituting (Eq. 4.15) in eq. (Eq. 4.14), a new expression is obtained:

$$Q_{hot} = \Delta T \sqrt{2t}\,(\lambda c_p \rho) \tag{4.15}$$

In this case, since (Eq. 4.15) refers to the maximum heat that can be stored in a unit area of the insulated wall, to minimize the heat losses Q_{hot} must be maximized. The material index is the same of the previous example but in this case it has to be maximized: therefore this can be done by selecting a material, with the **higher material index value $\boldsymbol{M_h}$**:

$$M_h = (\lambda c_p \rho)^{\frac{1}{2}} \tag{4.16}$$

The two cases share the same material index $\boldsymbol{M = (\lambda c_p \rho)^{\frac{1}{2}}}$ but in the cold scenario, where a rigid weather is present, the best TIM is selected such as it posses the lower value whereas in temperate hot-warm climate the best TIM is the one which posses the highest index value.

4.4.3 Compression test

Compression tests were performed using a Shimadzu Autograph 2,AG-10TA equipped with a 100 kN load cell with a constant compression speed of 1.3 mm/min. The tested samples had a square shape with an average side length of 50 mm and an average thickness of 18 mm. The compression modulus was determined by the linear deformation regime in the stress-strain curve. Different conditioning procedures were tested to highlight the effect of moisture uptake:

- dry: after conditioning for 24 h in a ventilated oven at 45 $\circ$C
- 40RH: conditioning in a 44 % RH environment (using a K_2CO_3 saturated solution). The samples, weighted at regular intervals, were tested after that a plateau in the percentage weight gain was reached.

Data processing was performed according to ASTM D 1621 standard.

4.4.4 Sound Absorption - Kundt's Apparatus

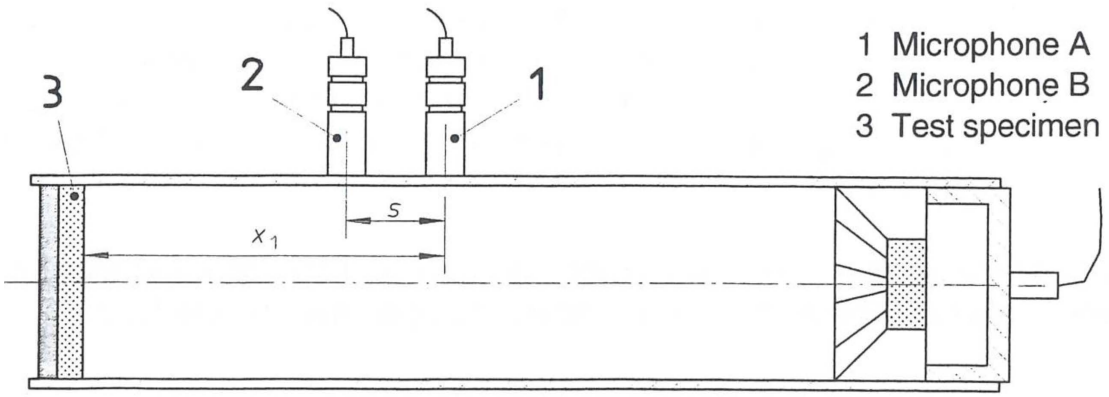

Figure 4.8: Impedance tube geometry, from ISO 10534-2:1998

Sound absorption analysis was performed with a Kundt tube apparatus (impedance tube) with an internal diameter of 45 mm according to ISO 10534-2:1998 and ISO 11654:1998. Sound absorption of a porous material can be calculated by recording the pressure field that is generated from the interference of the reflected and the generated wave by the use of the complex acoustic transfer function[223]. The

specimen is placed at one end of a closed tube, in close contact with a rigid backplate, and having, at the closed opposed extremity, a sound source capable, thanks to the tube geometry, of producing a plane wave spanning the range of the testing frequency. Two microphones are then present near to the surface of the sample which are needed to sampling the pressure field inside the tube.The absorption coefficient is then calculate as a function of the frequency (100 - 4000 kHz). Tests were performed in triplicate, for each sample, oCAF and rCAF, with a constant thickness of 18 mm.

4.4.5 XRD

X-ray diffraction was used to asses the presence of $Al(OH)_3$ in fGO-AL samples. X-Ray Diffraction (XRD) patterns were recorded on a Bruker D5005 diffractometer operating at 40 kV and 20 mA using Cu K_α (E = 8.04 keV; λ = 1.5406 Å) as X-Ray source.

4.4.6 TGA

Thermogravimetric analysis (TGA) was used to characterize fGO-ED, fGO-NH3, fGO-TEPA and fGO-pN samples. TGA is a widely used technique that use a small amount of sample ($\approx 0.5\ mg$) to detect its weight loss during a slow heating ramp. By taking advantage of this information it is possible to asses the thermal stability of the material (in ambient air or N_2 atmosphere). Differently from graphene, which is stable up to $\approx 1000°C$ oxygen moieties on GO surface lead to thermal decomposition and weigth loss, for this reason the presence of amine on GO surface can be assessed only by comparison against pristine GO in N_2 atmosphere. TGA were performed under N_2 atmosphere (25 mL/min flow rate) using a TGA Discovery (TA Instruments). The samples ($\approx 0.5\ mg$) were equilibrated at 100 °C for 20 min and then heated 10 ° C/min before running the measurement up to 800 °C. Separately, fGO-Al (15 mg)was analysed in ambient air atmosphere to evaluate the weight fraction of inorganic oxides residue using a STA 429 EP Netzsch in air with a heating rate of 10 ° C/min, in alumina crucibles, up to 800 °C after 24 h of vacuum conditioning.

4.4.7 DSC

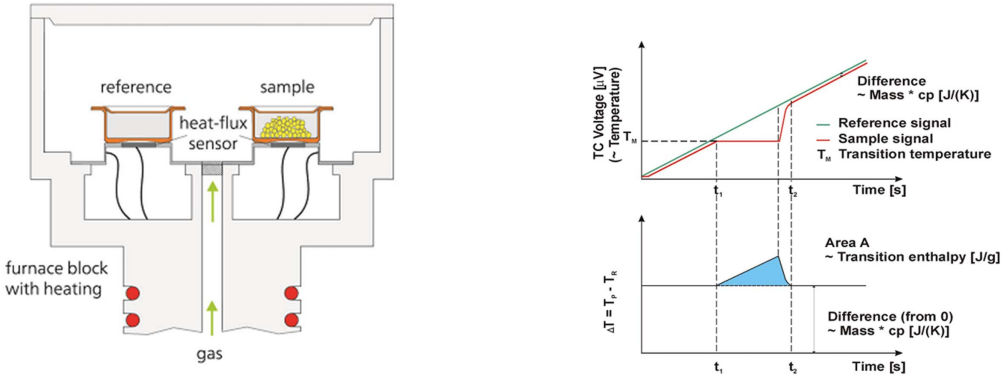

(a) DSC chamber

(b) DSC working principle.

Figure 4.9: Images taken from [224]

Differential scanning calorimetry is a useful characterization technique used to acquire quantitative information on endothermic or exothermic reactions that take place during the controlled heating (or cooling) of a sample. In such a way transition temperature of polymers, endothermic decompositions of hydroxides or, in general, phase and physical transformation can be followed determining quantitatively their relative calorific values (endothermic or exothermic). The working principle of DSC is simple: a small quantitative of sample is usually needed ($\approx$ mg) and it is placed (in a crucible) in a controlled furnace over a heat-flux sensor, beside a reference sample (normally an empty crucible). The two samples are then heated and the temperature difference between the sample and the reference, together with the heat-flux exchanged between the heater and the sample, is recorded. In this way, by differentiating the two signals, an endothermic (upward) or an exotermic (downward) peak is generated and by mean of accurate system calibration the area is correlated with the transformation's energy[Fig. 4.9].

DCS was mainly used to evaluate the $Al(OH)_3$ mass fraction of fGO-AL samples. Differential Scanning Calorimetry (DSC) has been performed with a Netzsch DSC 200 F3 Maia® differential scanning calorimeter. 10 mg of each sample was weighted and placed within closed aluminium crucibles, and heated, 10 $^\circ$ C/min, from room temperature up to 500°C. DSC traces have been analysed with Netzsch Proteus – Thermal Analysis – Version 6.1.0.

4.4.8 μ-CT

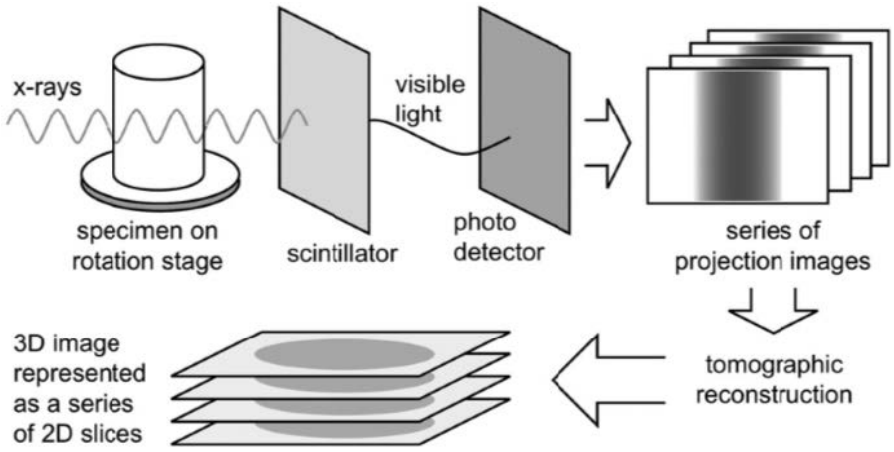

Figure 4.10: Schematic illustration of μCT image acquisition and reconstruction process, taken from[225]

X-ray micro-computed tomography (μ-CT) technique has its roots in medical computer tomography (CT) which in turn is based on X-ray radiography. The basic physic principle is the Beer-Lambert law applied to X-ray (Eq. 4.17) which gives the number of transmitted photons N_1 of energy E, with respect to the number N_0 of incident photons, as a function of the attenuation coefficient $\mu(s)$ integrated through the space that the X-ray cross:

$$N_1/N_0 = exp\left[-\int_{S \in ray} \mu(s)ds\right] \tag{4.17}$$

with μ that varies across the space S as a function of the density (ρ) and the atomic number (Z) of the different materials that the X-ray crosses through its path:

$$\mu(x, y, z) \propto K\rho\frac{Z^4}{E^3} \tag{4.18}$$

with K being a constant. The dependencies of the attenuation coefficient with respect to the materials properties gives the possibility to resolve heterogeneous structures in the projected image acquired by a detector positioned behind the sample. In addition, if a polychromatic source it is used, (Eq. 4.17) has to be

integrated across the spectrum. Despite a single X-ray radiography can give only a bi-dimensional information, which is a single plane projection, CT overcome this problem by taking multiple acquisition, rotating the specimen on a orthogonal plane (with respect to the detector plane) therefore being able to compute the local (in space) value of the attenuation coefficient, reconstructing in this way a three dimensional representation of the object[Fig. 4.10]. Common medical CT possesses a resolution of 300μm limited from X-ray source, optical and sample size constrains (*i.e.*human-body)[225]. The spatial resolution of the image is primarily affected by the geometry of the x-ray beam and by the technological characteristics of the detector: point-wise X-ray sources reduce the *penumbral blurring effect* of each image improving its quality. Another important factor is the image magnification factor, which is the ratio between the real dimension of the specimen and that of its projection on the detector plane: it strongly depends on the geometry of the beam and for conical shaped beams (e.g coming from pointwise radiation source) it is equal to the ratio of the distance between the source and the specimen and the distance of the specimen from the detector. It can therefore be deduced that a higher magnification results in a reduced scanned volume. Typical scanning volumes of micro-CT system may vary from few millimeters up to few centimeters[225]. μ-CT of samples, oAF and rAF, was obtained by means of a custom-made cone-beam system called TOMOLAB (Elettra, Trieste). μ-CT acquisitions were performed with a resolution of 8 μm, beam energy of 40 kV and intensity of 200 μA, and an exposure time of 2.5 s. The slices reconstruction process and the correction of artefacts were realized by a commercial software (Cobra Exxim) on a core portion of each sample (5 mm x 5 mm x 5 mm). Pore3D software [226] was used for the quantitative analyses. Amira software (Thermo Fisher Scientific, Waltham, USA) was used for the 3D rendering.

4.4.9 Porosity

Due to the limited reconstructed scanned size (5 mm x 5 mm x 5 mm) obtained from μ-CT, porosity (P) has been calculated separately according to (Eq. 4.19) for oCAF and rCAF samples. The bulk density ρ_b was calculated according to Archimedes principle in hexane, to overcome swelling problems. A thin film was

produced according with (Par. 4.1) and (Par. 4.2), respectively for oCAF and rCAF porosity determination, completely avoiding the freeze drying step and using oven drying (48 h at 50 °C) to obtain a collapsed structure. By measuring the dry (D) and wet (W) weight, in hexane, sample porosity can be calculated (Eq. 4.19) ($\rho_{hexane} = 659.5\ kg/m^3$ at 20 °C). Apparent density ρ_a was calculated by weight and volume measurement of standard samples as described in (Par. 4.4.2).

$$P = 1 - \left(\frac{\rho_a}{\rho_b}\right) \tag{4.19}$$

$$\rho_b = \rho_{hexane}\left(\frac{D}{D-W}\right) \tag{4.20}$$

4.4.10 Kaiser Test

Kaiser test (KT) is a colorimetric test, traditionally used in heterogeneous peptides synthesis, that provides qualitative and quantitative information about the presence of free primary amino groups. In [Fig. 4.11] the KT mechanism is depicted: the test involves the reaction of a primary amine (bonded to a secondary carbon) with a solution of ninhydrin, producing in such a way a characteristic dark blue product which can quantitatively be determined by UV-VIS-absortion at λ=570 nm according to (Eq. 4.21)using a JASCO V-630Bio UV-Vis spectrophotometer. KT was performed using a commercial kit purchased from Sigma Aldrich, composed of three solutions:

- **S1** 80 $g$of phenol in 20 mL of EtOH
- **S2** 2 mL of KCN 1 mM in H2O in 98 mL of pyridine;
- **S3** 1 g of ninhydrin in 20 mL of EtOH.

For the determination of primary amines ($F_{Am} = \mu mol/g$) 0.5 mg of sample (fGO) were added to 75 μL of S1 and 100 μL of S2 and sonicated, in a bath sonicator, for 15 min. Afterwards, 75 μL of S3 were added and the mixture was heated at 120 °C for 10 min, turning blue if primary amine were present. Later, the mixture was diluted to a final volume of 3 mL, with a 60% EtOH water solution, and

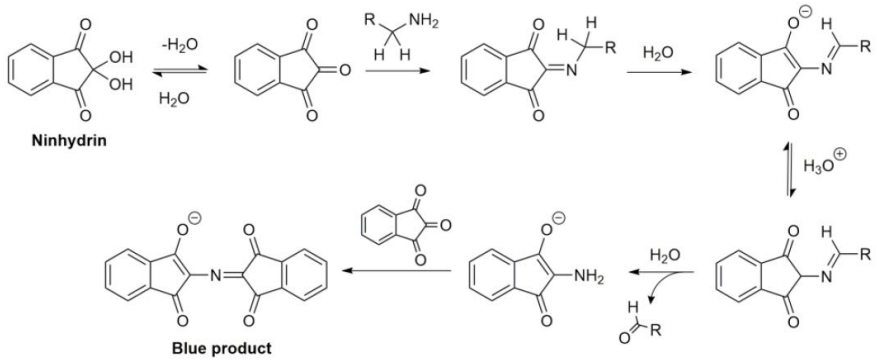

Figure 4.11: Schematic illustration of Kaiser Test mechanism

centrifugated for 5 min before UV-Vis determination of F_{Amm} accdording to (Eq. 4.21).

$$F_{Am}\ [\mu mol/g] = \left[\frac{Abs_{570nm} \cdot V \cdot 10^6}{\epsilon \cdot m}\right] \tag{4.21}$$

where V is the final volume after the dilution (3 mL), ϵ is the extinction coefficient (15000 $M^{-1}cm^{-1}$) and m is the weight of the sample in mg. KT was replicated twice for every sample. KT was used to asses the presence of free primary amino group in fGO-NH3, fGO-ED, fGO-TEPA and fGO-pN samples. Amine groups in fGO-MEL sample cannot be detected due to the fact that amine are not bonded to a secondary carbon.

4.4.11 Z-potential

Z-potential is a common characterization technique used to asses the elektrokinetic potential of colloidal systems or dispersion in solution: an external electric field is applied to a capillary cell, by means of two electrodes, in which the sample resides and, by using a laser Doppler velocimeter, the electrophoretic mobility (U_E) of particle migration toward the opposite charged electrode is acquired, which is then used to calculate the zeta potential by applying the Henry equation(Eq.

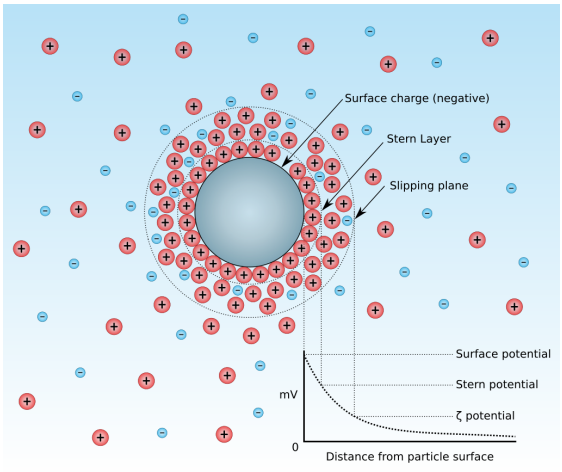

Figure 4.12: Charged state of colloidal particle in solution.

4.22):

$$U_E = \frac{2\ \epsilon\ \zeta}{3\ \eta}\ \mathfrak{f}(ka) \tag{4.22}$$

Where, ϵ is the dielectric constant, η is the viscosity of the solution and $\mathfrak{f}(ka)$ is the Henry's function[227]. Zeta potential of Go, fGO-NH3, fGO-ED, fGO-TEPA and fGO-pN was acquired by diluting each sample in Milli-q solution at a concentration of 0.1 mg/mL and by adding 15 mM of NaCl to stabilize the solution ionic strength at pH 7. The measurement was acquired with a Malvern Panalytical Zetasizer Nano ZS.

4.4.12 TEM

Transmission electron mycroscopy was used to characterize all GO and fGO sample. Each samples was previously dispersed in water, 0.1 mg/mL, and then deposited over a previously plasma treated Lacey carbon (400 mesh) Copper TEM grid. TEM was carried out on LaB6-TEM of type JEOL JEM-1400PLUS ($40kV$ - $120kV$) equipped with a GATAN US1000 CCD camera (2k x 2k).

4.4.13 SEM

A 10 $mm \times 10\ mm \times 10\ mm$ volume was extracted from the centre of the sample (oCAF and rCAF), and images were collected using a Leica-Stereoscan 430i Scanning Electron Microscope (SEM).

4.4.14 XPS

X-rays photoelectron spectroscopy (XPS) is a quantitative spectroscopic technique commonly used to perform surface elemental analysis in vacuum. X-rays are used to excite and emit core-level electrons from the surface atoms ($\approx 10nm$) of the sample. These electron are then extracted a passed thought a variable kinetic energy selector before being detected by a electron multiplier detector. In this way, by collecting simultaneously the kinetic energy and the counting of the photoemitted electron quantitative information about elemental composition, chemical state are acquired since the single electron binding energy (peculiar of the chemical state of each element) can be easily calculate by knowing the exciting X-ray photon energy jointly with a calibration factor.
XPS was used to confirm amine functionalization on fGO sample. The analyses were carried out with a SPECS Sage HR 100 spectrometer with a non-monochromatic X-ray source of Aluminium with a K_α line of 1486.6 eV energy and 250 W. The samples were placed perpendicular to the analyzer axis and calibrated using the 3d5/2 line of Ag with a full width at half maximum (FWHM) of 1.1 eV. An electron flood gun was used to compensate for charging during XPS data acquisition. The selected resolution was 30 and 15 eV of Pass Energy and 0.5 and 0.15 $eV/step$ for the survey and high-resolution spectra, respectively. Measurements were made in an ultra-high vacuum (UHV) chamber at a pressure below $8 \cdot 10^{-8}\ mbar$. Fitting of the XPS data were done using CasaXPS 2.3.16 PR 1.6 software: the Shirley-type background subtraction was used, and all curves were defined as a linear combination of Lorentzian and Gaussian. Atomic ratios were computed from experimental intensity ratios and normalized by atomic sensitivity factors.

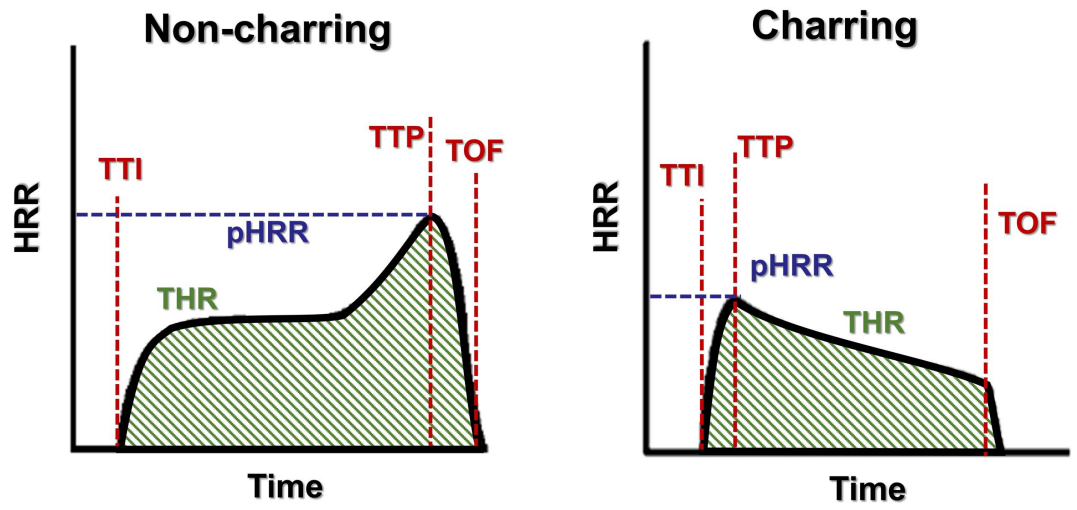

(a) Non-Char forming polymer **(b)** Char forming polymer

Figure 4.13: Typical HRR curves and related parameters

4.4.15 Cone Calorimetry (CC)

As anticipated in (Par. 2.1), cone calorimetry (CC) is a standardized test (ASTM E1354 and ISO 5660) used to specifically characterize polymer fire behavior: the main calculated parameter is the heat release rate per unit of surface **HRR** (KW/m^2) which comes from the measurement of the decreasing oxygen concentration in the collected gasses evolved from a specimen subjected to a defined heat flux. This calculation is based on the quantitative Huggett's relation in which the heat release of a burning polymeric specimen is proportional to the consumed oxygen[228][229]. In addition to HRR, other parameters are obtained from CC test:

- Ignition time, or time to ignition (**TTI**), which is the time elapsed between the exposure of the sample to the irradiation and the development of flame.
- peak Heat Release Rate (**pHRR**), which is the maximum thermal power developend by the sample during combustion.
- Total Heat Released (**THR**), which is the integral of the HRR with respect to time expressed in kJ/m^2.

- Time of flame out (**TOF**), which is the time elapsed between the ignition time to the flame out.
- Mass loss and mass loss rate (**MLR**).
- Char yield ($\mathbf{C_y}$), which is the organic residue [%] after the test.

In [Fig. 4.13] two typical curves of a charring and a non-charring polymer are represented in wich the CC parameters are shown: non-charring polymers usually shows a gradual increase of the HRR, after the initial flame out until the pHRR at the end of the test where no material is left. Contrarily, the pHRR appears immediately after the initial flame out in charring polymer since after that char start to limit the combustion development. A Fire Testing Technology Limited FFT Cone Calorimeter model was used to characterize sample's fire behavior with a set radiant heat flux of 35 kW/m^2 with spark igniter. Tested specimen dimensions were 100 x 100 mm, with an exposed surface area of 88.4 cm^2, placed at a distance of 25 mm from the cone heater in horizontal position. At least 2 specimens for each formulation were tested : oCAF, rCAF-G, oCAF-GO2, rCAF-GO2, oCAF-ED and oCAF-NH3.

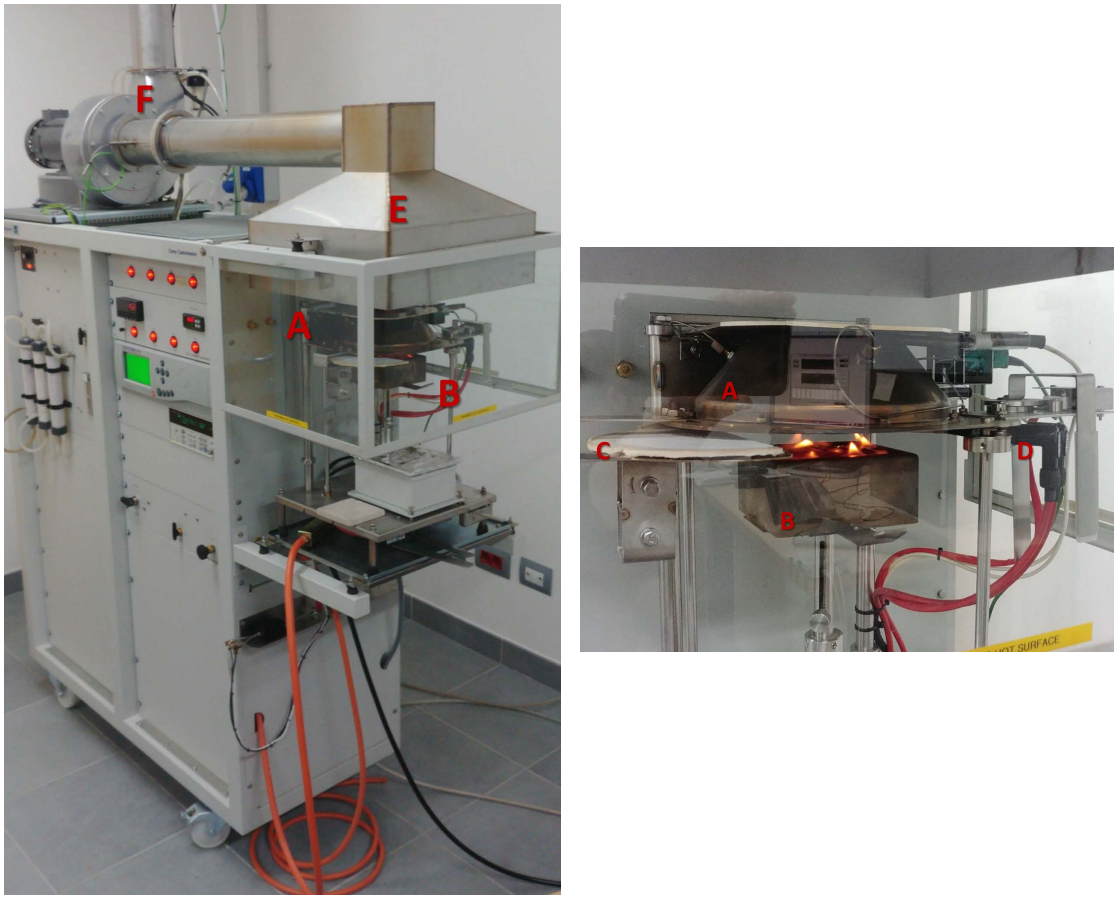

(a) Cone calorimeter apparatus **(b)** Cone calorimeter - Specimen holder

Figure 4.14: Cone calorimeter: **A** cone heater, **B** specimen holder, **C** removable heat shield, **D** spark igniter, **E** collecting gas hood, **F** gas sampling, sensors and fan system.

4.4.16 Micro Combustion Calorimetry (MCC)

Micro combustion calorimetry or pyrolysis combustion flow calorimetry is a technique capable of evaluating combustion behavior of polymeric a sample in limited amounts: if tens of grams are minimum required by CC, MCC test usually require *mg* size sample thus facilitating the analysis when only reduced amount of material can be provided. During MCC the sample is slowly heated under nitrogen atmosphere and the released gases are collected and separately mixed with pure oxygen before combustion, in this way the HRR can be calculated according to Huggett's relation. In MCC a new parameter is introduced, in addition to THR and pHRR

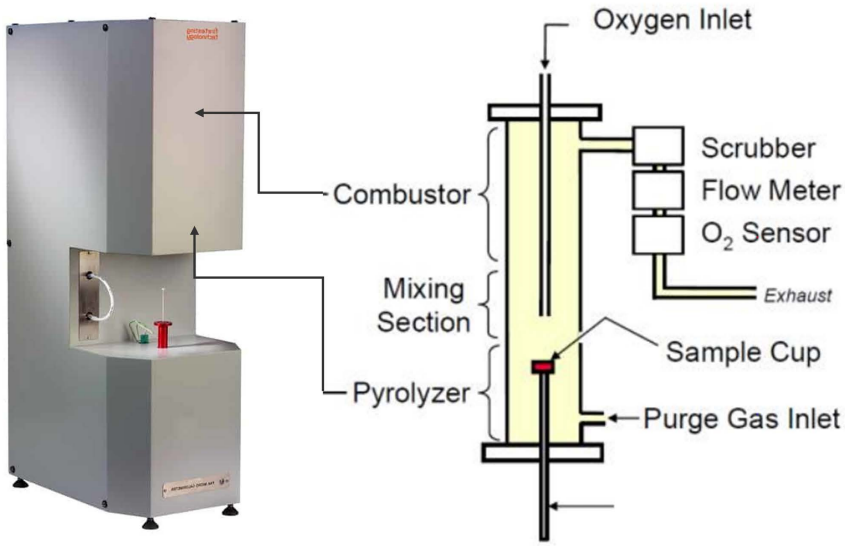

Figure 4.15: Micro (Scale) Combustion Calorimetry apparatus, image adapted from [230] and [231]

typical of CC test, which is the heat release capacity (**HRC**) corresponding to the value of the pHRR divided by the heating rate: such a parameter is independent of the heating rate and can be related to intrinsic characteristic of a material[232]. Due to the fact that the sample undergoes a complete pyrolysis in place of a combustion mechanism and extremely reduced sample size, MCC is little or no sensitive to physical flame retardant mechanism and HRC reductions tends to be always lower than pHRR reductions identified with CC techniques[232]. Therefore MCC was used, as a preliminary tool, to evaluate non-physical FR effects of GO in pure alginate foams (AF-GOx).

Microscale combustion calorimetry (MCC) was used to assess the flammability of small samples (mg) of AF and AF-GO foams. The sample was heated under nitrogen flow up to 750 °C at 30 $°C/min$.

Chapter 5

LCA

Life Cycle Assessment (LCA) is a powerful method which allows to describe the environmental impact of a specific product (service) by taking in to account the contribution of all the subsidiaries processes (enclosed in a well defined system boundary) which are connected to a single final product (service). This is done by defining a product system in which the main involved processes are defined (main unit processes) and an inventory (LCI) that includes all the resources that these processes requires (streams). After that, all the subsidiaries processes involved into the production (provision) of the required streams are linked to the main unit processes. The procedures herein adopted for the LCA evaluation and method presentation and description follow the ISO 14040[233] and ISO 14044[234] standards.

5.1 General goal and scope definition

In this work, 3 different *craddle-to-gate* LCA system have been analysed to compare the environmental impacts of the original production process against those associated with the recycling process, using an attributional approach. In this chapter these LCA studies will be defined whereas the detailed results will be presented in (Ch. 8), in the following section. In the first place, the environmental impacts associated with the production of rCAF samples were compared with

Table 5.1: Functional units calculated for PO, PR and PRI product systems.

R [m^2 K/W]	A [m^2]	λ [W/m K]	ρ [W/m k]	thickness [m]	Volume [m^3]	f.u. [kg]	Product System
1	1	0.04323	78.26	0.043	0.043	3.383	PO
1	1	0.04923	127.91	0.049	0.049	6.297	PR
1	1	0.04923	127.91	0.049	0.049	6.297	PRI

those derived from the production of oCAF. In this way, two distinct products systems were analysed: PO and PR, respectively modeling the original production process (as described in (Par. 4.1)) and the recycling process (as described in (Par. 4.2) in its rCAF-G variant) at the lab scale. Following, to have a broader understanding of the general impacts of rCAF production and to make the resulting calculated impact comparable with those of common TIMs, a third product system was studied: PRI in which the the rCAF-G production was up-scaled at the industrial level. In addition, a total of 7 different scenarios, applied to PRI, were calculated, by varying the renewable and non-renewable content of electric energy mix used. This was done to analyse the potential reduction of the environmental impact of PRI product system. To make the results of PO, PR and PRI comparable, a consistent functional unit (*f.u.*) was defined as the amount of material, in kg, needed to produce a panel of 1 m^2 having a thermal resistance equal to 1 $m^2\,K/W$ (Eq. 5.1):

$$f.u. = R\,\lambda\,\rho\,A \tag{5.1}$$

where λ is the thermal conductivity, ρ is the density and A is the area. The calculated values are presented in [Tab. 5.1]. All data, referred to each product system, have been acquired with respect to the a reference unit (*r.u.*) of 1 kg of final product and scaled up to the respective *f.u.* before performing LCA calculation (a detailed description of the data is presented, for each product system, in the respective LCIA). LCA allows to present the environmental impacts trough different indicator that groups together the calculated outputs, as described in the ILCD handbook[235][236] The mains *end-point* categories that have been used in this study are:

Primary Energy Usage

In this category the primary energies (direct and indirect), required by the process are calculated, divided in sub-categories depending on the source:

- Non Renewable (n-RER)
  - Fossil
  - Nuclear
  - Primary Forest
- Renewable (RER)
  - Biomass
  - Geothermal
  - Solar
  - Wind
  - Water

The summ of all the energy allow the determination of the prymary embodied energy. All contribution are expressed in terms of $MJ_{eq.}$

Climate Change

Climate change groups all the outputs and calculate their effects regarding the changes in the average global temperature. It is expressed in terms of Global Warming Potential over different time horizons, with the most common being 100 years (GWP100), using CO_{2eq} [kg] as reference unit.

Acidification

Acidification reflects the increase of *acid rain* formation due to the emission of acid gasses into the atmosphere, such as SO_x, NH_3 or NO_x, and the increase of pH level of soil and water. The model account only for the acidification caused by SO_2 and NO_x (according with the recommendation of the IPCC[1]) it is expressed in terms of SO_{2eq} [kg]

[1]International Panel on Climate Change

Resources (abiotic) This accounts for the reduction of non-biological (*i.e.* abiotic) resources such as fossil fuels, minerals or water. Weight factors consider the relative abundance of singular fluxes and it is expressed in terms of Sb_{eq} [kg].

Photochemical Oxidation The build up of ozone at the ground-level is dangerous and toxic to human life: it is formed by reaction between volatile organic compounds (*e.g. smallalkanes*) and NO_x in presence of uv-light (*e.g.* sun light) and heat. This category assesses the amount of ozone which is created as a result of process emission, evaluated in terms of O_3-formed [kg]

All the calculations have been performed using OPEN-LCA software and using *Ecoinvent v3.5* database as process provider. All the energy mixes used, extracted from *Ecoinvent v3.5* database, are based on the "*IEA World Energy Statistics and Balances report*" (IEA 2017 database [237]) and are representative of the energy production mix of each state for year 2014.

5.2 PO product system

In [Fig. 5.1] the scheme of the PO product system in which the lab scale production of oCAF is modeled is represented. The system boundaries extends from the Algae harvesting toward the production of the composite foam oCAF (with the final optimized composition described in (Ch. 6)) in a *cradle-to-gate* approach in which all the processes involved in the production and transportation of required chemicals, energy and raw materials used are included starting from primary resources (with some exceptions afterwards described). The PO product system is subdivided in five different main unit processes each of which possess its input and output streams inventory (LCI). The first two units, PO.1 and PO.2, account respectively for the algae harvesting and the alginate extraction process and their model (and relative data entries) were taken from the alginate extraction LCA study of Villanueva Rey[209][208] which was based on another alginate LCA study[238]. The harvesting and the extraction were modelled to take place in two separate locations of the European mainland continent and to be able to deliver the output

product (respectively the seaweed and the sodium alginate) in any location of the European mainland, for such a reason an european production energy mix was used, as energy provider (detailed energy mix composition is presented in [Tab. 5.10]), and transportation was included in each unit process (PO.1 and PO.2). In the first unit, PO.1, the algae is harvested by small boat operation and collected in the port where is stored and then shipped in refrigerated truck to PO.2 location. Boat and equipment maintenance together with fuel (*e.g.* *diesel*) consumption and emission and antifouling paint metal leaching were considered in PO.1. The extraction process in PO.2 was modelled on the basis of the previously described process (Par. 3.1.1.1) with secondary data obtained from lab scale extraction[209], chemicals production processes together with transportation to site were linked to PO.2. Transportation of sodium alginate in European mainland was accounted in PO.2 unit process. Equipment maintenance and allocated fabrication impact was not considered. In accordance with what prescribed by the ISO 14044 all generated waste were modelled and treated with suitable processes accounting the associated environmental impacts. The production process of oCAF foam, as described in (Par. 4.1) was subdivided in three system unit: PO.3, PO.4, and PO.5 respectively modelling step 1-3 (alginate solubilization and component dispersion), step 4 (hydrogel freezing) and step 5 (the lyophilization). Italian production energy mix was used in PO.3, PO.4 and PO.5 (detailed energy mix composition is presented in [Tab. 5.10]). For PO.3, chemicals production processes together with transportation to site were included with the exception of fibre-glass waste. Fibre-Glass waste enter in the PO.3 as an external boundary flux, without any link to its source process due to the fact that, as prescribed by ISO 14044, the associated environmental impacts of generated waste are allocated to the relative production process (*i.e.* fibre-glass production). As a consequence fibre-glass enter with a zero neat pending environmental balance. Transportation of fibre-glass to the oCAF production site were included in the system boundary. No equipment maintenance or fabrication allocated impact were considered in PO.3, PO.4 and PO.5 with the exception of the consideration of lubricant oil substitution of pumping system of the lyophilizator in PO.5. With the exception of those derived by all the sub-linked processes used (and present in the *Eco-invent* database), no allocation are presented in PO product system since no other products are delivered aside from

oCAF.

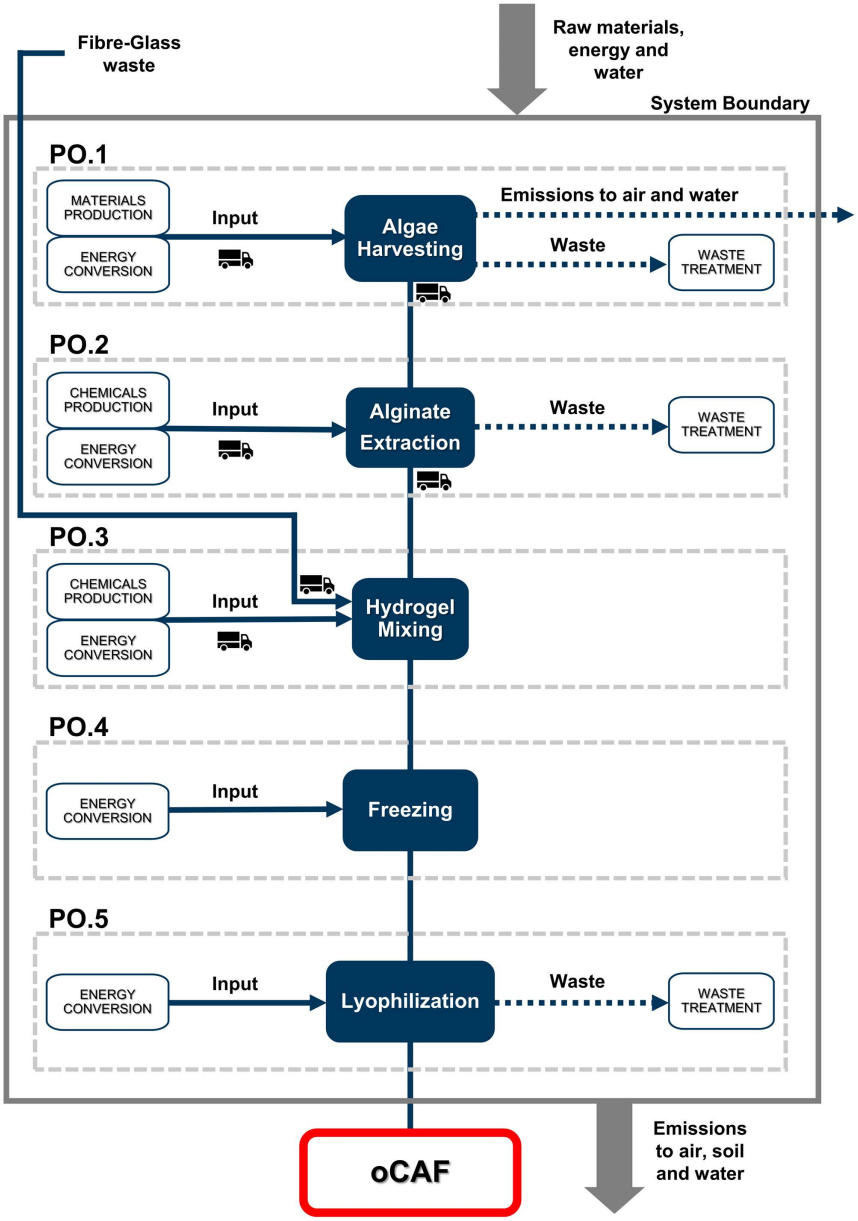

Figure 5.1: PO product system scheme

5.2.1 PO - Life Cycle Inventory Analysis (LCIA)

In this section the procedure and the data used in the definition of the PO production system are detailed. As previously stated, all the data were collected referring to a reference flux of 1 kg of oCAF produced. Secondary data have been used for modelling input and output of PO.1 and PO.2 unit processes from [208] and respective life cycle inventory (LCI) are presented in [Tab. 5.2] and [Tab. 5.3]. In PO.1, boat maintenance data input (*e.g.* glass fiber and steel) were calculated on the basis of a service life of 15 and 30 year for the main engine and the hull whereas substitution of degraded antifouling paint and metal leaching was based on the assumption that $\approx 70\%_{wt}$ is released into the marine environment. The system boundaries includes also the polyethylene and nylon from nets maintenance, calculated from [238]. Air emission derived from fuel consumption were also extrapolated from [208] on the basis of EMEP-Corinair inventory[239]. Seaweed transportation was calculated on a 2200 km of transit basis via refrigerated lorry. In [Tab. 5.2] all the processes that have been used to model the input and output data are also elencated: all processes defined as *"market"* consider the transportation to production (treatment) site of the reference flux. In PO.2 a 90% recovery of Ethanol was assumed, by Villanueava[208], between different washings and on this basis the overall amount was calculated. Sodium alginate transportation was calculated on a 2000 km of transit basis via conventional truck (30%) and train vector (70%). Primary laboratory data were used as source for chemicals consumption data and waste generation in PO.3 PO.4 and PO.4 unit processes, respective LCI are presented in [Tab. 5.4][Tab. 5.5][Tab. 5.6]. Required electric energy LCI inputs were identified as follow. In PO.3, taking the equipment nominal power in account, the total energy consumption was calculated considering the total process duration (mixing). Similarly, for PO.4 energy was computed by considering nominal power, process duration (24h of freezing) and assuming that a total of 6 samples could be stored, at the same time, in the conventional lab freezer used (avoiding thermal overload). In PO.5 electric load was calculated considering the number of oCAF samples (2 x 700ml of frozen hydrogel) that can be stored in the chamber, the process duration (72h) and assuming that power consumption is maximum during the first 0.5h (during cold trap cooling and vacuum condition

establishment, 6 mbar) and then decrease to 10% during steady state operation. Glass-fiber waste transportation to site was calculated on a 300 km basis via truck vector, following the assumption that waste are provided by local industries. Each chemical, involved in oCAF production, was correctly modelled in PO product system by connecting its stream to the correct corresponding provider (*i.e.* the parent production process present in the Ecoinvent database). An exception was made for glucono-δ-lactone (GDL), in PO.3 unit process, due to its absence in the database. In consideration of the fact that GDL is derived from glucose fermentation, glucose was then chosen as substituting stream for GDL and its production process was defined as GDL provider in PO.3 LCI [Tab. 5.4].

Table 5.2: PO.1 unit process, algae harvesting life cycle inventory. All data refers to a reference final flux of 1kg of oCAF produced

Input			**Provider**
Glass Fiber	6.332	g	Ecoinvent - market for glass fibre reinforced plastic
Steel	1.900	g	Ecoinvent - market for steel, low-alloyed
Antifouling	4.031	g	Ecoinvent - market for alkyd paint
Paint	1.015	g	Ecoinvent - market for alkyd paint
Lubricant Oil	5.030	g	Ecoinvent - market for lubricating oil
Polyethylene (LDPE)	3.122	g	Ecoinvent - market for fleece, polyethylene
Nylon	1.718	g	Ecoinvent - market for Nylon 6-6
Diesel	2.252	kg	Ecoinvent - market for diesel - EU
Algae	0.484	kg	Ecoinvent - primary - Biomass
Refrigerated transport	1065.641	kg·km	Ecoinvent - market for transport, freight, lorry with refrigeration machine
Output			
Seaweed	0.484	kg	
Waste			
Polyester /glass fiber	6.332	g	Ecoinvent - treatment of inert waste, sanitary landfill
Steel	1.901	g	Ecoinvent - treatment of scrap steel, inert material landfill
Polyethylene	3.122	g	Ecoinvent - treatment of waste polyethylene, sanitary landfill
Nylon	1.718	g	Ecoinvent - treatment of municipal solid waste, incineration
Emission to air			
Carbon dioxide	20.386	kg	Ecoinvent - emission in low density population areas
sulfur dioxide	12.871	g	Ecoinvent - emission in low density population areas
NMVOC	190.343	g	Ecoinvent - emission in low density population areas
methane	1.158	g	Ecoinvent - emission in low density population areas
Nitrogen oxide	151.066	g	Ecoinvent - emission in low density population areas
Carbon monoxide	47.623	g	Ecoinvent - emission in low density population areas
Emission to water			
Xylene	0.360	g	Ecoinvent - emission to water/ocean
Cobalt	0.023	mg	Ecoinvent - emission to water/ocean
Copper	0.836	g	Ecoinvent - emission to water/ocean
Zinc	0.377	g	Ecoinvent - emission to water/ocean

Table 5.3: PO.2 unit process, Alginate extraction, life cycle inventory. All data refers to a reference final flux of 1kg of oCAF produced.

Input			**Provider**
Seaweed	0.484	kg	PO.1
Formaldehyde	0.197	kg	Ecoinvent - market for formaldehyde
Sulphuric acid	4.459	kg	Ecoinvent - market for sulphuric acid
Sodium carbonate	0.243	kg	Ecoinvent - market fo soda production, solvay process
Ethanol	3.949	kg	Ecoinvent - market for ethanol, without water
Acetone	2.875	kg	Ecoinvent - market for acetone, liquid
Water	118.504	kg	Ecoinvent - market for water, deionised
Electricity	5.728	kWh	Ecoinvent - market group for electricity, low voltage - EU
Transportation	257.846	kg·km	Ecoinvent - market for transport, freight train
Transportation	110.505	kg·km	Ecoinvent - market for transport, freight lorry
Output			**Provider**
Sodium Alginate	0.184	kg	
Waste			
waste water	0.119	m^3	Ecoinvent - treatment of wastewater

Table 5.4: PO.3 unit process, Hydrogel Mixing, life cycle inventory. All data refers to a reference final flux of 1kg of oCAF producedMixing oCAF.

Input			**Provider**
Alginate	0.184	kg	PO.2
Transport	193.836	kg·km	Ecoinvent - market for transport, freight lorry
Calcium carbonate	0.020	kg	Ecoinvent - market for calcium carbonate, precipitated
GDL	0.150	kg	Ecoinvent - market for glucose | glucose
Fibre-glass	0.646	kg	
Water	11.069	L	Ecoinvent - market for water, deionised
Electricity	3.759	kWh	Ecoinvent - market group for electricity, low voltage - IT
Output			**provider**
Hydrogel	13.155	L	

Table 5.5: PO.4 unit process, Freezing, life cycle inventory. All data refers to a reference final flux of 1kg of oCAF produced

Input			**Provider**
Hydrogel	13.155	L	PO.3
Electricity	0.257	kWh	Ecoinvent - market group for electricity, low voltage - IT
Output			**Provider**
Frozen-hydrogel	12.069	kg	

Table 5.6: PO.5 unit process, lyophilization, life cycle inventory. All data refers to a reference final flux of 1kg of oCAF produced

Input			**Provider**
Frozen-hydrogel	12.068	kg	PO.4
Electricity	154.395	kWh	Ecoinvent - market group for electricity, low voltage - IT
Output			**Provider**
1pt oCAF	1	kg	
Waste			
Water	11.069	L	Ecoinvent - treatment of wastewater
Lubricant oil	0.338	kg	Ecoinvent - market for waste mineral oil - incineration

5.3 PR - product system

In [Fig. 5.2] the PR production system which model the lab scale recycling process as described in (Par. 4.2) (in its rCAF-G variant) is presented. Respectively, steps 1-3 were grouped and modelled in system process PR.1 (dissolution) whereas steps 4 (freezing) and 5 (lyophilization) were modelled in system process PR.2 and PR.3. Since rCAF is produced from oCAF no alginate production is considered and, similarly to what was done in defining fibre-glass stream in PO product system, and in compliance with ISO 14044, oCAF enters with a neat zero environmental balance in PR.1. Transportation of oCAF waste from, hypothetical, installation site to recycling site was also considered. The same considerations made in the previous

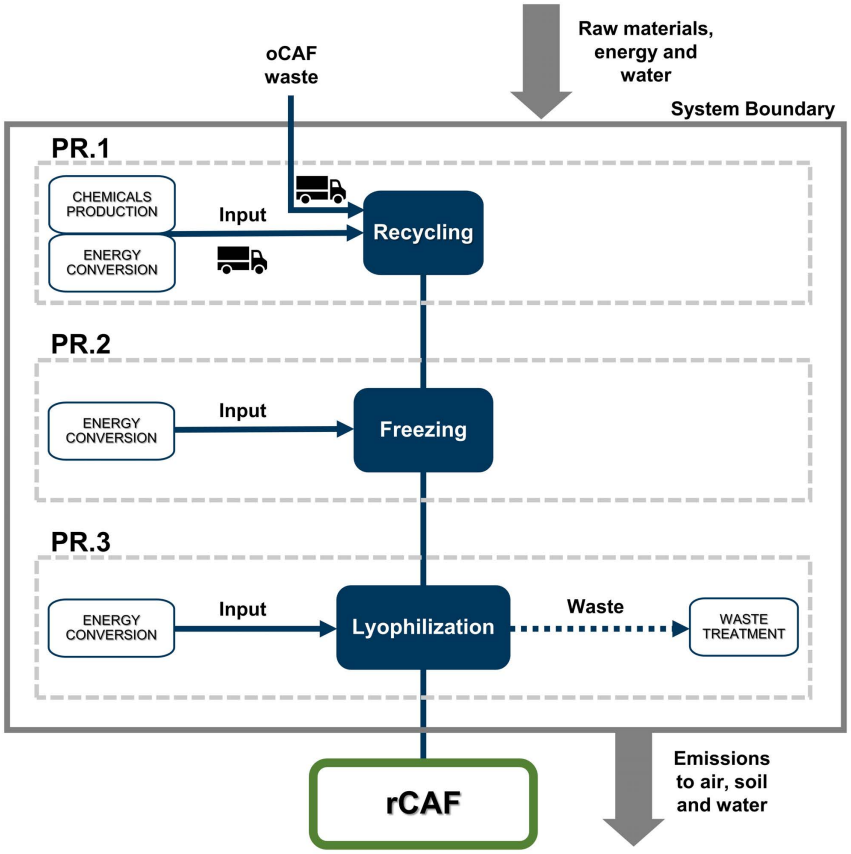

Figure 5.2: PR product system scheme

paragraph for PO.4 and PO.5 apply respectively to PR2, and PR.3 (freezing and lyophilization).

5.3.1 PR - Lyfe Cycle Inventory LCI

Primary laboratory data were used as source for electric energy input, chemicals consumption and waste generation in PR.1, PR.2 and PR.3 unit processes, respective LCI are presented in [Tab. 5.7][Tab. 5.8][Tab. 5.9]. oCAF waste transportation to site was calculated on a 300 km basis via truck vector, following the assumption that waste are provided by, hypothetical, local construction sites. Each chemical, involved in rCAF production, was correctly modelled in PR product system by connecting its stream to the correct corresponding provider. The same exception made for GDL in PO.3 was applied in PR.1.

Table 5.7: PR.1 unit process, Recycling, life cycle inventory. All data refers to a reference final flux of 1kg of rCAF produced.

Input			**Provider**
oCAF	0.613	kg	
EDTA	0.136	kg	Ecoinvent - market for EDTA
GDL	0.260	kg	Ecoinvent - market for glucose | glucose
Transport	184.028	kg*km	Ecoinvent - market for transport, freight lorry
Water	7.674	L	Ecoinvent - market for water, deionised
Electricity	3.472	kWh	Ecoinvent - market group for electricity, low voltage - IT
Output			**Provider**
Hydrogel	8.102	L	

Table 5.8: PR.2 unit process, Freezing, life cycle inventory. All data refers to a reference final flux of 1kg of rCAF produced.

Input			**Provider**
Hydrogel	8.102	L	PR.1
Electricity	0.158	kWh	Ecoinvent - market group for electricity, low voltage - IT
Output			**Provider**
Frozen-hydrogel	8.713	kg	

Table 5.9: PR.3 unit process, Lyophilization, life cycle inventory. All data refers to a reference final flux of 1kg of rCAF produced.

Input			**Provider**
Frozen-hydrogel	8.713	kg	PR.2
Electricity	95.090	kWh	Ecoinvent - market group for electricity, low voltage - IT
Output			**Provider**
rCAF	1.000	kg	
Waste			
Water	7.674	L	Ecoinvent - treatment of wastewater
Lubricant oil	0.208	kg	Ecoinvent - market for waste mineral oil - incineration

5.4 PRI - product system

In [Fig. 5.3] the PRI production system which model an industrial scaled version of the recycling process described in (Par. 4.2) (in its rCAG-G variant) is presented. PRI product system was developed from PR product system by merging PR.2 and PR.3 processes (freezgin and lyophilization) into a single freeze-drying unit process (PRI.2). This was done on the assumption that an industrial freeze-dryer possesses a built-in samples freezing system. The use of an industrial mixer was modelled into the calculation of the energy required in PRI.1. Electric energy input calculation are described in LCI section. Same consideration made in PR.1 herein were applied into modelling oCAF stream. No equipment maintenance or construction allocated impacts were considered. As anticipated in the main LCA goal description, 7 different scenarios were considered for PRI-LCA by varying the production energy mix used:

PRI-ITA Baseline scenario in which Italian production energy mix was used as electric energy provider in PRI LCI [Tab. 5.11] and [Tab. 5.11]. Unless further specified this scenario was used in all the presented results.

PRI-DE Alternative scenario in which German production energy mix was used as electric energy provider in PRI LCI [Tab. 5.11] and [Tab. 5.11].

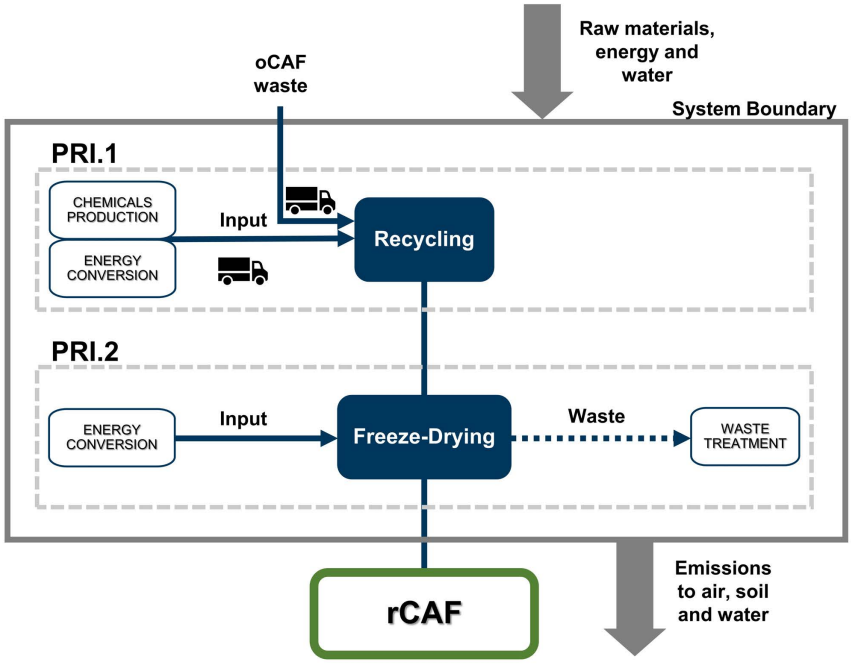

Figure 5.3: PRI product system scheme

PRI-FR Alternative scenario in which French production energy mix was used as electric energy provider in PRI LCI [Tab. 5.11] and [Tab. 5.11].

PRI–DK Alternative scenario in which Danish production energy mix was used as electric energy provider in PRI LCI [Tab. 5.11] and [Tab. 5.11].

PRI-Wi Alternative scenario in which a synthetic 100% wind energetic source was used as electric energy provider in PRI LCI [Tab. 5.11] and [Tab. 5.11].

PRI-Pv Alternative scenario in which a synthetic 100% photovoltaic energetic source was used as electric energy provider in PRI LCI [Tab. 5.11] and [Tab. 5.11].

PRI-Hy Alternative scenario in which a synthetic 100% hydroelectric energetic source was used as electric energy provider in PRI LCI [Tab. 5.11] and [Tab. 5.11].

Detailed composition of states and synthetics energy mixes are presented in [Tab. 5.10].

Table 5.10: Production energy mixes used. State mixes (IT, FR,DK, DE and EU) taken *as they are defined* from *Ecoinvent* Database. Synthetic renewable mixes (P.V., Hy and Wi) created from *Ecoinvent* Database. RER = Renewable Energy Resource, n-RER = non Renewable Energy Resource

	IT	FR	DK	DE	EU	P.V.	Hy	Wi
Coal	15.37%	2.19%	29.19%	44.12%	27.05%	-	-	-
Oil	3.68%	0.19%	0.28%	0.28%	1.40%	-	-	-
N. Gas	25.39%	1.61%	4.71%	6.48%	11.34%	-	-	-
Nuclear	7.81%	79.52%	6.65%	18.55%	29.50%	-	-	-
Geother.	1.84%	0.00%	0.00%	0.02%	0.31%	-	-	-
Hydro	24.32%	12.26%	15.48%	4.81%	18.12%	-	100.00%	-
Wind	5.29%	3.20%	32.96%	10.10%	7.70%	-	-	100.00%
Solar	0.00%	0.01%	0.00%	0.00%	0.14%	-	-	-
Biomass	5.45%	0.24%	8.56%	6.78%	3.24%	-	-	-
P.V.	10.85%	0.76%	2.16%	8.87%	1.20%	100.00%	-	-
RER	47.75%	16.48%	59.17%	30.58%	30.71%	100.00%	100.00%	100.00%
n-RER	52.25%	83.52%	40.83%	69.42%	69.29%	0.00%	0.00%	0.00%

5.4.1 PRI - Lyfe Cycle Inventory LCI

Energy input in PRI.1, for hydrogel mixing, was extrapolated from secondary data of plaster mixing (process present in the *Ecoinvent* database) that requires 0.08 kWh/L based on the assumption that both rCAF solution (after the dissolution step) and standard plaster share similar shear viscosity (1 - 2 Pa·s). Electric energy requirement for industrial freeze-drying (PRI.2) was calculated on the basis of secondary producer data (modelling a CUDDON FD300 Freeze Dryer[240]), considering 2 kWh/kg (on wet product weight basis, *i.e.* hydrogel produced in PRI.1). This assumption was further validated by similar calculations performed in the consulted literature, in which the energy consumption of freeze drying of strawberries was assessed[241]. Strawberries water content ($\approx 85\%_{wt}$) is similar

to the water content ($\approx 85\%_w t$) of the hydrogel produced as result of step 3 of the recycling process (Par. 4.2) (modelled as PRI.1 output). As it was done in PO and PI system product definition, all chemicals involved in sample production were correctly modelled in PRI product system by connecting its stream to the correct corresponding provider. The same exception made for GDL in PO.3 and PR.1 was herein applied in PRI.1. oCAF input in PRI.1 was modelled just as it was done in PR.1. Detailed LCI for PRI.1 and PRI.2 are presented in [Tab. 5.11] and [Tab. 5.12].

Table 5.11: PRI.1 unit process, Recycling, life cycle inventory. All data refers to a reference final flux of 1kg of rCAF produced.

Input			**Provider**
oCAF	0.613	kg	
EDTA	0.136	kg	Ecoinvent - market for EDTA
GDL	0.260	kg	Ecoinvent - market for glucose | glucose
Transport	184.028	kg*km	Ecoinvent - market for transport, freight lorry
Water	7.674	L	Ecoinvent - market for water, deionised
Electricity	0.648	kWh	Ecoinvent - market group for electricity, low voltage - IT
Output			**Provider**
hydrogel	8.712	kg	

Table 5.12: PR.2 unit process, Freeze-Drying, life cycle inventory. All data refers to a reference final flux of 1kg of rCAF produced. Data referred to PRI-ITA scenario.

Input			**Provider**
Hydrogel	8.712	kg	PRI.1
electricity	17.424	kWh	Ecoinvent - market group for electricity, low voltage - IT
Output			**Provider**
rCAF	1.000	kg	
Waste			
Water	7.674	L	Ecoinvent - treatment of wastewater

Part III

Result and Discussion

Chapter 6

Optimization of oCAF composition

As anticipated in the introduction, this initial part of the work was conducted in collaboration with industrial partners in a project (*GGTDoors - Green Gas Tight Doors*) that had as its main objective the delivering of a gas thigh door for the ship-building sector. As an internal component, an optimized version of the composite alginate foam (CAF-*GGTDoors*) was used as alternative thermal insulator panel in substitution to standard Rock-Wool tiles. Due to the nature of the project its detailed composition is currently covered by a *non-disclosure agreement*, therefore only relevant informations with respect to the final composite alginate foam (oCAF) composition that was then used thereafter in this work will be herein discussed.

As depicted in [Fig. 6.1] the composite alginate foam was produced, as described in (Par. 4.1), starting from a water solution of alginate in which both fibre-glass and glass waste were dispersed together with a natural plasticizer and $CaCO_3$ (as Ca^{2+} precursor). The gelification starts only after the addition of glucono-δ-lactone (GDL) which, by slow hydrolyzation, decreases the pH of the solution triggering the release of Ca^{2+} ions that build up the ionic junction zones therefore forming the alginate gel matrix. The porous structure of the composite foam is obtained by

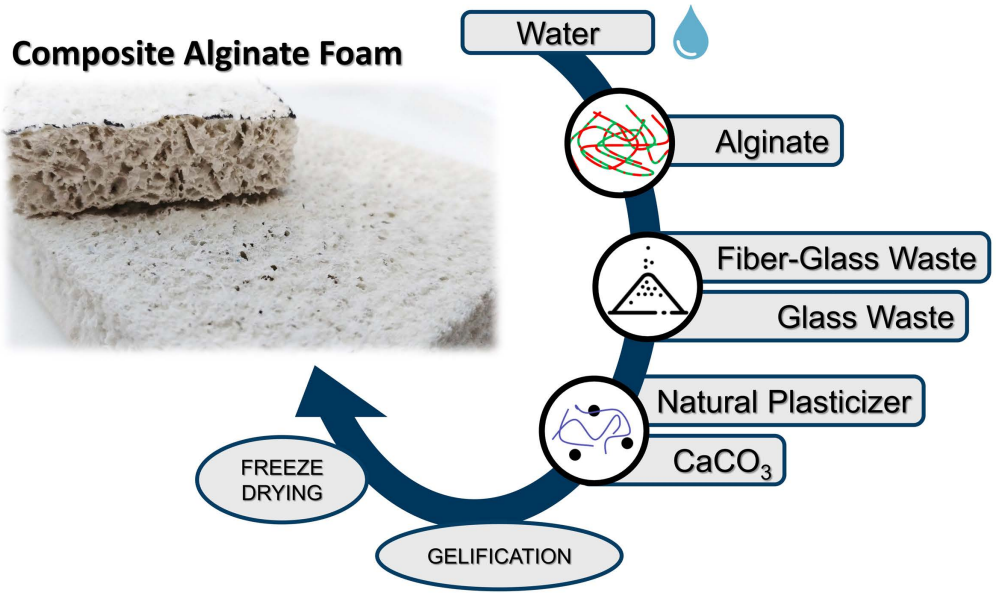

Figure 6.1: Composition of the Composite Alginate Foam optimized as a part of the *GGTDoors* project (CAF-*GGTDoors*).

drying the formed gel via *freeze-drying*. The main scope of the originally developed composite alginate foam[1][108] was to introduce a new option for the re-use of industrial waste, such as glass and fiber-glass. However, the recycle of glass waste is not as critical as the one of fibre-glass: glass can be easily remelted to produce new glass products. Differently, fibre-glass, which is a common name for fiber-glass reinforced polymer (more commonly reinforced polyester resins), are mainly disposed to landfills due to the low economic value of the recovered glass fibres (by pyrolysis or chemical degradation of the resin) and the impossibility (or with no economical advantage) of resin recovery[109][112](See par. 1.3.4). Nevertheless, the FTP code[1] places some restrictions, to materials intended to be used in the ship-building sector, one of these constrains requires to a material to maintain $> 50\%$ of residue after a heat treatment at 750 °C in air: since only the glass and $Al(OH)_3$ content of fiber-glass (plus a minimum contribution of $CaCO_3$) can contribute to the residue, glass waste were added to the composition to increase the total inorganic content. The optimized oCAF composition, as described in

[1]2010 FTP code: Fire testing Procedures adopted by the *Maritime Safety Committee*[131]

(Par. 4.1), was expressed in terms of alginate, waste-filler (fibre-glass), and $CaCO_3$ and GDL concentration[Tab. 6.2] and it was optimized in order to maximize the waste filler concentration. Herein are reported the consideration deducted from the production of *GGTDoors*-CAF:

Alginate	The minimum, initial, alginate concentration in water (1.4 %) was defined in order to prevent filler sedimentation during mixing and gelification, whereas, by increasing the alginate content, a reduction in the apparent density was observed which, being detrimental to thermal properties was maintained fixed.
$CaCO_3$	The minimum amount of $CaCO_3$ (15 mM) was required to prevent sedimentation during gelification: Ca^{2+} is released by slow acidification of the solution, and gelling time can be reduced by increasing the concentration of $CaCO_3$. Further increase in $CaCO_3$ induced unwanted syneresis effect with water expulsion and gel volume contraction without any increase in the mechanical stiffness of gelled sample (determined with frequency rheometry).
GDL	The optimal molar $CaCO_3$/GDL ratio was identified with 4 (60 mM of GDL) since a lower GDL concentration, maintaining constant $CaCO_3$, increased the gelling time (with the rise of sedimentation problem) whereas a higher GDL concentratoin lead to the formation of inhomogeneites with entrapped CO_2 bubbles.
Fiber-Glass and Glass Waste	As described above, filling concentration was constrained by FTP code requirements, but a maximum concentration of $75\%_{dry,wt}$ was identified before particulate leaking occurred in the dried foam. Further addition of the plasticizer had no effect on reducing the leaking.

In [Fig. 6.2] and [Tab. 6.1] thermal and mechanical properties of the *CAF-GGTDoor* are reported with respect to the rock wool standard used in the GGTDoors

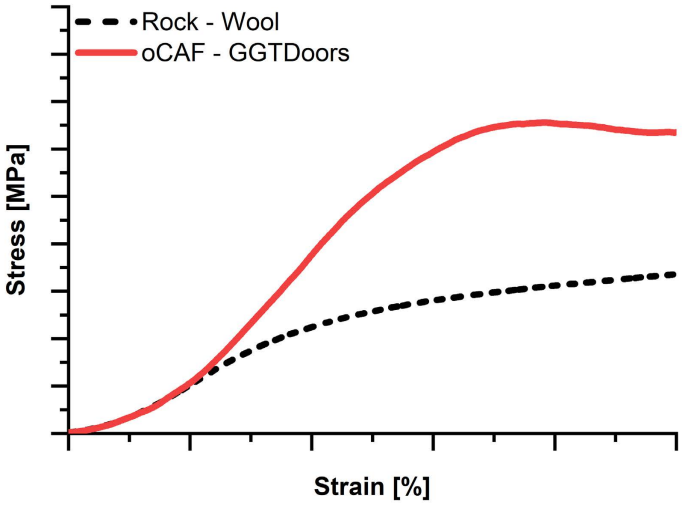

Figure 6.2: Compression resistance comparison between commercial Rock-Wool and the Composite Alginate Foam optimized as a part of the *GGTDoors* project.

project.

As previously highlighted, since the intended use of the oCAF is not limited to the shipbuilding industry the restriction on inorganic [$\%_{wt}$] fraction does not apply and only fiber-glass waste were used as filler and in [Fig. 6.3] the thermal conductivity of various CAF sample produced varying the fibre-glass(FG) content are represented. As previously stated, the maximization of the total fibre-glass concentration was the primary objective during the optimization of oCAF composition: a maximum load of 67.10% was possible before fibre-glass leaking occurs.

Table 6.1: Properties of the composite alginate foam developed as a part of the GGT-Doors project with respect to common Rock-Wool TIM

TIM	**Thermal conductivity (20 °C)** [**mW/m K**]	**Density** [**kg/m^3**]
Rock Wool	37	150
CAF-*GGTDoors*	47	151

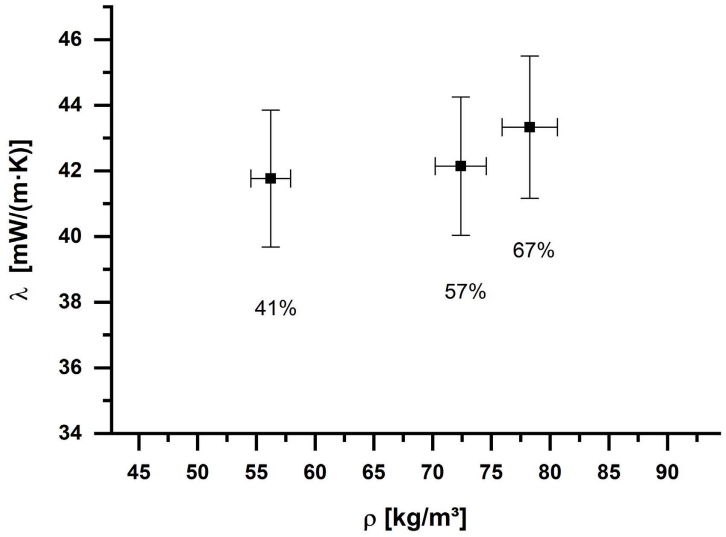

Figure 6.3: Thermal conductivity vs Density of Composite Alginate Foams at different fibre-glass concentration. A relative instrumental precision error of 5% and 3% was attributed to each single measurement, respectively for thermal conductivity and density.

Table 6.2: oCAF composition, value for 700 mL of final gel volume.

Alginate		Fiber-Glass		Ca		GDL	
[g]	[$\%_{wt,dry}$]	[g]	[$\%_{wt,dry}$]	[g]	[$\%_{wt,dry}$]	[g]	[$\%_{wt,dry}$]
9.80	17.59	37.38	67.10	1.05	1.88	7.48	13.43

The linear relation between the thermal conductivity and the density is a typical phenomenon that is present in porous and fibrous material caused by the higher contribution, to the overall thermal conductivity, of the solid fraction (λ_s)[242]. The final composition of the oCAF was therefore obtained [Tab. 6.2] and [Fig. 6.4], as result of the above mentioned consideration, balancing the maximization of the fiber-glass content and thermal properties.

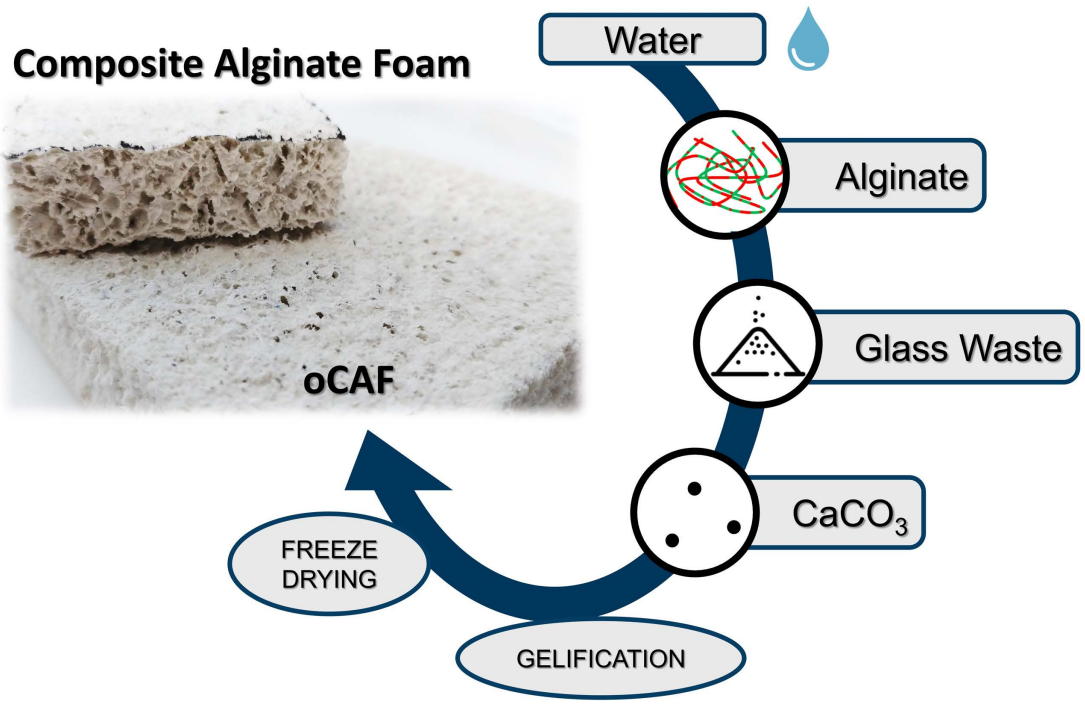

Figure 6.4: Composition of the Composite Alginate Foam optimized in this work (o-CAF).

Chapter 7

Recycling oCAF

In this section the working principles and the development of the recycling process will be reviewed, followed by the discussion on the functional properties of the recycled samples (rCAF), which are then compared with oCAF. Parts of these results have been published in [243].

7.1 Working Principle

As stated in (Par. 3.1.1), alginate is an anionic block copolymer formed by β-D-Glucuronate (M) and α-L-Guluronate (G) monomers linked together by a $1 \rightarrow 4$ glycosidic linkage capable to form a gel through the chelation of calcium ions, operated by GG blocks (*i.e* ionotropic gelation). To avoid instantaneous and inhomogeneous gelification, following the introduction of dissociated cations (*e.g.* the direct introduction of CaCl), a controlled internal gelation approach was used for the production of CAF sample using glucono-δ-lactone(GDL): GDL slowly hydrolyze in water forming gluconic acid, which, upon acidification of the solution, promotes the release of Ca^{2+} by decomposition of the previously dispersed $CaCO_3$. Once the ionic gel is formed, it can withstand temperatures up to 100 °C [206]. The recycling process herein developed, and summarized in [Fig. 7.1], exploits the reversible ionic interactions that build up the alginate matrix of the oCAF samples: simple grinding and dispersion in water do not lead to the dissolution of

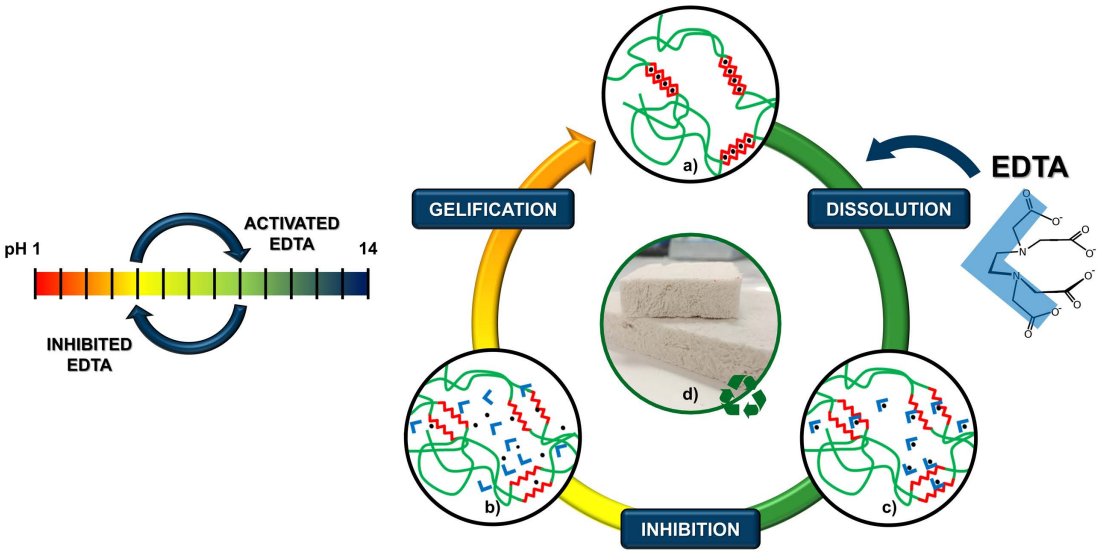

Figure 7.1: Representation of the recycling process. The alginate foam (d) is dissolved in activated EDTA solution by subtraction of calcium ions from alginate gel junction zones, obtaining a homogeneous viscous solution (b). Upon inhibition of the chelator, by a pH drift, calcium ions are released (c) and the gel structure is reobtained (a).

the oCAF (or oAG) due to the high stability of the ionotropic calcium alginate gel. The addition of a chelator, however, capable of interfering with the ionic bonds between the alginate chain and calcium by subtracting the cross-linking cations, can lead to the dissolution of the matrix. The chelator can be therefore inhibited thus releasing the cation which are then available again to cross-link the alginate, re-obtaining, in this way, the alginate foam. In order, for the chelator, to be effective and to sequester the Ca^{2+} ions its association constant has to be higher that of the alginate. In addition, these values have to be easily tunable (in compatible conditions) in order to make the process reversible. EDTA, [Fig. 7.2], is a polyprotic acid with 6 different dissociation constant, pK_a, (2 tertiary amines and 4 carboxylic groups) therefore can exist, depending on pH, in 7 different form: from the full protonated $[EDTA^{2+}]$ to the complete de-protonated $[EDTA^{4-}]$ with their relative fraction commonly expressed as $\alpha_{Y^{m\pm}}$. By using (Eq. 7.1) the fraction of the full de-protonated species can be easily calculated:

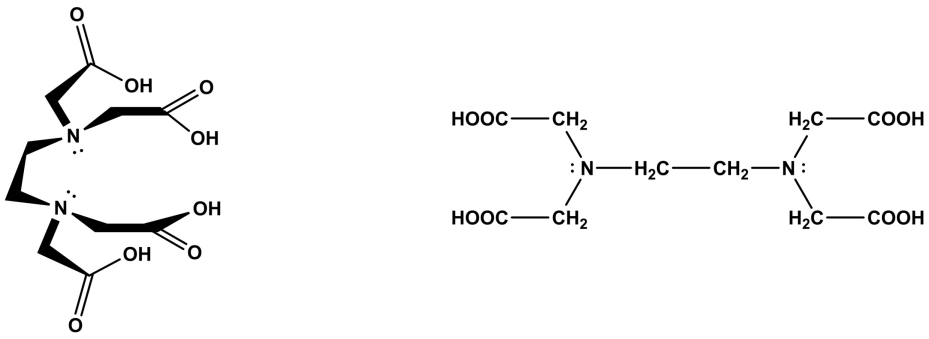

Figure 7.2: EDTA structure

$$\begin{aligned}\alpha_{EDTA^{4-}} &= \frac{[EDTA^{4-}]}{C_{EDTA}} \\ &= \frac{\prod_{i=1}^{6} 10^{-pK_{ai}}}{10^{-6\cdot pH} + \left(\sum_{i=1}^{6} \left(10^{(-(6-i)\cdot pH)} \prod_{i=1}^{n} 10^{-pK_{ai}}\right)\right)}\end{aligned} \tag{7.1}$$

with

$$\begin{aligned}C_{EDTA} = &[EDTA^{2+}] + [EDTA^{+}] + [EDTA] \\ &+ [EDTA^{-}] + [EDTA^{2-}] + [EDTA^{3-}] + [EDTA^{4-}]\end{aligned} \tag{7.2}$$

In [Fig. 7.3] the relative concentration of EDTA species ($\alpha_{EDTA^{n\pm}}$) with respect to the pH value are represented. Since only the full de-protonated form ($EDTA^{4-}$), is capable to bind Ca^{2+}, forming $Ca - EDTA^{2-}$ with a $Log(K_{Ca-EDTA^{2-}}) = 10.65$, the complex stability, expressed in respect of the total EDTA concentration ($K_{Ca-EDTA^{2-}}$), is inherently a function of $[EDTA^{4-}]$, thus depending on the pH of the solution, as shown by (Eq. 7.3):

$$\begin{aligned}K'_{Ca-EDTA} &= \alpha_{EDTA^{4-}} \cdot K_{Ca-EDTA^{2-}} \\ &= \frac{[EDTA^{4-}]}{C_{EDTA}} \cdot \frac{[Ca{-}EDTA^{2-}]}{[Ca^{2+}][EDTA^{4-}]}\end{aligned} \tag{7.3}$$

Similarly, the conditional association constant for the $Ca-Alg$ complex can be defined by assuming, in a simplified model, that the alginate is immediately capable of binding Ca^{2+} after de-protonation of the α-L-guluronic acid monomer (Alg_GH)

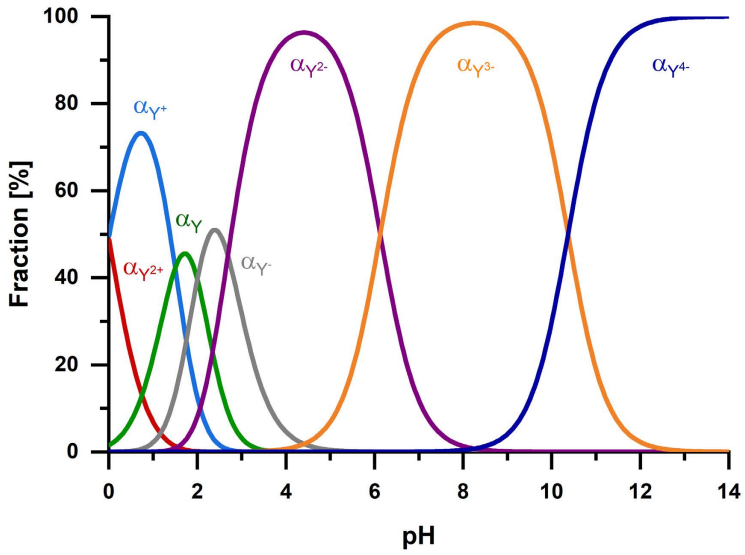

Figure 7.3: different EDTA fractions in water as a function of pH level: $\alpha_{Y^{n\pm}}$, with Y=EDTA. EDTA dissociation constant: $pK_{a1} = 0$, $pK_{a2} = 1.5$, $pK_{a3} = 2$, $pK_{a4} = 2.67$, $pK_{a5} = 6.16$, $pK_{a6} = 10.26$) , Value referenced at T=25 °C and $\mu = 0.1$ M, source [244]

to α-L-guluronate (Alg_{G^-}). β-D-mannuronic acid and α-L-guluronic acid possessing $pK_M = 3.65$ and $pK_G = 3.38$ respectively(Eq. 7.4)[245].

$$K'_{Ca-Alg_G} = \alpha_{Alg_{G^-}} \cdot K_{Ca-Alg_G} \tag{7.4}$$

The association constant for the Guluronate-Ca^{2+} complex, has been taken from literature with an estimated value of $Log(K_{Gul/Ca^{2+}}) \approx 4$ [245][244]. In [Fig. 7.4] and [Tab. 7.1] are presented the calculated value of the conditional associated constant as defined in (Eq. 7.3) and (Eq. 7.4). As it can be seen, at pH ≈ 5, K'_{Ca-Alg} is higher than $K'_{Ca-EDTA}$. As a consequence the dissolution step has to be performed maintaining the solution above this threshold value whereas, the inhibition of the chelating activity is reached below.

This is clearly visible by looking at species fraction as a function of the pH value in the simulated Alginate-Ca-EDTA system: [Fig. 7.5] and [Fig. 7.6] have been obtained by numerically solving the associated equation system(Eq. 7.5). The same

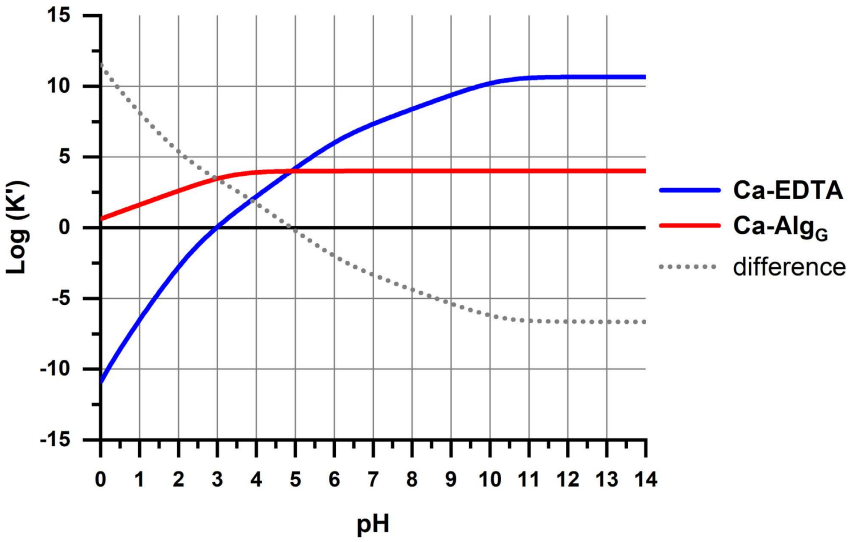

Figure 7.4: Graphical representation of the calculated value of conditional association constants of Ca^{2+} complexes with respect to pH.

assumption, made in [Fig. 7.4] and (Eq. 7.4), of modelling alginate using the sole α-L-guluronic acid monomer, was used in these calculation. Above pH 7.5 the calcium is completely displaced by the EDTA in the form of $Ca{-}EDTA^{2-}$ and alginate is de-protonated. By lowering the pH, Ca^{2+} ion start to be exchanged between the alginate and the EDTA by reaching the full fraction of $Ca{-}Alg_G$ at pH 2.5, below this point the alginic acid gel fraction (Alg_{GH}) starts to increase and Ca^{2+} ions are relesed from $Ca{-}Alg_G$. In first approximation, during the recycling of oCAF (Par. 4.2) 18 mM of Alg_G are presented (calculated by using the Mannuronic/Guluronic ratio), together with 45 mM of EDTA and 15 mM of Ca^{2+}. The results of the calculation performed with these concentration are presented in [Fig. 7.7]. Experimentally, it was observed that a minimum of pH 5 was needed to start the dissolution of oCAF sample but was not until maintaining the pH above 7 that a homogeneous and clear viscous solution was obtained (this was observed during oAG recycling, whereas the solutions of rCAF sample, due to the fibre-glass, were opaque but still homogeneous). This is caused by the partial protonation (*i.e* deactivation) of the EDTA as it can be seen by the arising $EDTA^{-3}$ fraction at

Table 7.1: Calculated value of conditional association constant of Ca^{2+} complex composition.

pH	Alginate-Ca^{2+}	EDTA-Ca^{2+}
	$Log\left(K'_{Ca\text{-}Alg}\right)$	$\mathrm{Log}(K'_{Ca\text{-}EDTA^{2-}})$
3.01	3.47	0.07
4.01	3.91	2.23
4.21	3.94	2.63
4.41	3.96	3.03
4.61	3.97	3.43
4.81	3.98	3.82
5.01	3.99	4.21
6.01	4	6.02
7.01	4	7.34
8.01	4	8.39

pH 5-6[Fig. 7.5]. Analogously, it was observed that, during the inhibition step, the viscosity of the solution increases at pH $\approx$ 5 and eventually a complete gelled sample is obtained upon reaching pH 4. None of the tested conditions for the prodution of rCAF lead to a lower final pH value. This is probably due to the presence of a plateau in the tritation curve of the system: both β-D-mannuronic and α-L-guluroninc respectively possesses a dissociation constant of 3.65 (pK_G) and 3.38 (pK_M) whereas pK_{a4} of the EDTA is equal to 2.67. Further consideration based on rheological evaluation are presented in the following section(Par. 7.2). One of the main advantages of this system is represented by the fact that once inhibited, the chelator is stable and remains in the lyophylized samples (*i.e.* rCAF). Multiple recycling cycles are therefore possible, following the procedure described in (Par. 4.2.1), by simple re-activation of the EDTA in mild basic condition by rising the pH above the critical value. Thermal characterization of double recycled sample 2rCAF are presented in (Par. 7.3).

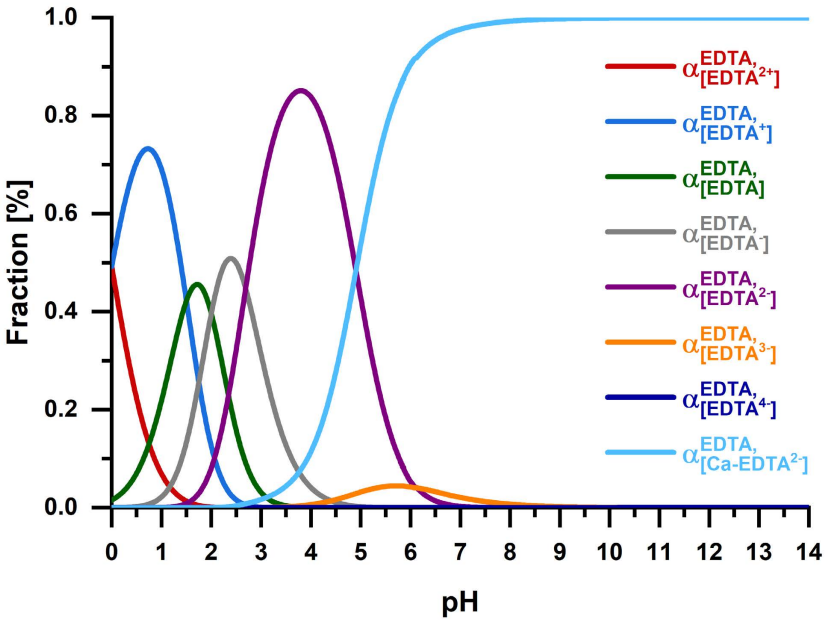

Figure 7.5: Calculated EDTA species fractions in a simulated system composed by Alginate-α-L-guluronate (15mM), Ca^{2+} (15mM) and EDTA (15mM). α superscript refers to the expression of fractions with respect to the total EDTA concentration.

$$
\begin{cases}
[Alg_GH]K_G - [H^+][Alg_G^-] = 0 \\
[Alg_G^-][Ca^{+2}]K_{Ca-Alg_G} - [Ca{-}Alg_G] = 0 \\
[EDTA^{2+}]K_{a1} = [H^+][EDTA^+] \\
[EDTA^+]K_{a2} = [H^+][EDTA] \\
[EDTA]K_{a3} = [H^+][EDTA^-] \\
[EDTA^-]K_{a4} = [H^+][EDTA^{2-}] \\
[EDTA^{2-}]K_{a5} = [H^+][EDTA^{3-}] \\
[EDTA^{3-}]K_{a6} = [H^+][EDTA^{4-}] \\
[EDTA^{4-}][Ca^{+2}]K_{Ca-EDTA^{2-}} = [Ca{-}EDTA^{2-}] \\
[Ca^{2+}] + [Ca{-}EDTA^{2-}] + [Ca - Alg_G] = [Ca_{TOT}] \\
[Alg_GH] + [Alg_G^-] + [Ca{-}Alg_G] = [Alg_{G_{TOT}}] \\
\left(\sum_{i=-2}^{4}[EDTA^i]\right) + [Ca{-}EDTA^{2-}] = [EDTA_{TOT}]
\end{cases}
\tag{7.5}
$$

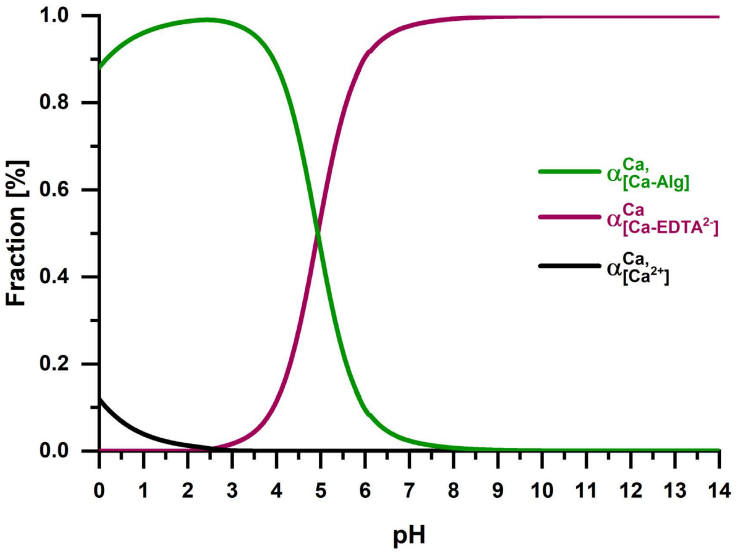

(a) Calculated Calcium species fractions in a simulated system composed by Alginate-α-L-guluronate (15mM), Ca^{2+} (15mM) and EDTA (15mM). α superscript refers to the expression of fractions with respect to the total Calcium concentration.

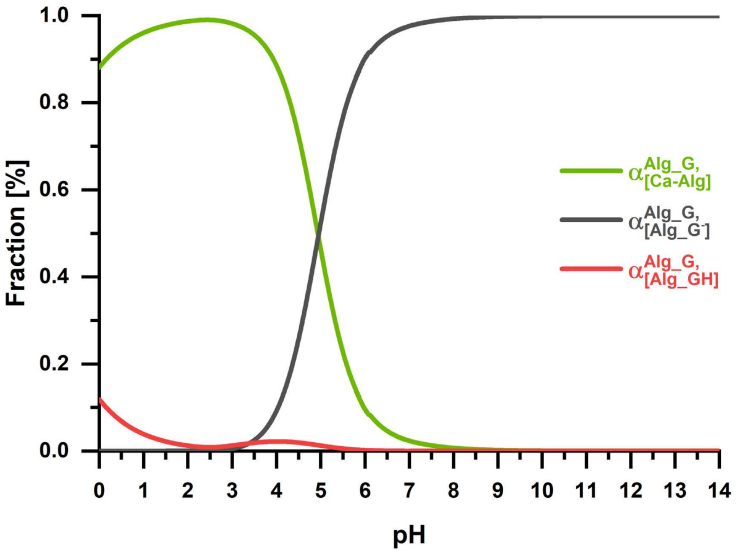

(b) Calculated Alginate species fractions in a simulated system composed by Alginate-α-L-guluronate (15mM), Ca^{2+} (15mM) and EDTA (15mM). α superscript refers to the expression of fractions with respect to the total Alginate-α-L-guluronate (Alg_G) concentration.

Figure 7.6

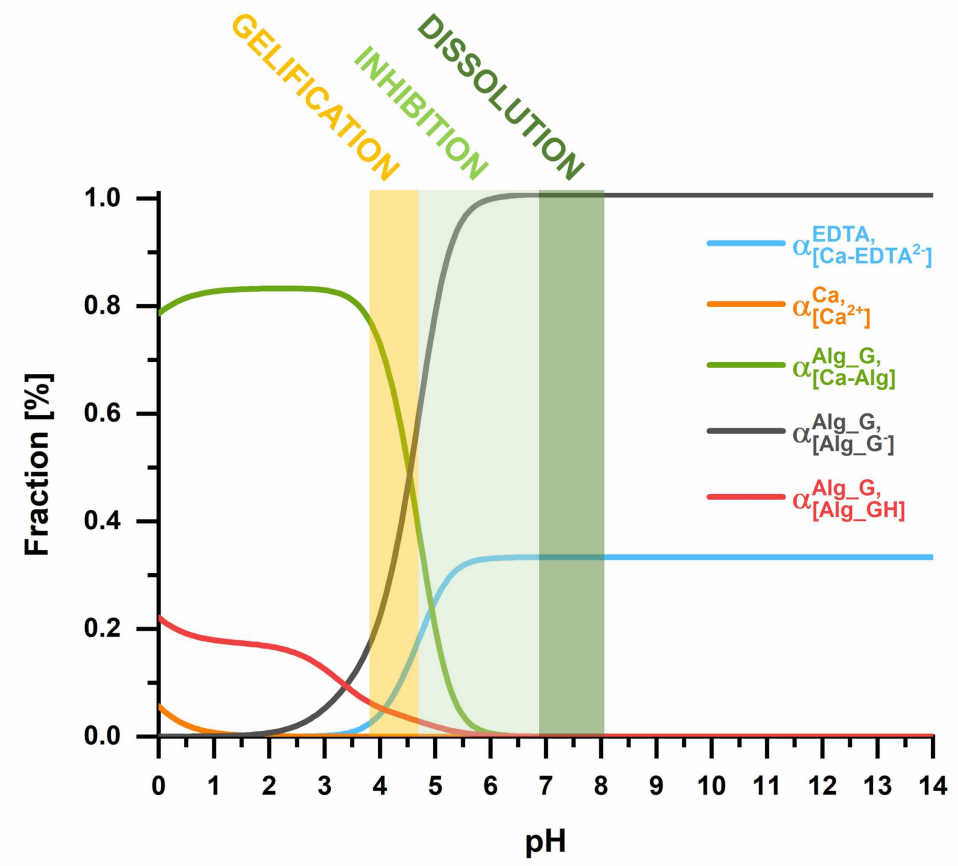

Figure 7.7: Calculated species fraction in a simulated system composed by Alginate-α-L-guluronate (18mM), Ca^{2+} (15mM) and EDTA (45mM). α superscript refers to the expression of fractions respecive concentration: Alg_G = total Alginate-α-L-guluronate concentration, Ca = total Ca^{2+} concentration, EDTA = total EDTA concentration.

7.2 Rheological evaluation of rAG

7.2.1 Dissolution Step

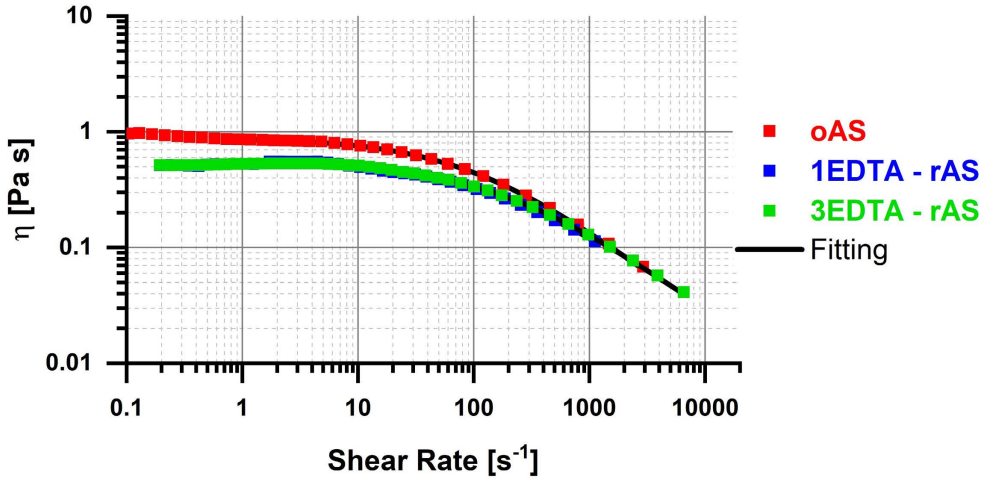

Figure 7.8: Shear viscosity, Flow Curves of original alginate solutions (oAS) and recycled alginate solution (rAS). Recycling of oAF was tested with $[EDTA]/[Ca^{2+}] = 1$ and $[EDTA/Ca^{2+}] = 3$, corresponding respectively to 15 and 45 mM

Steady state-shear viscosity [Fig. 7.8] has been used to evaluate signs of possible chain degradation in basic environment, due to the addition of concentrated $NaOH$ solution during the process. Both the original and the recycled alginate solution (oAS and rAS) shown a shear thinning behavior, typical of polymeric solutions. The initial reduction of the zero-shear viscosity (η_0) of the recycled samples can be attributed to the presence of the EDTA since an analogous behavior was evident in a control experiment where EDTA was added to a clean alginate solution at both the tested EDTA concentrations: 15mM corresponding to a molar ratio between the EDTA and the Ca^{2+} concentration in the original alginate foam sample (oAF) and 45mM corresponding to a molar ratio equal to 3. As anticipated in (Par. 4.4.1) the curves have been fitted with the Cross model equation (Eq. 4.2) since information about the alginate's polydispersibility can be inferred and parameters are given in [Tab. 7.2]. The values and the dispersions of the exponential parameter

Table 7.2: Cross model fitting parameters of fitted curves in [Fig. 7.8]. Mean absolute deviation in parentheses(Eq. 4.2)

	τ	m	η_∞	η_∞
oAS	0.010 (0.001)	0.750 (0.009)	1.000 (0.075)	0.003 (0.004)
1EDTA–rAS	0.007 (0.001)	0.724 (0.019)	0.579 (0.063)	0.003 (0.002)
3EDTA–rAS	0.006 (0.001)	0.736 (0.013)	0.601 (0.044)	0.002 (0.002)

m obtained from the data for the original and for the recycled samples are in line with those reported in the literature [246]. The variations on the value of m, due to uncertainty on the measure, are such that the observed variation cannot be considered meaningful and no sign of polymer degradation can be deduced. In case of degradation, a sharp reduction of the exponential value would be expected since, for linear non-blended polymers, m is inversely proportional to the PI of the polymer (*i.e.* the ratio between the weight averaged molecular weight and the numeric averaged molecular weight M_w/M_n (Eq. 4.3)). This is also visible directrly in [Fig. 7.8] : at high shear rate all the curves are asymptotic. Alginate degradation was tested at different EDTA concentration (15 mM e 45 mM) due to higher required amount of NaOH which has to be added to buffer the solution at the dissolution pH level, therefore a required higher EDTA concentration could have lead to the onset of a high chain degradation rate due to local peaks of high alkaline environment during the initial stage of the dissolution step.

7.2.2 Inhibition and Gelification step

Once that the oCAF is dissolved, and a viscous homogeneous solution is obtained, the following step of the recycling process involves the inhibition of the chelator and the subsequent gelification of the matrix. By reversing the trend of the dissolution step, the pH of the solution is lowered leading to the preferential binding of the Ca^{2+} ions to the alginate thus leading to the formation of a stable ionic alginate gel. This was done by using a stoichiometric amount of GDL, enough to protonate the four carboxyl groups of the EDTA. In (Par. 4.2) four different recycling routes were studied to highlight their effect on the complete recovery of the alginate gel structure, and in the functional properties of the final material (as it will be

presented later on(Par. 7.3)). Recalling, the following condition were tested:

rCAF–G	no addition before the use of GDL
rCAF–CG	further addition of $CaCO_3$ before the use of GDL.
rCAF–CG–A	use of HCl, jointly with the GDL
rCAF – G–A	addition of CaCO3 and joint use of HCl and GDL ° C.

The preferential recycling route involves the use of GDL alone (rCAF–G). Further addition of CaCO3 after the dissolution phase has been studied in order to increase the concentration of Ca^{2+} available to cross-link the alginate (rCAF – GC). With the same purpose the use of HCl was tested to further promote the acidification of the solution thus the release of Ca^{2+} from the Ca-$EDTA^{2-}$ complex (rCAF–G–A and rCAF–GC–A). The use of GDL is preferred to HCl due to the instantaneous formation of alginic gel (acid) upon contact with a 6 M HCl solution therefore leading to local pH values below the acid gel formation point (≈ 3.5). To prevent the formation of non-thermally stable alginic gel clusters, in which the HCl remains trapped, it is crucial that the HCl solution (jointly with freshly prepared GDL solution) is added after heating the solution at 75 °C and under vigorous mixing. The assumption that gelification of all rCAF samples occurs through ionotropic gelation, avoiding acid gelation, is supported by the fact that the final pH of all rAF gels (before lyophilization) reached a plateau at pH = 4. The recovery of the gel structure was determined via frequency sweep test rheometry, with a clean alginate gel sample (oAG) used as reference. Mechanical Spectra of both oAF and all rAF samples show a frequency-independent behavior of both the storage (G') and the loss (G') modulus within the linear strain regime which is characteristic of an elastic gelled systems[Fig. 7.9]. This further supports the fact that the dissolution step did not degrade the polymer, which maintained its gel-forming capabilities. However the elestic (G') and the viscous (G'') components of the systems gelled witouth the addition of $CaCO_3$ (rAF–G) and (rAF–G –A) are decreased with with respect to the reference value of oAF, whereas rAF–GC and rAF–GC–A samples shows comparable values. No increase of the storage modulus (G') was observedd as a consequence of the addition of $CaCO_3$ (which is result in

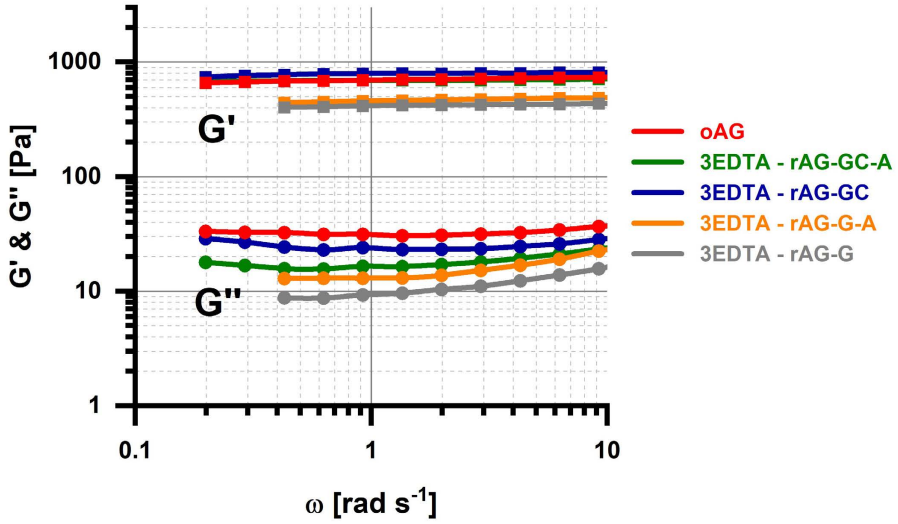

Figure 7.9: Frequency Sweep test on original alginate gel (oAG) and recycled alginate gel (rAG), recycling tested with molar EDTA/Ca^{2+} = 3

doubling the concentration of Ca^{2+} in rAG respect to oAG). This is in accordance with what was observed during the initial optimization stage in which any increase in $CaCO_3$ (above the optimum level) only leads to syneresis effect(Par. 6). The tested composition in which no additional calcium was added (rAF-G) shows the higher deviation denoting a incomplete back release of Ca^{2+}. This is in accordance with the result of the simulated system [Fig. 7.7]: as previously stated, after 12h, from the addition of the acid and before freezing, all the gel reached a value of pH ≈ 4, point at which only ≈ 90% of the total calcium is released by Ca-$EDTA^{2-}$. The role of the HCl can be better understood by taking account the gelling kinetics: the gelification setting time for oAF is ≈ 30 min whereas for rAF 1–2 h are needed when HCl or additional CaCO3 is used (R –rAF–G–A,rAF–GC–A and rAF –GC). Conversely, 3R – rAF – G samples are characterized by a longer setting time (≈ 3–4 h). HCl thus increase the release rate of Ca^{2+}but with little change in its final amount. Equivalent results were obtained with recycled alginate foam with a molar ratio EDTA/Ca^{2+} = 1. Shorter setting times are favourable to prevent waste fibre-glass sedimentation while recycling oCAF.

7.3 Characterization of rCAF

rCAF samples were characterized mainly from a thermal and acoustic perspective since the main objective was the validation of the capability of the recycling process through the maintaining of the oCAF functional properties.

7.3.1 Morphology and Sound Absorption

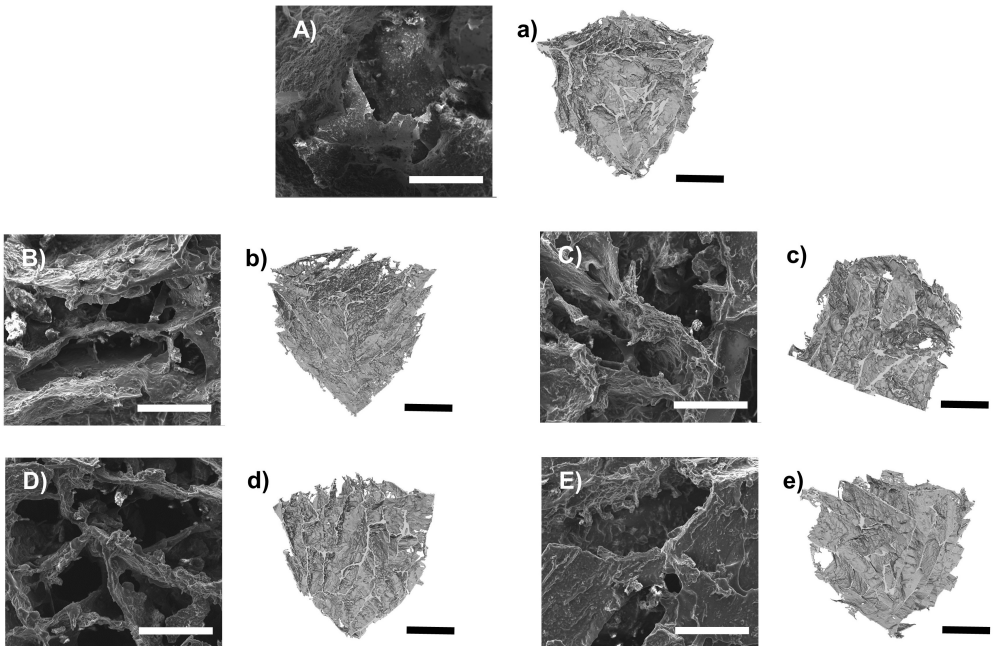

Figure 7.10: SEM and μCT images of: (A) (a) oCAF; (B) (b) rCAF–GC–A; (C) (c) rCAF–GC; (D) (d) rCAF–G–A; (E) (e) rAF–G; SEM scale bar equal to 500 μm, μCT scale bar equal to 2 mm.

SEM images and µCT reconstructions were collected to investigate the internal morphology of rCAF samples. A well-interconnected millimetre range open porous structure is preserved in all the rAF samples as it can be clearly seen in [Fig. 7.10]. A close porous structure is preferred in high performing thermal insulator whereas an open cell structure and, in particular, the presence of a millimetre range porosity leads to a strong contribution of convection in heat transfer thus increasing the thermal transfer. On the other hand a closed porosity has a detrimental impact on sound insulation performance were pore interconnectivity plays a major role [247].

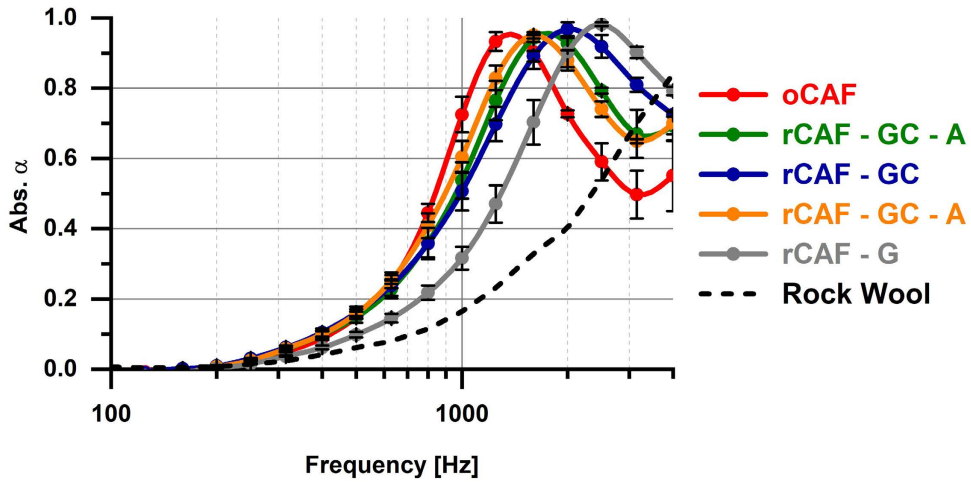

Figure 7.11: Averaged sound absorption coefficients of oAF and rAF samples, mean absolute deviation for each data-point was calculated. Absorption curve of Rock-Wool has been added as reference from literature [1]. Rock-Wool sample thickness: 10 mm.

As reported in [Fig. 7.11], sound absorption capability of rCAF is preserved in all the tested recycled composition: it is shown to be effective in the human-speech region (500-2000 Hz), reaching value close to unity (*i.e. complete absorption of the incident sound wave*) at higher frequencies. The preserved open cell structure of the rCAF is fundamental for obtaining a high sound absorption: air needs to travel through the material to dissipate its energy interacting with the solid material structure through viscous, thermal and damping effects[247]. The shift of the peak toward higher absorption factors and frequencies is commonly referred in literature to a decrease in the internal structure tortuosity[248]: tortuosity can be defined as the ratio between the length of the path that a sound wave needs to propagate through a materials with respect to the length which would have covered in free space and it is related to the dispersion of the velocities of the sound waves. Sound waves propagating in high tortuous systems tends to be highly scattered which limits absorption at high frequencies[249]. Preserving an open cell structure in foam materials represent a compromise to maintain good sound absorption and thermal insulation performance.

7.3.2 Mechanical Properties

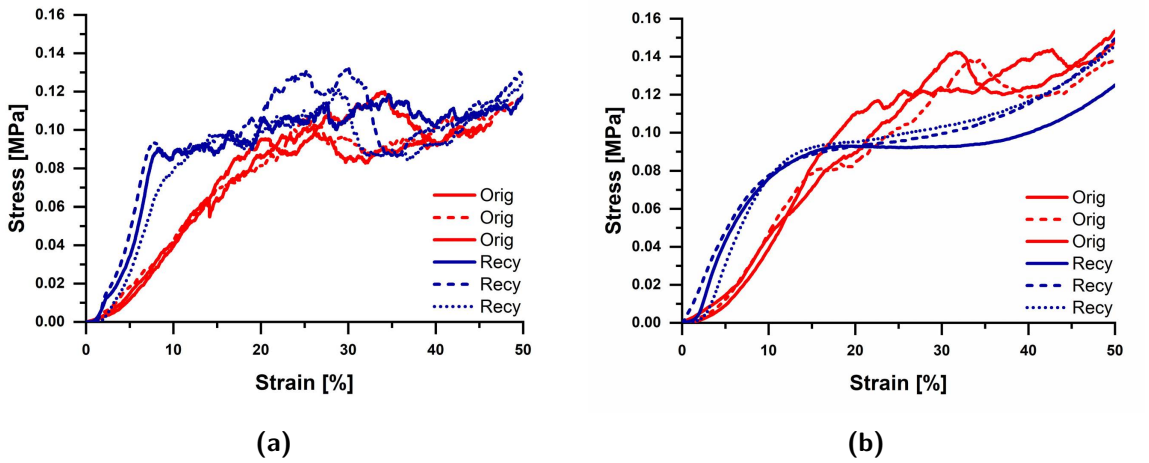

Figure 7.12: Compression resistance of oCAF (Orig) and rCAF–G (recy) tested as-lyophilized (dry)**a** and conditioned at 40 RH (**b**).

[Fig. 7.12] reports a typical compression stress-strain curve of an oCAF and a rCAF samples tested in dry contidion (*i.e.* as-lyophilized) and after a conditioning treatment at 40 RH. No statistically significant differences were detected in the mechanical properties between any of the rAF and oAF samples tested in dry condition except for an increase of the average Young's Modulus. Both the original and the recycled material showed a brittle behavior, with a failure stress at around 80–200 kPa. Interestingly, after conditioning in a 40RH chamber, a marked visco-elastic behavior emerges in all rCAF samples. In particular, 40RH-conditioned rCAF samples were capable to recover 75 % of the compression strain (after a compression strain of 50 %), compared to the 30 % of the oAF which however displayed brittle failure. This behavior can be traced back to the higher GDL content of rCAF samples, which amount to $33\%_{wt}$: as a matter of fact GDL is a well known plasticizer in food industry[250]. During conditioning at 40 RH weight gain, due to water uptake, stops respectively for oCAF and rCAF samples at 0.8% and 3% (on average) for oCAF and rCAF samples respectively, mainly attributed to the high hygroscopicity of EDTA and GDL. Compressive Strain and Young's Modulus data are detailed in [Tab. 7.3].

Table 7.3: Mechanical properties of oCAF and rCAF, conditioned (40 RH) and dry. E = Young's modulus

Sample	Conditioning	E [MPa]		Com. Str. [MPa]	
		mean	dev. st.	mean	dev. st.
oAF	dry	0.54	0.03	0.05	0.01
	40 RH	0.73	0.07	0.07	0.01
rAF-G-C	dry	1.70	0.71	0.16	0.02
	40 RH	1.56	1.01	0.12	0.07
rAF-G	dry	1.53	0.46	0.07	0.02
	40 RH	1.59	0.49	0.11	0.04
rAF-GC-A	dry	1.46	0.44	0.07	0.01
	40 RH	0.92	0.32	0.08	0.02
rAF-G-A	dry	1.71	0.78	0.19	0.31
	40 RH	1.14	0.62	0.03	0.01

7.3.3 Thermal Properties

As it can be seen in [Fig. 7.13] and , the consequent increase in the densities of recycled sample (caused by the addition of EDTA adn GDL) resulted into a slight increase in thermal conductivity. Nevertheless, λ remains still below the threshold value of 50 $mW/m\,K$ at 20 °C, which is commonly used as threshold value to indicate a good thermal insulator candidate. Another consequence of the increased mass density can be seen in the increased heat capacity of rCAF samples observed upon addition of EDTA and GDL during the recycling process which respectively represent the 12 $\%_{wt}$ and 33 $\%_{wt}$ of the final recycled sample [Tab. 7.5]. In [Fig. 7.14] are reported the thermal conductivity of the double recycled composition (2rCAF-G) which, recalling the procedure in (Par. 4.2.1), are produced by recycling rCAF-G sample. The further increase in thermal conductivity is again caused by the added mass of GDL which now contribute to the 46$\%_{wt}$[Tab. 4.2]. By extrapolating the thermal conductivity at $\rho = 0$ from the whole set of thermal conductivities a value comprised between 31 and 34 $mW/m\,K$ is obtained (the linear extrapolations were performed for each subset defined by the combination

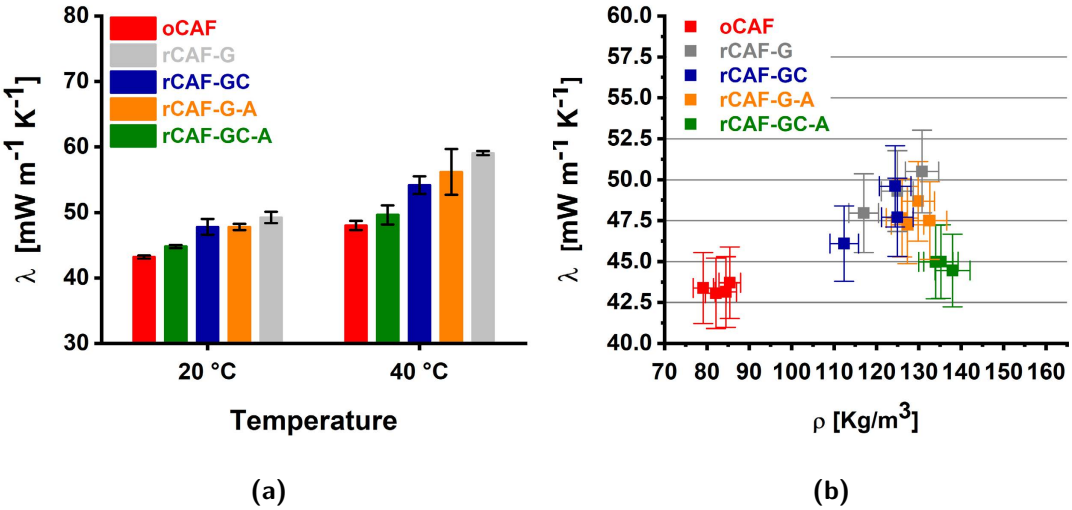

Figure 7.13: Thermal conductivity of oCAF, rCAF. (**a**) average thermal conductivity values are presented, with the corresponding average absolute error. (**b**) a plot of density vs thermal conductivity at 20 °C of each tested specimen. A relative instrumental precision error of 5% and 3% was attributed to each single measurement, respectively for thermal conductivity and density

of all the samples). This is clearly visible in [Fig. 7.14b] in which the linear fit of the rCAF-G sub-group, spanning along two recycled generations, is plotted. The extrapolated value, higher than the thermal conductivity of still air ≈26 mW/m K, suggests a small but not neglectable contribution of convection to the overall CAF thermal conductivity. It is worth noting that rAF–GC–A samples generally possess a lower thermal conductivity with respect to the other rAF samples, despite an average higher density. This could be explained with the different pore size distribution [Fig. 7.15]: oCAF and rCAF–GC–A both possess a lower population of larger pores (in the millimetre range), which mostly contribute to the convection heat transfer. This also suggests that a better control of the internal structure of the foam could have a relevant impact on the thermal properties of both oCAF and rCAF. The problem related to the increase of material density can be easily addressed by addition of fresh alginate solution after the dissolution stage in order to increase the final matrix volume. Nevertheless, it is worth mentioning that this is not associated with the chelation-driven recycling process herein described,

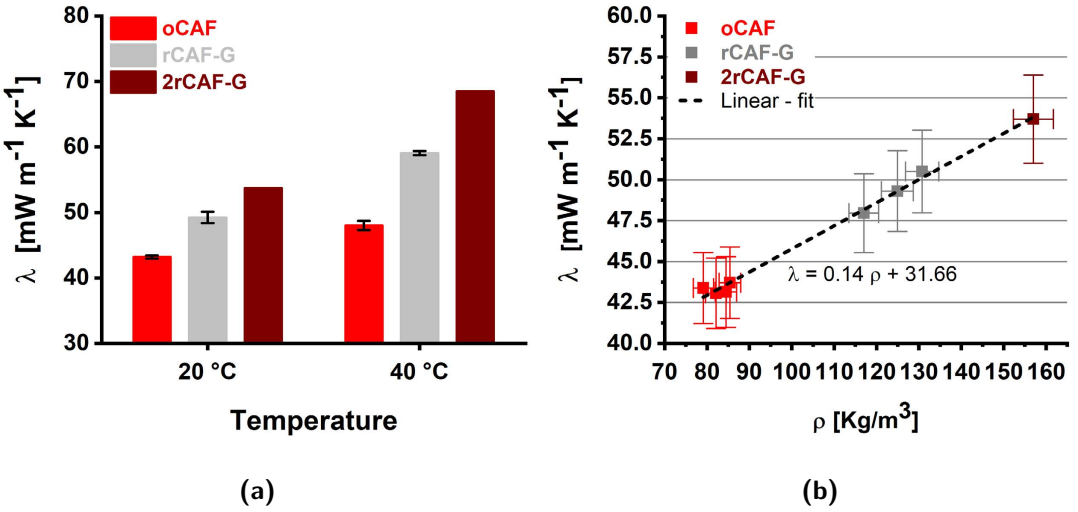

Figure 7.14: Thermal conductivity of oCAF, rCAF-G and 2rCAF samples. (**a**) average thermal conductivity values are presented, with the corresponding average absolute error. (**b**) a plot of density vs thermal conductivity at 20 °C of each tested specimen. A relative instrumental precision error of 5% and 3% was attributed to each single measurement, respectively for thermal conductivity and density.

which instead, has been proved to work in a second recycling test. As a matter of fact, the presence of the chelator in the rCAF samples, in an inactive form, confers an added value to the new recycled material which can be therein recycled multiple times by an inherited simple pH driven process, without addition of new chelating agent. Thermal conductivity, density and specific heat capacity are the three main parameters that characterize the efficiency of a thermal insulation material and their contribution can be summarized in a single index $M = (\lambda\, c_p\, \rho)^{1/2}$ which can be used to rank different thermal insulator materials, in terms of their overall performance, depending on the climate conditions in which they are intended to be used. Normally, heating and cooling loads are not constant during the day but are tailored to maintain internal comfort during residency time. In hot and warm climates, especially those with large diurnal temperature variation (e.g. southern Europe), a high heat capacity is preferred since it helps to stabilize the internal temperature due to the thermal damping effect. Conversely, in cold

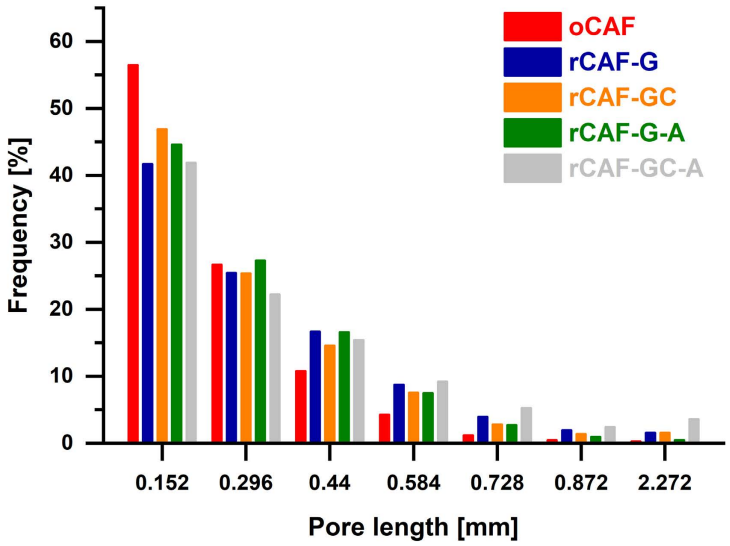

Figure 7.15: Pore length distribution obtained by uCT scan of oAF and rAF samples.

climates (e.g. northern Europe), with an extensive use of internal heating, a wall with a high thermal capacity can have a detrimental effect since more heat is lost through the wall heating [251][31]. On those grounds, materials with a lower M index perform well in cold climate whereas in hot warm climate best performance follows the highest value of M [Fig. 4.4.2.1]. In [Fig. 7.16] several thermal insulation materials are sorted by M and as it can be seen, both the rCAF and the 2rCAF remains competitive against commercial options and natural alternatives. In particular, the increase in density and specific heat lead to an improvement in insulation performances whenever they would be employed in cold regions.

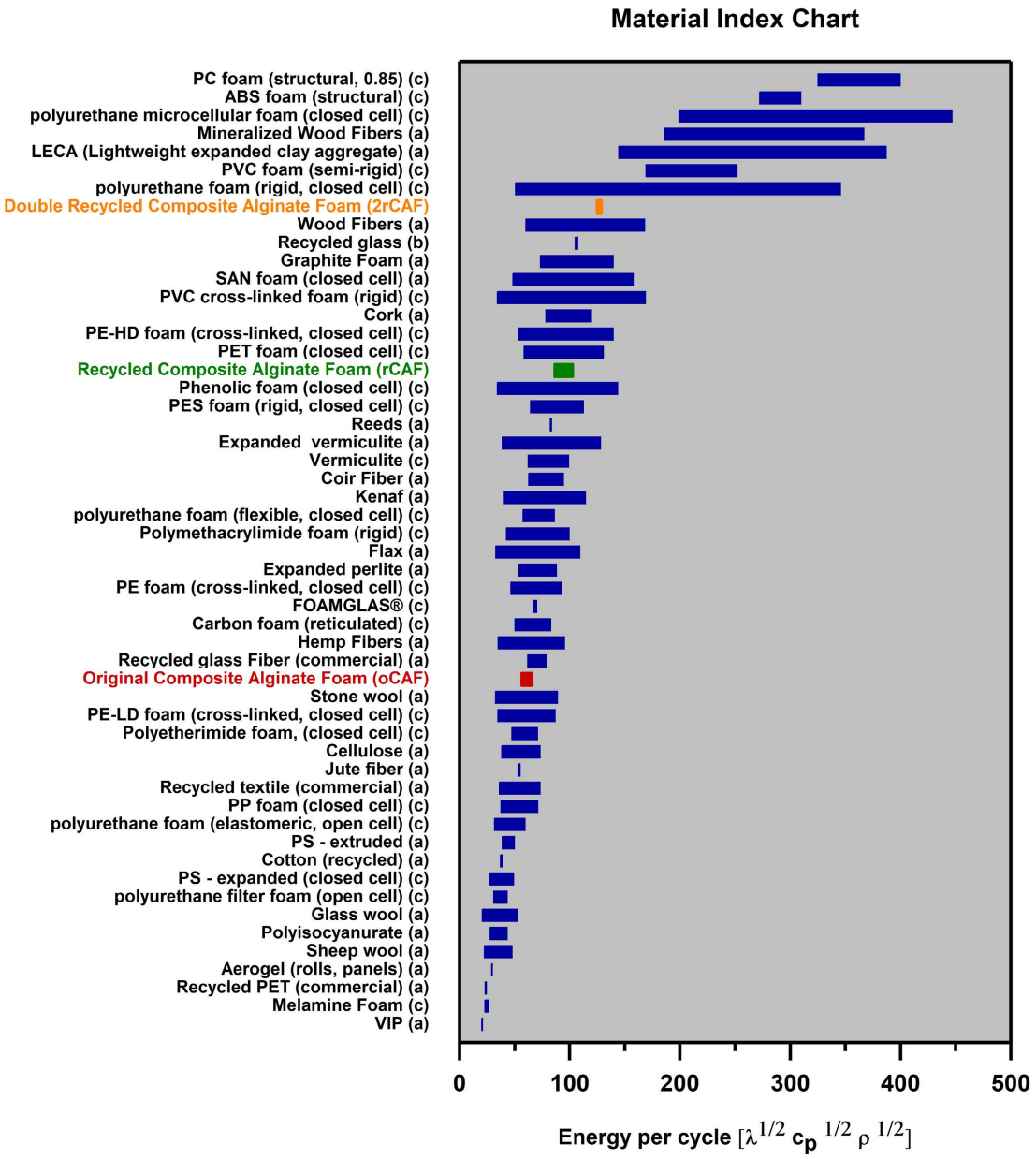

Figure 7.16: Thermal insulation materials performance ranked by material index M. Data source: a) [36] b) [75] c) CES Selector 2018. Data for the original and the recycled alginate foam (grouped), respectively in red, green and orange, from [Tab. 7.4] and [Tab. 7.5].

Table 7.4: Density and thermal properties of oCAF, rCAF and 2rCAF. Mean absolute deviation in parentheses

Sample	**Density** $[kg/m^3]$	**Thermal Conductivity 20 °C** $[mW/m\,K]$	**Thermal Conductivity 40 °C** $[mW/m\,K]$
oCAF	78.26 (7.19)	43.23 (0.22)	48.64 (0.70)
rCAF–G	127.91 (6.96)	49.23 (0.86)	59.06 (0.33)
rCAF–GC	120.57 (5.45)	47.80 (1.20)	54.18 (1.35)
rCAF–G–A	128.95 (2.26)	47.77 (0.46)	56.18 (3.49)
rCAF–GC–A	137.19 (2.61)	44.80 (0.24)	49.63 (1.45)
2rCAF–G	157.19	53.73	68.52

Table 7.5: Porosity and thermal properties of oCAF, rCAF and 2rCAF. Mean absolute deviation in parentheses

Sample	**Specific heat capacity 20 °C** $[KJ/m^3\,K]$	**Specific heat capacity 30 °C** $[KJ/m^3\,K]$	**Porosity** [%]
oCAF	1.11 (0.07)	1.19 (0.09)	93.57
rCAF–G	1.57 (0.02)	1.75 (0.02)	91.55
rCAF–GC	1.49 (0.02)	1.74 (0.01)	92.26
rCAF–G–A	1.46 (0.06)	1.75 (0.04)	91.65
rCAF–GC–A	1.31 (0.06)	1.51 (0.13)	91.27
2rCAF–G	1.93	1.99	-

Chapter 8

Life Cycle Assessment of the Original and Recycling Process

In this chapter LCA results of the defined system products PO (which models the lab scale production of oCAF), PR (which models the lab scale production of rCAF-G) and PRI (which models the industrial scale production of rCAF-G) will be analysed. PRI was further studied by varying the used energy mixes with the scope of evaluating the potential reduction of its environmental impact. As a first thing, it will be analysed the impact of the three different product systems which share the same production mix and subsequentially the results which regard the different PRI energetic scenarios will be presented. Recalling what was defined in (Ch. 5), all environmental impacts herein presented were calculated respectively to two distinct units: the *reference units* (*r.u.*) which correspond to 1 kg of material produced and the *functional unit* (*f.u.*) which was previously defined as the amount of material capable to produce a panel of 1 m^2 with a thermal resistance of 1 $m^2\,K/W$. Relative *f.u.* value for defined product systems are re-presented in [Tab. 8.1]((Eq. 5.1)). Due to the complexity of data analysis and the intrinsic branched nature of a product system the following definitions applies:

- **Direct contribution** is defined, for a single unit process, as the sum of the contributions of all of its primary streams defined in its life cycle inventory (LCI). Primary streams are, for example, direct emissions or primary

collected resources which are not connected to any production process (*e.g.* CO_2, biomass, solar energy, natural gas).

- **Cumulative contribution** is iteratively defined, for a single unit process, as the sum of its direct contributions with the cumulative contributions of all the connected subsidiaries processes. Which means that sum all the direct contributions of all sub-linked processes.
- **Principal cumulative contribution** is defined for a principal process unit in a product system (*e.g.* PO.1, PO.2) as the difference between its cumulative contribution and the cumulative contribution of all subsidiaries principal process units directly connected (*e.g.* PR.4 principal cumulative contribution excludes the cumulative contribution of PR.3).

Table 8.1: Functional units calculated for PO, PR and PRI product systems.

R [m^2 **K/W**]	**A** [m^2]	**λ** [**W/m K**]	**ρ** [**W/m k**]	**thickness** [**m**]	**Volume** [m^3]	**f.u.** [**kg**]	**Product System**
1	1	0.04323	78.26	0.043	0.043	3.383	PO
1	1	0.04923	127.91	0.049	0.049	6.297	PR
1	1	0.04923	127.91	0.049	0.049	6.297	PRI

8.1 Product systems comparison

Grouped LCA result comparing the impacts of PO, PR and PRI product sistems, calculated on *f.u.* basis, are shown in [Tab. 8.2] and graphical representations of relative impacts are available in [Fig. 8.2] and [Fig. 8.3]. Due to the lacking definition of the contribution of equipment production impacts, during the definition of the product systems, direct comparison between lab scale (PO and PR) and industrial (PIR) system have to be done with caution. Analysing the associated environmental impacts of PO and PR system, it is immediately worth mentioning that the PR possesses a reduced footprint in all the analysed categories, leading to the conclusion that the recycling option is, at least in the lab scale, environmentally preferable to landfill and insulator substitution. Furthermore, PO shows a reduced embodied energy, despite the fact that $2.37 \cdot 10^3$ MJ/*f.u.* of secondary

energy (electricity) are directly used in the defined product system with respect to $1.99{\cdot}10^3$ MJ/*f.u.* which are needed by PO. This is due to the fact that the embodied energy is calculated by taking in to account for all the primary energy which is required, not only by the defined system units (*e.g.* electric energy production), but also by all the subsidiaries processes. As it will be clear at the end of this section, oCAF and rCAF production is an extremely energy intensive process with considerable impacts but alginate production does not have to be underrated since its extraction represents a solid mark in numerous categories.

Table 8.2: Impacts calculated for PO, PR and PRI product systems, calculated on *f.u.* basis. RER = Renewable Energy Resource, n-RER = non Renewable Energy Resource

	PO f.u.	**PR** f.u.	**PRI** f.u.	**Unit**
Acidification Potential	2.56E+00	2.12E+00	4.05E-01	kg SO_{2eq}
Climate Change (GWP 100)	2.81E+02	2.68E+02	5.27E+01	kg CO_{2eq}
Photochemical Oxidation	1.07E-01	2.74E-02	6.20E-03	kg formed O_3
Resources Depletion (Abiotic)	2.54E+00	1.94E+00	3.89E-01	Sb_{eq}
Embodied Energy	6.85E+03	5.64E+03	1.12E+03	$MJ_{eq.}$
total n-RER	5.65E+03	4.27E+03	8.51E+02	$MJ_{eq.}$
fossil (n-RER)	4.84E+03	3.49E+03	7.04E+02	$MJ_{eq.}$
nuclear (n-RER)	8.09E+02	7.84E+02	1.46E+02	$MJ_{eq.}$
primary forest (n-RER)	1.23E-01	3.77E-02	7.91E-03	$MJ_{eq.}$
total RER	1.20E+03	1.36E+03	2.71E+02	$MJ_{eq.}$
geothermal (RER)	7.85E+01	9.05E+01	1.62E+01	$MJ_{eq.}$
biomass (RER)	1.69E+02	2.03E+02	6.06E+01	$MJ_{eq.}$
solar (RER)	2.38E+02	2.73E+02	4.87E+01	$MJ_{eq.}$
water (RER)	5.85E+02	6.55E+02	1.19E+02	$MJ_{eq.}$
wind (RER)	1.31E+02	1.43E+02	2.60E+01	$MJ_{eq.}$

It is, indeed, interesting to focus the attention on the fossil primary energy demand, which pose the biggest contribute to the total material embodied energy, both in PO and PR system. As it can be seen in [Fig. 8.1], in which the principal cumulative contributions to fossil primary energy demand are represented, the lyophilization principal process unit (PR.3 and PO.5) shares the highest impact contributing respectively to 91% and 57% in PR and PO. These contributions, recalling their respective inventories, PO.5 [Tab. 5.6] and PO.3[Tab. 5.9], are derived by the subsidiary processes responsible for electric energy (E.E.) production (oil

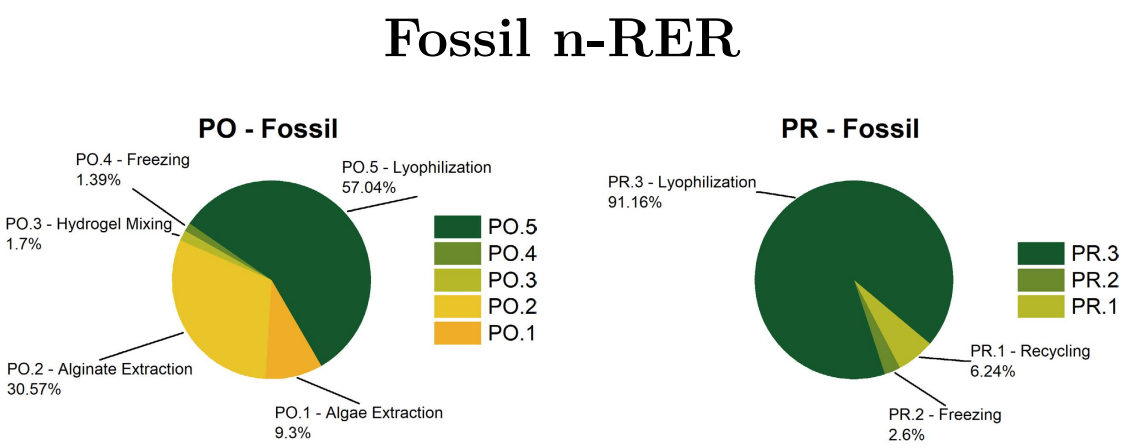

(a) PO product system **(b)** PR product system

Figure 8.1: Principal cumulative contribution to Fossil n-RER with respect to the total system product impact.

and water waste processes contributions are neglectable, $< 0.01\%$). Interestingly, PO.2, despite sharing only $\approx 2\%$ of the total E.E. consumed by principal processes, impacts for about 30%: by raw data analysis this can be directly brought back to the direct contribution of ethanol and acetone production (respectively accounting for 12% and 13% of total PO fossil n-RER impact). As a matter of fact, Ethanol, as defined in the *Ecoinvent* database, is provided by synthesis route (from hydration of ethylene of steam cracking origin), whereas acetone is obtained by cumene oxidation process. Another important contribution of PO to fossil origin embodied energy is derived by fuel consumption in PO.1 (algae harvesting) due to small-boat operation (8.27% of cumulative contribution from diesel refinery process). PRI embodied energy is drastically reduced, with respect to its lab scale counterpart and this is manly due to reduced secondary energy demand. Relative direct process contributions to PIR embodied energy is similar to those of PR, also visible in [Fig. 8.3], with chemical cumulative contribution accounting for a 3% maximum.

By analysing the other categories, by single process principal cumulative contributions, it can be immediately noticed how the impacts associated with the electric energy production dominates, as the shares of PO.5, PR.3 and PRI.2 (*i.e*

Table 8.3: Principal cumulative contribution of principal processes units of PO, PR and PRI product systems, calculate on *f.u.* basis. Percentage share with respect to overall impact.

Product System	Principal Process Unit	Principal Cumulative Contribution			
		GWP 100	Acidification Potential	Resources Depletion (abiotic)	Photochemical Oxidation
PO	PO.5	76.26%	66.74%	60.69%	19.56%
	PO.4	1.84%	1.62%	1.48%	0.48%
	PO.3	2.25%	1.87%	1.77%	0.61%
	PO.2	17.79%	12.39%	28.17%	77.18%
	PO.1	1.83%	17.35%	7.89%	2.16%
PR	PR.3	91.78%	92.72%	91.39%	87.74%
	PR.2	2.59%	2.65%	2.61%	2.50%
	PR.1	5.63%	4.63%	6.00%	9.75%
PRI	PRI.1	84.31%	88.47%	83.10%	70.65%
	PRI.2	15.69%	11.54%	16.90%	29.35%

the lyophilization step) remain higher with respect to other principal process units (waste and transportation contributions remains neglectable $< 1\%$)[Tab. 8.3]. The sole exception is presented by the photochemical oxidation impact of PO product system: here the process associated with the alginate extraction (PO2) contributes, alone, with a 77%. This is caused by the emission of small volatile alkanes and ketones during acetone and ethanol production (respectively marking a solid 33.71% and 42.05% cumulative contribution to overall impact)[Fig. 8.13]. By eliminating the need of new alginate, PR indeed drastically cuts its emissions associated with this category (*i.e.* coming from organic solvents production)[Fig. 8.2]. Alginate extraction, and in particular solvent associated production process, is the main responsible for the higher oCAF production process (PO) impacts. Calculations, indeed, show that the absolute contribution of oCAF foam making processes (*i.e.* summing PO.3, PO.4 and PO.5 principal cumulative contributions) with respect to rCAF foam making (*i.e.* PR.1, PR.2 and PR.3) processes is lower in all the analysed categories. As stated above, solvents make a huge impact in photochemical oxidation category which then decrease, by order, in abiotic resources depletion (due to their petrol-chemical origin) GWP100 and acidification potential (in these two categories, associated production process emissions are the main responsi-

bles). In this last category, sulphuric acid manufacture (a subsidiary process of PO.2, used in alginate extraction) makes a direct contribution of about 4.13% (due to release of SO_x and NO_x)[Fig. 8.7]. The second higher direct contribution, regarding acidification potential, is however represented by the emissions derived by small-boat operation during Algae harvesting (PO.1) which alone counts for more than 15%. Regarding the impact of chemicals used during PR process, EDTA and GDL, their cumulative contributions do not exceed, respectively, 5.48% and 1.19% with the maximum share reached in photochemical oxidation[Fig. 8.14]. The relative high impact of EDTA suggests that by reducing its amount of 2/3, which does not impair the recycling process (as previously demonstrated in (Par. 7.2)), an overall reduction of 1.5% and 3.3% in GWP and Photochemical oxideation of PR can be reached. Differences between PR and PRI product systems impacts simply derive by the reduced electric energy required by the process from the moment that chemicals concentration were unchanged [Fig. 8.3][Fig. 8.2]: as defined in (Par. 5.4.1)[Tab. 5.12], the required energy is reduced to 19% with respect to its lab scale counterpart. As a consequence the electric energy cumulative contribution is drastically reduced in all the impact categories and chemical cumulative contribution share is raised. As a consequence the reduction of EDTA concentration could lead to more important impact reductions: up to 4.2% in GWP100 and 13.5% in photochemical oxidation. As a matter of fact the industrial scale system product, PRI, of the recycling process rCAF (as defined in (Par. 5.4)) can only lead to a first estimation of rCAF production environmental impacts due to the several limitations which are presented in the model: first of all, equipment production and maintenance were not considered. However, the analysis of PO and PR system highlighted so far that electrical energy consumption is the critical parameter that had to be precisely addressed in order to quantify oCAF and rCAF production impacts, which were accurately modelled in PRI-LCI(Par. 5.4.1).

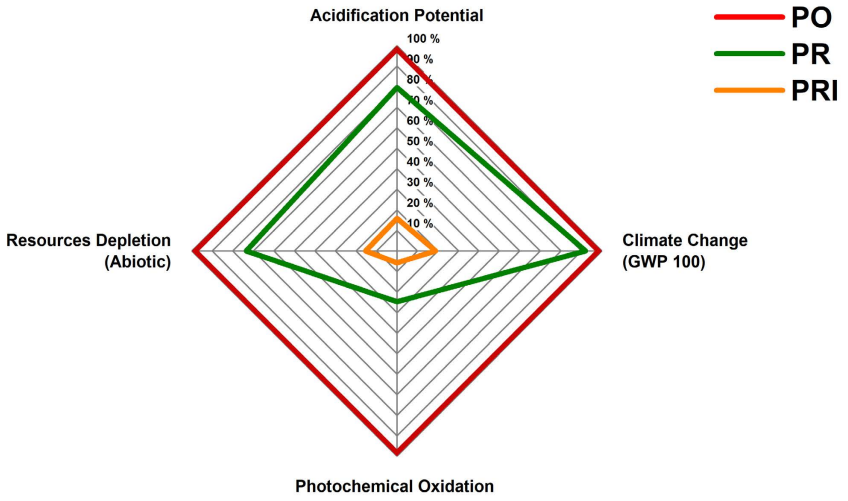

Figure 8.2: Relative impact results of PO, PR and PRI product systems in the studied CML2001 indicators. For each impact category, the maximum result is set to 100% and the other are expressed as relative results with respect to it

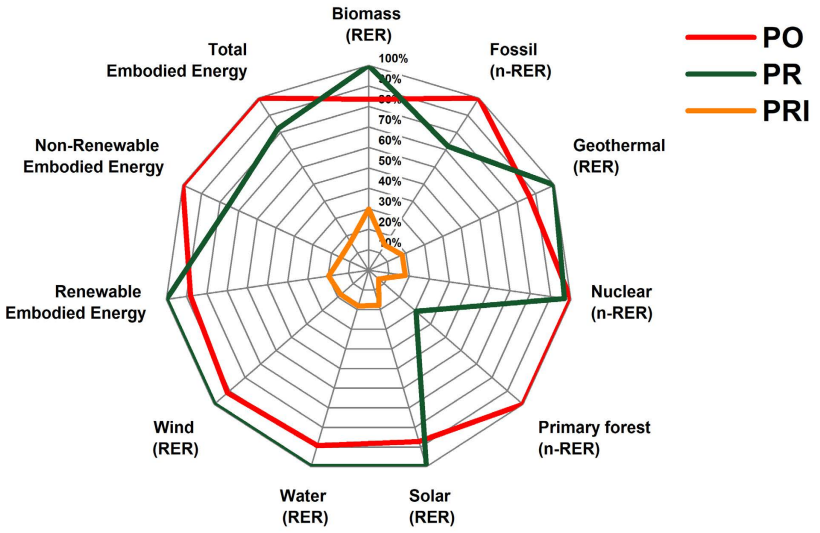

Figure 8.3: Relative impact results of oCAF and rCAF product systems in the main Cumulative Energy Demand indicators. For each impact category, the maximum result is set to 100% and the other are expressed as relative results with respect to it. RER = Renewable Energy Resources, nRER = non Renewable Energy Resources.

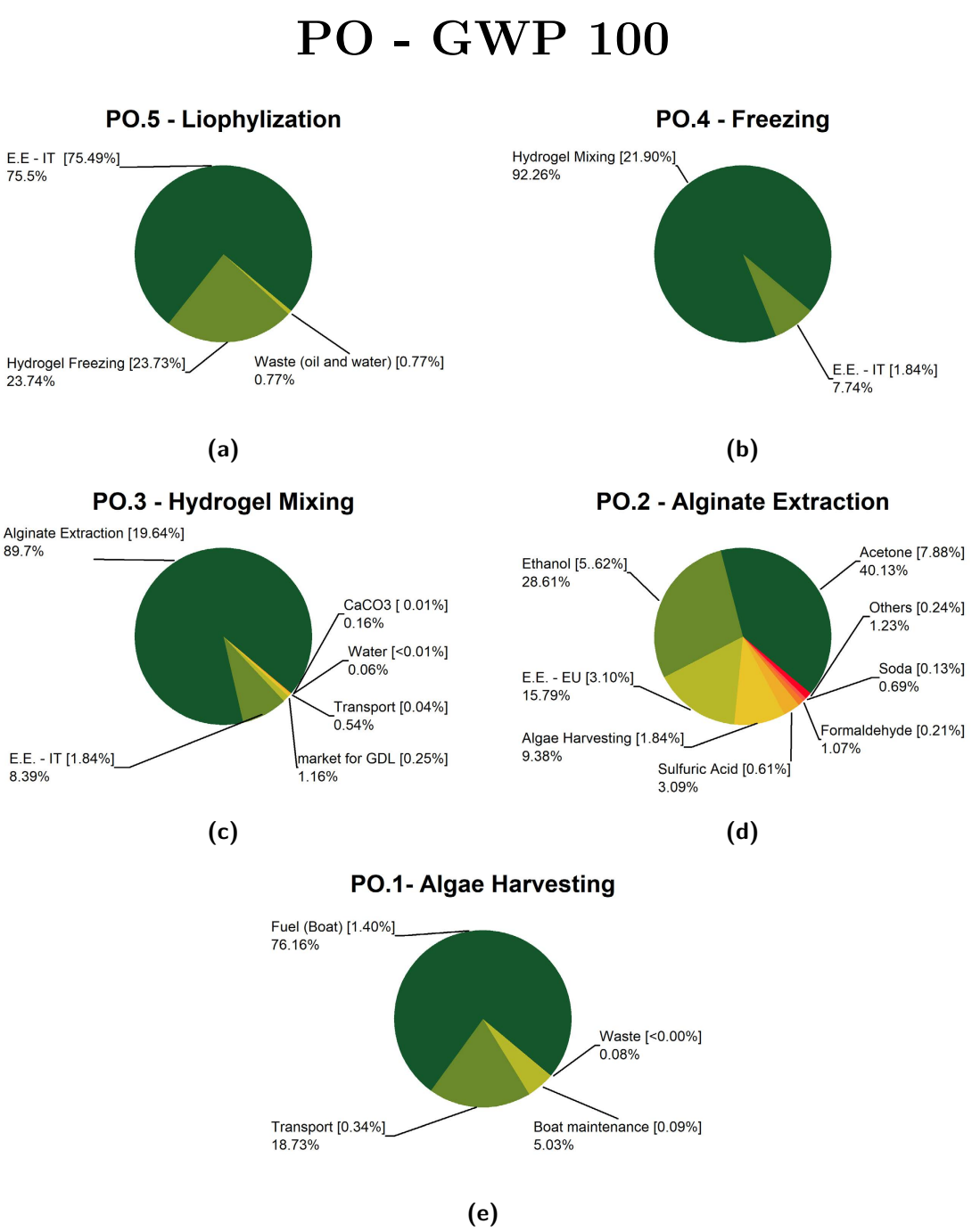

Figure 8.4: Subsidiaries processes cumulative contribution share with respect to parent principal unit process. GWP100 impact category. Inside [ ] are presented the single process cumulative contribution share with respect to the entire PO product system.

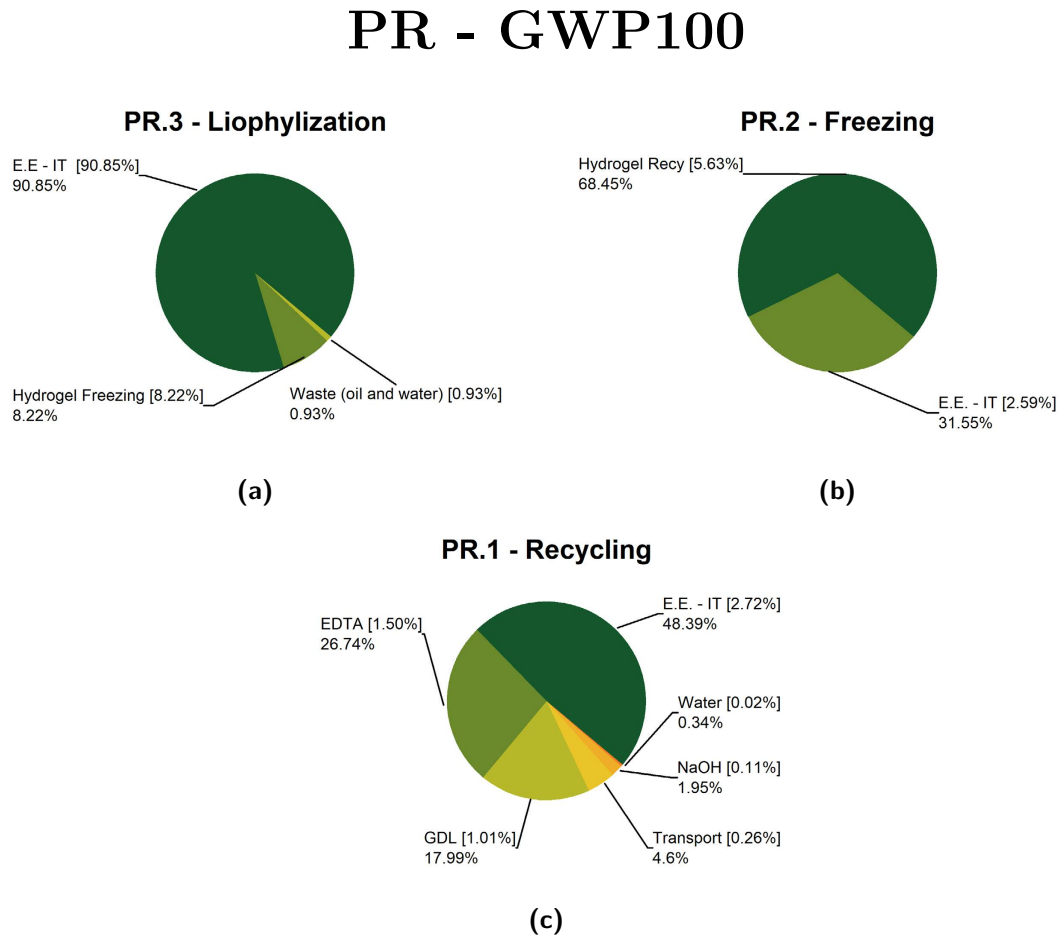

Figure 8.5: Subsidiaries processes cumulative contribution share with respect to parent principal unit process. GWP100 impact category. Inside [ ] are presented the single process cumulative contribution share with respect to the entire PR product system.

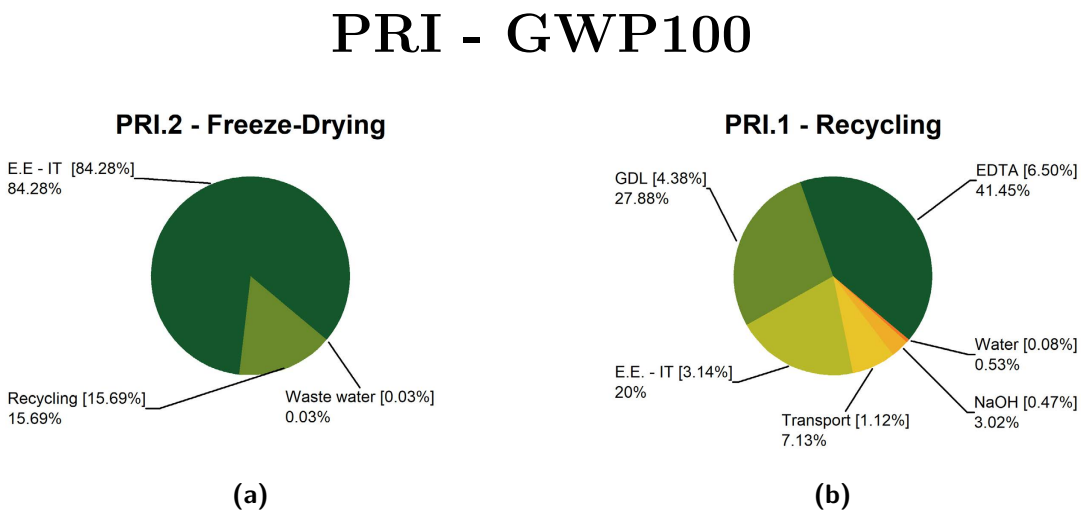

Figure 8.6: Subsidiaries processes cumulative contribution share with respect to parent principal unit process. GWP100 impact category. Inside [ ] are presented the single process cumulative contribution share with respect to the entire PRI product system.

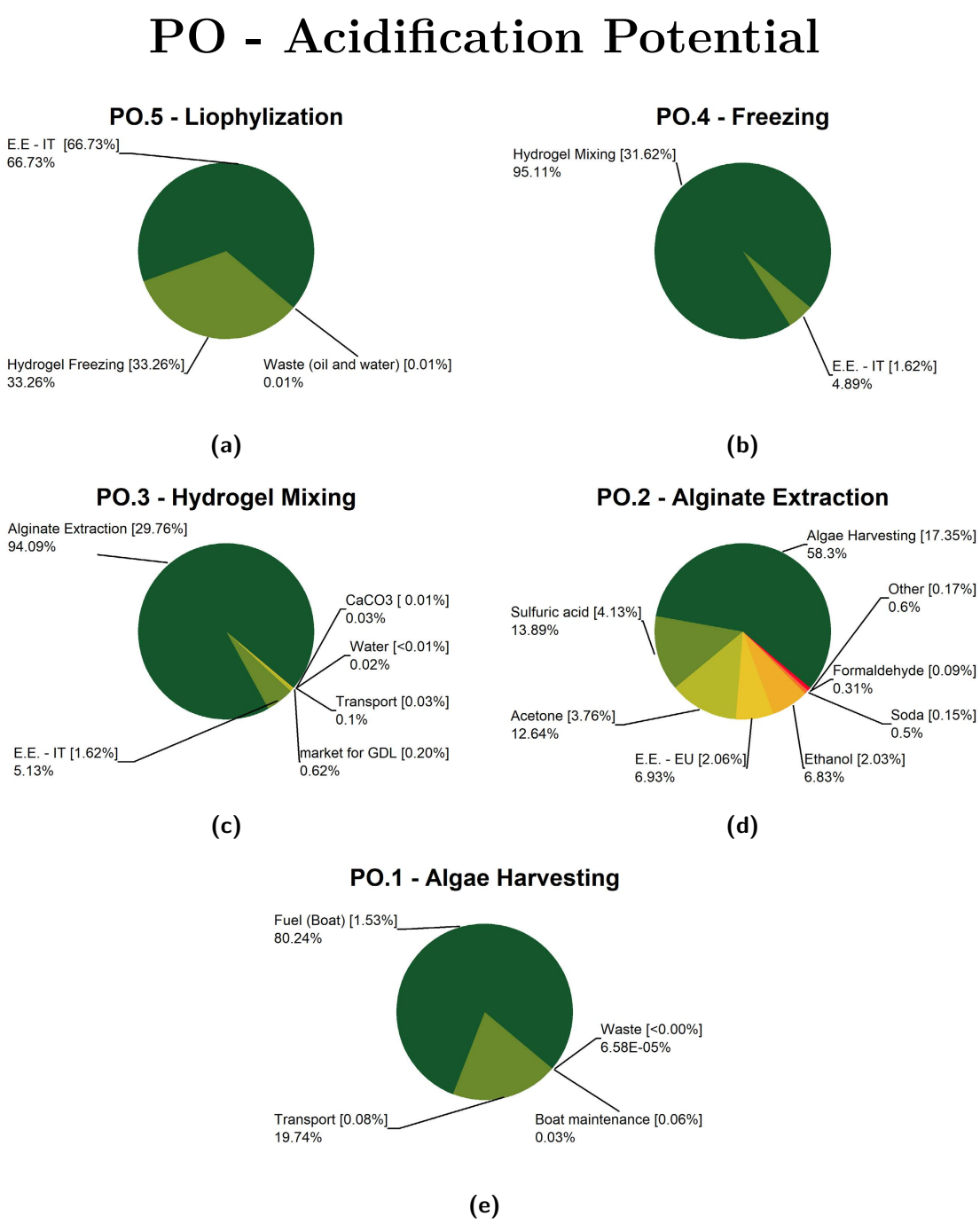

Figure 8.7: Subsidiaries processes cumulative contribution share with respect to parent principal unit process. Acidification Potential impact category. Inside [ ] are presented the single process cumulative contribution share with respect to the entire PO product system.

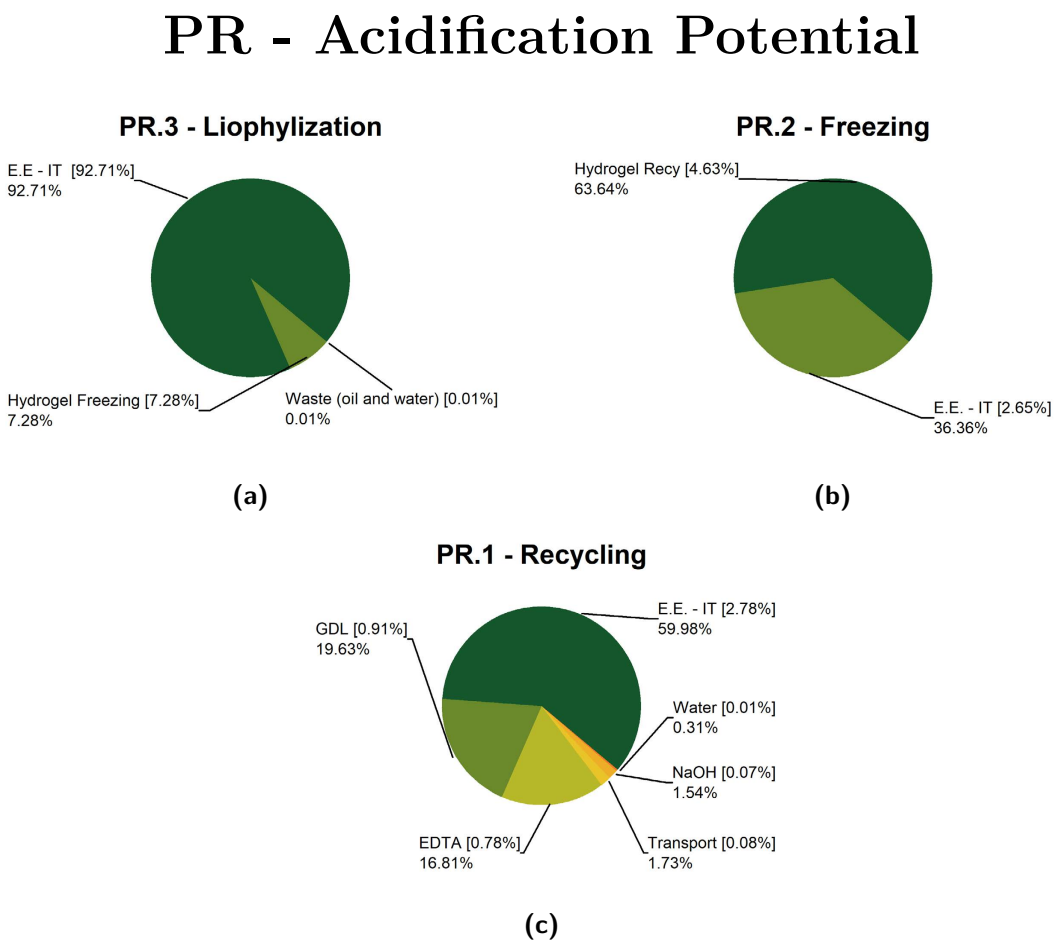

Figure 8.8: Subsidiaries processes cumulative contribution share with respect to parent principal unit process. Acidification Potential impact category. Inside [ ] are presented the single process cumulative contribution share with respect to the entire PR product system.

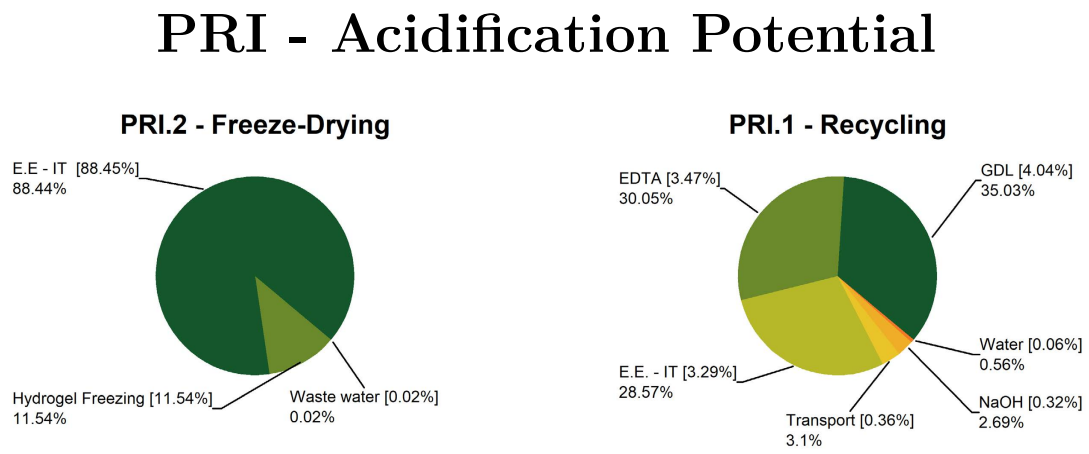

(a) PRI.2 contribution to acid

(b) PRI.1 contribution to acid

Figure 8.9: Subsidiaries processes cumulative contribution share with respect to parent principal unit process. Acidification Potential impact category. Inside [ ] are presented the single process cumulative contribution share with respect to the entire PRI product system.

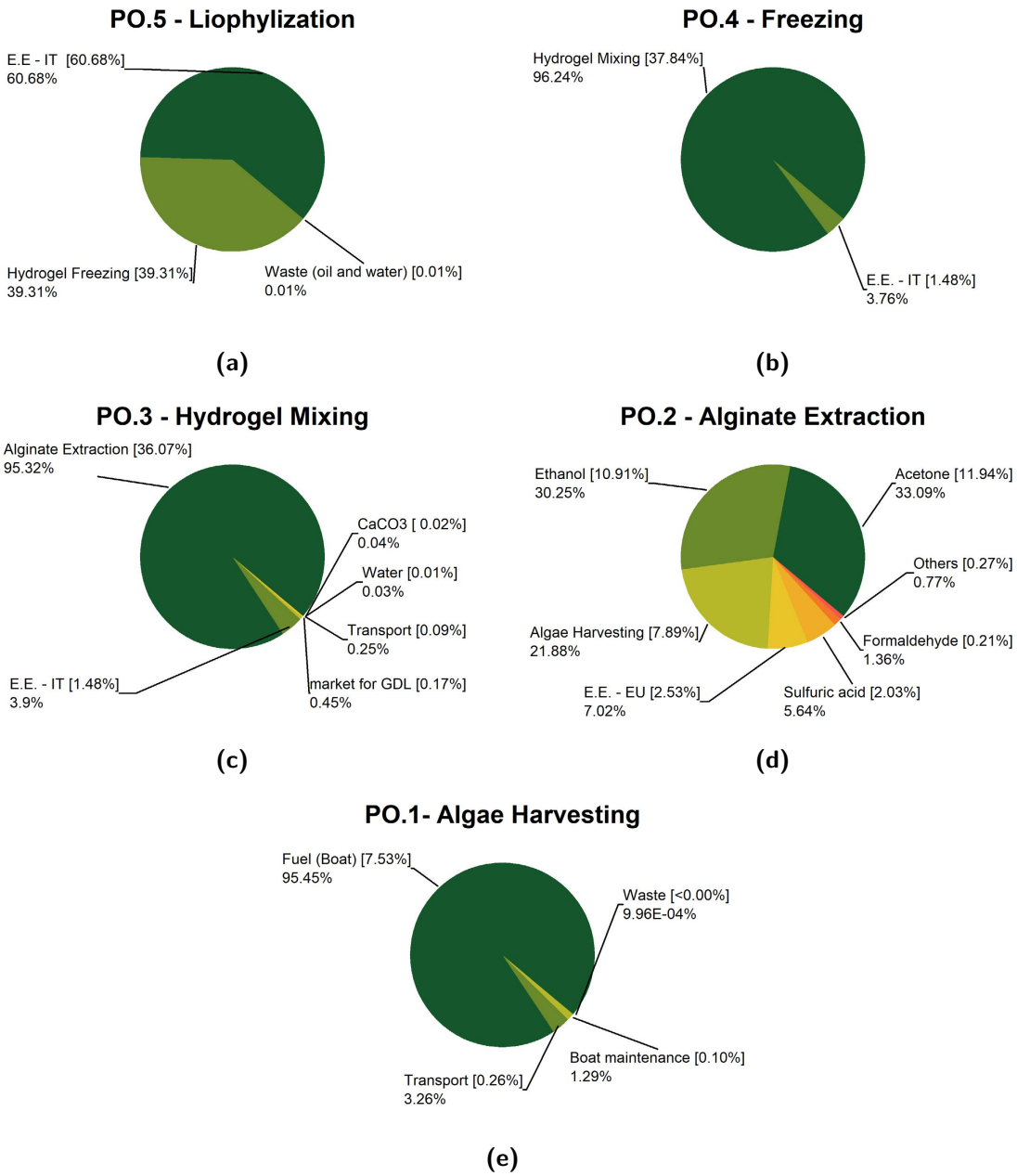

Figure 8.10: Subsidiaries processes cumulative contribution share with respect to parent principal unit process. Resources depletion (abiotic) impact category. Inside [ ] are presented the single process cumulative contribution share with respect to the entire PO product system.

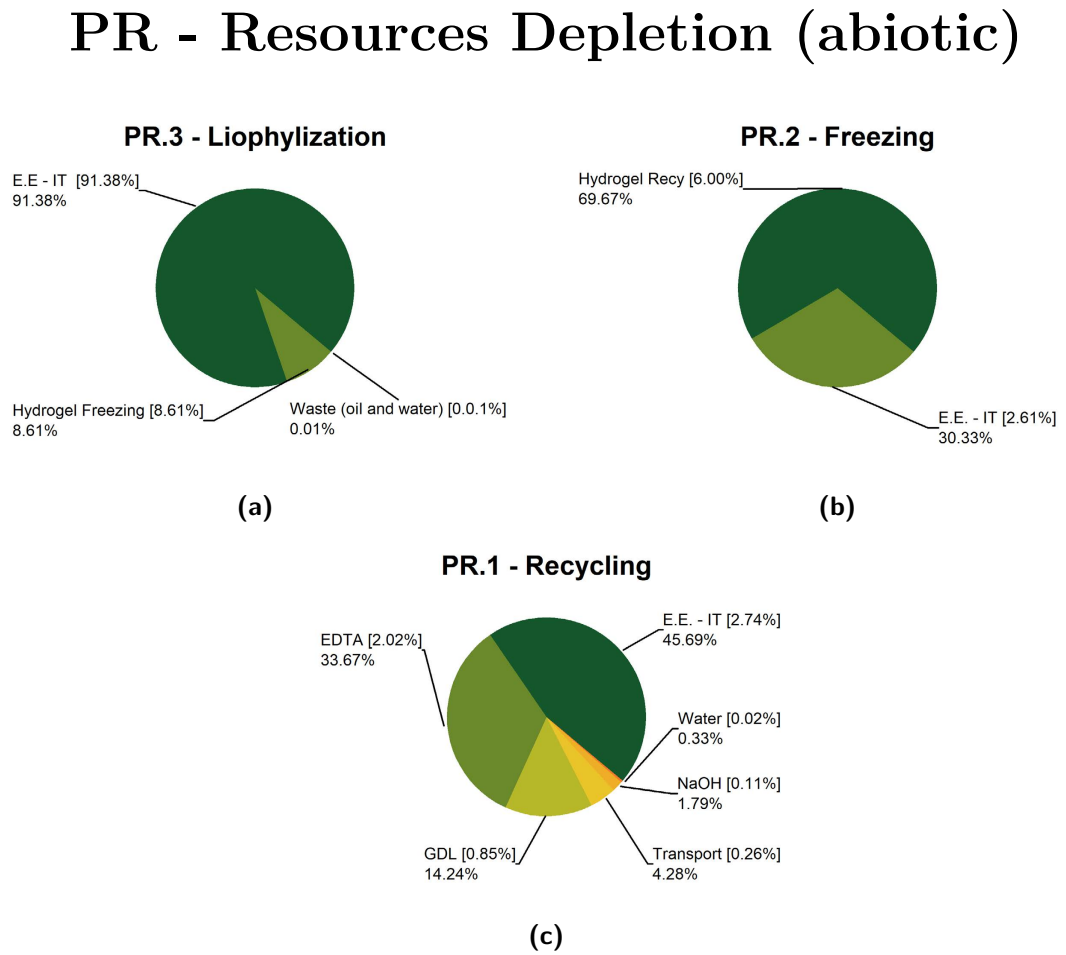

Figure 8.11: Subsidiaries processes cumulative contribution share with respect to parent principal unit process. Resources depletion (abiotic) impact category. Inside [ ] are presented the single process cumulative contribution share with respect to the entire PR product system.

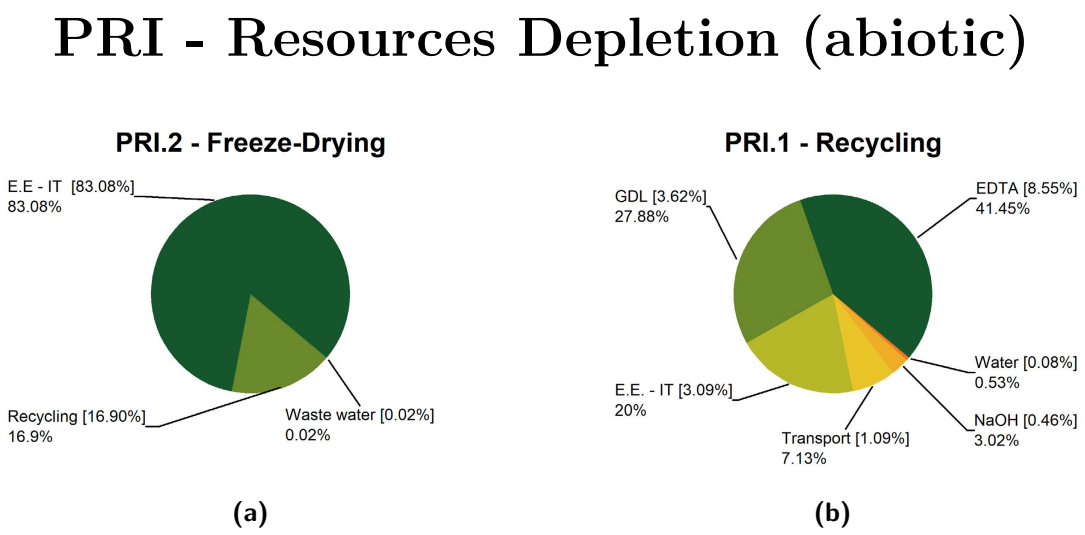

Figure 8.12: Subsidiaries processes cumulative contribution share with respect to parent principal unit process. Resources depletion (abiotic) impact category. Inside [ ] are presented the single process cumulative contribution share with respect to the entire PRI product system

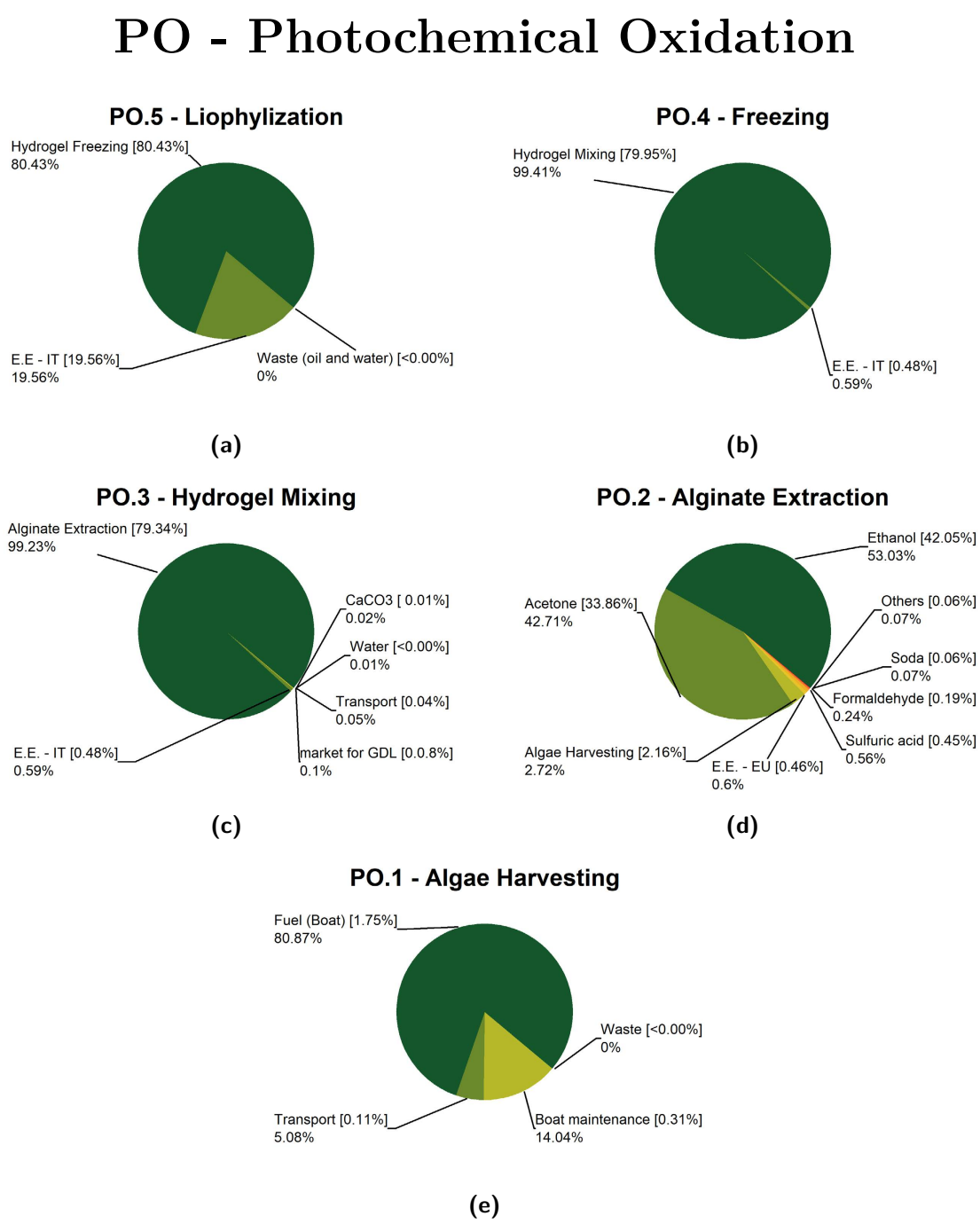

Figure 8.13: Subsidiaries processes cumulative contribution share with respect to parent principal unit process. Photochemical Oxidation impact category. Inside [ ] are presented the single process cumulative contribution share with respect to the entire PO product system

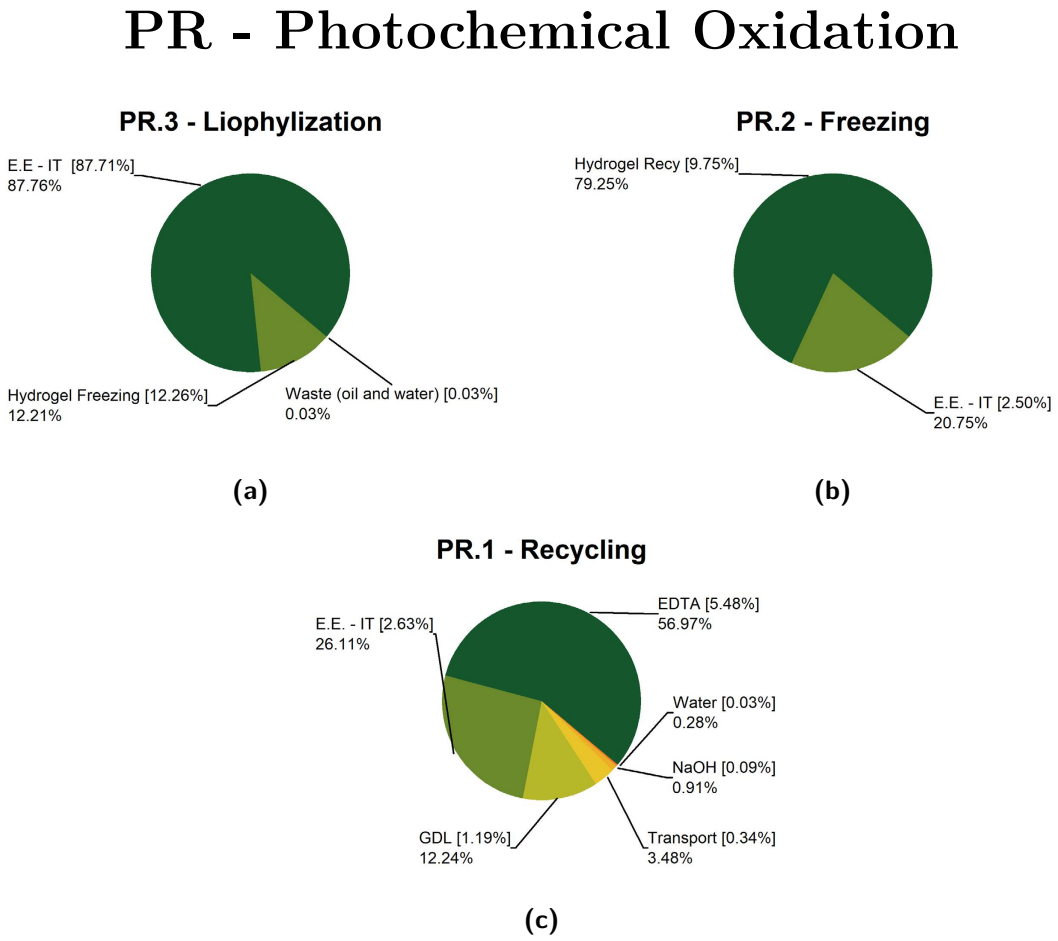

Figure 8.14: Subsidiaries processes cumulative contribution share with respect to parent principal unit process. Photochemical Oxidation impact category. Inside [ ] are presented the single process cumulative contribution share with respect to the entire PR product system

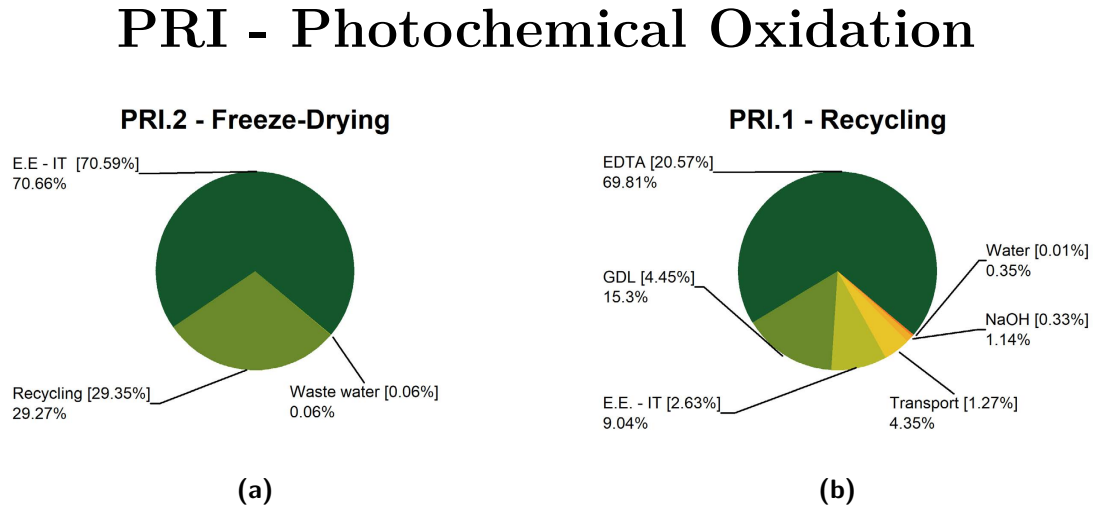

Figure 8.15: Subsidiaries processes cumulative contribution share with respect to parent principal unit process. Photochemical Oxidation impact category. Inside [ ] are presented the single process cumulative contribution share with respect to the entire POR product system

Table 8.4: Principal cumulative contribution of PO, PR and PRI product systems,calculate on *r.u.* basis. Percentage share with respect to overall impact. RER = Renewable Energy Resource, n-RER = non Renewable Energy Resource

	PO r.u.	**PR** r.u.	**PRI** r.u.	
Acidification potential (generic)	7.56E-01	3.36E-01	6.43E-02	kg SO_{2eq}
Climate change (GWP 100a)	8.29E+01	4.26E+01	8.37E+00	kg CO_{2eq}
Photochemical oxidation	3.15E-02	4.35E-03	9.85E-04	kg O_2-for.
Resources Depletion (abiotic)	7.51E-01	3.08E-01	6.18E-02	kg Sb_{eq}
Embodied Energy	2.02E+03	8.95E+02	1.78E+02	$MJ_{eq.}$
total n-RER	1.67E+03	6.78E+02	1.35E+02	$MJ_{eq.}$
fossil (n-RER)	1.43E+03	5.54E+02	1.12E+02	$MJ_{eq.}$
nuclear (n-RER)	2.39E+02	1.24E+02	2.32E+01	$MJ_{eq.}$
primary forest (n-RER)	3.64E-02	5.99E-03	1.26E-03	$MJ_{eq.}$
total RER	3.55E+02	2.17E+02	4.30E+01	$MJ_{eq.}$
biomass (RER)	5.00E+01	3.22E+01	9.63E+00	$MJ_{eq.}$
geothermal (RER)	2.32E+01	1.44E+01	2.58E+00	$MJ_{eq.}$
solar (RER)	7.02E+01	4.33E+01	7.73E+00	$MJ_{eq.}$
water (RER)	1.73E+02	1.04E+02	1.90E+01	$MJ_{eq.}$
wind (RER)	3.87E+01	2.28E+01	4.13E+00	$MJ_{eq.}$

8.2 Different energetic scenario - PRI

The analysis performed in the previous section highlighted how the electric energy, used principally during the lyophilization process, has the most considerable impact on the environmental footprint of both the original and recycled material. However, "*not all electric energy is created equal*": as a matter of fact differences in production or production mix could lead to important variation into a material's impact (that is, indeed, the whole point of the ongoing global energetic *agenda*). A total of 7 different energetic scenarios were computed by varying the production energy mix used: 4 are based on real state production mixes whereas the other 3 are synthetic scenarios in which the whole energy is supplied by one single renewable energy source. The main objective of this analysis is the assessment of the range of potential variation of the environmental impact of rCAF production. The "state" scenarios where chosen with the main aim of testing realistic conditions

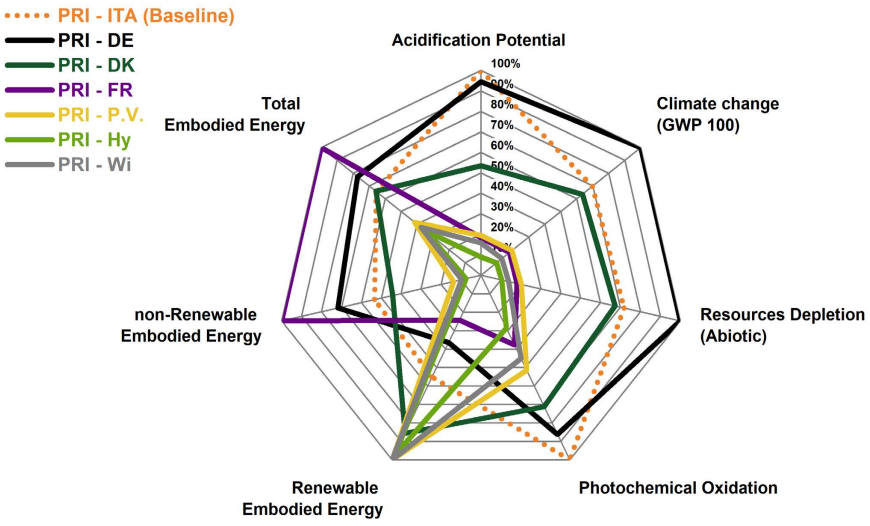

Figure 8.16: Relative impact results of different energetic scenarios of PRI product system in the studied CML2001 and Cumulative Energy Demand indicators. For each impact category, the maximum result is set to 100% and the other are expressed as relative results with respect to it.

whereas the three "synthetic" scenarios where chosen in behalf of a realistic near-future perspective in which electric energy is totally provided by renewable energy sources (at least for some restricted sectors or applications). The four selected energy production mixes were: the italian mix (which is the base-line scenario which was used in the previous section), the German mix (whose energy is mainly provided by hard coal source), the French mix (in which nuclear is the biggest energetic provider, with more than 79% of share) and the Danish (which possesses one of the highest renewable share in the EU area). For the "synthetic" scenarios, photovoltaic, wind power and hydroelectric were chosen as renewable providers (detailed composition is provided in [Tab. 5.10]).

In [Tab. 8.5] and [Tab. 8.6] respectively, the associated impacts of the three scenarios are presented, a graphical representation of relative impacts is also presented in [Fig. 8.16]. By focusing the attention on the climate change indicator (GWP100) it can be directly noticed that the results span over a whole order of magnitude. Among the four "state" scenarios, as easily predictable, PRI-DE possesses the

worst impact (due to emission of coal power plants) whereas PRI-FR the lower. Low impact of PRI-FR in GWP100 comes from the reduced share of fossil fuel in energy mix while nuclear energy production shows up only due to fuel enrichment ($\approx 6\%$). In this scenario the relative cumulative impacts of chemicals (EDTA adn GDL) rise up to cover 42% of the total impact share in GWP100, reaching 54% in photochemical oxidation category (with 20% of direct contribution of EDTA synthesis due to emission of formaldehyde precursor). Low envoronmental impacts, however, are payed off by an increase in the total embodied energy due to the high uranium primary embodied energy. Still high non renewable fraction of Denish electric energy mix lead to a softer reduction of associated impacts (Interestingly, photochemical oxidation and acidification potential reduction is caused by lower share of N. Gas and Biogas in Danish energy mix with respect to the Italian one).

As far the "synthetic" energy scenarios are concerned the major contribution, for GWP100, still comes from the electric energy provider process in PRI-P.V.,$\approx$ 56%, with a nested cumulative contribution of $\approx$37% (with respect to the whole PRI impact) derived by photovoltaic panel production. Electric energy production cumulative impact is drastically reduced in PRI-Wi ($\approx$32%, with the wind turbine subsidiary construction process that contribute with a 28% on the total impact) and it is further diminished in PRI-Hy where it accounts only for 10% (mainly shared by implant construction). In this last scenario, EDTA production process alone accounts for more than 45% (cumulative) of the shared impact. By lowering the electric energy impact share, the influence of the ammount of EDTA which is used in the process becomes significat (even some in state scenarios), therefore in the optic of the overall environmental impact reduction of rCAF material production, a finer tuning of EDTA concentration becomes fundamental. As a matter of fact, a potential reduction of $\approx$ 30% (calculated for PRI.Hy) in GWP100 is possible by using a Ca/EDTA molar ratio equal to 1.

Eventually, in [Tab. 8.7] a comparison between the calculated impacts of PRI and those of conventional TIM is presented. rCAF production modelled by PRI using state energy mix is not competitive against other TIMs in terms of both GWP100 and embodied energy with the exception of PRI-FR scenario (due to the energy

intensive lyophilization process). However, by taking advantage of low electric energy impact of renewable resources, rCAF impact becomes comparable to those of conventional TIMs.

Two consideration have to be made at this point: this LCA study is far from being exhaustive since the as-modelled industrial-scaled product system (PRI) was developed by focusing on the scaling of electric energy consumption and no equipment maintenance is considered nor the final production step of GDL(*e.g. fermentation from glucose* was modelled. nevertheless it allows to highlight the more critical, environmentally speaking, aspect of the recycling process toward which future research has to be done (*i.e.* finer tuning of chemicals concentrations, EDTA as first).

Table 8.5: Impacts calculated for state energy mixes of PRI product systems, calculated on *f.u.* basis. RER = Renewable Energy Resource, n-RER = non Renewable Energy Resource

	PRI - DE	**PRI - DK**	**PRI - FR**	**PRI - ITA (Baseline)**	**unit**
Climate Change (GWP 100)	7.56E+01	4.80E+01	1.35E+01	5.27E+01	kg CO_{2eq}
Acidification Potential	3.83E-01	2.17E-01	7.41E-02	4.05E-01	kg SO_{2eq}
Photochemical Oxidation	5.35E-03	4.42E-03	2.34E-03	6.20E-03	kg O_3-for.
Resources Depletion (Abiotic)	5.42E-01	3.65E-01	9.80E-02	3.89E-01	kg Sb_{eq}
total Embodied Energy	1.32E+03	1.13E+03	1.71E+03	1.12E+03	$MJ_{eq.}$
total n-RER	1.79E+02	4.20E+02	1.19E+02	2.71E+02	$MJ_{eq.}$
total RER	1.15E+03	7.07E+02	1.60E+03	8.51E+02	$MJ_{eq.}$

Table 8.6: Impacts calculated for synthetic energy mix scenarios of PRI product systems, calculate on *f.u.* basis. RER = Renewable Energy Resource, n-RER = non Renewable Energy Resource

	PRI - P.V.	**PRI - Hy**	**PRI - Wi**	unit
Climate Change (GWP 100)	1.46E+01	7.35E+00	9.88E+00	kg CO_{2eq}
Acidification Potential	7.86E-02	3.61E-02	6.37E-02	kg SO_{2eq}
Photochemical Oxidation	3.19E-03	1.78E-03	2.79E-03	kg O_3-for.
Resources Depletion (Abiotic)	1.10E-01	5.68E-02	7.56E-02	Sb_{eq}
total Embodied Energy	7.10E+02	5.98E+02	6.45E+02	$MJ_{eq.}$
total n-RER	4.91E+02	4.79E+02	4.91E+02	$MJ_{eq.}$
total RER	2.19E+02	1.19E+02	1.54E+02	$MJ_{eq.}$

Table 8.7: Environmental impacts (Embodied energy and GWP100) comparison between conventional TIMs (data from [36]) and rCAF produced and modelled in this work.

Material	**f.u.**	**Thermal Conductivity**	**Embodied Energy**	**GWP**
	[kg]	[W/m K]	[MJ_{eq}]	[kg] CO_{2eq}
Cellulose	2.00	0.04	20.97	3.66
Cork	7.53	0.05	378.65	5.93
EPS	1.13	0.04	118.67	8.25
EPS	0.80	0.04	127.31	5.05
Polyurethane (expanded)	0.99	0.03	126.40	5.31
XPS	1.75	0.04	127.31	13.22
Glass-wool	8.00	0.05	229.02	9.89
Stone Wool	2.40	0.04	63.34	3.26
Recycled textile(commercial)	1.79	0.04	17.57	1.55
rCAF	6.29	0.05		
PRI-IT			1121.58	52.69
PRI-DK			1127.00	47.98
PRI-FR			1714.81	13.48
PRI-DE			1324.65	75.61
PRI-P.V.			710.06	14.65
PRI-Hy			598.44	7.35
PRI-Wy			644.86	9.88

Chapter 9

Graphene Oxide - composite Alginate Foam

Graphene Oxide was introduced in oCAF composition with the main scope of enhancing its flame resistance behavior. Micro-combustion calorimetry and cone-calorimetry were initially used, respectively, to asses graphene oxide behavior in alginate foam and nanocomposite alginate foam samples (oCAF-GO2). Contemporarily, tests toward the compatibility of the so formed nanocomposite with respect to the recycling process were conducted and, similarly to what was done in (Par. 7.3), the conservation of oCAF-GO functional properties in rCAF-GO (thermal and acoustical) were evaluated. Eventually the preservation of GO functional properties (*i.e.* flame retardant) on recycled samples were further assessed through cone-calorimetry.

9.1 GO dispersion in alginate

The production of oCAF-GOx sample has been described in details in (Par. 4.1.1). To ensure a good dispersion and compatibilization with alginate, GO solution ($0.4\%_{wt}$) was firstly sonicated and treated via mechanical homogenization before being mixed with alginate solution. Thenceforth, the alginate-GO solution (AS-GO) was further homogenized. Frequency sweep rheology was used to charac-

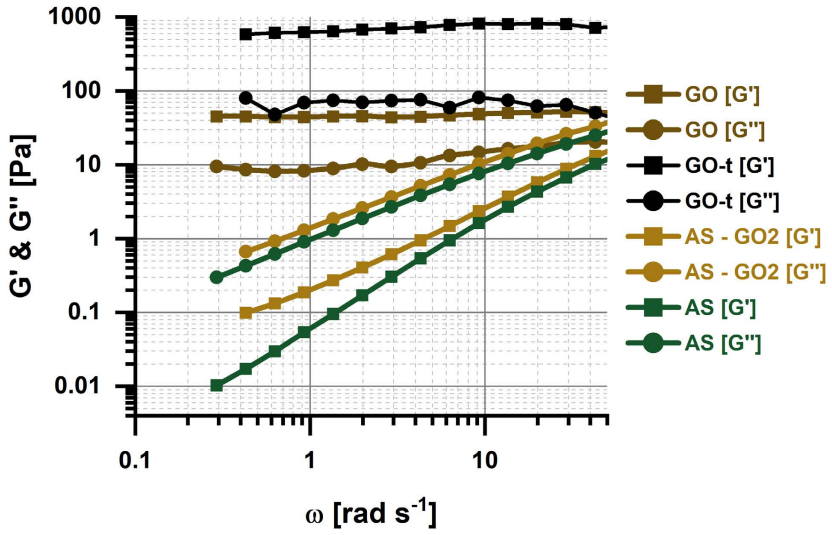

Figure 9.1: Frequency Sweep test of mild sonicated GO solution (GO), homogenized GO solution (GO-t), AS= Clean Alginate solution and Graphene oxide - Alginate solution (AS-GO2).

terize, for both the treated GO (GO-t) and the final AS-GO solution, the compatibilization of GO with alginate. By focusing the attention on low frequency mechanical spectra of GO and GO-t,[Fig. 9.1], it can be immediately noticed that both solutions present an elastic gel behavior (both G′ and G″ shows a frequency-independent behavior) with a marked increase in both the storage (G′ , *i.e.* elastic component) and loss (G″ , *i.e.* viscous component) modulus in the treated GO solution. However, if compared with the value of AG sample ([Fig. 7.9]) it can be noticed that G′ and G″ values of GO untreated solution are one order of magnitude lower. This behavior is typical of concentrated GO solution ($> 0.04\%_{wt}$) in which GO sheets tend, in solution, to re-stack in large crystalline domain reaching and, if the mechanical percolation limits is reached G′, increase over G″[252][253]. Mechanical homogenization is commonly used to temporarily enhance nanoparticle dispersion in liquid or in low-viscouse polymeric solutions, here it has been used to induce exfoliation of GO layer to increase its dispersion in the alginate ma-

trix. Both G′ and G″ increase after homogenization treatment, a behavior that is compatible with the increase of the interconnection degree of the mechanical network. In accordance with the percolation theory, by having maintained constant the mass fraction in the solution the increase of the magnitude of the mechanical response can be associated with an increase of the volumetric concentration of GO which is only possible as a result of a better exfoliation degree[254]. From a phenomenological point of view, the GO solution, after mechanical homogenization, shifts from showing a weak-thixotropic behavior to form a highly viscous gel. After the treatment, GO was mixed with alginate and the solution was further homogenized. By having a look at the treated AS-GO2 dispersion with respect to a clear reference alginate solution curve (obtained at the same alginate concentrations and testing conditions) an increase in bot the loss and storage modulus together with a decrease in the slope of G′ can be noted. Such an increase, at low frequencies, is indicative of a lower degree of freedom of alginate chain which is attributed to the interaction between the alginate and the dispersed GO.

9.2 Functional properties of GO nanocomposite Foams

Graphene Oxide was added to oCAF sample at a final concentration of $2\%_{wt.org.}$, calculated over the total organic fraction. This was justified by the fact that only the organic fraction needs to be protected against flame since glass and $CaCO_3$ cannot sustain combustion. As anticipated, the GO nanocomposite alginate foam (oCAF-GO2) was tested against its compatibility toward the recycling process and herein, thermal and acoustical properties of oCAF-GO2 and rCAF-GO2 are presented together. In [Fig. 9.2] acoustic absorption of both GO original (oCAF-GO2) and recycled nanocomposite (oCAF-GO2-G) are confronted respect to their analogues composite foams (oCAF and oCAF-G). The original nanocomposite show a slight shift of the peak toward higher frequencies, with respect to its original composite formulation: such a behavior, shown also by all the recycled sample, ([Fig. 7.11]), can be ascribed to a reduced internal tortuosity of the porous structure. The recycled nanocomposite formulation, however does not show any marked

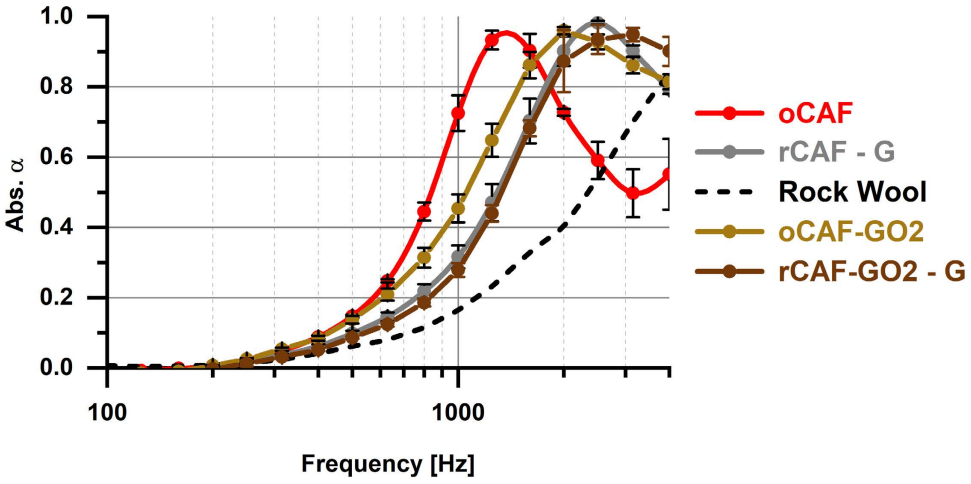

Figure 9.2: Averaged sound absorption coefficients of oCAF, oCAF-GO, rCAF and rCAF-GO samples, mean absolute deviation for each data-point was calculated. Absorption curve of Rock-Wool has been added as reference from literature [1]. Rock-Wool sample thickness: 10 mm.

deviation with respect to its recycled analogous composite (rCAF-G). As far as thermal conductivity is concerned ([Fig. 9.3] and [Tab. 9.1]), despite the fact that GO is a well known good thermal conductor ($\approx$ 50-100 W/mK [255]) its inclusion did not impaired thermal insulation properties of oCAF-GO2. On the contrary, both oCAF-GO2 and rCAF-GO2-G show a reduction in their average thermal conductivity, with respect to their counterparts, which cannot be attributed to a statistical deviation of samples densities (as it is clearly visible in [Fig. 9.3b]). A deeper study of GO nanocomposite pore structure should be performed and μ-CT has been identified as the best characterization method to address this anomalous behavior: an hypotheses is that GO interaction with alginate could have induced a reduced pore size structure. In general, GO nanocomposite, as far as thermal and acoustical functional properties are considered, show its completely compatibility toward the developed recycling process.

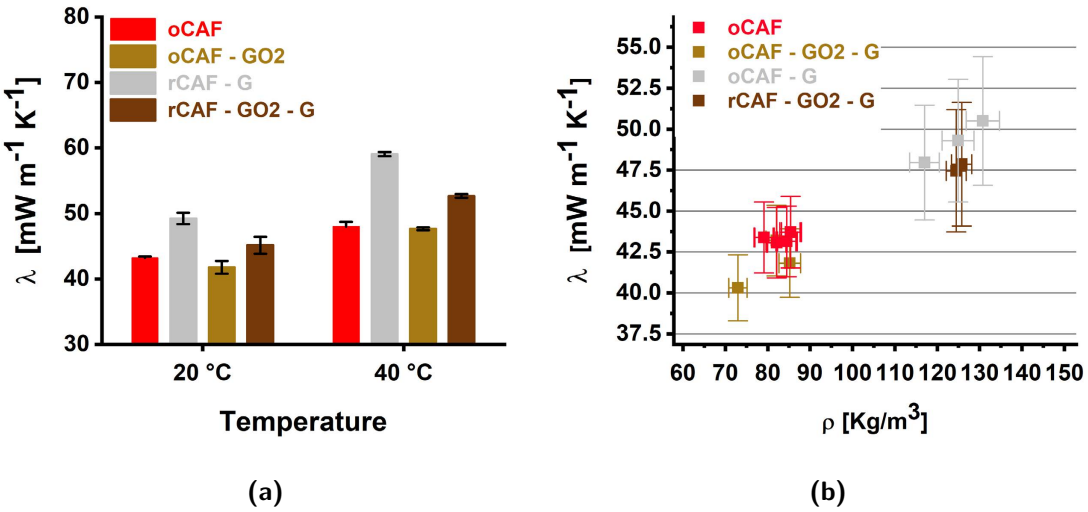

Figure 9.3: Thermal conductivity of oCAF, rCAF, oCAF-GO2 and rCAF-GO2. (**a**) average thermal conductivity values are presented, with the corresponding average absolute error. (**b**) a plot of density vs thermal conductivity at 20 °C of each tested specimen. A relative instrumental precision error of 5% and 3% was attributed to each single measurement, respectively for thermal conductivity and density

Table 9.1: Density and thermal properties of oCAF-GO and rCAF-GO2. Mean absolute deviation in parentheses

Sample	**Density** $[kg/m^3]$	**Thermal Conductivity 20 °C** $[mW/m\,K]$	**Thermal Conductivity 40 °C** $[mW/m\,K]$
oCAF-GO2	80.07 (4.75)	41.77 (0.98)	45.14 (1.29)
rCAF-GO2	125.12 (0.64)	47.66 (0.20)	52.67 (0.26)

9.3 Fire behavior of GO nanocomposite foams

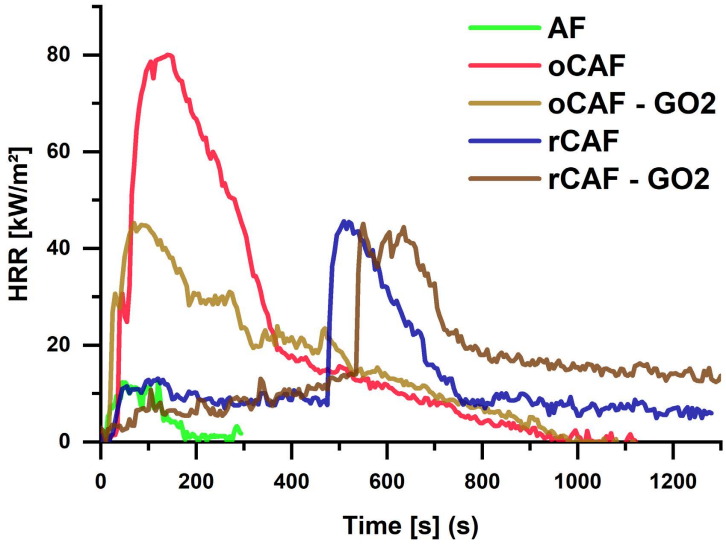

Figure 9.4: Representative cone calorimetry curves of tested samples, detailed data are presented in [Tab. 9.3].

In this paragraph the behavior of the original and recycled alginate foams (oCAF and rCAF-G) at the cone-calorimeter test and the effects of GO, used as flame retardant and added during oCAF production (oCAF-GO2) on the enhancement of flame resistance properties of both the original and the recycled foam (rCAF-GO2-G) will be discussed. In [Fig. 9.4] a typical heat release rate profile of all the tested samples is depicted, whereas averaged values are presented in [Tab. 9.3]. It is worth immediately mentioning that the non flame retarded oCAF shows an average pHRR of 80.78 kW/m^2, which is already a relative low value if compared with those shown by other conventional TIMs such as polyurethane and EPS[Tab. 9.2]. Moreover, no spontaneous ignition was observed, in any tested composition, without the use of the external igniter. The major contribution to the HRR of oCAF is derived by Fibre-Glass waste, which build up 67.10 $\%_{wt}$ of the total sample mass, containing 33.6 $\%_{wt}$ of $Al(OH)_3$[Tab. 9.4]. As a a matter of fact, alginate, as previously described in (Par. 2.6), is a well known char forming polymer which, once tested, showed a pHRR of only 9.35 kW/m^2 and failed to ignite even with

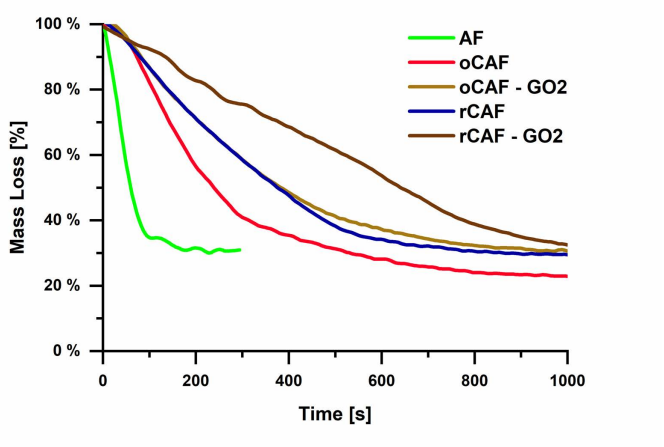

Figure 9.5: Mass loss curve of cone calorimeter tested samples. Averaged and smoothed (20pt Savitzky–Golay filter).

external igniter(visible in [Fig. 9.4]). The char forming contribution of alginate to fire behavior of composite samples is clearly visible in all HRR curves that show the typical progression of a burning char forming polymers: the pHRR is reached straight after the ignition followed by a reduction of the heat release. The addition of only 2 $\%_{wt,org.frac.}$ of GO is enough to reduce the pHRR of oCAF of about 42% which is followed by a reduction of the THR of 19%. The interpretation of THR [Fig. 9.6] and mass loss [Fig. 9.5] allows to hypothesize that GO (thanks to its high aspect ratio) primarily acts by enhancing the formation of a non-continuous char layer yet capable of limiting the diffusion of volatiles and thus limiting the combustion rate which eventually leads to flame extinction: this is primarily visible in the overall reduction of the pHRR and in the reduction of mass loss rate in oCAF-GO2 sample with respect to oCAF. In addition, the final residue, with respect to the overall organic content (*i.e. the char yield* $\mathbf{C_y}$, increases from 6.86% to 10.20%. However, a compact protective char is not formed since after the test both samples completely loosed their mechanical stability: this also due to the powder and high inorganic nature of fibre glass filler, which is the major component (by weight) of both oCAF and rCAF. The formation of continuous char layer is also difficult in foam materials due to the high surface area that easily allows combustibles and oxygen exchange with respect to bulk solid materials. The reduction of TTI asso-

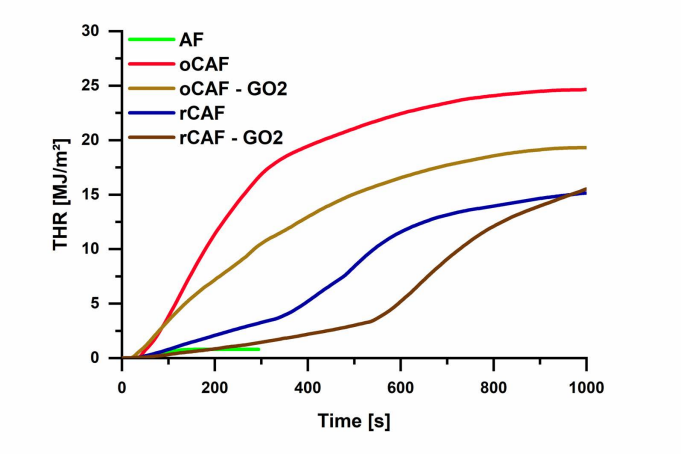

Figure 9.6: Total Heat Release (THR) curves of cone calorimeter tested samples. Averaged.

ciated with GO addition is a frequently reported phenomenon, mainly correlated with carbon based nano-flame retardant, and its commonly associated to the high infrared absorption of nano-filler which locally increase the materials temperature [168]. As far as recycled samples are concerned both show a drastic increase of the TTI which is higher in the sample in which GO was present in origin (rCAF-GO2-G). The ignition is anticipated by a long period of low heat release (without flame) in which both the samples start to loose weight. This shift could be primarily ascribed to the high concentration of organic acid (EDTA, ≈13.05 $\%_{wt}$, and gluconic acid from GDL ≈ 33 $\%_{wt}$) that could act both as char forming and char catalyzing agents with a similar mechanism by which phosporic acid and other organic acids, used in intumescent system act (Par. 2.4.2.1). In addition EDTA could release non flammable N-rich compouds that can dilute the oxygen concentration thus limiting the combustion during the first stage and hence retarding the ignition. The higher final residue of recycled samples, the further reduction of the THR and the reduction of pHRR (with respect to oCAF) support the enhanced char forming hypotheses which, however, fails into building up a continuous layer from the moment that, after the flame out, smouldering occurs (flameless combustion characterized by low heat release)(Par. 2.1). This behavior is particularly observable in rCAF-GO2-G sample in which the THR fails to reach a plateau at

Table 9.2: Typical cone calorimeter test data for non flame retarded TIMs.

non flame retarded TIMs	**THR** [MJ/m^2]	**TTI** [s]	**pHRR** [kW/m^2]
Cellulose [256]	9.5	12	126.6
Polyurethane (expandable foam) [257]	-	5	194.27
XPS [258]	24.07	30	210.5
Polyurethane (rigid foam) [259]	40.7	10	310
EPS [260]	-	54	355.47
XPS [258]	-	39	403.36
Polyurethane (rigid foam) [261]	10.7	0	232.7

Table 9.3: Cone Calorimeter data. THR = Totoal Heat Release, TTI = Time To Ingition, pHRR = peak Heat Release Rate, $\mathbf{C_y}$ = char yield.

Sample	**Res.**		**THR** [MJ/mm^2]		**TTI** [s]		**pHRR** [kW/m^2]	
	$\%_{wt,tot}$	$\mathbf{C_y}$	mean	dev. St.	mean	dev. St.	mean	dev. St.
AF	31.71%	32.45%	0.80	-	NO	NO	9.35	-
oCAF	25.61%	6.86%	23.99	0.93	47.50	17.68	80.78	1.17
oCAF - GO2	28.00%	10.20%	19.31	-	19.31	3.54	46.32	4.55
rCAF	32.03%	22.34%	15.16	1.46	402.50	102.53	49.68	5.73
rCAF - GO2	30.76%	21.00%	15.53	1.04	547.50	17.68	44.32	1.08

1000s. GO presence in the recycled sample leads to a small reduction of the pHRR, with respect to the value of rCAF-G. Nevertheless, a marked change in the mass loss curve is observable which is indicative of its effectiveness in further delaying the combustion (that is degradation) rate of the polymeric matrix. Both in the original and recycled formulation GO seems therefore capable to reduce the mass loss and heat release rate, mainly via a physical barrier mechanism, but fails in inducing the formation of a stable char. This can be ascribed to its reduced thermal stability that leads to its decomposition, failing to act as continuous barrier (in accordance with what is reported in literature (See (Par. 2.5.3)).

Table 9.4: $\%_{wt}$ composition of samples tested at the cone calorimeter. FG = fibre-glass

	oCAF	rCAF	oCAF - GO2	rCAG-GO2 -G
Alg	17.59%	10.90%	17.32%	10.80%
FG	67.10%	41.59%	66.05%	41.18%
CaCO3	1.88%	1.17%	1.86%	1.16%
GDL	13.43%	33.29%	13.22%	32.96%
EDTA	-	13.05%	-	13.22%
GO	-	-	1.57%	0.98%
$\%_{Inorganic}$	20.13%	12.48%	19.81%	12.35%
$\%_{Organic}$	79.87%	87.52%	80.19%	87.65%

9.3.1 Micro combustion calorimetry of alginate GO systems

Micro combustion calorimetry was used to asses the efficacy of GO, and analyze its FR mechanism, in alginate foam (*i.e.* without the addition of fibre-glass) by increasing its content from 1% to 6%. These preliminary tests were also conducted with the aim of understanding if MCC could be used as a reliable technique for characterizing FR efficacy of the different functionalized graphene oxides whose synthesis are discussed in (Ch. 10). The curves presented in [Fig. 9.7] clearly show the double decomposition peaks of alginate: between 200-300 °C esterification and decarboxylation and partial de-polymerization (due to glycosidic bond fraction) reactions take place with main evolution of CO_2 whereas final decomposition and carbonization began above 450 °C with CO evolution[262]. In [Tab. 9.5] detailed average data are presented. The limited but constant reduction of HRC with respect to the increase of GO concentration tends to confirm the physical FR effect mechanism of GO and no sign of a chemical FR effect, that would have lead to a marked decrease in HRC with GO content, can be inferred from these data. However, despite the fact that this decreasing trend was confirmed by multiple repetition of these measurement (at least 4 for each composition) none of the above tested conditions allowed to reach a minimum of 10% of oxygen drop in the combustion chamber, which is defined as the minimum concentration required to obtain reliable results (lower oxygen drops mean a lower concentration of combustible gasses released by the sample).

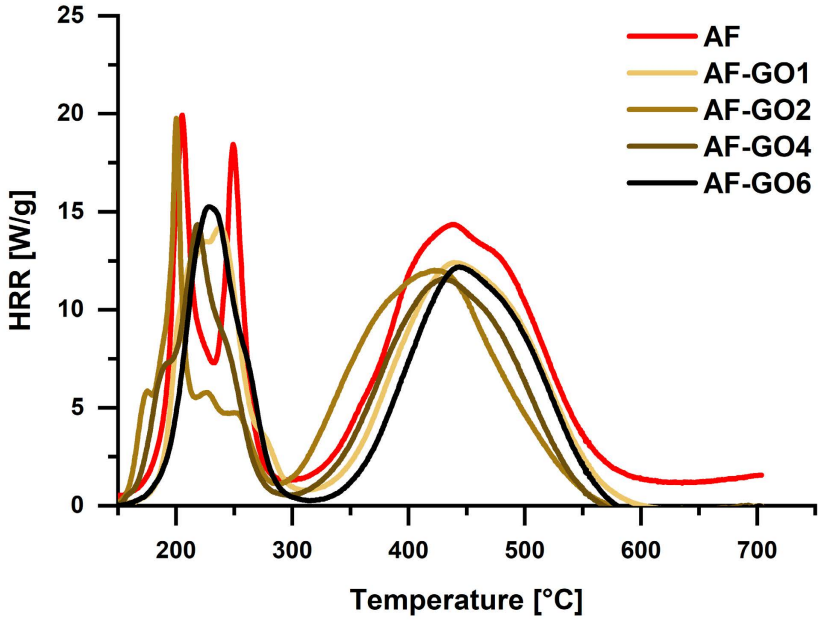

Figure 9.7: Averaged MCC cuves for all the tested compositions.

Table 9.5: Micro Combustion Calorimeter data. THR = Totoal Heat Release, HRC = Heat Release Capacity, pHRR = peak Heat Release Rate.

Sample	**THR** [kJ/g]		**HRC** [J/g K]		**pHRR** [W/g]	
	mean	dev. St.	mean	dev. St.	mean	dev. St.
AF	2.90	0.24	38.67	13.02	34.43	12.31
AF-GO1	2.63	0.12	23.00	4.32	20.18	3.62
AF-GO2	2.60	0.08	30.00	16.97	26.70	6.09
AF-GO3	2.40	0.14	18.33	1.25	16.23	1.23
AF-GO6	2.37	0.09	20.33	3.30	18.30	3.29

Chapter 10

GO functionalization

The main objective of GO functionalization was, initially, the synthesis of a positively charged GO to have a better compatibility with alginate with the scope of enhancing its FR capability. The synthesis and characterization of amine GO are presented in the first part of this chapter whereas the second part is dedicated to the synthesis of fGO-AL. Due to several external contributing factors, final tests on flame retardant capabilities of fGO have not been assessed but some preliminary results obtained at the cone calorimeter in which fGO-ED and fGO-NH3 have been incorporated in oCAF, are presented.

10.1 Amine fGO

Simple GO amination throught Leuckart and epoxy ring opening reactions, directly using amine as precursors, have been chosen in place of more sophisticated functionalization routes such as two step esterification (with thionyl chloride [185]) or selective amine orthogonal protection (with BOC and tryfluoroacetyl groups[263][264]) due to difficulties associated with their scalability (prymary related to the work up). Early laboratory attempts of selective orthogonal protection led to the consideration that synthesis of high amounts of fGO would have been unpractical, despite the expected higher yield of active primary amines that would have been obtained. As a matter of fact, quantities in the order of grams, are actu-

Table 10.1: XPS atomic mass composition, values calculated by dividing the total peak area with respect to the sum of N1s C1s and O1s areas. Each area was multilied by respective atomic mass and photoionization cross-section factor

Sample	$\%_{\mathbf{wt}}$		
	C	N	O
GO - pristine	60.81%	0.66%	38.54%
Go-ctrl - 80 °C	68.47%	0.68%	30.85%
Go-ctrl - 135 °C	67.82%	0.30%	31.88%
fGO - NH3 - 5	86.47%	5.10%	8.43%
fGO - NH3 -10	82.54%	6.30%	11.17%
fGO - ED	69.48%	11.00%	19.51%
fGO - TEPA	73.13%	12.55%	14.30%
fGO - pN	73.71%	15.42%	10.87%
fGO - MEL	3.68%	82.49%	13.83%

ally required to be synthesized, in order to test fGO FR efficacy in cone calorimeter test size samples. On the contrary, the adopted methods described in (Par. 4.3) require just a simple work-up filtration. XPS spectra of all synthesized fGO are given in the following pages. Deconvolution of C1s peak has been done by trying to fit 5 different components each identifying a particular carbon species: the main peak is assigned to sp^3/sp^2 carbon (respectively centred around 280.3 eV and 280.8 eV depending on which hybridization majorly contribute to the peak, C−C and C=C); the second, around 286.3 eV, was assigned to the contributions of hydroxyl, epoxy, ether and nitrogen single-bonded carbon atoms (C−O , C−N); double bonded carbons with oxygen contribution are present at around 287.5 eV for carbonyl (C=O) and, approximately at 289.3 for ester and carboxyl groups. Eventually, around 291.2 eV, the $\pi^* \leftarrow \pi$ *shake-up* satellite peak identifies the interaction caused by HOMO - LUMO transition in aromatic structures. Similarly, N1s deconvolution was based on 3 peaks: aromatic nitrogen contribution around 398.4 eV, amine and amide nitrogen around 399.5 eV, and graphitic / $-NH_3^+$ at 401.5 eV. Finally 2 peaks were used as base for the deconvolution of O1s: around 531.2 eV and 532.5 eV respectively, referable to O=C and O−C. Peaks attribution have been operated according to literature [265][266][267], a higher resolved

deconvolution was not feasible due to low instrumental resolution (≈ 0.5 eV).

By starting with having a look at fGO-NH3-5 XPS spectra, it is immediately noticeable the extensive reduction of oxygen moieties contributions and, by the different sp^2/sp^3 shape (an asymmetric Gaussian-Lorentz curve was used) and position (2.84.37 eV) peak together with the presence of the $\pi^* \leftarrow \pi$, the partial restoration of C sp^2 in GO structure in [Fig. 10.4b] with respect to [Fig. 10.3b]. This is attributable to the reaction between ammonium formate and GO, since only partial reduction (visible also in [Fig. 10.1]) and minimal change in the sp^3/sp^2 peak's shape, coupled with the absence of the $\pi^* \leftarrow \pi$ peak is detected in its control reaction spectra (GOctr - 135°C [Fig. 10.5c]). Total N concentration, calculated from total-area ratio XPS, reached 5.10%$_{wt}$ and GO amination is confirmed by the presence of the relative amine peak (399.71 eV)[Fig. 10.4c]. However others peaks suggest the presence of nitrogen into the GO structure both in aromatic and graphitic structure (respectively at 398.25 eV and 401.97 eV). Traces of nitrogen oxydes formation are also detected (404.75 eV)[Fig. 10.4c]. The increase of ammonium formate initial concentration (fGO - NH3 - 10) leads only to a slight rise in total N concentration, reaching 6.30%$_{wt}$ with analogous XPS deconvoluted spectra. Considering the extensive reduction of GO, O=C in O1s has been successfully detected by fitting due to reduction of total oxygen concentration (which reaches 8.43%$_{wt}$ from 33.54%$_{wt}$ in GO).

No differences in peaks identification occurs among fGO - ED, fGO - TEPA and fGO - pN: with respect to GO - pristine, a partial reduction of oxygenated group peaks is identified in all the samples (with total oxygen concentration that is reduced up to 10.87%$_{wt}$ in GO - pN) but with no detected increase in sp^3 C nature due to the symmetric Gaussian-Lorentz profile of fitted peak at 284.80 eV. Nitrogen presence was mainly attributed to its amine form which assessed the successful functionalization and no sign of aromatic nitrogen was detected by deconvolution[Fig. 10.6c][Fig. 10.7c][Fig. 10.8c]. Calculated total nitrogen mass concentration was 11.00%$_{wt}$, 12.55%$_{wt}$ and 15.42%$_{wt}$ respectively for fGO - ED, fGO - TEPA and fGO - pN. (detailed value are presented in [Tab. 10.1]). Melamine presence on fGO-MEL was assesed by N1s deconvolution in which only the aromatic nitrogen and amine peak were successfully fitted (other components fitting did not

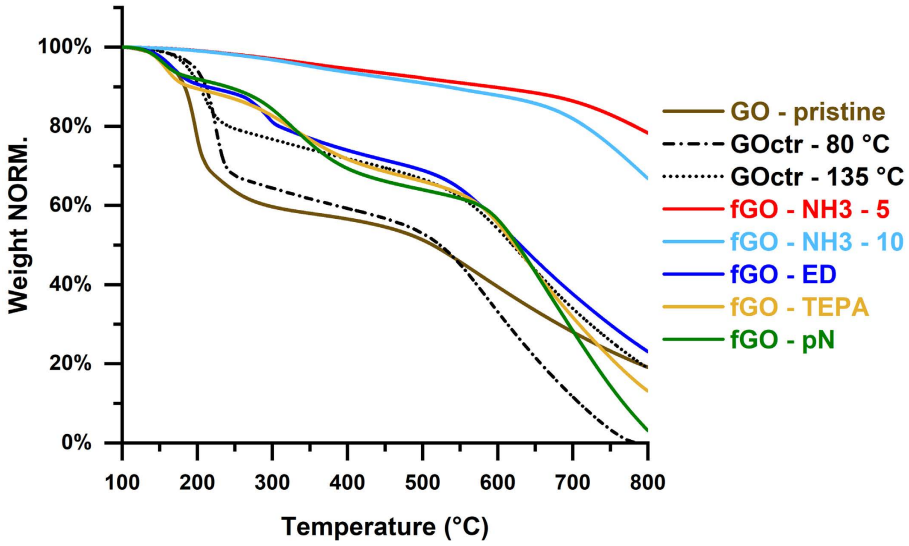

Figure 10.1: representative TGA curves of fGO samples with relatives control reactions. N_2 atm.

succeed)[Fig. 10.10]. Nevertheles, calculated nitrogen concentration for fGO-MEL was the lowest in aminated fGO (3.68%$_{wt}$), which can be reconducted to the lower nucleophilic nature of melamine primary amines.

Thermal degradation of GO is characterized by a first major mass loss region which starts around 150 °C up to 250 °C, with degradation of most labile oxygen groups (such as edge carbonyl, carboxyl, hydroxyl and start of epoxydes decomposition) followed by a gradual weight loss region up to 500°C and a final decomposition of in plane remaining oxygen groups (such as in plane carbonyl, phenols and ethers) accompanied by the final degradation of scheletal carbon. All degradation steps concurs to the elimination of both carbon and oxygen yielding to the evolution of CO and CO_2[268][266]. TGA analysis confirms the extensive reduction of both fGO-NH3-5 and fGO-NH3-10 with respect to both the GO-pristine and the corresponding control reaction (GOctr-135°C) with a mass loss of only ≈7% at 450°C with respect to ≈46% ad ≈30% of GO-pristine and relative control reaction. No amine specific weight loss step was detected in fGO-NH3-5 and fGO-NH3-10. Interestingly, despite sharing the same relative oxygen concentration (≈30%$_{wt}$ [Tab.

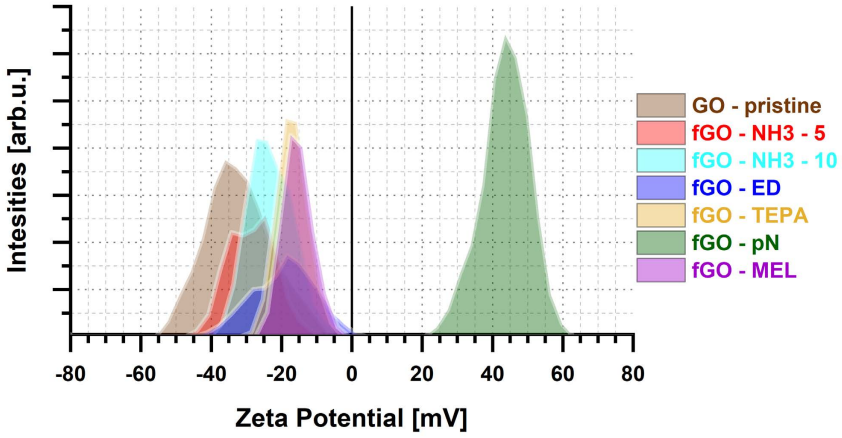

Figure 10.2: Z-pot representative curves of fGO, mean data presented in [Tab. 10.2] curves of fGO sample with relatives control reaction.

10.1], reduced from GO-pristine caused by a general partial reduction) GOctr-80°C shows an higher mass loss in the first region with respect to GOctr-135°C: this could be attributed to a localized, in air, re-oxidation (or transformation of labile hydroxyls and epoxides) of GOctr-135°C with the formation of more stable in-plane carboxy and ether groups[268]. Aminated fGO shows an additional degradation step around 280-400°C which is attributable to amine partial decomposition [269] [270]. Partial reduction of fGO-ED, fGO-TEPA and fGO-pN, as identyfied by XPS, is confirmed in TGA due to their higher thermal stability at 500°C with respect to both GO-pristine and their relative control reaction (GOctr-80°C). The specific weight loss, traceable back to the amine decomposition step, was calculated from the difference between the weight loss and the linearly back-extrapolated value (from the linear decomposition range between 420°C and 500°C) both taken at 250°C. Respectively these value are equal to 7.51% (± 0.96), 13.45% (± 0.65) and 17.79% (± 0.82) for fGO-ED, fGO-TEPA and fGO-pN. The calculated mass fractions of grafted TEPA and ED can be easily converted in primary amines molar concentration by considering that only one primary amine group is added to GO surface for each molecule (as described in (Par. 4.3.1)): this leads, respectively to to 1249.19 $\mu mol/g_{GO}$ and 710.48 $\mu mol/g_{GO}$ for fGO-ED and fGO-TEPA (detailed value in [Tab. 10.3]. Even though this approach was used for

Table 10.2: Z-potential averaged peak values. Obtained at pH7, 0.01 mg/ml, 15mM CaCl

Sample	mV	
	average	St. dev.
GO_pristine	-37.43	4.76
Go-ctrl - 135 °C	-38.30	2.15
fGOctr - MEL	-31.77	2.32
fGO - NH3 - 5	-31.03	2.32
fGO - NH3 -10	-25.03	1.82
fGO - ED	-20.27	4.56
fGO - TEPA	-18.47	1.37
fGO - pN	44.10	2.92
fGO - MEL	-15.73	0.35

initial amount calculation of pN during syntheses, its polymeric nature prevents any valid conversion. Kayser test was therefore used to directly asses primary amine concentration and values are reported in [Tab. 10.3]. With respects to the theoretical value of 0.166 mol/g_{GO} (NH_2/g_{GO}) the calculated KT primary amines concentrations are extremely low; moreover, they are also one order of magnitude lower than the calculated values based on TGA amine step weight loss for fGO-ED and fGO-TEPA. From the moment that kaiser test (KT) detects only primary amines, this reduction could be indicative of the fact that both the terminal amines of ED and TEPA are convalently attached to another active site of the GO (thus being in-active in KT condition). However, it has to be taken in account that KT was originally designed for peptide synthesys and the obtainment of an homogeneous water dispersion is fundamental to achieve reliable results which is not easy to obtain, working with partially reduced GO water dispersions. Nevertheless, it has to be reminded that the primary objective was not to obtain active primary amine sites on GO but rather having a net positively charged fGO. Information about fGO effective surface charge were therefore obtained through Z-potential which results are reported in [Tab. 10.2] and depicted in [Fig. 10.2]. GO, due to its high oxygen functional groups, possesses a net negative charge[271] [272][273] which is maintained also in al partially reduced control reactions (fGOctr-80°C,

Table 10.3: Kaiser test, active primary amine goups in fGO-ED, fGO-TEPA and fGO-pN.

Sample	$\mathbf{F}_a$ μmol/g		**TGA - amine step loss at 250°C** μmol/g	
	average	St. dev.	average	St. dev.
fGO - NH3 - 5	25.18114	7.497623	-	d
fGO - ED	118.8937	39.13115	1249.19	240
fGO - TEPA	96.71547	24.01709	710.48	31.48
fGO - pN	122.9987	69.42128	-	-

fGOctr-135°C) due to the non complete elimination of oxygen which is reported to contribute to the negative surface charge also in extremely low mass concentration (≈1.8%[274]). A net negative charge is maintained, despite an increasing shift toward zero, in fGO-NH3, fGO-ED, fGO-TEPA and fGO-MEL functionalization. Only fGO-TEPA shows positive value (≈ 13 eV) when stabilized at pH 5 (due to amine protonation). Only fGO-pN successfully reached a net positively charge (+44.10 eV) when stabilized at pH 7 which is important if a good compatibilization with alginate has to be maintained of recycling (in which the main dissolution step is carried out at pH 7.5 (Par. 7.1)).

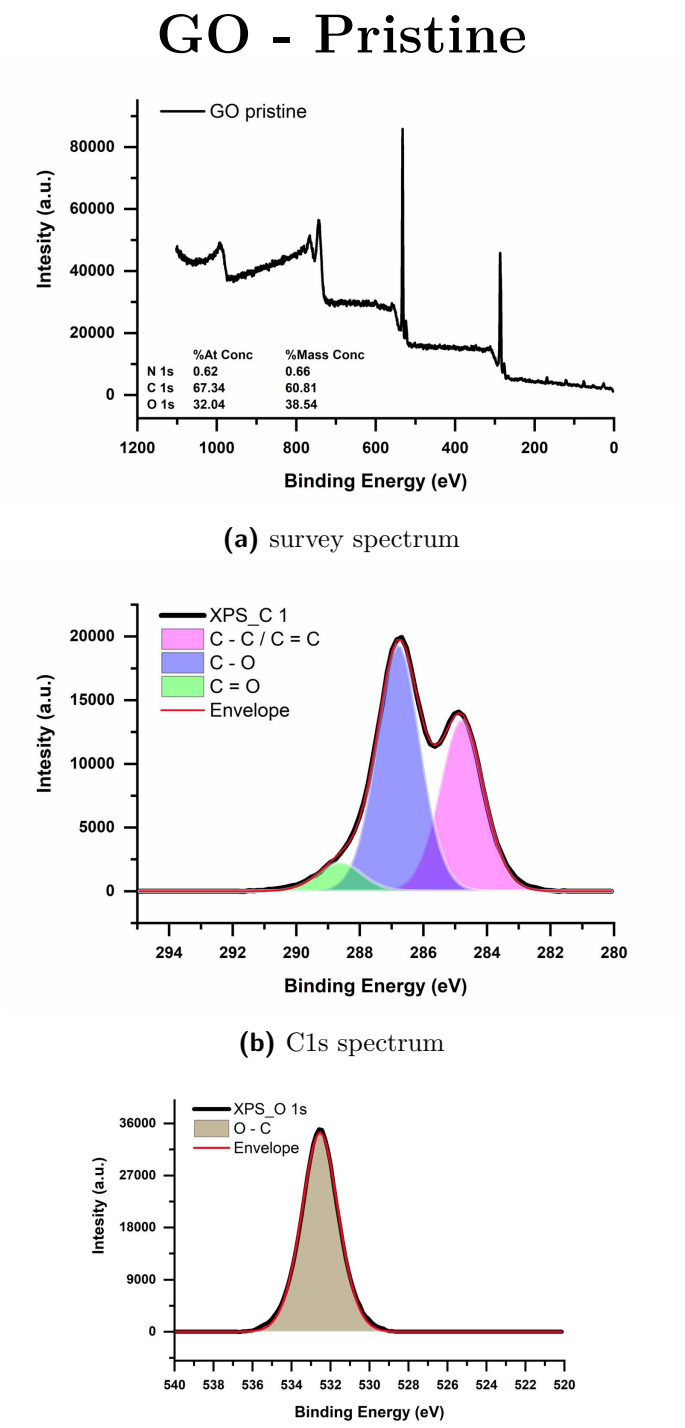

(a) survey spectrum

(b) C1s spectrum

(c) O1s spectrum

Figure 10.3: XPS acquired spectra of GO - Pristine

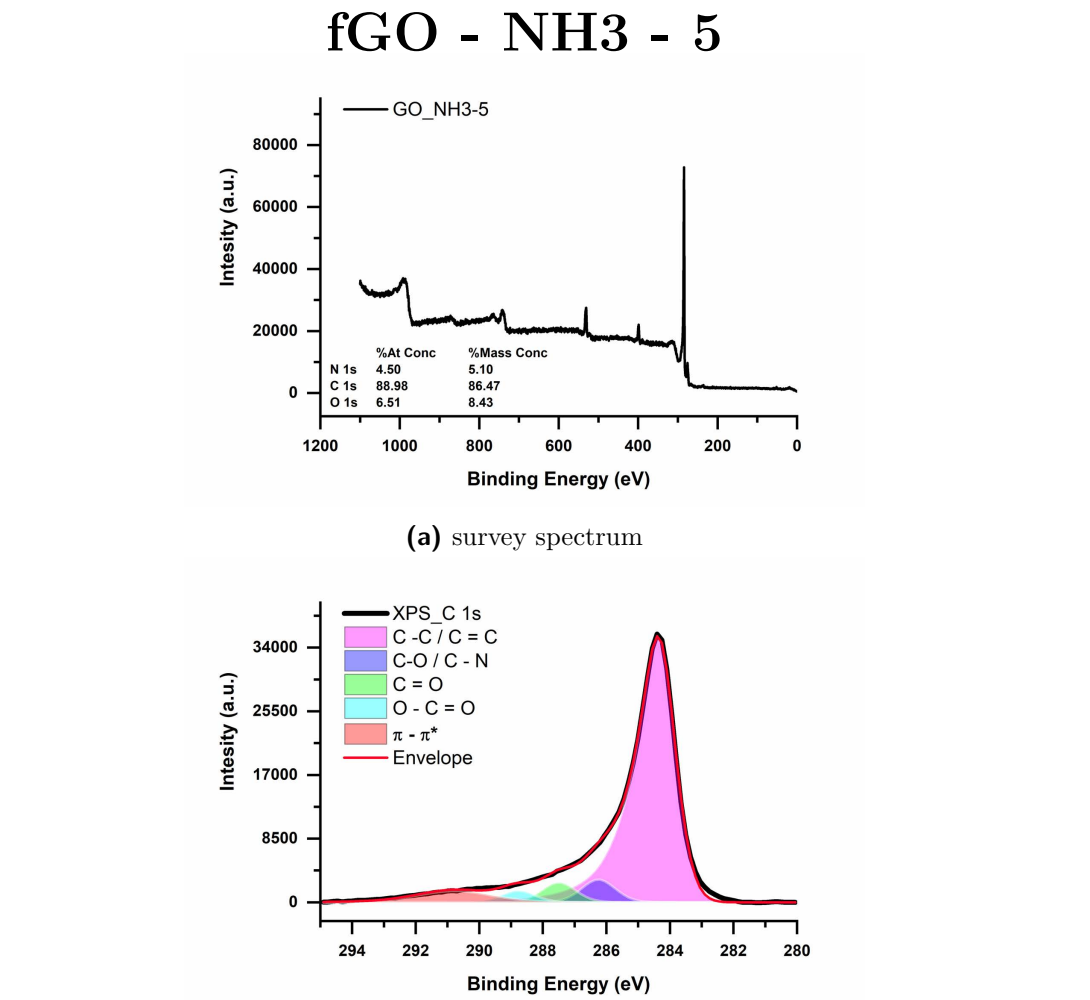

(a) survey spectrum

(b) C1s spectrum

(c) N1s spectrum

(d) O1s spectrum

Figure 10.4: XPS acquired spectra of fGO-NH3-5

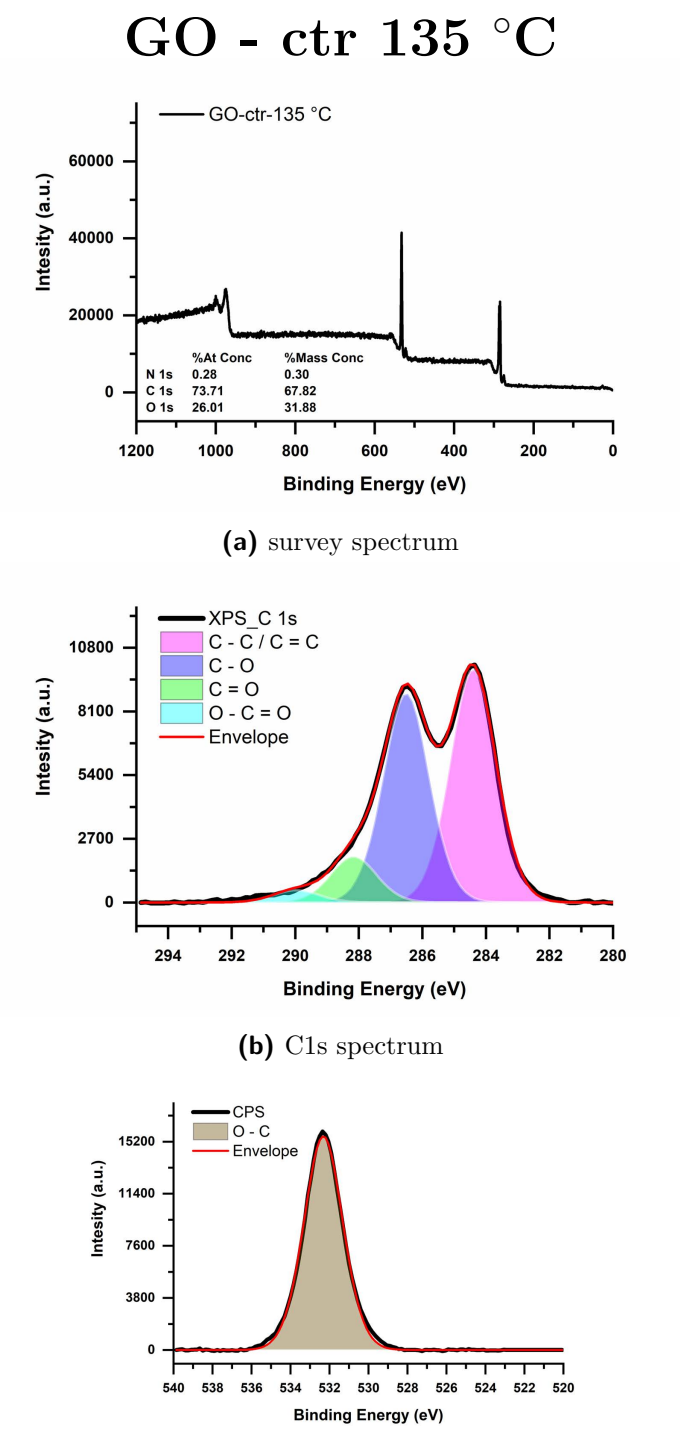

(a) survey spectrum

(b) C1s spectrum

(c) O1s spectrum

Figure 10.5: XPS acquired spectra of GO-ctr135: control reaction of fGO - NH3 - 5 and fGO - NH3 - 10

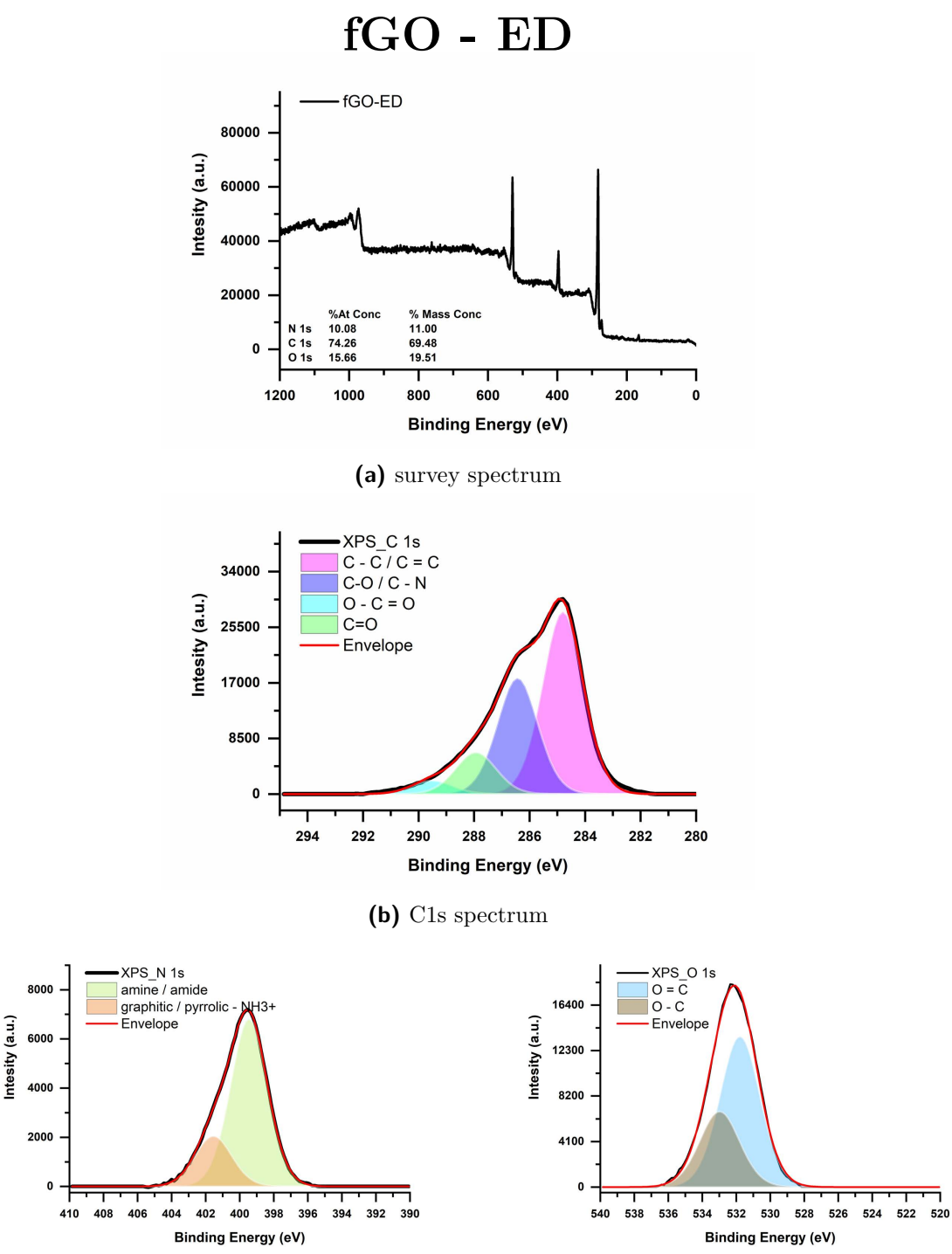

(a) survey spectrum

(b) C1s spectrum

(c) N1s spectrum

(d) O1s spectrum

Figure 10.6: XPS acquired spectra of fGO-ED

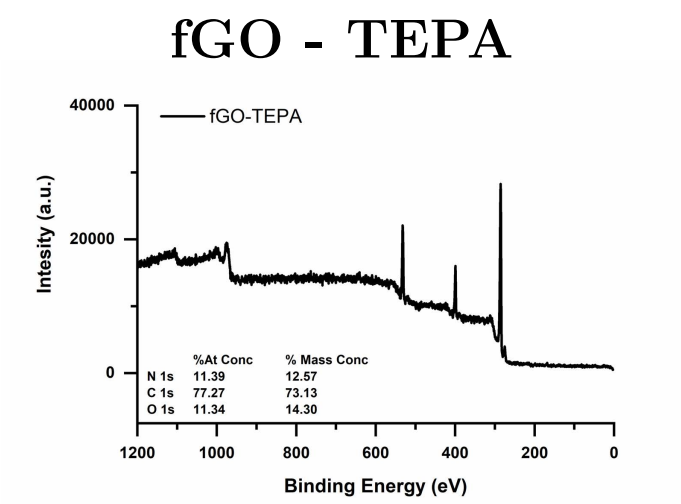

(a) survey spectrum

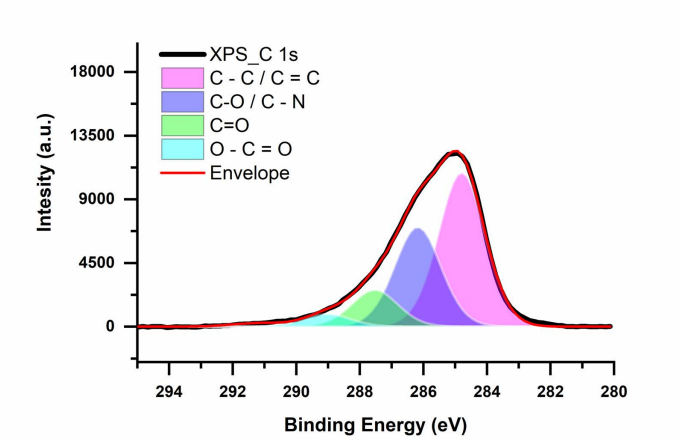

(b) C1s spectrum

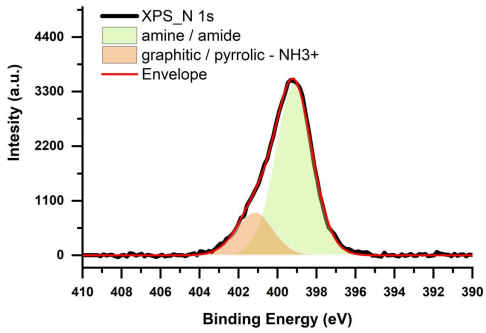

(c) N1s spectrum

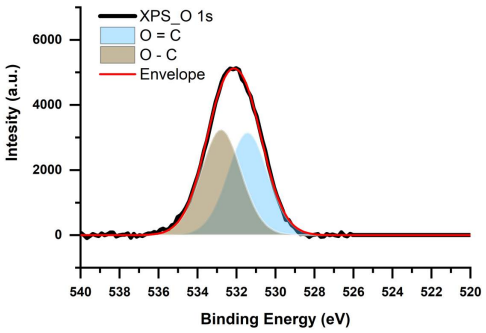

(d) O1s spectrum

Figure 10.7: XPS acquired spectra of fGO-TEPA

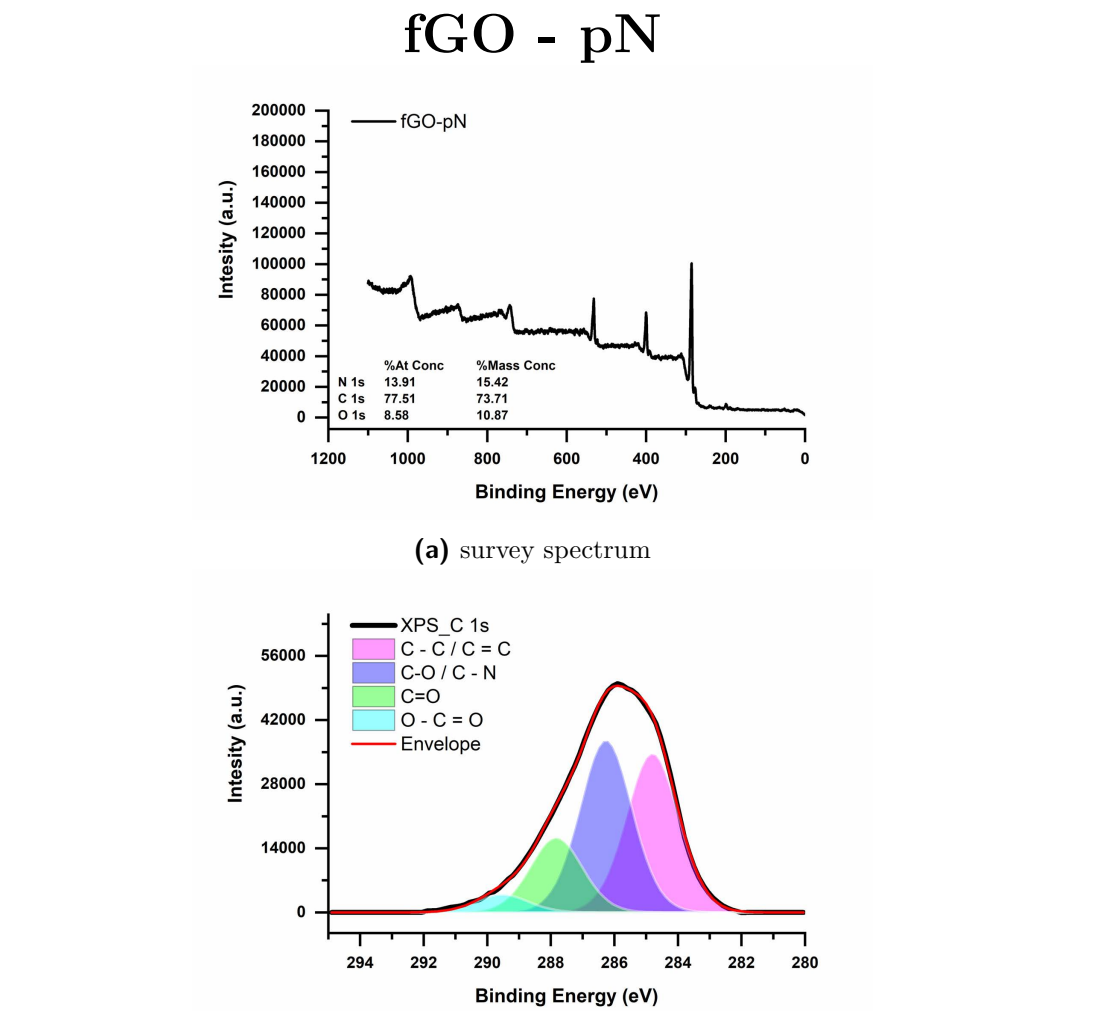

(a) survey spectrum

(b) C1s spectrum

(c) N1s spectrum

(d) O1s spectrum

Figure 10.8: XPS acquired spectra of GO-fpN

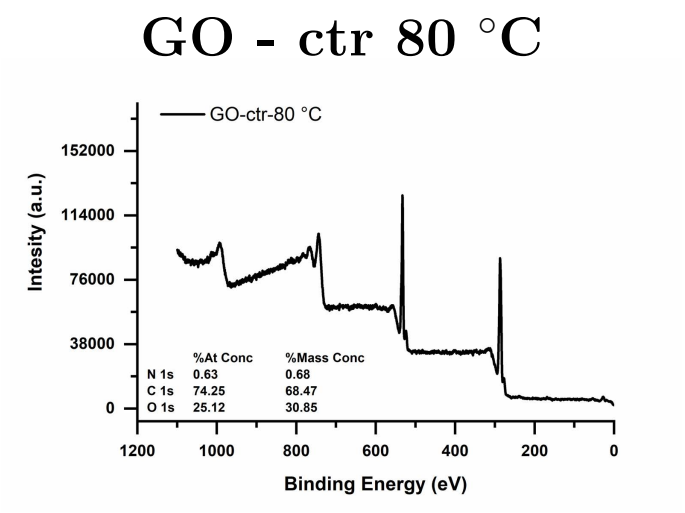

(a) survey spectrum

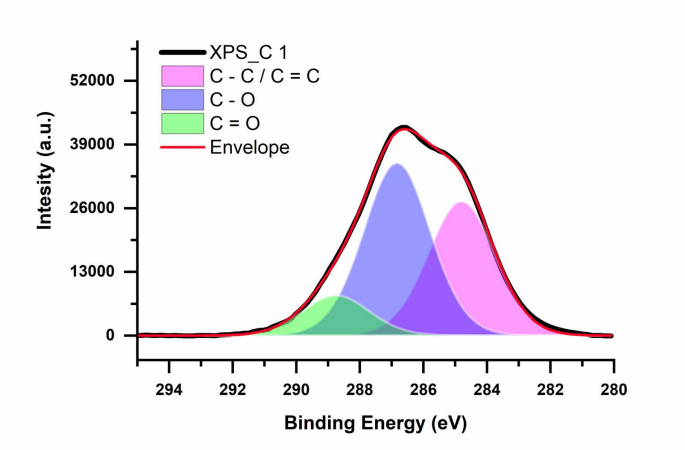

(b) C1s spectrum

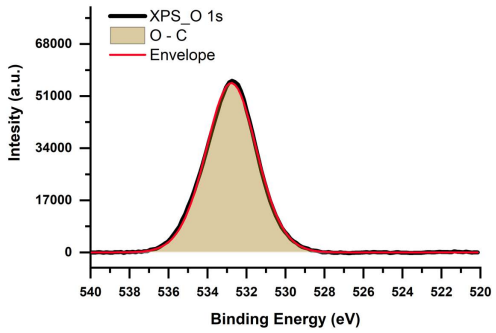

(c) O1s spectrum

Figure 10.9: XPS acquired spectra of GO-ctr 80 °C, control reaction of fGO-ED, fGO -TEPA, fGO-pN.

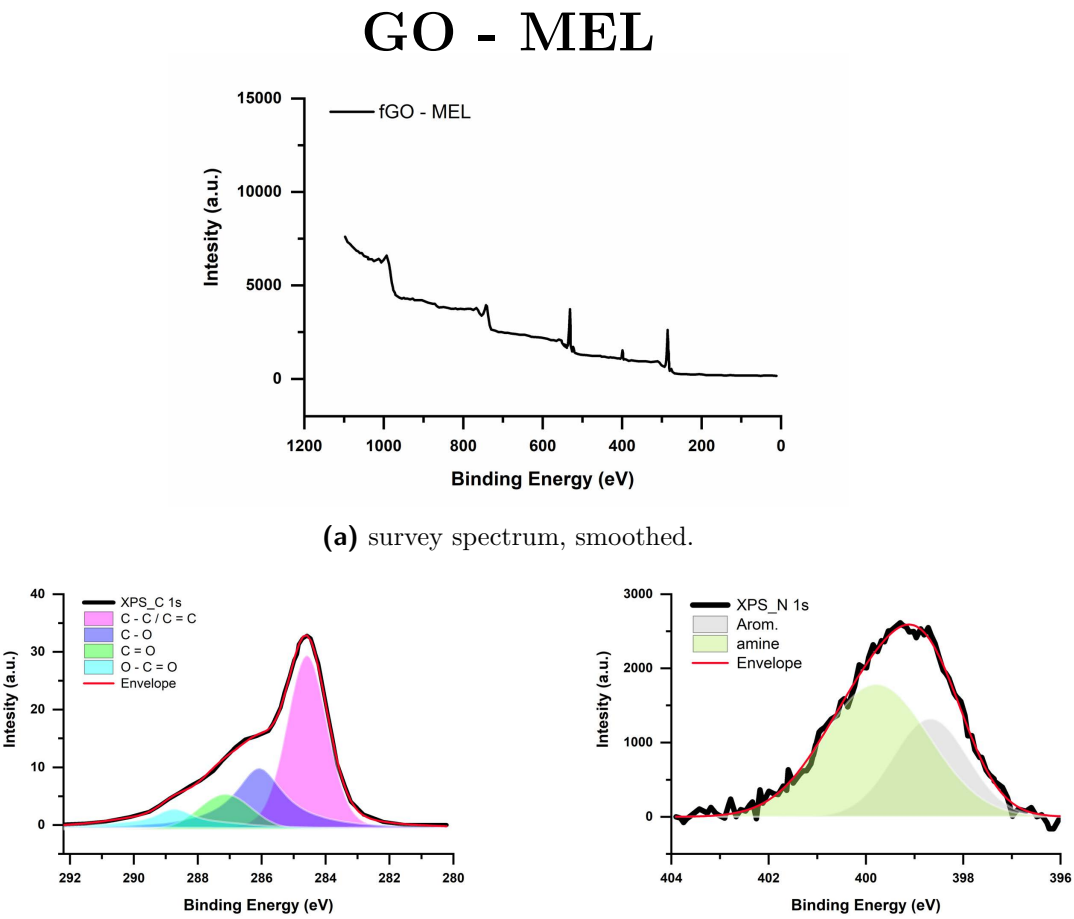

(a) survey spectrum, smoothed.

(b) C1s spectrum, smoothed.

(c) N1s spectrum

Figure 10.10: XPS acquired spectra of fGO-MEL

10.2 fGO-AL

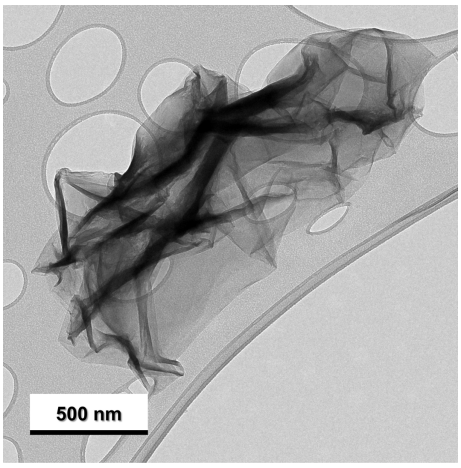

(a) GO - pristine.

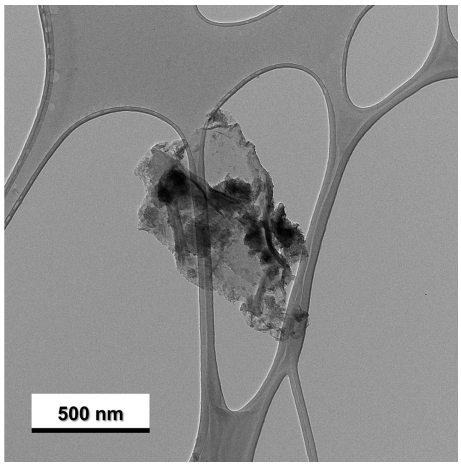

(b) fGO-AL. Synthesized at pH 11.

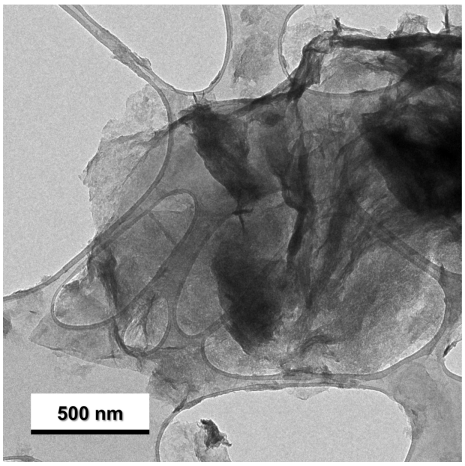

(c) fGO - AL - b. Synthesized at pH 9.

Figure 10.11: TEM images of fGO-Al

$AlOH_3$ is a well known physical FR (due to its endothermic decomposition (Par. 2.4.4)) and its deposition on GO was carried out by *in-situ* nucleation from aqueous dispersion of $Al_2(SO_4)_3 \cdot 16H_2O$ in basic conditions as result of precursor hydrolyzation[276]. From an initial brownish solution, a light gray product was then obtained by maintaining the pH at 11 (fGO-AL) during the reaction, whereas only a black powder was produced at lower pH level (pH 9)(fGO-AL-b). XRD

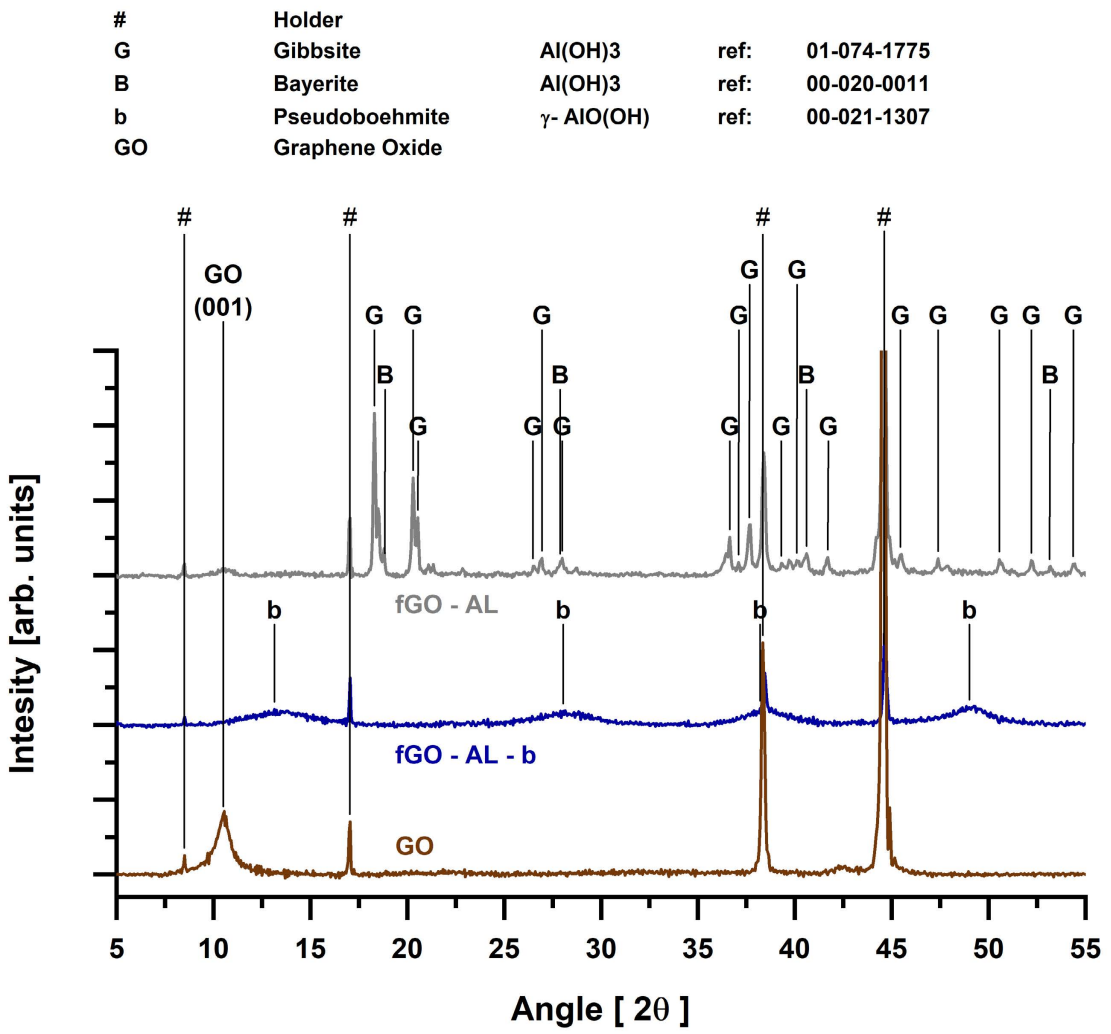

Figure 10.12: XRD difractograms of fGO-pristine, fGO-AL and fGO-AL-b. Aluminum sample holder peaks are referenced with # label. Referenced peaks for Gibbsite, Pseudobohemite and Bayerite were obtained from PDF-2 ICDD materials diffraction database[275]

was used to identify the crystallographic nature of the deposited nano-crystal on the GO surface which, presence was confirmed by TEM images [Fig. 10.11]. As it can be seen in [Fig. 10.12], two distinct products were deposited on GO surface: at pH 9 an oxy-hydroxide hydrate $AlO(OH)\cdot nH_2O$ form, identified as Pseudobohemite, was present whereas $AlOH_3$ was obtained at pH 11 as a mixture of

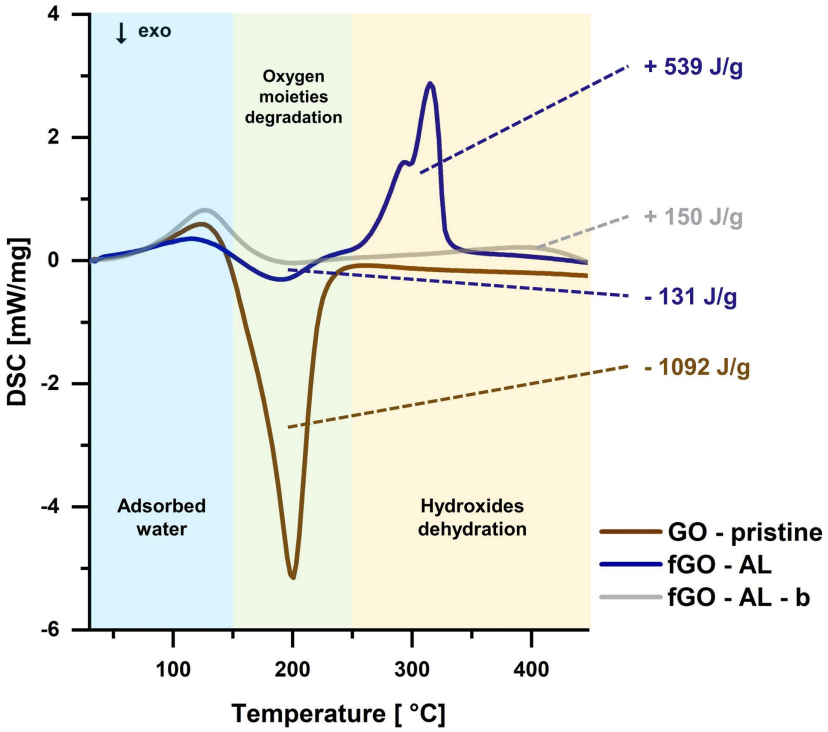

Figure 10.13: DSC curves of GO-pristine and aluminium functionalized fGO.

Gibbsite and Bayerite (fGO-AL). Pseudobohemite is a non stoichiometric form of Bohemite in which water molecules are intercalated into its double ocatehedral oxygen layers whereas, Gibbsite and Bayerite are two polymorph of $AlOH_3$ with the first being its more common in nature[277]. Bayerite, Gibbsite and Pseudobohemite all endothermically decompose in α-allumina through metastable allumina phases formation [Fig. 10.14]) but with a different starting transformation temperature: while Bayerite and Gibbsite posses an endothermic peak at $\approx$ 300 °C, Pseudobohemite is reported to transform at $\approx$ 450 - 550 °C [276]. DSC was used to confirm the endothermic activity of fGO-AL samples and curves are reported in [Fig. 10.13]. As expected from literature, fGO-AL shows an endothermic peak (539 J/g) in the range of 250-300°C with an associated energy of 539 J/g. By comparing this value with DSC data of pure $AlOH_3$ (which shows a endothermic decomposition energy of 1006 J/g) a 63.17%$_{wt}$ fraction of $AlOH_3$ was calculated

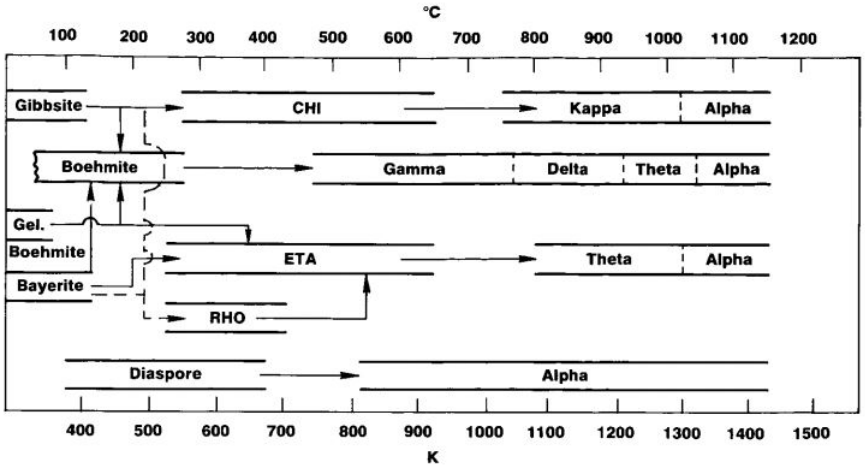

Figure 10.14: Thermal decomposition pathways of Al-hydroxides, greeks letters refers to metastable allumina forms. From[278].

for fGO-AL. Interestingly, DSC data also reportes a strong reduction of fGO-AL inferred by the diminished exothermic peak at 200°C which is associated to labile oxygen groups decomposition as discussed in the previous paragraph.

10.3 Early Cone Calorimetry tests of fGO FR activity

By analogy with what was done for GO in (Par. 9.3), fGO-NH3-5 and fGO-ED flame retardant activity was tested at the cone calorimeter by incorporation, at $2\%_{wt,org.frac.}$ in oCAF: respective produced samples are labeled oCAF-NH3 and oCAF-ED. A different fiberglass waste batch (batch 2 (Par. 3.1.3)) was used in these tests, since the original waste reservoir was consumed: this second batch was characterized by a higher $AlOH_3$ content and lower glass content. As a consequence these result cannot be directly related to previous cone calorimetry test data presented in (Par. 9.3). Due to the higher concentration of $AlOH_3$ in the fibreglass conentent, oCAF(batch2) shows average better flame resistance resulting in a lower efficacy of GO into improoving cone calorimetry parameters. However, with the sole exception of the total heat released, data are compatible with the considerations made in (Par. 9.3). As a matter of fact, smouldering combustion

after flame out occurs in oCAF-GO2(batch2) which was not shown in any tested oCAF-GO2 samples. This, could be caused by a lower stability of the char formed which, considering the higher pHRR of oCAF-GO2(batch2) with respect to oCAF-GO2, could also suggest the rise of an antagonist effect between $AlOH_3$ and GO. Little FR activity is shown by fGO-ED adn fGO-NH3 in which THR, pHRR are comparable with those of the oCAF(batch2) sample. This cloud be derived by the reduced compatibility of fGO with alginate as a result of the enhance hydrophobic behavior (caused by GO reduction) which was not counter-balanced by an attractive electrostatic interaction between the polymer and the fGO. However, both fGO remarkably induced a shift of the TTI which could have been caused by the release of non combustible N-rich moieties that cause a delay of the ignition. These early results seem to suggest the addition of gas diluting effect to the potential FR activity of positively charged fGO-pN.

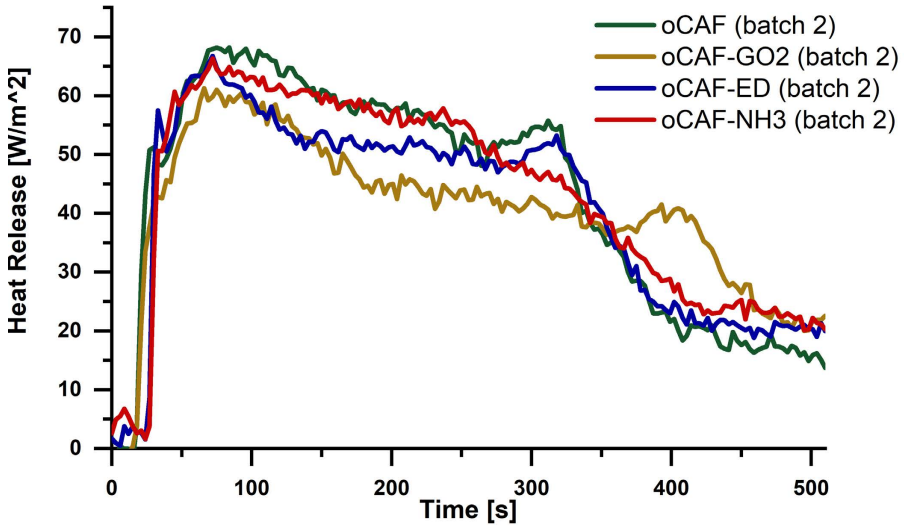

Figure 10.15: Representative cone calorimetry curves of tested samples, detailed data are presented in [Tab. 10.4].

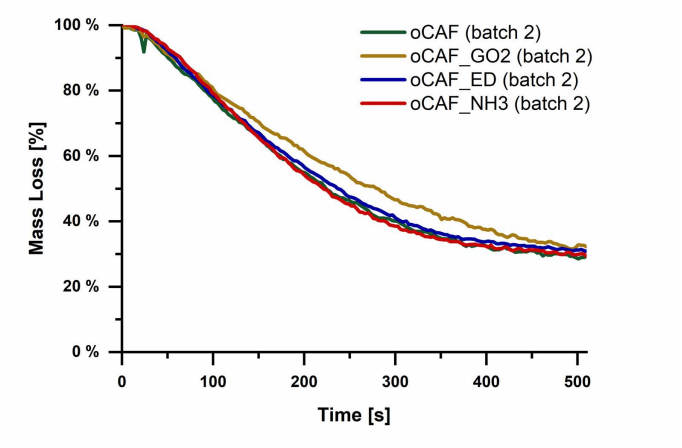

Figure 10.16: Mass loss curve of cone calorimeter tested samples.

Table 10.4: Cone Calorimeter data. Res. = residue, THR = Totoal Heat Release, TTI = Time To Ingition, pHRR = peak Heat Release Rate, $\mathbf{C_y}$ = char yield

Sample	**Res.**		**THR** [MJ/m^2]		**TTI** [s]		**pHRR** [kW/m^2]	
	$\%_{wt,tot}$	$\mathbf{C_y}$	mean	dev. St.	mean	dev. St.	mean	dev. St.
oCAF (batch2)	25.53%	2.68%	21.24	1.21	18.5	2.12	71.63	4.89
oCAF - GO2 (batch2)	25.52%	3.13%	20.70	0.17	16.00	8.49	61.64	0.51
oCAF - ED (batch2)	29.86%	8.77%	22.13	1.77	25.00	8.46	66.09	0.92
oCAF - NH3 (batch2)	32.63%	12.38%	21.29	1.14	45.50	-	69.45	4.41

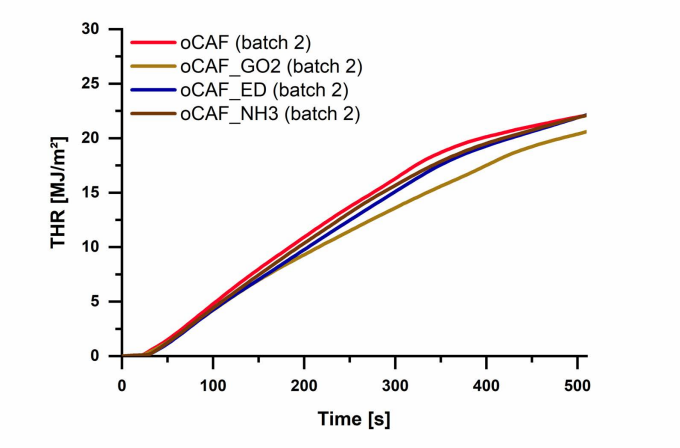

Figure 10.17: Total Heat Release (THR) curves of cone calorimeter tested samples. Averaged.

Part IV

Conclusions and Future Perspective

Chapter 11

Conclusions and Future perspectives

This research work started with the study and optimization of a previously developed thermal insulation material and rapidly evolved, expanding its original horizons, through designing a recycling process which was thereafter analyzed through a life cycled assessment study. Concurrently, the topic of flame resistance enhancement has been handled with the foresight of a complete material's recyclability. Nanotechnology, due to its reviewed higher efficacy, was identified as the favorable alternative to conventional flame retardant approaches that commonly bring around several drawbacks, impacting on material functional properties or, in some cases, even carrying risks of toxicological effects.

In (Ch. 6) a first optimization of original composite alginate foam (oCAF) composition was carried out, briefly discussing the most relevant considerations (not covered by the *N.D.A*) that affected the production process of the original material which was firstly optimized for the shipbuilding sector as a part of the GGTDoors project.

In (Ch. 7) a completely new recycling approach, capable of dismantling and then rebuilding the matrix of an ionotropic alginate-based composite, was designed by taking advantage of a chelating agent easily controlled via pH shift. Its efficacy and

robustness, were demonstrated through the assessment of the complete preservation, or improvement, of thermal, acoustical and mechanical functional properties of the original material. As clearly stated, the selection of the best thermal insulation option does not rely only on thermal properties but also strongly depends on local variables (*e.g.*climate, place of installation and occupancy profile of the building). These considerations lead to the conclusion that both the oCAF and rCAF can potentially represent a valuable alternative solution to conventional thermal insulation options. Moreover, due to the persistence of the chelating agent in the recycled material, multiple recycling cycles can be performed, by its simply re-activation in mild basic aqueous environment, therefore leading to a cradle-to-cradle perspective. The field of application of this process is not limited to alginate-based systems but can in principle be applied to the recycling any composite material whose matrix is stabilized by ion-polymer junctions. This includes other polyanionic systems such as: hyaluronic acid, pectin and cellulose. Additionally, the recycling process, within the herein described specific application, has proved to be robust with with respect to the process parameters which is, together with the unnecessarly needs of specialized equipment, which is an undoubtedly valuable advantage in terms of industrial scalability. Morphology and thermal characterization of oCAF samples highlighted that a better control of the porous structure could lead to major performance improvement. This could be easily done by adopting different freezing techniques (*e.g.* liquid nitrogen deep freezing) regardless of the original adopted technique, shape, dimension, density and micro-structure of the oCAF, since these characteristics are lost in the process. In a similar fashion, the properties of the recycled material could be tailored to new specific target applications: anti-fungal chemicals or plasticizers can be easily added after the alginate matrix dissolution. Another important aspect that has to be tackled in future works regard the magnitude of the effects that humidity and water vapor uptakes have on material performances.

The environmental impact evaluation analysis conducted in (Ch. 8) concluded that, at least at current lab-scale, the recycling process possesses a lower environmental footprint (in all the anaylized cathegories) thus indicating that the recycling option is preferable to oCAF landfill disposal and simple substitution. The electric

energy consumed during the lyophilization process was identified as the major contributing factor in almost all the impact categories of all the analyzed production systems. This is followed, for oCAF manufacture, by the cumulative contribution of solvents production (used in the alginate extraction process) and by EDTA and GDL production (used in the recycling process). The elimination of the need of new alginate, in rCAF production, is therefore the main contributing factor that brings to the cumulative reduced environmental impact of rCAF manufacture. LCA analysis thus draws to the identifications of the main parameters and aspects that should be optimized to further reduce the ecological footprint of rCAF which (not considering lyophilization) are represented by the total EDTA and GDL concentrations. Chemicals relative impacts are further increased in the industrial scaled product system, due to the abatement of the electric energy required, hence emphasizing the importance of chemicals concentrations optimization. An overall reduction of 66% of EDTA has already been proved to be compatible with the recycling process (as tested in (Ch. 7)) but its effects on functional material properties have not yet been studied. The use of alternative drying systems, as substitutes to lyophilization, should also be considered in future works. The PRI product system has given an initial estimation of the impacts associated to rCAF industrial production, allowing a comparison with others conventional TIMs: an analysis based on different production energy mixes leads to the conclusion that, at the current state, the rCAF process start to becomes competitive against other commercial solutions only if green (*i.e.* renewable) electric energy is used as energy source in the main process units. However, in order to obtain a better estimation, an improved definition of PRI units processes should be considered in future studies, also by taking in to accounts the newly identified optimized parameters.

The effects of GO addition were studied in (Ch. 9), at first as far as thermal and acoustical properties were concerned and subsequently regarding fire resistance, of both the original and the recycled version of the nanocomposite. In terms of thermal and acoustical properties, GO seems to have little impact on both the original and recycled material. Nevertheless, the reduction of the thermal conductivity, which could be ascribed by a reduced pore size distribution, will be studied by μCT in the following works. On the other hand, by testing the nanocomposite at

the cone calorimeter (oCAF-GO2), GO has shown to be effective as FR even at low concentrations (2%) with a reduction of up to 42% of the pHRR of the original composite (oCAF). The main action mechanism of GO was identified in the formation of a non-continuous char layer capable of reducing the diffusion of oxygen and combustible species thus limiting the combustion and reducing the mass loss rate. GO, mainly due to its limited thermal stability, however, fails to build up a stable char which decomposes with a limited enhancement of the final char yield. with Respect to other commercial thermal insulation materials the oCAF-GO2 nanocomposite, according to cone calorimeter data, shows a competitive flame resistance behavior. Interesting, the recycled composite (rCAF) showed an improved fire resistance behavior with respect to the original composite (oCAF): pHRR and THR were both diminished followed by an increased resistance to ignition (which was preceded by smoldering). As a matter of fact, rCAF showed an increase of the time to ignition (TTI) to minutes with respect to the few seconds exhibited by the original composite, even with the addition of GO (oCAF and oCAF-GO2). This behavior was ascribed to the presence of N-rich EDTA which triggered char formation mechanisms (by dehydration reaction of alginate chain) and, at the same time, acted through gas dilution by relasing of non combustible N-rich species (*e.g.* NH_3 or NO_x). The FR effect of GO in the recycled nanocomposite (rCAF-GO2) was still evident: it showed better fire resistance parameters with respect to both the original composite (oCAF) and nanocomposite (oCAF-GO2), but it displayed a limited improvements with respect to the recycled composite (rCAF). At this point we demonstrated the compatibility of the recycling process toward the GO presence, which maintained its FR capability. Future steps will involve testing the material for the Limiting Oxygen Index and, by coupling a gas-chromatography (or IR) analysis with the cone calorimeter, the identification of evolved species during combustion to confirm the gas dilution mechanism of EDTA.

As a final part of this work, in order to improve its efficacy as flame retardant, GO was functionalized with amine rich species (to enhance its compatibility with the negatively charged alginate matrix) and $Al(OH)_3$(Ch. 10). Effective amination (fGO-NH3) and GO grafting (with ethlendiammine (fGO-ED), tetraethylendiammine (fGO-TEPA), polyethylenimine (fGO-pN) and melamine (fGO-MEL))

were confirmed mainly trough XPS and TGA analysis. Functionalized GO showed an improved thermal stability, primarily ascribed to the partial reduction of its oxidized structure, that seemed to have partially influenced its FR efficacy. Eventually, a completely positive charged GO was obtained via pN graft (fGO-pN). Successful deposition of $Al(OH)_3$ on GO surface was proved by XRD and DSC analysis which also confirmed the appearance of an endothermic decomposition peak. Due to external factors, it has not been possible to evaluate the flame retardant efficacy of fGO. Nevertheless, a preliminary test, conducted on non-optimized fGO composition (*i.e.* GO-ED and GO-NH3), despite of showing a reduced FR effect with respect to pristine GO a limited, but new, shift of TTI was detected on those samples in which fGO was present. This behavior was ascribed to a mild gas dilution effect caused by amine decomposition. A chemical analysis of the evolved gases should be carried in future works with the intent of supporting this hypothesis. In addition, a complete assessment of the FR activity of all the synthesized fGO will be conducted in future works.

In conclusion, as a result of this work, a completely recyclable thermal insulator nanocomposite was developed which is intended to be used as non-structural insulator component in building envelopes. This was done by developing a new recycling method (currently patent pending) capable of fully maintains or even improves the original functional properties of the nanocomposite material. In addition, according to cone calorimetry tests, thanks also to the incorporation of GO, the nanocomposite showed a competitive fire resistance behavior against others conventional thermal insulation solutions.

Part V

Bibliography and Acknowledgments

Bibliography

[1] Giada Kyaw Oo D'Amore et al. "Innovative thermal and acoustic insulation foam from recycled waste glass powder". In: *Journal of Cleaner Production* 165 (2017), pp. 1306–1315. ISSN: 09596526. DOI: 10.1016/j.jclepro.2017.07.214. URL: http://dx.doi.org/10.1016/j.jclepro.2017.07.214.

[2] *Insulation Market Size, Share & Trends Analysis Report By Product (EPS, XPS, Glass Wool, Mineral Wool), By Application (Infrastructure, Industrial, HVAC & OEM), By Region, And Segment Forecasts, 2019 - 2025.* Tech. rep. Grand View Research, June 2019. URL: https://www.grandviewresearch.com/industry-analysis/insulation-market.

[3] Kiran Pulidindi and Hemant Pandey. *Building Thermal Insulation Market Size, Share & Industry Analysis, By Material (Mineral Wool Glass Wool, Stone Wool, Foamed Plastics Expanded Polystyrene [EPS], Extruded Polystyrene [XPS], Polyurethane [PU], Polyisocyanurate [PIR], and Other Foamed Plastics, Cellulose, Aerogels, and Others), By End-Use (Residential and Non-residential), By Application Area (Floor & Basement, Wall, and Roof & Ceiling), and Regional Forecast, 2019-2026.* Tech. rep. GMInsights, 2020. URL: https://www.fortunebusinessinsights.com/enquiry/covid19-impact/building-thermal-insulation-market-102708.

[4] Laszlo Bax, Judith Cruxent, and Jacques Komornicki. *Advanced materials for energy efficient buildings. Key to innovation integrated solution. Innovative chemistry for energy efficiency of buildings in smart cities.* Tech. rep. Smart Cities Stakeholder Platfor, 2019.

[5] C. C. Pavel and D. T. Blagoeva. *Competitive landscape of the EU's insulation materials industry for energy-efficient buildings, EUR 28816 EN, Publications Office of the European Union, Luxembourg, 2018, PUBSY No. JRC10869*. Tech. rep. JRC, 2018. DOI: 10.2760/750646.

[6] IEA. *Technology Roadmap. Energy efficent building envelopes*. Tech. rep. IEA, 2013, p. 68. DOI: 10.1007/SpringerReference_7300. URL: https://www.iea.org/publications/freepublications/publication/TechnologyRoadmapEnergyEfficientBuildingEnvelopes.pdf.

[7] European Commision. *Questions and Answers on the Renovation Wave*. 2020. URL: https://ec.europa.eu/commission/presscorner/detail/en/QANDA_20_1836 (visited on 10/14/2020).

[8] Fleiter Tobias et al. *Baseline scenario of the heating and cooling demand in buildings and industry in the 14 MSs until 2050*. Tech. rep. Fraunhofer Institute for Systems and Innovation Research, 2017. URL: http://www.heatroadmap.eu/resources/HRE4_D3.3andD3.4_final.pdf.

[9] T.M. Gulotta et al. "A bottom-up harmonized energy-environmental models for europe (BOHEEME): A case study on the thermal insulation of the EU-28 building stock". In: *Energy and Buildings* (Oct. 2020), p. 110584. ISSN: 03787788. DOI: 10.1016/j.enbuild.2020.110584.

[10] Stefan Lechtenböhmer and Andreas Schüring. "The potential for large-scale savings from insulating residential buildings in the EU". In: *Energy Efficiency* 4.2 (2011), pp. 257–270. ISSN: 1570646X. DOI: 10.1007/s12053-010-9090-6.

[11] Constantin Ionescu et al. "The historical evolution of the energy efficient buildings". In: *Renewable and Sustainable Energy Reviews* 49 (2015), pp. 243–253. ISSN: 18790690. DOI: 10.1016/j.rser.2015.04.062.

[12] Marina Economidou, Valeria Todeschi, and Bertoldi. *Accelerating energy renovation investments in buildings - Financial andfiscalinstrumentsacross the EU*. 2019, p. 174. ISBN: 978-92-76-12195-4. DOI: 10.2760/086805. URL: https://ec.europa.eu/jrc/en/publication/eur-scientific-and-technical-research-reports/accelerating-energy-renovation-investments-buildings.

[13] Thomas Boermans et al. *Renovation tracks for Europe Up to 2050. Building renovation in Europe- what are the choices?* Tech. rep. Ecofys 2012, 2012, p. 52. URL: http://www.eurima.org/uploads/ModuleXtender/Publications/90/Renovation_tracks_for_Europe_08_06_2012_FINAL.pdf.

[14] BPIE. *Factsheet 97% of Buildings in the EU Need to be Upgraded*. Tech. rep. Building Performance Institute Europe, 2017, p. 2. URL: http://bpie.eu/wp-content/uploads/2017/12/State-of-the-building-stock-briefing_Dic6.pdf.

[15] *Transition to Sustainable Buildings - Strategies and Opportunities to 2050*. Tech. rep. IEA, June 2013. DOI: 10.1787/9789264202955-en. URL: https://www.oecd-ilibrary.org/energy/transition-to-sustainable-buildings_9789264202955-en.

[16] European Commision. "COMMUNICATION FROM THE COMMISSION TO THE EUROPEAN PARLIAMENT, THE COUNCIL, THE EUROPEAN ECONOMIC AND SOCIAL COMMITTEE AND THE COMMITTEE OF THE REGIONS - A Renovation Wave for Europe - greening our buildings, creating jobs, improving lives - COM(2020) 662 final". In: *Official Journal of the European Union* (2020).

[17] Anne Esser et al. *Comprehensive study of building energy renovation activities and the uptake of nearly zero-energy buildings in the EU Final report*. Tech. rep. EU, 2019, p. 87. DOI: 10.2833/14675. URL: https://ec.europa.eu/energy/sites/ener/files/documents/1.final_report.pdf.

[18] European Commision. *New rules for greener and smarter buildings will increase quality of life for all Europeans*. 2019. URL: https://ec.europa.eu/info/news/new-rules-greener-and-smarter-buildings-will-increase-quality-life-all-europeans-2019-apr-15_en (visited on 11/10/2020).

[19] European Commision. *European strategy for plastics*. 2020. URL: https://ec.europa.eu/environment/waste/plastic_waste.htm (visited on 10/14/2020).

[20] European Commision. *EU Circular Economy Action Plan*. 2020. URL: https://ec.europa.eu/environment/circular-economy/index_en.htm (visited on 10/14/2020).

[21] European Commision. *Bioeconomy policy Policy background, strategy and contribution to the Commission's political agenda of bioeconomy policy*. 2020. URL: https://ec.europa.eu/research/bioeconomy/index.cfm?pg=policy&lib=strategy (visited on 10/14/2020).

[22] European Commision. "COMMUNICATION FROM THE COMMISSION TO THE EUROPEAN PARLIAMENT, THE COUNCIL, THE EUROPEAN ECONOMIC AND SOCIAL COMMITTEE AND THE COMMITTEE OF THE REGIONS -A new Circular Economy Action Plan For a cleaner and more competitive Europe - COM(2020) 98 final". In: *Official Journal of the European Union* (2020).

[23] Margareta Wahlström et al. *Construction and Demolition Waste: Challenges and opportunities in a circular economy; European Enviroment Agency European Topic Centre Waste and Materials in a Green Economy*. Tech. rep. January. EIONET, 2020.

[24] Paola Villoria Sáez and Mohamed Osmani. "A diagnosis of construction and demolition waste generation and recovery practice in the European Union". In: *Journal of Cleaner Production* 241 (Dec. 2019), p. 118400. ISSN: 09596526. DOI: 10.1016/j.jclepro.2019.118400. URL: https://linkinghub.elsevier.com/retrieve/pii/S0959652619332706.

[25] R. V. Silva, J. de Brito, and R. K. Dhir. "Availability and processing of recycled aggregates within the construction and demolition supply chain: A review". In: *Journal of Cleaner Production* 143 (2017), pp. 598–614. ISSN: 09596526. DOI: 10.1016/j.jclepro.2016.12.070.

[26] European Commission. *A sustainable bioeconomy for Europe: strengthening the connection between economy, society and the environment*. Tech. rep. Directorate-General for Research and Innovation, 2018, p. 107. DOI: 10.2777/792130.

[27] David Bozsaky. "Nature-Based Thermal Insulation Materials From Renewable Resources – A State-Of-The-Art Review". In: *Slovak Journal of Civil*

Engineering 27.1 (2019), pp. 52–59. ISSN: 1210-3896. DOI: 10.2478/sjce-2019-0008.

[28] Wenqing Yang et al. "Recycling and Disposal Methods for Polyurethane Foam Wastes". In: *Procedia Environmental Sciences* 16.September (2012), pp. 167–175. ISSN: 18780296. DOI: 10.1016/j.proenv.2012.10.023.

[29] Vladimír Ihnát et al. "SIZE REDUCTION DOWNCYCLING OF WASTE WOOD - A REVIEW". In: *Wood Research* 65.2 (May 2020), pp. 205–220. ISSN: 1336-4561. DOI: 10.37763/wr.1336-4561/65.2.205220. URL: http://www.woodresearch.sk/wr/202002/03.pdf.

[30] Azra Korjenic et al. "Development and performance evaluation of natural thermal-insulation materials composed of renewable resources". In: *Energy and Buildings* 43.9 (Sept. 2011), pp. 2518–2523. ISSN: 03787788. DOI: 10.1016/j.enbuild.2011.06.012.

[31] Aidan Reilly and Oliver Kinnane. "The impact of thermal mass on building energy consumption". In: *Applied Energy* 198.April 2017 (July 2017), pp. 108–121. ISSN: 03062619. DOI: 10.1016/j.apenergy.2017.04.024. URL: https://linkinghub.elsevier.com/retrieve/pii/S0306261917304178.

[32] Tim Yates. *Study to evaluate the need to regulate within the Framework of Regulation (EU) 305 / 2011 on the toxicity of smoke produced by construction products in fires Final Report*. Tech. rep. October. European Commision, 2017.

[33] Anna A. Stec and T. Richard Hull. "Assessment of the fire toxicity of building insulation materials". In: *Energy and Buildings* 43.2-3 (2011), pp. 498–506. ISSN: 03787788. DOI: 10.1016/j.enbuild.2010.10.015.

[34] F. Asdrubali, S. Schiavoni, and K. V. Horoshenkov. "A review of sustainable materials for acoustic applications". In: *Building Acoustics* 19.4 (Dec. 2012), pp. 283–312. ISSN: 1351010X. DOI: 10.1260/1351-010X.19.4.283. URL: http://journals.sagepub.com/doi/10.1260/1351-010X.19.4.283.

[35] Gajanan Deshmukh et al. "Thermal Insulation Materials: A Tool for Energy Conservation". In: *Journal of Food Processing & Technology* 08.04 (2017). DOI: 10.4172/2157-7110.1000670.

[36] S Schiavoni et al. “Insulation materials for the building sector: A review and comparative analysis”. In: *Renewable and Sustainable Energy Reviews* 62 (Sept. 2016), pp. 988–1011. ISSN: 13640321. DOI: 10.1016/j.rser.2016.05.045. URL: https://linkinghub.elsevier.com/retrieve/pii/S1364032116301551.

[37] Theresa Sattler et al. “Mineral wool waste in Austria, associated health aspects and recycling options”. In: *Detritus* 9.3 (2020), pp. 174–180. ISSN: 26114135. DOI: 10.31025/2611-4135/2020.13904.

[38] Eurima. *EURIMA - Health & Safety*. URL: https://www.eurima.org/about-mineral-wool/health-safety.html (visited on 11/19/2020).

[39] Seung-hyun Hyun Park. “Types and Health Hazards of Fibrous Materials Used as Asbestos Substitutes”. In: *Safety and Health at Work* 9.3 (2018), pp. 360–364. ISSN: 20937911. DOI: 10.1016/j.shaw.2018.05.001. URL: https://linkinghub.elsevier.com/retrieve/pii/S2093791118300933.

[40] Eurima Information Sheet. *Waste Handling of Mineral Wool Insulation*. Tech. rep. 5. EURIMA, 2016.

[41] Timo Ka et al. “Mineral wool waste in Europe: A review of mineral wool waste quantity, quality, and current recycling methods”. In: *Journal of Material Cycles and Waste Management* 16.1 (2014), pp. 62–72. ISSN: 1436378X. DOI: 10.1007/s10163-013-0170-5.

[42] *What is the difference between XPS and EPS Insulation? - Soprema United Kingdom*. URL: https://www.soprema.co.uk/en/article/sopravoice/what-is-the-difference-between-xps-and-eps-insulation (visited on 11/24/2020).

[43] *The REACH REFIT Evaluation (REACH Review 2017) - REACH - Chemicals - Environment - European Commission*. URL: https://ec.europa.eu/environment/chemicals/reach/review_2017_en.htm (visited on 11/24/2020).

[44] *Persistant Organic Pollutants - Environment - European Commission*. URL: https://ec.europa.eu/environment/chemicals/international_conventions/index_en.htm (visited on 11/24/2020).

[45] Constantine D. Papaspyrides and Pantelis Kiliaris. *Polymer Green Flame Retardants*. Ed. by Constantine D. Papaspyrides and Pantelis Kiliaris. Else-

vier, 2014, p. 924. ISBN: 9780444538086. DOI: 10.1016/C2010-0-66406-6. URL: https://linkinghub.elsevier.com/retrieve/pii/C20100664066.

[46] Hidetaka Takigami, Mafumi Watanabe, and Natsuko Kajiwara. "Destruction behavior of hexabromocyclododecanes during incineration of solid waste containing expanded and extruded polystyrene insulation foams". In: *Chemosphere* 116 (Dec. 2014), pp. 24–33. ISSN: 00456535. DOI: 10.1016/j.chemosphere.2014.01.082. URL: https://linkinghub.elsevier.com/retrieve/pii/S0045653514001738.

[47] Maja Wiprächtiger et al. "A framework for sustainable and circular system design: Development and application on thermal insulation materials". In: *Resources, Conservation and Recycling* 154.December 2019 (2020). ISSN: 18790658. DOI: 10.1016/j.resconrec.2019.104631.

[48] C. Demacsek et al. "PolyStyreneLoop – The circular economy in action". In: *IOP Conference Series: Earth and Environmental Science* 323.1 (Sept. 2019), p. 012149. ISSN: 1755-1315. DOI: 10.1088/1755-1315/323/1/012149. URL: https://iopscience.iop.org/article/10.1088/1755-1315/323/1/012149.

[49] Niklas Heller and Sabine Flamme. "Waste management of deconstructed External Thermal Insulation Composite Systems with expanded polystyrene in the future". In: *Waste Management & Research: The Journal for a Sustainable Circular Economy* 38.4 (Apr. 2020), pp. 400–407. ISSN: 0734-242X. DOI: 10.1177/0734242X20904413. URL: http://journals.sagepub.com/doi/10.1177/0734242X20904413.

[50] *Tris[2-chloro-1-(chloromethyl)ethyl] phosphate - Substance Infocard*. URL: https://echa.europa.eu/it/substance-information/-/substanceinfo/100.033.767 (visited on 11/30/2020).

[51] Cheryl Fairfield Estill et al. "Worker exposure to flame retardants in manufacturing, construction and service industries". In: *Environment International* 135 (Feb. 2020), p. 105349. ISSN: 18736750. DOI: 10.1016/j.envint.2019.105349.

[52] Sara Petty et al. *End-of-life Foams and Plastics Containing Flame Retardants Report by Green Science Policy Institute: Methods of Responsibly*

Managing End-of-Life Foams and Plastics Containing Flame Retardants. Tech. rep. GREEN SCIENCE POLICY INSTITUTE - Berkley, June 2017.

[53] *Recycling Rigid PU Foam Residues - Pofi*. URL: https://www.pofi.eu/recycling-rigid-pu-foam-residues/?lang=en (visited on 11/30/2020).

[54] Polyurethane Foam et al. *FLEXIBLE POLYURETHANE FOAM IN MATTRESSES AND FURNITURE - AN OVERVIEW OF POSSIBLE END OF LIFE SOLUTIONS*. Tech. rep. EUROPUR, 2013. URL: http://www.hospicefoundation.org/endoflife.

[55] Pablo Lopez Hurtado et al. "A review on the properties of cellulose fibre insulation". In: *Building and Environment* 96 (Feb. 2016), pp. 170–177. ISSN: 03601323. DOI: 10.1016/j.buildenv.2015.09.031. URL: https://linkinghub.elsevier.com/retrieve/pii/S0360132315301311.

[56] Bjørn Petter Jelle. "Traditional, state-of-the-art and future thermal building insulation materials and solutions – Properties, requirements and possibilities". In: *Energy and Buildings* 43.10 (Oct. 2011), pp. 2549–2563. ISSN: 03787788. DOI: 10.1016/j.enbuild.2011.05.015. URL: https://linkinghub.elsevier.com/retrieve/pii/S0378778811002295.

[57] *ISOCELL - THE PERFECT CYCLE*. URL: https://www.isocell.com/en/news/77/the-perfect-cycle/ (visited on 12/01/2020).

[58] Ikbal Cetiner and Andrew D. Shea. "Wood waste as an alternative thermal insulation for buildings". In: *Energy and Buildings* 168 (June 2018), pp. 374–384. ISSN: 03787788. DOI: 10.1016/j.enbuild.2018.03.019. URL: https://linkinghub.elsevier.com/retrieve/pii/S0378778817326749.

[59] A.R. Horrocks and D. Price. *Fire Retardant Materials : First Edition*. Ed. by A. Richard Horrocks and D. Price. Cambridge England: Woodhead Publishing, 2001. ISBN: 9781855737464.

[60] Ya-Ling He and Tao Xie. "Advances of thermal conductivity models of nanoscale silica aerogel insulation material". In: *Applied Thermal Engineering* 81 (Apr. 2015), pp. 28–50. ISSN: 13594311. DOI: 10.1016/j.applthermaleng.2015.02.013. URL: https://linkinghub.elsevier.com/retrieve/pii/S1359431115001210.

[61] Ruben Baetens et al. “Vacuum insulation panels for building applications: A review and beyond”. In: *Energy and Buildings* 42.2 (2010), pp. 147–172. ISSN: 03787788. DOI: 10.1016/j.enbuild.2009.09.005.

[62] Bjørn Petter Jelle, Ruben Baetens, and Arild Gustavsen. “Aerogel Insulation for Building Applications”. In: *The Sol-Gel Handbook* 3-3.4 (2015), pp. 1385–1412. ISSN: 03787788. DOI: 10.1002/9783527670819.ch45. URL: http://dx.doi.org/10.1016/j.enbuild.2010.12.012.

[63] Vinayak G. Parale, Kyu Yeon Lee, and Hyung Ho Park. “Flexible and transparent silica aerogels: An overview”. In: *Journal of the Korean Ceramic Society* 54.3 (2017), pp. 184–199. ISSN: 12297801. DOI: 10.4191/kcers.2017.54.3.12.

[64] Basim Abu-Jdayil et al. “Traditional, state-of-the-art and renewable thermal building insulation materials: An overview”. In: *Construction and Building Materials* 214 (July 2019), pp. 709–735. ISSN: 09500618. DOI: 10.1016/j.conbuildmat.2019.04.102. URL: https://linkinghub.elsevier.com/retrieve/pii/S0950061819309845.

[65] *Product Documents | Aspen Aerogel*. URL: https://www.aerogel.com/products-and-solutions/product-documents/ (visited on 12/07/2020).

[66] *Aerogel Blanket | Cabot Corporation*. URL: https://www.cabotcorp.com/solutions/products-plus/aerogel/blanket (visited on 12/07/2020).

[67] Gabrijela Horvat et al. “Preparation and characterization of polysaccharide - silica hybrid aerogels”. In: *Scientific Reports* 9.1 (2019), pp. 3–12. DOI: 10.1038/s41598-019-52974-0.

[68] Shafiqul Islam and Gajanan Bhat. “Environmentally-friendly thermal and acoustic insulation materials from recycled textiles”. In: *Journal of Environmental Management* 251 (Dec. 2019), p. 109536. ISSN: 03014797. DOI: 10.1016/j.jenvman.2019.109536. URL: https://doi.org/10.1016/j.jenvman.2019.109536%20https://linkinghub.elsevier.com/retrieve/pii/S030147971931254X.

[69] I. C. Valverde et al. “Development of new insulation panels based on textile recycled fibers”. In: *Waste and Biomass Valorization* 4.1 (Mar. 2013), pp. 139–146. ISSN: 18772641. DOI: 10.1007/s12649-012-9124-8. URL: https://link.springer.com/article/10.1007/s12649-012-9124-8.

[70] Amine Tilioua, Laurent Libessart, and Stéphane Lassue. "Characterization of the thermal properties of fibrous insulation materials made from recycled textile fibers for building applications: Theoretical and experimental analyses". In: *Applied Thermal Engineering* 142 (Sept. 2018), pp. 56–67. ISSN: 13594311. DOI: 10.1016/j.applthermaleng.2018.06.071.

[71] *ISOLANTE ACUSTICO ANTICALPESTIO IN FIBRE TESSILI RICICLATE: RECYCLEPAV PLUS – Isolanti ecosostenibili isolamento termico acustico isolanti fibre naturali | Manifattura Maiano*. URL: http://www.maiano.it/edilizia/recyclepav-plus-isolante-acustico-anticalpestio-fibre-tessili-riciclate.html (visited on 12/10/2020).

[72] *Inno-Therm® | Thermal Insulation*. URL: http://www.inno-therm.com/product-information/thermal-applications/ (visited on 12/11/2020).

[73] Francesca Intini and Silvana Kühtz. "Recycling in buildings: an LCA case study of a thermal insulation panel made of polyester fiber, recycled from post-consumer PET bottles". In: *The International Journal of Life Cycle Assessment* 16.4 (May 2011), pp. 306–315. ISSN: 0948-3349. DOI: 10.1007/s11367-011-0267-9. URL: https://link.springer.com/article/10.1007/s11367-011-0267-9%20http://link.springer.com/10.1007/s11367-011-0267-9.

[74] Mohamadreza Massoudinejad et al. "Use of municipal, agricultural, industrial, construction and demolition waste in thermal and sound building insulation materials: A review article 09 Engineering 0912 Materials Engineering". In: *Journal of Environmental Health Science and Engineering* 17.2 (July 2019), pp. 1227–1242. ISSN: 2052336X. DOI: 10.1007/s40201-019-00380-z. URL: https://doi.org/10.1007/s40201-019-00380-z.

[75] F. Asdrubali, F. D'Alessandro, and S. Schiavoni. "A review of unconventional sustainable building insulation materials". In: *Sustainable Materials and Technologies* 4.2015 (July 2015), pp. 1–17. ISSN: 22149937. DOI: 10.1016/j.susmat.2015.05.002. URL: https://linkinghub.elsevier.com/retrieve/pii/S2214993715000068.

[76] Satta Panyakaew and Steve Fotios. "New thermal insulation boards made from coconut husk and bagasse". In: *Energy and Buildings* 43.7 (July 2011), pp. 1732–1739. ISSN: 03787788. DOI: 10.1016/j.enbuild.2011.03.015.

[77] Nor Azlina Ramlee, Jesuarockiam Naveen, and Mohammad Jawaid. "Potential of oil palm empty fruit bunch (OPEFB) and sugarcane bagasse fibers for thermal insulation application – A review". In: *Construction and Building Materials* (Nov. 2020), p. 121519. ISSN: 09500618. DOI: 10.1016/j.conbuildmat.2020.121519.

[78] Kazem Doost-Hoseini, Hamid Reza Taghiyari, and Abdollah Elyasi. "Correlation between sound absorption coefficients with physical and mechanical properties of insulation boards made from sugar cane bagasse". In: *Composites Part B: Engineering* 58 (Mar. 2014), pp. 10–15. ISSN: 13598368. DOI: 10.1016/j.compositesb.2013.10.011.

[79] Rajendran Muthuraj et al. "Sustainable thermal insulation biocomposites from rice husk, wheat husk, wood fibers and textile waste fibers: Elaboration and performances evaluation". In: *Industrial Crops and Products* 135.May (Sept. 2019), pp. 238–245. ISSN: 09266690. DOI: 10.1016/j.indcrop.2019.04.053. URL: https://doi.org/10.1016/j.indcrop.2019.04.053%20https://linkinghub.elsevier.com/retrieve/pii/S0926669019303024.

[80] C. Buratti et al. "Rice husk panels for building applications: Thermal, acoustic and environmental characterization and comparison with other innovative recycled waste materials". In: *Construction and Building Materials* 171 (May 2018), pp. 338–349. ISSN: 09500618. DOI: 10.1016/j.conbuildmat.2018.03.089.

[81] Miguel Sánchez-Soto et al. "Thermal, Electrical, Insulation and Fire Resistance Properties of Polysaccharide and Protein-based Aerogels". In: *RSC Green Chemistry*. Vol. 2018-January. 58. Royal Society of Chemistry, July 2018, pp. 158–176. ISBN: 9781782624127. DOI: 10.1039/9781782629979-00158. URL: https://pubs.rsc.org/en/content/chapter/bk9781782627654-00158/978-1-78262-765-4.

[82] Kathirvel Ganesan et al. "Review on the production of polysaccharide aerogel particles". In: *Materials* 11.11 (2018), pp. 1–37. ISSN: 19961944. DOI: 10.3390/ma11112144.

[83] Danny Illera et al. "Cellulose Aerogels for Thermal Insulation in Buildings: Trends and Challenges". In: *Coatings* 8.10 (Sept. 2018), p. 345. ISSN: 2079-

6412. DOI: 10.3390/coatings8100345. URL: https://www.mdpi.com/2079-6412/8/10/345.

[84] Farouk Ayadi et al. "Mechanically flexible and optically transparent three-dimensional nanofibrous amorphous aerocellulose". In: *Carbohydrate Polymers* 149 (Sept. 2016), pp. 217–223. ISSN: 01448617. DOI: 10.1016/j.carbpol.2016.04.103.

[85] Bastien Seantier et al. "Multi-scale cellulose based new bio-aerogel composites with thermal super-insulating and tunable mechanical properties". In: *Carbohydrate Polymers* 138 (Mar. 2016), pp. 335–348. ISSN: 01448617. DOI: 10.1016/j.carbpol.2015.11.032. URL: https://linkinghub.elsevier.com/retrieve/pii/S0144861715011212.

[86] Yuri Kobayashi, Tsuguyuki Saito, and Akira Isogai. "Aerogels with 3D Ordered Nanofiber Skeletons of Liquid-Crystalline Nanocellulose Derivatives as Tough and Transparent Insulators". In: *Angewandte Chemie* 126.39 (Sept. 2014), pp. 10562–10565. ISSN: 00448249. DOI: 10.1002/ange.201405123. URL: http://doi.wiley.com/10.1002/ange.201405123.

[87] Bernd Wicklein et al. "Thermally insulating and fire-retardant lightweight anisotropic foams based on nanocellulose and graphene oxide". In: *Nature Nanotechnology* 10.3 (2015), pp. 277–283. ISSN: 17483395. DOI: 10.1038/nnano.2014.248. URL: http://www.nature.com/doifinder/10.1038/nnano.2014.248.

[88] Gabrijela Horvat et al. "Thermal properties of polysaccharide aerogels". In: *Journal of Thermal Analysis and Calorimetry* 127.1 (2017), pp. 363–370. DOI: 10.1007/s10973-016-5814-y.

[89] P. Gurikov et al. "A novel approach to alginate aerogels: carbon dioxide induced gelation". In: *RSC Advances* 5.11 (2015), pp. 7812–7818. ISSN: 2046-2069. DOI: 10.1039/C4RA14653K. URL: http://xlink.rsc.org/?DOI=C4RA14653K.

[90] Lucile Druel et al. "Starch Aerogels: A Member of the Family of Thermal Superinsulating Materials". In: *Biomacromolecules* 18.12 (Dec. 2017), pp. 4232–4239. ISSN: 15264602. DOI: 10.1021/acs.biomac.7b01272. URL: https://pubmed.ncbi.nlm.nih.gov/29068674/.

[91] Satoru Takeshita and Satoshi Yoda. "Chitosan Aerogels: Transparent, Flexible Thermal Insulators". In: *Chemistry of Materials* 27.22 (Nov. 2015), pp. 7569–7572. ISSN: 15205002. DOI: 10.1021/acs.chemmater.5b03610. URL: https://pubs.acs.org/doi/10.1021/acs.chemmater.5b03610.

[92] Bitao Fan et al. "Fabrication of Cellulose Nanofiber/AlOOH Aerogel for Flame Retardant and Thermal Insulation". In: *Materials* 10.3 (Mar. 2017), p. 311. ISSN: 1996-1944. DOI: 10.3390/ma10030311. URL: http://www.mdpi.com/1996-1944/10/3/311.

[93] Nga H.N. Do et al. "Recycling of Pineapple Leaf and Cotton Waste Fibers into Heat-insulating and Flexible Cellulose Aerogel Composites". In: *Journal of Polymers and the Environment* (2020). ISSN: 15728919. DOI: 10.1007/s10924-020-01955-w. URL: https://doi.org/10.1007/s10924-020-01955-w.

[94] Imrana I. Kabir et al. "Alginate/Polymer-Based Materials for Fire Retardancy: Synthesis, Structure, Properties, and Applications". In: *Polymer Reviews* 0.0 (2020), pp. 1–58. ISSN: 15583716. DOI: 10.1080/15583724.2020.1801726. URL: https://doi.org/10.1080/15583724.2020.1801726.

[95] Thierry Vincent et al. "Fire behavior of innovative alginate foams". In: *Carbohydrate Polymers* 250.April (2020). ISSN: 01448617. DOI: 10.1016/j.carbpol.2020.116910.

[96] Thierry Vincent et al. "New alginate foams: Box-Behnken design of their manufacturing; fire retardant and thermal insulating properties". In: *Journal of Applied Polymer Science* 135.7 (2018), pp. 1–12. ISSN: 10974628. DOI: 10.1002/app.45868.

[97] Gabrijela Tkalec et al. "Optimisation of critical parameters during alginate aerogels' production". In: *Journal of Non-Crystalline Solids* 443 (July 2016), pp. 112–117. ISSN: 00223093. DOI: 10.1016/j.jnoncrysol.2016.04.014. URL: https://linkinghub.elsevier.com/retrieve/pii/S0022309316301119.

[98] Yuhuan Jiang et al. "An alginate hybrid sponge with high thermal stability: Its flame retardant properties and mechanism". In: *Polymers* 11.12 (2019). ISSN: 20734360. DOI: 10.3390/polym11121973.

[99] Ke Shang et al. “Nonflammable Alginate Nanocomposite Aerogels Prepared by a Simple Freeze-Drying and Post-Cross-Linking Method”. In: *ACS Applied Materials & Interfaces* 8.1 (Jan. 2016), pp. 643–650. ISSN: 1944-8244. DOI: 10.1021/acsami.5b09768. URL: https://pubs.acs.org/doi/10.1021/acsami.5b09768.

[100] Clément Lacoste et al. “Sodium alginate adhesives as binders in wood fibers/textile waste fibers biocomposites for building insulation”. In: *Carbohydrate Polymers* 184 (Mar. 2018), pp. 1–8. ISSN: 01448617. DOI: 10.1016/j.carbpol.2017.12.019.

[101] M. Palumbo et al. “Performance of biobased insulation board from crop byproducts and natural gums”. In: *Academic Journal of Civil Engineering* 33.2 (2015), pp. 189–196. DOI: https://doi.org/10.26168/icbbm2015.29.

[102] M. Palumbo et al. “Improvement of fire reaction and mould growth resistance of a new bio-based thermal insulation material”. In: *Construction and Building Materials* 139 (May 2017), pp. 531–539. ISSN: 09500618. DOI: 10.1016/j.conbuildmat.2016.11.020. URL: https://linkinghub.elsevier.com/retrieve/pii/S0950061816317743.

[103] Ruifang Xia and Guoqing Cheng. “Study on mechanics and thermal performance of new building energy-saving wall insulation materials”. In: *Gongneng Cailiao/Journal of Functional Materials* 50.9 (Sept. 2019), pp. 09110–09114. ISSN: 10019731. DOI: 10.3969/j.issn.1001-9731.2019.09.018. URL: http://www.gncl.cn/CN/abstract/abstract17777.shtml.

[104] Narimane Mati-Baouche et al. “Mechanical, thermal and acoustical characterizations of an insulating bio-based composite made from sunflower stalks particles and chitosan”. In: *Industrial Crops and Products* 58 (2014), pp. 244–250. ISSN: 09266690. DOI: 10.1016/j.indcrop.2014.04.022.

[105] Girts Bumanis et al. “Gypsum, Geopolymers, and Starch—Alternative Binders for Bio-Based Building Materials: A Review and Life-Cycle Assessment”. In: *Sustainability* 12.14 (July 2020), p. 5666. ISSN: 2071-1050. DOI: 10.3390/su12145666. URL: https://www.mdpi.com/2071-1050/12/14/5666.

[106] Boyu Zhou et al. “Preparation and properties of bio-geopolymer composites with waste cotton stalk materials”. In: *Journal of Cleaner Production* 245

(Feb. 2020), p. 118842. ISSN: 09596526. DOI: 10.1016/j.jclepro.2019.118842.

[107] Narimane Mati-Baouche et al. "Polysaccharidic binders for the conception of an insulating agro-composite". In: *Composites Part A: Applied Science and Manufacturing* 78 (2015), pp. 152–159. ISSN: 1359835X. DOI: 10.1016/j.compositesa.2015.08.006.

[108] Giada Kyaw Oo D'Amore et al. "Towards the Use of Novel Materials in Shipbuilding: Assessing Thermal Performances of Fire-Doors by Self-Consistent Numerical Modelling". In: *Applied Sciences* 10.17 (Aug. 2020), p. 5736. ISSN: 2076-3417. DOI: 10.3390/app10175736. URL: www.mdpi.com/journal/applsci%20https://www.mdpi.com/2076-3417/10/17/5736.

[109] Géraldine Oliveux, Luke O. Dandy, and Gary A. Leeke. "Current status of recycling of fibre reinforced polymers: Review of technologies, reuse and resulting properties". In: *Progress in Materials Science* 72 (July 2015), pp. 61–99. ISSN: 00796425. DOI: 10.1016/j.pmatsci.2015.01.004. URL: https://linkinghub.elsevier.com/retrieve/pii/S0079642515000316.

[110] *Wind Turbine Blades Can't Be Recycled, So They're Piling Up in Landfills - Bloomberg*. URL: https://www.bloomberg.com/news/features/2020-02-05/wind-turbine-blades-can-t-be-recycled-so-they-re-piling-up-in-landfills (visited on 12/14/2020).

[111] Nicholas Sakellariou. "Current and potential decommissioning scenarios for end-of-life composite wind blades". In: *Energy Systems* 9.4 (Nov. 2018), pp. 981–1023. ISSN: 1868-3967. DOI: 10.1007/s12667-017-0245-9. URL: http://link.springer.com/10.1007/s12667-017-0245-9.

[112] Sankar Karuppannan Gopalraj and Timo Kärki. "A review on the recycling of waste carbon fibre/glass fibre-reinforced composites: fibre recovery, properties and life-cycle analysis". In: *SN Applied Sciences* 2.3 (Mar. 2020), p. 433. ISSN: 2523-3963. DOI: 10.1007/s42452-020-2195-4. URL: https://doi.org/10.1007/s42452-020-2195-4%20http://link.springer.com/10.1007/s42452-020-2195-4.

[113] Liqing Wei, Shaobo Liang, and Armando G. McDonald. "Thermophysical properties and biodegradation behavior of green composites made from polyhydroxybutyrate and potato peel waste fermentation residue". In: *In-*

dustrial Crops and Products 69 (July 2015), pp. 91–103. ISSN: 09266690. DOI: 10.1016/j.indcrop.2015.02.011.

[114] Rajendran Muthuraj, Manjusri Misra, and Amar Kumar Mohanty. "Biocomposite consisting of miscanthus fiber and biodegradable binary blend matrix: Compatibilization and performance evaluation". In: *RSC Advances* 7.44 (May 2017), pp. 27538–27548. ISSN: 20462069. DOI: 10.1039/c6ra27987b. URL: https://pubs.rsc.org/en/content/articlehtml/2017/ra/c6ra27987b%20https://pubs.rsc.org/en/content/articlelanding/2017/ra/c6ra27987b.

[115] Rajendran Muthuraj, Manjusri Misra, and Amar Kumar Mohanty. "Biodegradable biocomposites from poly(butylene adipate- co -terephthalate) and miscanthus: Preparation, compatibilization, and performance evaluation". In: *Journal of Applied Polymer Science* 134.43 (Nov. 2017), p. 45448. ISSN: 00218995. DOI: 10.1002/app.45448. URL: http://doi.wiley.com/10.1002/app.45448.

[116] Charles A. Wilkie and Alexander B. Morgan, eds. *Fire Retardancy of Polymeric Materials*. Second. CRC Press, Dec. 2009. ISBN: 9781420083996.

[117] Grand View Research. *Flame Retardant Market Analysis By Product (Halogenated (Brominated, Antimony Trioxide), Non Halogenated (Aluminum Hydroxide, Magnesium Dihydroxide, Phosphorous)), By Application, By End-Use And Segment Forecasts, 2018 - 2025*. 2016.

[118] Sudip Ray and Ralph P. Cooney. "Thermal Degradation of Polymer and Polymer Composites". In: *Handbook of Environmental Degradation of Materials: Second Edition*. Second Edi. Elsevier Inc., 2012, pp. 213–242. ISBN: 9781437734560. DOI: 10.1016/B978-1-4377-3455-3.00007-9.

[119] Simone T. Lazar, Thomas J. Kolibaba, and Jaime C. Grunlan. "Flame-retardant surface treatments". In: *Nature Reviews Materials* (2020). ISSN: 2058-8437. DOI: 10.1038/s41578-019-0164-6.

[120] F. Laoutid et al. "New prospects in flame retardant polymer materials: From fundamentals to nanocomposites". In: *Materials Science and Engineering: R: Reports* 63.3 (2009), pp. 100–125. DOI: 10.1016/j.mser.2008.09.002.

[121] Alberto Fina and Giovanni Camino. "Ignition mechanisms in polymers and polymer nanocomposites". In: *Polymers for Advanced Technologies* 22.7

(July 2011), pp. 1147–1155. ISSN: 10427147. DOI: 10.1002/pat.1971. URL: http://doi.wiley.com/10.1002/pat.1971.

[122] ASTM Standard D1929-16. *Standard Test Method for Determining Ignition Temperature of Plastics*. 2016.

[123] ASTM Standard E176-15a. *Standard Terminology of Fire Standards*. 2015.

[124] P.M. Visakh and Y. Arao. *Flame Retardants: Polymer Blends, Composites and Nanocomposites*. Engineering Materials. Springer International Publishing, 2015. ISBN: 9783319034676. URL: https://books.google.com.ua/books?id=DleEBgAAQBAJ.

[125] Guillermo Rein. "Smouldering Combustion Phenomena in Science and Technology". In: *International Review of Chemical Engineering* 1 (2009), pp. 3–18.

[126] E. H. Cornish. *Properties of polymers*. Ed. by D. W. VAN KREVELEN and K. TE NIJENHUIS. Fourth. Elsevier B.V, 2009. ISBN: 9780080548197.

[127] ASTM Standard D2863-13. *Standard Test Method for Measuring the Minimum Oxygen Concentration to Support Candle-Like Combustion of Plastics (Oxygen Index)*. 2013.

[128] ISO 4589-2:1996(E). "Plastic - Determination of burning behaviour by oxygen index - Part 2: Ambient-temperature test". In: (1996).

[129] UL - 94. "Tests for Flammability of Plastic Materials for Parts in Devices and Appliances". In: (). URL: https://standardscatalog.ul.com/standards/en/standard_94_6.

[130] THE COMMISSION OF THE EUROPEAN COMMUNITIES. "COMMISSION DECISION of 8 February 2000 implementing Council Directive 89/106/EEC as regards the classification of the reaction to fire performance of construction products". In: *Official Journal of the European Communities* (2000).

[131] *INTERNATIONAL CODE FOR APPLICATION OF FIRE TEST PROCEDURES, 2010 - RESOLUTION MSC.307(88) (adopted on 3 December 2010)*. 2010.

[132] M Zarrelli et al. "FIREPROOF SILICONE SEALANTS FOR SHIPBUILDING". In: *ECCM15 - 15TH EUROPEAN CONFERENCE ON COMPOSITE MATERIALS, Venice, Italy, 24-28 June 2012*. 2012.

[133] T Richard Hull and Anna A Stec. "Polymers and fire : Chemical and physical processes". In: *Fire Retardancy of Polymers: New Strategies and Mechanisms*. Royal Society of Chemistry, 2009, pp. 1–18.

[134] Irvin Glassman et al. "Explosive and general oxidative characteristics of fuels". In: *Combustion (fifth edition)*. Academic Press, 2015, pp. 71–146. ISBN: 978-0-12-407913-7. DOI: 10.1016/B978-0-12-407913-7.00003-7. URL: https://www.sciencedirect.com/science/article/pii/B9780124079137000037.

[135] Takashi Kashiwagi. "Polymer combustion and flammability-Role of the condensed phase". In: *Twenty-Fifth Symposium (International) on Combustion*. Vol. 25. 1994, pp. 1423–1437. DOI: 10.1016/S0082-0784(06)80786-1. URL: https://linkinghub.elsevier.com/retrieve/pii/S0082078406807861.

[136] D.W. Van Krevelen et al. "Chapter 21 – Thermal Decomposition". In: *Properties of Polymers*. 2009, pp. 763–777. ISBN: 9780080548197. DOI: 10.1016/B978-0-08-054819-7.00021-2.

[137] Shui Yu Lu and Ian Hamerton. "Recent developments in the chemistry of halogen-free flame retardant polymers". In: *Progress in Polymer Science (Oxford)* 27.8 (2002), pp. 1661–1712. ISSN: 00796700. DOI: 10.1016/S0079-6700(02)00018-7.

[138] Alexander B. Morgan and Charles A. Wilkie. *Non-Halogenated Flame Retardant Handbook*. Scrivener Publishing, 2014, p. 419. ISBN: 978-1-118-68624-9.

[139] Bernhard Schartel. "Phosphorus-based Flame Retardancy Mechanisms—Old Hat or a Starting Point for Future Development?" In: *Materials* 3.10 (Sept. 2010), pp. 4710–4745. ISSN: 1996-1944. DOI: 10.3390/ma3104710.

[140] Kristin H Pawlowski and Bernhard Schartel. "Flame retardancy mechanisms of triphenyl phosphate, resorcinol bis(diphenyl phosphate) and bisphenol A bis(diphenyl phosphate) in polycarbonate/acrylonitrile–butadiene–styrene blends". In: *Polymer International* 56.11 (Nov. 2007), pp. 1404–1414. ISSN: 09598103. DOI: 10.1002/pi.2290. URL: http://doi.wiley.com/10.1002/pi.2290.

[141] Dennis Price et al. “Flame retarding poly(methyl methacrylate) with phosphorus-containing compounds: Comparison of an additive with a reactive approach”. In: *Polymer Degradation and Stability* 74.3 (2001), pp. 441–447. ISSN: 01413910. DOI: 10.1016/S0141-3910(01)00184-7.

[142] Xia Zhou et al. “Polyphosphazenes-based flame retardants: A review”. In: *Composites Part B: Engineering* 202 (Dec. 2020), p. 108397. ISSN: 13598368. DOI: 10.1016/j.compositesb.2020.108397.

[143] George M. Crews et al. “Melamine and Guanamines”. In: *Ullmann’s Encyclopedia of Industrial Chemistry*. Vol. 22. Weinheim, Germany: Wiley-VCH Verlag GmbH & Co. KGaA, July 2006, pp. 377–392. DOI: 10.1002/14356007.a16_171.pub2. URL: http://doi.wiley.com/10.1002/14356007.a16_171.pub2.

[144] S. Dyjak, W. Kiciński, and A. Huczko. “Thermite-driven melamine condensation to CxNyHz graphitic ternary polymers: Towards an instant, large-scale synthesis of g-C3N4”. In: *Journal of Materials Chemistry A* 3.18 (May 2015), pp. 9621–9631. ISSN: 20507496. DOI: 10.1039/c5ta00201j.

[145] Martin Klatt. “Nitrogen-based Flame Retardants”. In: *Non-Halogenated Flame Retardant Handbook*. 2014, pp. 143–168.

[146] Manfred Döring, Yana Bykov, and Ingmar E. Held. *Innovative and Sustainable Flame Retardants in Transportation Non-halogenated phosphorus, inorganic and nitrogen flame retardants*. Tech. rep. Brussels: Pinfa, 2010. URL: www.pinfa.eu.

[147] Li Li Wang et al. “Flame-retardant coating by alternate assembly of poly(vinylphosphonic acid) and polyethylenimine for ramie fabrics”. In: *Chinese Journal of Polymer Science (English Edition)* 32.3 (2014), pp. 305–314. ISSN: 14396203. DOI: 10.1007/s10118-014-1408-y.

[148] Tao Zhang et al. “A phosphorus-, nitrogen- and carbon-containing polyelectrolyte complex: Preparation, characterization and its flame retardant performance on polypropylene”. In: *RSC Advances* 4.89 (2014), pp. 48285–48292. ISSN: 20462069. DOI: 10.1039/c4ra09243k. URL: http://dx.doi.org/10.1039/C4RA09243K.

[149] Kelvin K. Shen and Roderick O’Connor. “Flame retardants: borates”. In: *Plastics Additives*. Springer, Dordrecht, 1998, pp. 268–276. DOI: 10.1007/

978-94-011-5862-6_30. URL: https://link.springer.com/chapter/10.1007/978-94-011-5862-6_30.

[150] Takashi Kashiwagi et al. “Flame retardant mechanism of silica gel/silica”. In: *Fire and Materials* 24.6 (Nov. 2000), pp. 277–289. ISSN: 0308-0501. DOI: 10.1002/1099-1018(200011/12)24:6<277::AID-FAM746>3.0.CO;2-A.

[151] Takashi Kashiwagi et al. “Flame-retardant mechanism of silica: Effects of resin molecular weight”. In: *Journal of Applied Polymer Science* 87.9 (Feb. 2003), pp. 1541–1553. ISSN: 0021-8995. DOI: 10.1002/app.11967. URL: http://doi.wiley.com/10.1002/app.11967.

[152] Jeffrey W. Gilman, Takashi Kashiwagi, and J D. Lichtenhan. “Nanocomposites: A Revolutionary New Flame Retardant Approach.” In: *Sampe Journal* 33.4 (Dec. 1997), pp. 40–46. URL: https://www.nist.gov/publications/nanocomposites-revolutionary-new-flame-retardant-approach.

[153] Yoshitsugu Kojima et al. “Mechanical properties of nylon 6-clay hybrid”. In: *Journal of Materials Research* 8.5 (May 1993), pp. 1185–1189. ISSN: 20445326. DOI: 10.1557/JMR.1993.1185. URL: https://www.cambridge.org/core/product/identifier/S0884291400020537/type/journal_article.

[154] Ravin Narain, ed. *Polymer Science and Nanotechnology - Fundamentals and Applications*. 1st Editio. 2554. ISBN: 9780128168066. DOI: 10.1016/C2018-0-01134-2. URL: http://library1.nida.ac.th/termpaper6/sd/2554/19755.pdf.

[155] Bok Nam Jang, Marius Costache, and Charles A. Wilkie. “The relationship between thermal degradation behavior of polymer and the fire retardancy of polymer/clay nanocomposites”. In: *Polymer* 46.24 (Nov. 2005), pp. 10678–10687. ISSN: 00323861. DOI: 10.1016/j.polymer.2005.08.085.

[156] JW. Gilman. “Flame retardant mechanism of polymereclay nanocomposites”. In: *Flame retardant polymer nanocomposites*. Ed. by Wiley. 2007, pp. 67–87.

[157] Chao Zheng, Dongfang Li, and Monica Ek. “Improving fire retardancy of cellulosic thermal insulating materials by coating with bio-based fire retardants”. In: *Nordic Pulp and Paper Research Journal* 34.1 (Mar. 2019),

pp. 96–106. ISSN: 20000669. DOI: 10.1515/npprj-2018-0031. URL: https://doi.org/10.1515/npprj-2018-0031.

[158] Andong Liu and Lars A. Berglund. "Fire-retardant and ductile clay nanopaper biocomposites based on montmorrilonite in matrix of cellulose nanofibers and carboxymethyl cellulose". In: *European Polymer Journal* 49.4 (Apr. 2013), pp. 940–949. ISSN: 00143057. DOI: 10.1016/j.eurpolymj.2012.12.017. URL: https://linkinghub.elsevier.com/retrieve/pii/S0014305712004260.

[159] Qi Zhang et al. "Effect of particle size on the properties of Mg(OH)2-filled rubber composites". In: *Journal of Applied Polymer Science* 94.6 (Dec. 2004), pp. 2341–2346. ISSN: 00218995. DOI: 10.1002/app.21037.

[160] S. Mishra et al. "Effect of Nano-Mg(OH)2 on the mechanical and flame-retarding properties of polypropylene composites". In: *Journal of Applied Polymer Science* 94.1 (Oct. 2004), pp. 116–122. ISSN: 00218995. DOI: 10.1002/app.20750.

[161] N. Koga. "A comparative study of the effects of decomposition rate control and mechanical grinding on the thermal decomposition of aluminum hydroxide". In: *Journal of Thermal Analysis and Calorimetry* 81.3 (2005), pp. 595–601. ISSN: 13886150. DOI: 10.1007/s10973-005-0830-3.

[162] *Boehmite*. URL: https://nabaltec.de/en/products/boehmite/ (visited on 12/18/2020).

[163] Pei Hsuan Huang et al. "Boehmite-based Microcapsules as Flame-retardants for Lithium-ion Batteries". In: *Electrochimica Acta* 228 (Feb. 2017), pp. 597–603. ISSN: 00134686. DOI: 10.1016/j.electacta.2017.01.094.

[164] Tao Sun et al. "Synthesis of boehmite and its effect on flame retardancy of epoxy resin". In: *High Performance Polymers* 27.1 (Feb. 2015), pp. 100–104. ISSN: 0954-0083. DOI: 10.1177/0954008314540312. URL: http://journals.sagepub.com/doi/10.1177/0954008314540312.

[165] Saman Kahkesh and Mehdi Rafizadeh. "Flame retardancy and thermal properties of poly(butylene succinate)/ nano-boehmite composites prepared via in situ polymerization". In: *Polymer Engineering and Science* 60.9 (2020), pp. 2262–2271. ISSN: 15482634. DOI: 10.1002/pen.25468.

[166] Francielen Kuball Silva et al. “Synthesis of aluminum hydroxide nanoparticles from the residue of aluminum anodization for application in polymer materials as antiflame agents”. In: *Journal of Materials Research and Technology* 9.4 (July 2020), pp. 8937–8952. ISSN: 22387854. DOI: 10.1016/j.jmrt.2020.05.108.

[167] Yanshan Gao et al. “Flame retardant polymer/layered double hydroxide nanocomposites”. In: *Journal of Materials Chemistry A* 2.29 (Aug. 2014), pp. 10996–11016. ISSN: 20507496. DOI: 10.1039/c4ta01030b. URL: https://pubs.rsc.org/en/content/articlehtml/2014/ta/c4ta01030b%20https://pubs.rsc.org/en/content/articlelanding/2014/ta/c4ta01030b.

[168] Bin Sang et al. “Graphene-based flame retardants : a review”. In: *Journal of Materials Science* 51.18 (2016), pp. 8271–8295. ISSN: 1573-4803. DOI: 10.1007/s10853-016-0124-0.

[169] Yanqun Pan et al. “Influence of fullerenes on the thermal and flame-retardant properties of polymeric materials”. In: *Journal of Applied Polymer Science* 137.1 (2020), pp. 1–18. ISSN: 10974628. DOI: 10.1002/app.47538.

[170] Ayesha Kausar, Irum Rafique, and Bakhtiar Muhammad. “Significance of Carbon Nanotube in Flame-Retardant Polymer/CNT Composite: A Review”. In: *Polymer-Plastics Technology and Engineering* 56.5 (Feb. 2017), pp. 470–487. ISSN: 0360-2559. DOI: 10.1080/03602559.2016.1233267. URL: https://www.tandfonline.com/doi/full/10.1080/03602559.2016.1233267.

[171] Maziyar Sabet et al. “The effect of graphene oxide on flame retardancy of polypropylene and polystyrene”. In: *Materials Performance and Characterization* 9.1 (2020), pp. 284–292. ISSN: 21653992. DOI: 10.1520/MPC20190256.

[172] Chenlu Bao et al. “Preparation of graphene by pressurized oxidation and multiplex reduction and its polymer nanocomposites by masterbatch-based melt blending”. In: *Journal of Materials Chemistry* 22.13 (2012), p. 6088. ISSN: 0959-9428. DOI: 10.1039/c2jm16203b. URL: http://xlink.rsc.org/?DOI=c2jm16203b.

[173] Chenlu Bao et al. “Functionalized graphene oxide for fire safety applications of polymers: a combination of condensed phase flame retardant strategies”.

In: *Journal of Materials Chemistry* 22.43 (2012), p. 23057. ISSN: 0959-9428. DOI: 10.1039/c2jm35001g. URL: http://xlink.rsc.org/?DOI=c2jm35001g.

[174] Shan Liu et al. "Effect of graphene nanosheets on morphology, thermal stability and flame retardancy of epoxy resin". In: *Composites Science and Technology* 90 (Jan. 2014), pp. 40–47. ISSN: 02663538. DOI: 10.1016/j.compscitech.2013.10.012. URL: https://linkinghub.elsevier.com/retrieve/pii/S0266353813004120.

[175] Yongqin Han et al. "Preparation and properties of polystyrene nanocomposites with graphite oxide and graphene as flame retardants". In: *Journal of Materials Science* 48.12 (June 2013), pp. 4214–4222. ISSN: 00222461. DOI: 10.1007/s10853-013-7234-8. URL: https://link.springer.com/article/10.1007/s10853-013-7234-8.

[176] Bettina Dittrich et al. "Flame retardancy through carbon nanomaterials: Carbon black, multiwall nanotubes, expanded graphite, multi-layer graphene and graphene in polypropylene". In: *Polymer Degradation and Stability* 98.8 (Aug. 2013), pp. 1495–1505. ISSN: 01413910. DOI: 10.1016/j.polymdegradstab.2013.04.009.

[177] Federico Carosio et al. "Graphene Oxide Exoskeleton to Produce Self-Extinguishing, Nonignitable, and Flame Resistant Flexible Foams: A Mechanically Tough Alternative to Inorganic Aerogels". In: *Advanced Materials Interfaces* 5.23 (Dec. 2018), p. 1801288. ISSN: 2196-7350. DOI: 10.1002/admi.201801288. URL: https://onlinelibrary.wiley.com/doi/abs/10.1002/admi.201801288.

[178] Xiaotao Zhang et al. "Graphene oxide-filled multilayer coating to improve flame-retardant and smoke suppression properties of flexible polyurethane foam". In: *Journal of Materials Science* 51.23 (2016), pp. 10361–10374. ISSN: 15734803. DOI: 10.1007/s10853-016-0247-3.

[179] Susana C. Pinto et al. "Hybrid structures made of polyurethane/graphene nanocomposite foams embedded within aluminum open-cell foam". In: *Metals* 10.6 (2020), pp. 1–15. ISSN: 20754701. DOI: 10.3390/met10060768.

[180] *FireStop - First Graphene*. URL: https://firstgraphene.net/firestop/ (visited on 12/19/2020).

[181] J. Xu, J. Liu, and K. Li. "Application of functionalized graphene oxide in flame-retardant polypropylene". In: *Journal of Vinyl and Additive Technology* 21.4 (Dec. 2015), pp. 278–284. ISSN: 1083-5601. DOI: 10.1002/vnl.21415. URL: https://onlinelibrary.wiley.com/doi/10.1002/vnl.21415.

[182] Yewen Cao, Jiachun Feng, and Peiyi Wu. "Polypropylene-grafted graphene oxide sheets as multifunctional compatibilizers for polyolefin-based polymer blends". In: *Journal of Materials Chemistry* 22.30 (Aug. 2012), pp. 14997–15005. ISSN: 13645501. DOI: 10.1039/c2jm31477k. URL: https://pubs.rsc.org/en/content/articlehtml/2012/jm/c2jm31477k%20https://pubs.rsc.org/en/content/articlelanding/2012/jm/c2jm31477k.

[183] Weizhao Hu et al. "Hyper-branched polymer grafting graphene oxide as an effective flame retardant and smoke suppressant for polystyrene". In: *Journal of Hazardous Materials* 300 (2015), pp. 58–66. ISSN: 18733336. DOI: 10.1016/j.jhazmat.2015.06.040.

[184] Yuqiang Guo et al. "In Situ Polymerization of Graphene, Graphite Oxide, and Functionalized Graphite Oxide into Epoxy Resin and Comparison Study of On-the-Flame Behavior". In: *Ind. Eng. Chem. Res* 50 (2011), pp. 7772–7783. DOI: 10.1021/ie200152x. URL: https://pubs.acs.org/sharingguidelines.

[185] Parisa Monji, Reza Jahanmardi, and Milad Mehranpour. "Preparation of melamine-grafted graphene oxide and evaluation of its efficacy as a flame retardant additive for polypropylene". In: *Carbon Letters* 27 (2018), pp. 81–89. DOI: 10.5714/CL.2018.27.081.

[186] Andreas Edenharter et al. "Superior flame retardant by combining high aspect ratio layered double hydroxide and graphene oxide". In: *Polymer* 91 (May 2016), pp. 41–49. ISSN: 00323861. DOI: 10.1016/j.polymer.2016.03.020.

[187] Wanting Zhao et al. "Morphology and thermal properties of calcium alginate/reduced graphene oxide composites". In: *Polymers* 10.9 (2018), pp. 1–11. ISSN: 20734360. DOI: 10.3390/polym10090990.

[188] Xin Wang et al. "Recent advances in construction of hybrid nano-structures for flame retardant polymers application". In: *Applied Materials Today* 20

(Sept. 2020), p. 100762. ISSN: 23529407. DOI: 10.1016/j.apmt.2020.100762. URL: https://linkinghub.elsevier.com/retrieve/pii/S2352940720302109.

[189] Giulio Malucelli. "The Role of Graphene in Flame Retardancy of Polymeric Materials: Recent Advances". In: *Current Graphene Science* 2.1 (Oct. 2018), pp. 27–34. ISSN: 24522732. DOI: 10.2174/2452273202666180706145545. URL: http://www.eurekaselect.com/163596/article.

[190] Richard E Lyon. "Plastics and Rubber". In: *Handbook of Materials for Fire Protection*. Ed. by C.A. In Harper. July 2004. Chap. 3.

[191] M. Palumbo, J. Formosa, and A.M. Lacasta. "Thermal degradation and fire behaviour of thermal insulation materials based on food crop by-products". In: *Construction and Building Materials* 79 (Mar. 2015), pp. 34–39. ISSN: 09500618. DOI: 10.1016/j.conbuildmat.2015.01.028. URL: https://linkinghub.elsevier.com/retrieve/pii/S0950061815000483.

[192] Feng Qi Zhang et al. "Convenient blending of alginate fibers with polyamide fibers for flame-retardant non-woven fabrics". In: *Cellulose* 27.14 (Sept. 2020), pp. 8341–8349. ISSN: 1572882X. DOI: 10.1007/s10570-020-03331-2.

[193] Xin Wang et al. "An eco-friendly way to fire retardant flexible polyurethane foam: Layer-by-layer assembly of fully bio-based substances". In: *RSC Advances* 4.86 (Sept. 2014), pp. 46164–46169. ISSN: 20462069. DOI: 10.1039/c4ra07972h. URL: https://pubs.rsc.org/en/content/articlehtml/2014/ra/c4ra07972h%20https://pubs.rsc.org/en/content/articlelanding/2014/ra/c4ra07972h.

[194] Yun Liu et al. "Thermal degradation properties of biobased iron alginate film". In: *Journal of Analytical and Applied Pyrolysis* 119 (May 2016), pp. 87–96. ISSN: 01652370. DOI: 10.1016/j.jaap.2016.03.014.

[195] Y. Liu et al. "The flame retardancy and thermal degradation behaviors of trivalent metal-alginate films". In: *Nanomaterials and Energy* 3.NME1 (2014), pp. 3–10. DOI: http://dx.doi.org/10.1680/nme.13.00030.

[196] Yun Liu et al. "Bio-based nickel alginate and copper alginate films with excellent flame retardancy: Preparation, flammability and thermal degradation behavior". In: *RSC Advances* 5.79 (June 2015), pp. 64125–64137.

ISSN: 20462069. DOI: 10.1039/c5ra11048c. URL: https://pubs.rsc.org/en/content/articlehtml/2015/ra/c5ra11048c%20https://pubs.rsc.org/en/content/articlelanding/2015/ra/c5ra11048c.

[197] Jiao Li et al. "Flame retardancy and thermal degradation mechanism of calcium alginate/CaCO3 composites prepared via in situ method". In: *Journal of Thermal Analysis and Calorimetry* 131.3 (2018), pp. 2167–2177. ISSN: 15882926. DOI: 10.1007/s10973-017-6767-5.

[198] Jianjun Zhang et al. "Pyrolysis products and thermal degradation mechanism of intrinsically flame-retardant calcium alginate fibre". In: *Polymer Degradation and Stability* 96.5 (2011), pp. 936–942. ISSN: 01413910. DOI: 10.1016/j.polymdegradstab.2011.01.029. URL: http://dx.doi.org/10.1016/j.polymdegradstab.2011.01.029.

[199] Jianjun Zhang et al. "Effects of divalent metal ions on the flame retardancy and pyrolysis products of alginate fibres". In: *Polymer Degradation and Stability* 97.6 (June 2012), pp. 1034–1040. ISSN: 01413910. DOI: 10.1016/j.polymdegradstab.2012.03.004.

[200] M Caniato and A. Travan. "Method for recycling waste material". EP Patent 16425023.5A. M Caniato and A. Travan. 2016.

[201] César Peteiro. *Alginate Production from Marine Macroalgae, with Emphasis on Kelp Farming*. Springer, Singapore, 2018. Chap. 2, pp. 27–66. ISBN: 9789811069109. DOI: 10.1007/978-981-10-6910-9_2. URL: https://link.springer.com/chapter/10.1007/978-981-10-6910-9_2.

[202] Pierre Agulhon et al. "Structural regime identification in ionotropic alginate gels: Influence of the cation nature and alginate structure". In: *Biomacromolecules* 13.1 (Jan. 2012), pp. 215–220. ISSN: 15257797. DOI: 10.1021/bm201477g. URL: https://pubs.acs.org/doi/10.1021/bm201477g.

[203] Jiri Brus et al. "Structure and Dynamics of Alginate Gels Cross-Linked by Polyvalent Ions Probed via Solid State NMR Spectroscopy". In: *Biomacromolecules* 18.8 (Aug. 2017), pp. 2478–2488. ISSN: 1525-7797. DOI: 10.1021/acs.biomac.7b00627. URL: https://pubs.acs.org/sharingguidelines%20https://pubs.acs.org/doi/10.1021/acs.biomac.7b00627.

[204] Pavel Gurikov and Irina Smirnova. "Non-Conventional Methods for Gelation of Alginate". In: *Gels* 4.1 (Feb. 2018), p. 14. ISSN: 2310-2861. DOI: 10.3390/gels4010014. URL: http://www.mdpi.com/2310-2861/4/1/14.

[205] Kurt Ingar Draget, Gudmund Skjåk-Bræk, and Bjørn Torger Stokke. "Similarities and differences between alginic acid gels and ionically crosslinked alginate gels". In: *Food Hydrocolloids* 20.2-3 (Mar. 2006), pp. 170–175. ISSN: 0268005X. DOI: 10.1016/j.foodhyd.2004.03.009. URL: https://linkinghub.elsevier.com/retrieve/pii/S0268005X05001049.

[206] Alena Sergeeva, Anna S. Vikulina, and Dmitry Volodkin. "Porous Alginate Scaffolds Assembled Using Vaterite CaCO3 Crystals". In: *Micromachines* 10.6 (May 2019), p. 357. ISSN: 2072-666X. DOI: 10.3390/mi10060357. URL: https://www.mdpi.com/2072-666X/10/6/357.

[207] Noelia González-López, Andrés Moure, and Herminia Domínguez. "Hydrothermal fractionation of Sargassum muticum biomass". In: *Journal of Applied Phycology* 24.6 (Mar. 2012), pp. 1569–1578. ISSN: 09218971. DOI: 10.1007/s10811-012-9817-1. URL: https://link.springer.com/article/10.1007/s10811-012-9817-1.

[208] Pedro Villanueva-Rey et al. "Quantifying environmental impacts associated to sodium alginate extraction from seaweed - hal-01682195". In: *8th international conference on Life Cycle Management*. Luxembourg, 2017. URL: https://hal-mines-paristech.archives-ouvertes.fr/hal-01682195.

[209] Pedro Villanueva-Rey. "From Vineyard to Sea. Application of Life Cycle Assessment to Wine and Seafood Sectors". PhD thesis. UNIVERSIDADE DE SANTIAGO DE COMPOSTELA, 2015.

[210] Edgar Jimenez-Cervantes et al. "Graphene-Based Materials Functionalization with Natural Polymeric Biomolecules". In: *Recent Advances in Graphene Research*. InTech, Oct. 2016. DOI: 10.5772/64001. URL: http://dx.doi.org/10.5772/64001.

[211] Artur T. Dideikin and Alexander Y. Vul'. *Graphene oxide and derivatives: The place in graphene family*. Jan. 2019. DOI: 10.3389/fphy.2018.00149. URL: www.frontiersin.org.

[212] Huitao Yu et al. “High-efficient Synthesis of Graphene Oxide Based on Improved Hummers Method”. In: *Scientific Reports* 6.October (2016), pp. 1–7. ISSN: 20452322. DOI: 10.1038/srep36143.

[213] Daniel R. Dreyer et al. “The chemistry of graphene oxide”. In: *Chem. Soc. Rev.* 39.1 (2010), pp. 228–240. ISSN: 0306-0012. DOI: 10.1039/B917103G. URL: http://xlink.rsc.org/?DOI=B917103G.

[214] Won Kyu Park et al. “Facile synthesis of graphene oxide in a Couette-Taylor flow reactor”. In: *Carbon* 83 (2015), pp. 217–223. ISSN: 00086223. DOI: 10.1016/j.carbon.2014.11.024. URL: http://dx.doi.org/10.1016/j.carbon.2014.11.024.

[215] Héctor Aguilar-Bolados et al. “Facile and Scalable One-Step Method for Amination of Graphene Using Leuckart Reaction”. In: *Chemistry of Materials* 29.16 (2017), pp. 6698–6705. ISSN: 15205002. DOI: 10.1021/acs.chemmater.7b01438.

[216] Anwei Yang et al. “One-step amine modification of graphene oxide to get a green trifunctional metal-free catalyst”. In: *Applied Surface Science* 346 (Aug. 2015), pp. 443–450. ISSN: 01694332. DOI: 10.1016/j.apsusc.2015.04.033. URL: http://dx.doi.org/10.1016/j.apsusc.2015.04.033%20https://linkinghub.elsevier.com/retrieve/pii/S0169433215008739.

[217] *Flow Properties of Polymers*. URL: https://polymerdatabase.com/polymer%20physics/Viscosity2.html (visited on 12/31/2020).

[218] *Viscosity Model for Thermoplastic*. URL: http://support.moldex3d.com/r16/en/standardinjectionmolding_material_materialmodels_viscositymodelforthermoplastic.html (visited on 12/31/2020).

[219] Malcolm M. Cross. “Polymer rheology: Influence of molecular weight and polydispersity”. In: *Journal of Applied Polymer Science* 13.4 (1969), pp. 765–774. ISSN: 10974628. DOI: 10.1002/app.1969.070130415.

[220] *Rheology 101 – Learning the Basics [AZO Matherials]*. URL: https://www.azom.com/article.aspx?ArticleID=16985 (visited on 01/02/2021).

[221] *With Heat Flow Meter : NETZSCH TAURUS Instruments GmbH*. URL: https://www.taurus-instruments.de/en/product/thermal-conductivity-measuring-devices/with-heat-flow-meter/ (visited on 01/02/2021).

[222] Michael F. Ashby. *Materials Selection in Mechanical Design*. 4th ed. Elsevier, 2011, p. 523. ISBN: 9781856176637. DOI: 10.1016/C2009-0-25539-5.

[223] ISO 10534-2:1998. "Determination of Sound absorption coefficient and impedance in impedance tubes - Part2: Transfer-Function method". In: (1998).

[224] *Principle of a heat-flux DSC - NETZSCH Analyzing & Testing*. URL: https://www.netzsch-thermal-analysis.com/en/landing-pages/principle-of-a-heat-flux-dsc/ (visited on 01/03/2021).

[225] Eric N. Landis and Denis T. Keane. "X-ray microtomography". In: *Materials Characterization* 61.12 (Dec. 2010), pp. 1305–1316. ISSN: 10445803. DOI: 10.1016/j.matchar.2010.09.012. URL: http://linkinghub.elsevier.com/retrieve/pii/S1044580310002706.

[226] Francesco Brun et al. "Pore3D: A software library for quantitative analysis of porous media". In: *Nuclear Instruments and Methods in Physics Research, Section A: Accelerators, Spectrometers, Detectors and Associated Equipment* 615.3 (Apr. 2010), pp. 326–332. ISSN: 01689002. DOI: 10.1016/j.nima.2010.02.063.

[227] *Zeta Potential Analysis - Particle Technology Labs*. URL: https://www.particletechlabs.com/analytical-testing/zeta-potential-analysis (visited on 01/03/2021).

[228] Hubert Biteau et al. "Calculation methods for the heat release rate of materials of unknown composition". In: *Fire Safety Science* (2008), pp. 1165–1176. ISSN: 18174299. DOI: 10.3801/IAFSS.FSS.9-1165.

[229] Clayton Huggett. "Estimation of rate of heat release by means of oxygen consumption measurements". In: *Fire and Materials* 4.2 (June 1980), pp. 61–65. ISSN: 0308-0501. DOI: 10.1002/fam.810040202. URL: http://doi.wiley.com/10.1002/fam.810040202.

[230] Tristan Hehnen. *DGS-SEE SEMINAR ON FIRE PROTECTION FOR PHYSICS RESEARCH FACILITIES CREATING A CABLE MATERIAL FOR FIRE SIMULATION-FIRST STEPS*. Tech. rep. CERN, 2015.

[231] *Micro Calorimeter ASTM D7309 - Fire Testing Technology*. URL: https://www.fire-testing.com/faa-micro-calorimeter-3/ (visited on 01/04/2021).

[232] R. Sonnier et al. “Combining cone calorimeter and PCFC to determine the mode of action of flame-retardant additives”. In: *Polymers for Advanced Technologies* 22.7 (2011), pp. 1091–1099. ISSN: 10427147. DOI: 10.1002/pat.1989.

[233] ISO 14040:2006(E). “ Environmental management — Life cycle assessment — Principles and framework Management”. In: (2006).

[234] ISO 14044:2006(E). “ISO 14044:2006(E) Environmental management — Life cycle assessment — Requirements and guidelines”. In: (July 2006). ISSN: -.

[235] European Commission – Joint Research Centre – Institute for Environment and Sustainability. *International Reference Life Cycle Data System (ILCD) Handbook – General guide for Life Cycle Assessment – Detailed guidance*. First. Publications Office of the European Union, 2010, p. 417.

[236] European Commission - Joint Research Centre - Institute for Environment and Sustainability. *ILCD Handbook: Framework and requirements for LCIA models and indicators First edition*. First. Publications Office of the European Union, 2010, p. 102.

[237] *Data & Statistics - IEA*. URL: %7Bhttps://www.iea.org/data-and-statistics?country=WORLD%5C&fuel=Energy%20supply%5C&indicator=TPESbySource%7D (visited on 01/21/2021).

[238] Paula Pérez-López et al. “Comparative environmental assessment of valorization strategies of the invasive macroalgae Sargassum muticum”. In: *Bioresource Technology* 161 (2014), pp. 137–148. ISSN: 18732976. DOI: 10.1016/j.biortech.2014.03.013.

[239] *EMEP/EEA air pollutant emission inventory guidebook — European Environment Agency*. URL: https://www.eea.europa.eu/themes/air/air-pollution-sources-1/emep-eea-air-pollutant-emission-inventory-guidebook (visited on 01/18/2021).

[240] *FD300 Freeze Dryer - Cuddon Freeze Dry*. URL: https://www.cuddonfreezedry.com/products/fd300-freeze-dryer/ (visited on 01/18/2021).

[241] Krstan Keselj et al. “Comparison of energy consumption in the convective and freeze drying of raspberries”. In: *Journal on Processing and Energy*

in Agriculture 21.4 (2017), pp. 192–196. ISSN: 1821-4487. DOI: 10.5937/jpea1704192k.

[242] A. G. Leach. "The thermal conductivity of foams. I: Models for heat conduction". In: *Journal of Physics D: Applied Physics* 26.5 (1993), pp. 733–739. ISSN: 13616463. DOI: 10.1088/0022-3727/26/5/003.

[243] Matteo Cibinel et al. "Recycling alginate composites for thermal insulation". In: *Carbohydrate Polymers* 251 (Jan. 2021), p. 116995. ISSN: 01448617. DOI: 10.1016/j.carbpol.2020.116995. URL: https://linkinghub.elsevier.com/retrieve/pii/S0144861720311681.

[244] David C. Bassett et al. "Competitive ligand exchange of crosslinking ions for ionotropic hydrogel formation". In: *Journal of Materials Chemistry B* 4.37 (2016), pp. 6175–6182. DOI: 10.1039/C6TB01812B. URL: http://xlink.rsc.org/?DOI=C6TB01812B.

[245] Marit Sletmoen, Kurt I. Draget, and Bjørn T. Stokke. "Alginate Oligoguluronates as a Tool for Tailoring Properties of Ca-Alginate Gels". In: *Macromolecular Symposia* 291-292.1 (June 2010), pp. 345–353. ISSN: 10221360. DOI: 10.1002/masy.201050541. URL: http://doi.wiley.com/10.1002/masy.201050541.

[246] Bommanahalli Shivegowda Roopa and Suvendu Bhattacharya. "Characterisation and modelling of time-independent and time-dependent flow behaviour of sodium alginate dispersions". In: *International Journal of Food Science & Technology* 44.12 (Dec. 2009), pp. 2583–2589. ISSN: 09505423. DOI: 10.1111/j.1365-2621.2009.02088.x. URL: http://doi.wiley.com/10.1111/j.1365-2621.2009.02088.x.

[247] Leitao Cao et al. "Porous materials for sound absorption". In: *Composites Communications* 10.June (Dec. 2018), pp. 25–35. ISSN: 24522139. DOI: 10.1016/j.coco.2018.05.001. URL: https://doi.org/10.1016/j.coco.2018.05.001%20https://linkinghub.elsevier.com/retrieve/pii/S2452213918300433.

[248] E. Knapen et al. "Acoustic properties of sound absorbing, polymer-modified porous cement mortars". In: *6th International Conference on Materials Science and Restoration, MSR-VI*. 2003.

[249] Kirill V Horoshenkov. "A Review of Acoustical Methods for Porous Material Characterisation". In: *The International Journal of Acoustics and Vibration* 22.1 (Mar. 2017). ISSN: 10275851. DOI: 10.20855/ijav.2017.22.1455. URL: https://doi.org/10.20855/ijav.2017.22.1455%20http://iiav.org/ijav/content/volumes/22_2017_497501490091138/vol_1/1166_fullpaper_1601601490091476.pdf.

[250] Sumitra Ramachandran et al. *Gluconic acid: Properties, applications and microbial production*. 2006.

[251] Jorge S. Carlos. "The impact of thermal mass on cold and hot climate zones of Portugal". In: *Indoor and Built Environment* 26.6 (2017), pp. 733–743. ISSN: 14230070. DOI: 10.1177/1420326X16635237.

[252] Cristina Vallés et al. "The rheological behaviour of concentrated dispersions of graphene oxide". In: *Journal of Materials Science* 49.18 (Sept. 2014), pp. 6311–6320. ISSN: 0022-2461. DOI: 10.1007/s10853-014-8356-3. URL: https://link.springer.com/article/10.1007/s10853-014-8356-3%20http://link.springer.com/10.1007/s10853-014-8356-3.

[253] Francesco Del Giudice and Amy Q. Shen. "Shear rheology of graphene oxide dispersions". In: *Current Opinion in Chemical Engineering* 16 (May 2017), pp. 23–30. ISSN: 22113398. DOI: 10.1016/j.coche.2017.04.003. URL: https://linkinghub.elsevier.com/retrieve/pii/S2211339816301307.

[254] Jiji Abraham et al. "Rheological Percolation in Thermoplastic Polymer Nanocomposites". In: *Rheology: Open access* 1.1 (2017), pp. 1–15.

[255] J. Chen and L. Li. "Thermal Conductivity of Graphene Oxide: A Molecular Dynamics Study". In: *JETP Letters* 112.2 (June 2020), pp. 117–121. ISSN: 10906487. DOI: 10.1134/S0021364020140015. URL: https://doi.org/10.1134/S0021364020140015.

[256] B. Schartel and T. R. Hull. "Development of fire-retarded materials — Interpretation of cone calorimeter data". In: *Fire and Materials* 31.5 (Aug. 2007), pp. 327–354. ISSN: 03080501. DOI: 10.1002/fam.949. URL: http://doi.wiley.com/10.1002/fam.949.

[257] Kamila Salasinska et al. "Analysis of flammability and smoke emission of rigid polyurethane foams modified with nanoparticles and halogen-free fire

retardants". In: *Journal of Thermal Analysis and Calorimetry* 130.1 (2017), pp. 131–141. ISSN: 15882926. DOI: 10.1007/s10973-017-6294-4.

[258] Heong Won Suh et al. "Fire spread of thermal insulation materials in the ceiling of piloti-type structure: Comparison of numerical simulation and experimental fire tests using small- and real-scale models". In: *Sustainability (Switzerland)* 11.12 (2019). ISSN: 20711050. DOI: 10.3390/su10023389.

[259] Xingxing Shi et al. "Establishment of a highly efficient flame-retardant system for rigid polyurethane foams based on bi-phase flame-retardant actions". In: *RSC Advances* 8.18 (2018), pp. 9985–9995. ISSN: 20462069. DOI: 10.1039/c7ra13315d.

[260] Weiguang An et al. "Correlation analysis of sample thickness, heat flux, and cone calorimetry test data of polystyrene foam". In: *Journal of Thermal Analysis and Calorimetry* 119.1 (2015), pp. 229–238. ISSN: 13886150. DOI: 10.1007/s10973-014-4165-9.

[261] Zhi Jie Cao et al. "Polyurethane foams with functionalized graphene towards high fire-resistance, low smoke release, superior thermal insulation". In: *Chemical Engineering Journal* 361.November 2018 (2019), pp. 1245–1254. ISSN: 13858947. DOI: 10.1016/j.cej.2018.12.176.

[262] Chuan Jie Zhang et al. "Bio-based calcium alginate nonwoven fabrics: Flame retardant and thermal degradation properties". In: *Journal of Analytical and Applied Pyrolysis* 122 (2016), pp. 13–23. ISSN: 01652370. DOI: 10.1016/j.jaap.2016.10.030.

[263] Mark E. Earll et al. "Synthesis of Cholesteryl Polyamine Carbamates: p K a Studies and Condensation of Calf Thymus DNA". In: *Bioconjugate Chemistry* 11.3 (2002), pp. 314–326. ISSN: 1043-1802. DOI: 10.1021/bc990115w.

[264] Ian S Blagbrough and Andrew J Geall. "Practical Synthesis of Unsymmetrical Polyamine Amides". In: *TETRAHEDRON LETTERS* 39 (1998), pp. 439–442.

[265] Joseph Gardella, Susan A. Ferguson, and Roland L. Chin. "pi * implied by pi SHAKEUP SATELLITES FOR THE ANALYSIS OF STRUCTURE AND BONDING IN AROMATIC POLYMERS BY X-RAY PHOTOELEC-

TRON SPECTROSCOPY." In: *Applied Spectroscopy* 40.2 (1986), pp. 224–232. ISSN: 00037028. DOI: 10.1366/0003702864509565.

[266] Abhijit Ganguly et al. "Probing the thermal deoxygenation of graphene oxide using high-resolution in situ X-ray-based spectroscopies". In: *Journal of Physical Chemistry C* 115.34 (2011), pp. 17009–17019. ISSN: 19327447. DOI: 10.1021/jp203741y.

[267] Jakub Ederer et al. "Determination of amino groups on functionalized graphene oxide for polyurethane nanomaterials: XPS quantitation vs. functional speciation". In: *RSC Advances* 7.21 (2017), pp. 12464–12473. ISSN: 20462069. DOI: 10.1039/c6ra28745j.

[268] Giang T.T. Le et al. "Divergent mechanisms for thermal reduction of graphene oxide and their highly different ion affinities". In: *Diamond and Related Materials* 89.March (2018), pp. 246–256. ISSN: 09259635. DOI: 10.1016/j.diamond.2018.09.006.

[269] Yuan Yuan et al. "An amine-bifunctionalization strategy with Beta/KIT-6 composite as a support for CO2adsorbent preparation". In: *RSC Advances* 10.56 (2020), pp. 34187–34196. ISSN: 20462069. DOI: 10.1039/d0ra05044j.

[270] Sunanda Roy, Le Van Hai, and Jaehwan Kim. "Synergistic effect of polydopamine - polyethylenimine copolymer coating on graphene oxide for EVA nanocomposites and high-performance triboelectric nanogenerators". In: *Nanoscale Advances* 1.6 (2019), pp. 2444–2453. ISSN: 25160230. DOI: 10.1039/c9na00142e.

[271] D. Stauffer et al. "An atomic charge model for graphene oxide for exploring its bioadhesive properties in explicit water". In: *Journal of Chemical Physics* 141.4 (July 2014), p. 044705. ISSN: 00219606. DOI: 10.1063/1.4890503. URL: http://aip.scitation.org/doi/10.1063/1.4890503.

[272] Febri Baskoro et al. "Graphene oxide-cation interaction: Inter-layer spacing and zeta potential changes in response to various salt solutions". In: *Journal of Membrane Science* 554 (May 2018), pp. 253–263. ISSN: 18733123. DOI: 10.1016/j.memsci.2018.03.006.

[273] Ming Jie Li et al. "The evolution of surface charge on graphene oxide during the reduction and its application in electroanalysis". In: *Carbon* 66 (2014), pp. 302–311. ISSN: 00086223. DOI: 10.1016/j.carbon.2013.09.004.

[274] Andrew N J Rodgers, Matěj Velický, and Robert A W Dryfe. "Electrostatic Stabilization of Graphene in Organic Dispersions". In: *Langmuir* 31.48 (Dec. 2015), pp. 13068–13076. ISSN: 0743-7463. DOI: 10.1021/acs.langmuir.5b04219. URL: https://pubs.acs.org/sharingguidelines%20https://pubs.acs.org/doi/10.1021/acs.langmuir.5b04219.

[275] *PDF-2 – ICDD*. URL: https://www.icdd.com/pdf-2/ (visited on 09/27/2020).

[276] Taichi SATO and Keiichi SATO. "Preparation of Gelatinous Aluminium Hydroxide from Aqueous Solutions of Aluminium Salts Containing Sulphate Group with Alkali". In: *Journal of the Ceramic Society of Japan* 104.1209 (1996), pp. 377–382. ISSN: 1882-1022. DOI: 10.2109/jcersj.104.377. URL: http://joi.jlc.jst.go.jp/JST.Journalarchive/jcersj1988/104.377?from=CrossRef.

[277] J. Theo Kloprogge et al. "XPS study of the major minerals in bauxite: Gibbsite, bayerite and (pseudo-)boehmite". In: *Journal of Colloid and Interface Science* 296.2 (2006), pp. 572–576. ISSN: 00219797. DOI: 10.1016/j.jcis.2005.09.054.

[278] Samir Lamouri et al. "Control of the γ-alumina to α-alumina phase transformation for an optimized alumina densification". In: *Boletin de la Sociedad Espanola de Ceramica y Vidrio* 56.2 (2017), pp. 47–54. ISSN: 21730431. DOI: 10.1016/j.bsecv.2016.10.001.

[279] Rolf Frischknecht et al. *Implementation of Life Cycle Impact Assessment Methods Data v2.0 (2007)*. Tech. rep. Dübendorf: Swiss Centre for Life Cycle Inventories, 2007. URL: www.ecoinvent.org.

[280] J.B. Guinée et al. *Handbook on life cycle assessment. Operational guide to the ISO standards. I: LCA in perspective. IIa: Guide. IIb: Operational annex. III: Scientific background.* Dordrecht: Kluwer Academic Publishers, 2002, p. 692.

[281] Bernhard Schartel, Charles A Wilkie, and Giovanni Camino. "Recommendations on the scientific approach to polymer flame retardancy: Part 2—Concepts". In: *Journal of Fire Sciences* 35.1 (Jan. 2017), pp. 3–20. ISSN: 0734-9041. DOI: 10.1177/0734904116675370. URL: http://journals.sagepub.com/doi/10.1177/0734904116675370.

[282] Sabu Thomas, René Muller, and Jiji Abraham. *Rheology and Processing of Polymer Nanocomposites*. Ed. by Sabu Thomas, Rene Muller, and Jiji Abraham. Hoboken, NJ, USA: John Wiley & Sons, Inc., Sept. 2016, pp. 1–600. ISBN: 9781118969809. DOI: 10.1002/9781118969809. URL: http://doi.wiley.com/10.1002/9781118969809.

[283] R. Kotsilkova. "Processing-structure-properties relationships of mechanically and thermally enhanced smectite/epoxy nanocomposites". In: *Journal of Applied Polymer Science* 97.6 (2005), pp. 2499–2510. ISSN: 00218995. DOI: 10.1002/app.21989.

[284] M. El Achaby and A. Qaiss. In: *[Materials & Design* (). ISSN: 02613069. DOI: 10.1016/j.matdes.2012.07.065.

[285] Naficy, Sina and Jalili, Rouhollah and Aboutalebi, Seyed Hamed and Gorkin, Robert A. and Konstantinov, Konstantin and Innis, Peter C. and Spinks, Geoffrey M. and Poulin, Philippe and Wallace, Gordon G. "Graphene oxide dispersions: Tuning rheology to enable fabrication". In: *Materials Horizons* 1.3 (2014), pp. 326–331. ISSN: 20516355. DOI: 10.1039/c3mh00144j.

[286] Cevdet Kaynak and B. Melike Sipahioglu. "Effects of nanoclays on the flammability of polystyrene with triphenyl phosphate–based flame retardants". In: *Journal of Fire Sciences* 31.4 (July 2013), pp. 339–355. ISSN: 0734-9041. DOI: 10.1177/0734904112473729. URL: http://journals.sagepub.com/doi/10.1177/0734904112473729.

[287] H. Benkreira, A. Khan, and K. V. Horoshenkov. "Sustainable acoustic and thermal insulation materials from elastomeric waste residues". In: *Chemical Engineering Science* 66.18 (Sept. 2011), pp. 4157–4171. ISSN: 00092509. DOI: 10.1016/j.ces.2011.05.047.

[288] L. Aditya et al. "A review on insulation materials for energy conservation in buildings". In: *Renewable and Sustainable Energy Reviews* 73.January (June 2017), pp. 1352–1365. ISSN: 13640321. DOI: 10.1016/j.rser.2017.02.034. URL: https://linkinghub.elsevier.com/retrieve/pii/S1364032117302484.

Acknowledgments

At this point, there are a lot of people, whose contributions went far beyond the intellectual one, to which I would like to express my thanks. They supported me all along during this journey by urging me on doing my best, especially in those moments where fatigue and frustration were at their peaks.

Firstly, I would like to express the deepest gratitude and appreciation to my supervisor, prof. Vanni Lughi, who always had time for me and who guided me in these three years with his patience and precious advice.

I would also like to express my gratitude to prof. Prato, who gave me the opportunity to work in his lab in the wonderful city of San Sebastian, and to prof. Loris Giorgini and Dr. Sabyasachi Gaan who spent their time and resources helping me through fire resistance assessment tests.

This project would not have been possible without the numerous people who have given up their time to teach me or assist me with patience during these years. Thank you to all the researchers and technicians of the CIC biomaGUNE, in particular those of the Carbon Bionanotechnology lab, who warmly welcomed me and taught me more that I would had never imagined. In particular, Alejandro Criado Fernández for his guidance during my terrific journey into the graphene chemistry world.

I would also extends my appreciation to Davide Porelli for his contribution regarding tomography analysis, to Alessandro Bordignon and Andrea Mio for their assistance during the performing of LCA investigation and to Luca Cozzarini for his advice.

I would also like to thank my collegues, Alessandro Esposito and Marco Beltrami who joined our office during my second year. Far from being just co-workers of an undoubted scientific value, they eventually become friends without those this journey would have been extremely arduous.

I would express my thankfulness to all of my friends and in particular to Alessandro and Margherita who always had a spare bottle to cheer me up.

I would like to thanks my family: mom, dad, grandma and my brother without whom I would have never been able to accomplish. In particular, a special thanks goes to my brother, Luca, who has never missed a chance to impress me with his value and support shown to me. In conclusion, last but definitely not least, I owe a very important debt to my girlfriend Arianna who has always sustained (and bore) me through the highs and lows of those years.